INVESTIGATIONS OF LIPID DYNAMICS AND POLYMORPHISMS IN LUNG SURFACTANT

By

REBA SUZANNE FARVER

A DISSERTATION PRESENTED TO THE GRADUATE SCHOOL
OF THE UNIVERSITY OF FLORIDA IN PARTIAL FULFILLMENT
OF THE REQUIREMENTS FOR THE DEGREE OF
DOCTOR OF PHILOSOPHY

UNIVERSITY OF FLORIDA

2011

To those who love me

ACKNOWLEDGMENTS

I take this opportunity to thank my advisor, Dr. Joanna R. Long for accepting me into her lab and not strangling me when I probably deserved it. I thank her for providing all the necessary tools for my training and lots of one-on-one guidance. If it wasn't for the valuable discussions in her office I wouldn't have made it this far. I also thank my committee members (Dr. Robert McKenna, Dr. Susan Frost, Dr. Gail Fanucci, and Dr. Arthur Edison) for their support and taking the time to attend numerous meetings, providing valuable feedback and criticisms. The Long and Fanucci groups have also been helpful in my training, providing resources and collaboration as well as an audience for practice presentations.

The AMRIS staff at the University of Florida have been behind me throughout my graduate school experience. I thank Jim Rocca for installing the 5 mm BBO probe every time I was scheduled to use the 500 MHz magnet. He has taught me a lot about NMR and has inspired my continued studies in this field. Our many conversations have helped me along the way as both moral support and encouragement. I also thank Kelly Jenkins for always being around when I needed help with various things and for being a friend.

I thank my parents, Bill and Rita Farver, for their encouragement and for always being there for me throughout my life. They told me I could do anything I wanted to and I believed them. Their faith in God and in my abilities is the reason I have become who I am today. My sister, Amy, has also been extremely supportive during my graduate studies. She has always been protective of me even though she is younger than me and I am truly thankful for her sisterly love.

My wonderful and loving fiancé, Casimir, has stuck with me through some of my hardest times in graduate school. He was there to listen when I needed encouragement and to distract me when I needed a break. I know he is looking forward to the completion of this degree. I thank him for loving me and putting up with my moods. I know we will have a wonderful and fulfilling life together.

Most of all I thank God for getting me through this degree and for giving me a purpose. I would be nothing without Him.

TABLE OF CONTENTS

page

LIST OF TABLES

LIST OF FIGURES

LIST OF ABBREVIATIONS

AAA	amino acid analysis
ARDS	acute respiratory distress syndrome
B_o	external magnetic field
BSA	bovine serum albumin
C-D	carbon-deuterium bond
CD	circular dichroism
chol	cholesterol
CLSE	calf lung surfactant extract
$CLSE^{L}$	lipids only calf lung surfactant extract
$CLSE^{Syn}$	synthetic calf lung surfactant extract
$CLSE^{T}$	therapeutic calf lung surfactant extract
C_p^{max}	maximum heat capacity
CSA	chemical shift anisotropy
D	diffusion coefficient
d(H)	hydrodynamic diameter
DLS	dynamic light scattering
DMF	dimethylformamide
DNA	deoxyribonucleic acid
DPPC	1,2-Dipalmitoyl-*sn*-Glycero-3-Phosphocholine
DSC	differential scanning calorimetry
E	energy
ER	endoplasmic reticulum
Fmoc	fluorenylmethyloxycarbonyl
FTIR	fourier-transform infrared spectroscopy

ΔG	change in Gibbs free energy
GPC	gel permeation chromatography
^{2}H	deuterium
H_I	hexagonal I phase
H_{II}	hexagonal II phase
ΔH_{cal}	change in calorimetric enthalpy
ΔH_{vH}	change in van Hoft enthalpy
HPLC	high performance liquid chormatography
k	Boltzmann's constant
kDa	kilodalton
kHz	kilohertz
KL_4	KLLLLKLLLLKLLLLKLLLLK (sinapultide)
L_β	liquid-crystalline phase of a phospholipid
L_α	gel phase of a phospholipid
LB	lamellar body
LBPA	lysobisphosphatidic acid
LPC	lysophosphatidyl choline
LS	lung surfactant
LUVs	large unilamellar vesicles
m_ε	molar ellipticity
MAS	magic angle spinning
MLVs	multilamellar vesicles
NMR	nuclear magnetic resonance
p	pressure across alveoli
^{31}P	phosphorus

PA	palmitic acid
PC	phosphatidylcholine
PCS	photon correlation spectroscopy
PDB	protein data bank
PE	phosphatidylethanolamine
PG	phosphatidylglycerol
PI	phosphatidylinositol
PL	phospholipid
POPC	1-Palmitoyl-2-Oleoyl-*sn*-Glycero-3-Phosphocholine
POPE	1-Palmitoyl-2-Oleoyl-*sn*-Glycero-3-Phosphoethanolamine
POPG	1-Palmitoyl-2-Oleoyl-*sn*-Glycero-3-[Phospho-*rac*-(1-glycerol)]
ppm	parts per million
PS	phosphatidylserine
QELS	quasi-electron light scattering
r	radius
R	universal gas constant (1.987 cal K^{-1} mol^{-1})
RDS	respiratory distress syndrome
rf	radio frequency
ΔS	change in entropy
S_{CD}	time averaged order parameter of a C-D bond
sn-1	first acyl chain position of the glycerol backbone
sn-2	second acyl chain position of the glycerol backbone
SM	sphingomyelin
SP-A	Lung surfactant protein A
SP-B	Lung surfactant protein B

SP-B_{1-25}	FPIPLPYCWLCRALIKRIQAMIPKG
SP-B_{59-80}	DTLLGRMLPQLVCRLVLRCSMD
SP-C	Lung surfactant protein C
SP-D	Lung surfactant protein D
SPPS	solid phase peptide synthesis
ssNMR	solid-state nuclear magnetic resonance
SUVs	small unilamellar vesicles
γ	surface tension
T	absolute temperature
$\Delta T_{½}$	peak-width at half height in a DSC trace
TEM	transmission electron microscopy
TFA	trifluroacetic acid
T_m	phase transition temperature
TM	tubular myelin
Tr	trace
tRNA	transfer ribonucleic acid
$\Delta\nu_Q$	quadrupolar splitting

Abstract Of Dissertation Presented To The Graduate School
Of The University Of Florida In Partial Fulfillment Of The
Requirements For The Degree Of Doctor Of Philosophy

INVESTIGATIONS OF LIPID DYNAMICS AND POLYMORPHISMS IN LUNG SURFACTANT

By

Reba Suzanne Farver

December 2011

Chair: Joanna R. Long
Major: Medical Sciences – Biochemistry and Molecular Biology

This work seeks to delineate the role specific peptide sequences and lipid composition play in regulating lipid dynamics, organization, and trafficking of lung surfactant (LS). LS is a lipid-rich substance containing key proteins that minimizes surface tension in the alveoli. Its lipid composition is highly conserved among mammalian species. However, the lipid composition of LS alone is not sufficient to maintain the organization and dynamics of the lipid assemblies observed in the lung surfactant fluid of intact lung tissue. It has been postulated that protein-induced lipid polymorphisms and protein-induced trafficking of lipids to the interface are critical for LS function at ambient pressure. In particular, surfactant protein B (SP-B), which is highly hydrophobic and present at low levels, is critical to lipid trafficking and formation of a lipid layer at the air/water interface. SP-B is absolutely necessary for proper breathing. Additionally, several synthetic peptides based on the N- and C- termini of SP-B have shown promise as replacements for native SP-B in synthetic LS formulations.

SP-B_{1-25}, an amphipathic peptide composed of the first 25 amino acids of the N-terminus of SP-B, retains much of the biological activity of SP-B. I have observed the induction of uncommon lipid polymorphisms by SP-B_{1-25} in synthetic lipid systems, which could be mirroring the activities of SP-B in the lung. These results led to the study of lipid polymorphisms in more complex lipid mixtures, including organic solvent extracts of lavaged calf lung surfactant, CLSE, which better mimic endogenous LS to give a deeper understanding of lipid behavior in LS.

The properties of lipids in CLSE were investigated and compared to model lipid systems to guide efforts in developing synthetic lipid/peptide formulations to replace CLSE and to better understand the underlying molecular mechanisms involved in LS function. In addition, I have seen differences in lipid dynamics as regulated by point mutations in the peptide sequence of SP-B_{1-25} suggesting a new direction for developing therapeutic peptides. My research primarily utilized ^{2}H NMR to investigate lipid-specific acyl chain dynamics and polymorphisms and ^{31}P NMR to monitor systemic lipid polymorphisms.

CHAPTER 1
INTRODUCTION TO LUNG SURFACTANT

Surface Active Agents in the Lung

Surfactants are surface active agents that contain hydrophobic and hydrophilic moieties with the ability to self-assemble at interfaces and lower surface tension to extremely low levels (*1*, *2*). Surface tension is the tension found at a gas/liquid interface. The distance between molecules in a liquid is much smaller than in a gas at atmospheric pressure causing gas molecules to exert little attractive force on interfacial molecules. A molecule in the interior of a liquid is attracted on all sides, but at the gas/liquid interface the attraction is unbalanced causing an inward attractive force on the liquid molecules and shrinkage of the surface area (*1*). The difference between the intermolecular forces at the surface of the liquid and within the liquid produces the surface tension (*3*).

Replacing surface water with surfactants, which have lower surface energy, reduces surface tension at the interface (*3*). The amphipathic nature of surfactant molecules causes them to prefer a location at an interface whereby the hydrophobic groups are located in the air and the hydrophilic portions are in the water (*1*). One important type of surfactant is lung surfactant (LS), which is found at the air/water interface of alveoli and reduces surface tension, stabilizing the alveoli and allowing efficient gas exchange. Much of the work of breathing involves expanding the alveolar airsacs against these forces in order for gas exchange to occur.

Function of LS in the Alveoli

The alveoli are the primary site of gas exchange between blood and air. Air travels to the lungs through the trachea and bronchi to tiny air sacs called alveoli which

are surrounded by capillaries. Oxygen diffuses into the blood vessels to be pumped by the heart to the rest of the body. Carbon dioxide diffuses out of the blood into the lungs to be exhaled. This rapid gas exchange cycle between oxygen and carbon dioxide within the alveoli keeps oxygenated blood flowing throughout the body, with the lungs playing a critical role (*4*). Mammals require high oxygen uptake which is made possible by the large inner surface area of the lung, with 300 cm^2 per cubic centimeter of lung tissue (*5*). Collectively, the surface area of the alveoli in human adult lungs is approximately that of a tennis court. Inflation and deflation of the lungs under ambient conditions requires low surface tension at the air/water interface of the alveoli in addition to a large gas exchange area. A lipid/protein complex known as LS lines the inside of the alveoli and reduces the work of breathing by minimizing surface tension.

LaPlace's Law, $p = 2\gamma/r$, states that the pressure difference at the air/water interface (p) is equal to twice the surface tension (γ) at this interface, divided by the radius of the alveolar air space (r). The human lung contains 300 to 500 million alveoli with small radii to allow for more surface area in a small total volume. Lung volume and the air space radius decrease during expiration, leading to a higher pressure difference and requiring an increased amount of energy to reverse the process to inflate the lungs during inhalation (if surface tension does not change). If the alveoli are subject to normal pressure and the surface tension is high, LaPlace's Law predicts that they would collapse (*6*) (Figure 1-1). However, this does not happen in healthy lungs, suggestive of the presence of a substance that must be reducing surface tension in the lungs. This substance, LS, covers the surface of the alveoli and prevents the lungs from collapsing by keeping the energy requirement low (*1*). LS also allows the lungs of newborn infants

to spontaneously inflate on their first breaths. Also worth noting is that the structure of the lung is not exactly like that of a sphere and Laplace's law may not apply to the entire alveolar structure. A journal article by Henry Prange brings to our attention the fact that alveoli are not shaped like individual bubbles; they are prismatic or polygonal in shape. He also states that LS does reduce surface tension, however, it may be restricted to small distensible airways. Thus, the Y-tube model of alveolar inflation may be an over simplification (*7*). Nevertheless, it is the most commonly used model for understanding the mechanics of alveolar inflation.

Respiratory Distress Syndrome (RDS) in premature infants results from producing inadequate amounts of pulmonary surfactant, leading to high surface tension and alveolar collapse (*8*). Another type of respiratory failure, Acute Respiratory Distress Syndrome (ARDS), occurs in children and adults and results from the inability to adequately oxygenate the blood when gas exchange cannot be performed normally due to low surfactant concentration caused by lung injury (*8*). Lung surfactant is needed so that the alveoli can expand and the lungs can inflate; otherwise, blood passing through the pulmonary circulation system cannot pick up oxygen and dispose of carbon dioxide. If this occurs, blood oxygen levels decrease and carbon dioxide increases, leading to high acid levels in the blood and hypoxia. Among the many complications of RDS are congenital heart defects, patent ductus arteriosus, low blood pressure, and defects in other vital organ functions.

LS Cycle

Type II pneumocytes are the site of LS production. LS is synthesized, processed, stored, secreted, and recycled by type II pneumocytes (also known as type II epithelial cells), a type of cell that covers 5% of the alveolar surface (*1*). These type II cells are

surfactant factories containing all components (fatty acids, glucose, choline, and amino acids) needed for surfactant synthesis. LS is synthesized in the endoplasmic reticulum and then processed through the Golgi apparatus before being packaged into specialized organelles known as lamellar bodies (LB). LS is recycled every 5-10 hours and some of the steps in its hypothesized pathway are commonly accepted while others are controversial. What is agreed upon is that LB are secreted into the alveolar subphase from type II cells and tubular myelin (TM) is formed by multiple secreted LB (*9*). The TM then forms a film by unraveling and adsorbing onto the air/water interface (Figure 1-2). However, some of the lamellar bodies maintain their packed structure; both tubular myelin and lamellar bodies are able to contribute to the *in vivo* formation of the interfacial film important for oxygen exchange. Tubular myelin is not essential but can optimize surfactant properties *in vivo* (*10*). The LB particles and TM are both able to transfer the lipid/protein complex directly to the air/water interface where it is able to overcome the intermolecular forces of surface tension (*8*). What is debated is the role particular constituents of LS play in the cycle and where they are located at different times in the cycle. A rigid, surface stable phospholipid, dipalmitoylphosphatidylcholine (DPPC), found at high levels in LS is thought to be the major component of the surface film. How it is specifically trafficked to the interface is not fully understood. Sorting of the LS during adsorption to the air/water interface seems to result in a DPPC-rich surface film and a DPPC-poor lipid/protein mixture in the subphase. It is believed that most of the non-DPPC components of LS are squeezed out during the compression/expansion cycles leaving a DPPC-rich surface film (*9*) (Figure 1-3).

A dynamic process of compression and decompression of the surfactant film occurs during the breathing process (Figure 1-4). During inspiration LS adsorbs rapidly to the air/water interface and during expiration compression of the surface film takes place resulting in low surface tension and alveolar stability. Eventually parts of the surface film collapse into the alveolar subphase and are recycled or taken up by macrophages. If they are to be recycled, the type II cells retrieve the used LS and repackage the materials back into LB (*9*)

Lipid Trafficking

While the life cycle of LS is mostly mapped out, the molecular level processes by which LS lipids are trafficked to the air/water interface are not well understood and have been a subject in recent studies (*11–15*). LS is an ideal system for studying the molecular basis of lipid trafficking. Its simple lipid and protein composition (relative to the plasma membrane) is highly conserved among mammalian species. LS lipids can adopt a variety of structures in addition to the bilayer phase, all of which may play roles in their movement in the LS cycle. Their supermolecular structure and organization depend on acyl chain length and degree of unsaturation, headgroup hydrogen bonding, temperature, and the presence of other biological molecules such as proteins. The LS proteins are thought to be responsible for moving lipids around the alveolar environment (Figure 1-3). More specifically, it is SP-B that has been determined absolutely required for efficient LS function by several recent studies (*16*, *17*). Humans with genetic SP-B dysfunction die soon after birth as do genetically engineered SP-B null mice.

Chemical Composition of Lung Surfactant

Lung surfactant is comprised of 90% lipids and 10% proteins by weight and its composition varies only slightly among mammalian species. Phospholipids make up

the bulk of its lipid content with phosphatidylcholine (PC) as the predominant phospholipid species. Dipalmitoylphosphatidylcholine (DPPC) makes up half of the PC content. The two saturated acyl chains of DPPC enable it to be packed tightly in the monolayer at the air/water interface. The remaining PC lipids are monounsaturated, which contributes to the fluidity of LS. Anionic, predominantly monounsaturated phosphatidylglycerol (PG) is another lipid present in relatively high amounts. Smaller amounts of palmitic acid (PA), sphingomyelin (SM), phosphatidylinositol (PI), phosphatidylserine (PS), phosphatidylethanolamine (PE), and cholesterol, along with a trace amount of lysophosphatidylcholine (LPC), are also present (*9*, *18*) (Table 1-1) (Figure 1-5). The lipid composition of LS alone is not enough to maintain the organization and dynamics of the lipid assemblies observed in LS. Its protein content is the factor that sustains the overall function of LS, discussed below.

LS Lipids, Bilayers, and Polymorphisms

The majority of LS lipids are phospholipids along with a small percentage of neutral lipids. Phospholipids are known for their biological role in forming cell membranes via self-assembly into lipid bilayers; however, they also play crucial roles as the largest component of LS, in organizing intracellular organelles, and in trafficking of intracellular and extracellular components. Phospholipids have two fatty acid chains (sn-1 and sn-2) attached by ester linkages to a 3-carbon glycerol backbone. Attached to the third carbon in the glycerol backbone is a polar phosphate headgroup which determines the class of phospholipid and the last two letters of the common naming acronym. Lipid acyl chain length and saturation determine the first two letters of the naming scheme, as in dipalmitoyalphosphatidylcholine or DPPC as this lipid has two fully saturated palmitoyl (or 16 carbon) chains. The main LS phospholipids are DPPC,

POPC, POPG, and POPE; small amounts of other species exist, particularly monounsaturated variants with different fatty acyl chain lengths (*19*). Zwitterionic phospholipids make up almost 85% of total LS phospholipids and PCs are the largest group of zwitterionic phospholipids present in mammalian LS. Other zwitterionic phospholipids species found in LS include PE and sphingomyelin (*20*). Of the 80% LS lipids by weight which are phosphatidylcholines, almost half are DPPC. PG is 10% by weight of total LS lipids. Cholesterol is the main component of the neutral lipids and comprises about 5 mol% of all LS lipids. Monoacylglycerol, diacylglycerol, and triacylglycerol also make up a small portion of the neutral lipids along with a very small amount of free fatty acids, which are technically acidic and should be classified differently but are included under neutral lipids in surveys of LS composition.

The melting temperature, T_m, of lipids depends on several physical properties but is mostly dependent on hydrocarbon chain length and structure, charge, and hydrogen bonding between the phospholipid headgroups (*19*). As the chain length increases, the melting temperature increases. T_m decreases substantially with unsaturation of an acyl chain.

It is thought that the stability of DPPC monolayers to lateral pressure during compression is critical to the integrity of the air/water interface in the lung. The gel to liquid transition temperature of DPPC is 41°C; at 37°C it is in a gel state. However, when present with other LS lipids its melting temperature decreases to just below physiologic levels (~ 36°C). Palmitoyloleoylphosphatidyl choline (POPC) and palmitoyloleoylphosphatidyl glycerol (POPG) contain monounsaturated fatty acids and both have a transition temperature of -2°C, well below that of the disaturated DPPC.

These lipids increase the fluidity of the DPPC rich lung surfactant, accelerating surface film formation to cover the surface of the alveoli during the dynamic compression and expansion cycle. The adsorption capacity of lipids is related to their fluidity (*21*). If the film only consisted of disaturated lipids, it would become too rigid during dynamic breathing cycles. During exhalation, it is thought the remaining monolayer at the interface contains mostly DPPC while the monounsaturated lipids and surfactant proteins are squeezed out from the monolayer into a surfactant aggregate. These components then form another layer connected to the monolayer so that certain materials can be transferred to the monolayer during inhalation (*1*).

Bilayers form spontaneously when phospholipids are placed in an aqueous environment and they are in the form of vesicles (liposomes) in the laboratory setting when studying membrane properties experimentally. While LS lipids also form bilayers, they do not have the same fluid consistency that cell membranes have and are packed more tightly due to the high DPPC content, which is not a common component in cell membranes.

When describing lipid behavior, polymorphism is the ability of a mixture of lipids to form a variety of self-assembled structures. It also refers to the range of lipid phases above and below the phase transition temperature of different lipids including membrane bilayers. Lipids can also arrange in non-bilayer configurations, such as tubes, rods, and cubic assemblies in addition to bilayer (lamellar) structures (Figure 1-6) (*19*, *22*). For example, under the right conditions, a major polymorphism known as the hexagonal phase may form in which the lipids are arranged as cylinders with the polar headgroups pointed towards an aqueous pore (H_{II}) or with the acyl chains oriented

inwards and the phosphate headgroups forming the exterior of the rods (H_I) (*23*). Other alternative structures include cubic, rhombic, and micellar arrangements in which isotropic motion occur (*22*). These polymorphisms have been implicated as playing a crucial role in the function of LS (*24*). The ability to study lipid polymorphism and lipid dynamics has been profoundly extended by development of NMR techniques, in particular ^{31}P and ^{2}H NMR spectroscopy, which will be discussed in Chapter 2.

LS Proteins, Function, and Structure

There are four proteins found in pulmonary surfactant: SP-A, SP-B, SP-C, and SP-D. Surfactant Protein-B (SP-B) has been shown to be absolutely necessary in maintaining lung function; SP-C also maintains lung function, and SP-A and SP-D are immunoprotective proteins which do not have any effect on respiratory capacity (*1*, *25*). The surfactant proteins SP-A and SP-D are hydrophilic, and the surfactant proteins SP-B and SP-C are highly hydrophobic and lipid-associated (Figure 1-7). SP-D, a member of the collectin family, is able to bind to pathogens, such as bacteria, viruses, and fungi. Members of the collectin family contain collagen-like and lectin domains (*25–27*). The defense mechanism of this protein has proven essential in maintaining sterile conditions at respiratory surfaces. SP-A, also in the collectin family, is needed in the formation of tubular myelin, which increases the efficiency of surfactant adsorption. Nevertheless, it is not absolutely necessary for normal LS function and respiration (*28*). Both SP-B and SP-C interact with LB particles and have helical structures. They are small proteins, and, in spite of their low abundance, are critical to the formation of surfactant films. However, SP-B is the protein in lung surfactant responsible for lowering the surface tension during expansion and reducing the work of breathing that is absolutely required for proper trafficking of LS. The phospholipids of surfactant are also directly implicated

in surface tension reduction; however, they cannot act effectively by themselves. Initial clinical studies to develop LS replacement therapies used only lipids in surfactant formulations, but were unsuccessful. More recently, protein/lipid complexes have been shown to more closely mimic the properties of human lung surfactant and have shown significant clinical success (*1*). In vitro studies of SP-B have demonstrated it to be critically important in fulfilling the three main properties important for lung surfactant activity. These include transferring material from the aqueous subphase to the interface to form the phospholipid-rich surface film, reducing surface tension, and re-spreading the surface film during expansion (*29*–*31*) (Figure 1-3).

Properties and Hypothesized Function and Structure of SP-B

SP-B is encoded by a single gene on chromosome 2 and is transcribed into a 2 kb mRNA (*32*). The translation product of SP-B is a 381 residue preprotein (Figure 1-8). A 23 amino acid residue signal peptide, which is cleaved when the protein reaches the endoplasmic reticulum, mediates the beginning of the post-translational modifications. Cleavage of the proprotein continues yielding an N-terminal peptide, mature SP-B, and a C-terminal peptide. The N-terminal portion is needed for transit out of the endoplasmic reticulum, and both the N-terminal and mature protein are needed for trafficking of SP-B to the lamellar bodies. The C-terminal peptide is not required for intracellular trafficking (*33*). Post-translational processing produces the mature homodimer form of SP-B, with 79-81 amino acid residues in each monomer, with >60% of its amino acids being hydrophobic. Final processing of SP-B occurs during transit to the lamellar bodies (*33*).

SP-B is found in secreted LS as a 17 kDa sulfhydryl-dependent homodimer. Intramolecular disulfide bridges formed by cysteine residues are thought to bundle four

or five amphipathic helices in the monomer. The pattern of disulfide bonding in the processed protein and a sequence similar to sphingolipid-activator proteins place SP-B in the saposin-like protein family. However, in contrast to saposins, SP-B exists in nature as a dimer, is more lipophilic than other saposin-like proteins, and is always lipid associated. SP-B is particularly difficult to make because of its hydrophobicity. A three-dimensional model of porcine SP-B (based on 22% sequence identity to NK-lysin) exists, which has predicted approximate locations of four major helices (*34*). However, NK-lysin is water-soluble, whereas SP-B is not, so this model is insufficient to predict tertiary structural information for SP-B in lipid environments (*17*, *35*). Moreover, SP-B has not been successfully expressed heterologously and human lung surfactant supply is limited so animal sources are most often used, posing a risk of infection or immune response (*36*). While there is no full structure solved for SP-B, shorter peptide sequences that include portions of the N-terminal sequence have contributed to partial structures and models via solution NMR (in organic solvent) and FTIR (in lipid bilayers) (*37*–*39*).

Surfactant Replacements

Surfactant replacements currently used in the clinic contain material from animal lungs. Despite the high activity of these LS clinical formulations, they pose a risk of immune response from the patient and can only be administered to those who have not yet formed antibodies against LS proteins or infectious material. Potential adverse effects from exposure to foreign animal products have not been studied intensively; however, efforts to develop safer LS replacements are warranted because of potential microbes, immune response to animal proteins, and inconsistent LS content (*40*). Multiple instillations of an animal-derived LS formulation over time would lead to an

amplified immune response making it necessary for premature infants who are given this drug to start making their own surfactant shortly after receiving animal LS. As a result of their type II alveolar cells maturing due to the mechanical stimulation of breathing, many infants are successfully treated with CLSE. Older patients are at a greater risk of immune response due to a more mature immune system and ARDS is not as easily remedied since it is caused by injury to the lungs and LS proteins are denatured by BSA and other blood products. Therefore, synthetic surfactant preparations are being developed to circumvent the problems that occur with animal-derived LS.

Endogenous Sources of LS

Clinical LS therapies have endogenous and exogenous characteristics. There are preparations that contain endogenous sources of LS from animals and those that only contain synthetic non-animal derived material. Both are considered exogenous LS replacements as they are either extracted and are no longer affiliated with their original source (animal derived) or are completely synthetic. Preparations containing endogenous LS include organic extracts of lavaged animal LS, organic extracts of processed animal lung tissue, and organic extracts of processed animal lung tissue that have been supplemented with synthetic LS components (*1*). *Infasurf*, *Curosurf*, and *Survanta* are examples of exogenous LS replacements from endogenous sources which are used clinically. Other replacements being pursued are either completely synthetic or contain synthetic lipids along with recombinant apoproteins. For the purposes of this dissertation, any animal-derived LS replacement will be deemed endogenous compared to the fully synthetic LS mimics in this study.

Both RDS and ARDS can be treated with endogenous pulmonary surfactant replacement therapies. Clinical trials have demonstrated the efficacy of natural animal-derived surfactant as it acts faster and the mortality rate is lower than when exogenous synthetic surfactant is used (*41*). Nevertheless, there are studies that have shown no significant difference in the effectiveness of LS replacements whether they are animal-derived or synthetic (*40*, *42*). Developing an exogenous LS replacement therapy having the same or better efficacy to replace the current animal-derived surfactant therapies to avoid adverse immunologic and infectious complications is one goal for investigators studying LS mimics. Many medical professionals agree that pulmonary surfactant treatment is much safer when using non-animal sources (*40*). It could also be substantially less expensive to produce and have greater stability and a longer shelf life.

Calf Lung Surfactant Extract (CLSE)

CLSE is a surfactant replacement prepared from chloroform extracts of lavaged natural surfactant from calf lungs. It is commonly administered to premature infants with respiratory distress syndrome under the name *Infasurf*. The lipids in CLSE are unusually surface active and form unique aqueous assemblies due to low levels of surfactant proteins SP-B and SP-C. The surface active properties of lipids in CLSE have been investigated and compared to model lipid systems to guide efforts in developing synthetic lipid/peptide formulations to replace CLSE and to better understand the underlying molecular mechanisms involved in LS function.

CLSE contains 93% phospholipid, 5% cholesterol and neutral lipids, and 2% SP-B and SP-C by weight. Considering its components, it is the closest surfactant replacement relative to natural LS on the market. It is manufactured by ONY Inc. and

was generously provided as a gift for the studies in this dissertation. Comparisons of CLSE to synthetic LS mimics containing SP-B_{1-25} will be discussed in Chapter 4.

Synthetic Peptides and Lipids

Given the tremendous importance of SP-B to LS function, surfactant replacement methods employing simple peptide analogs with surface-active properties have been investigated. Based on the helical content of SP-B, studies by Cochrane and Revak were undertaken to determine which peptide sequences in SP-B were most physiologically viable (*43*). The identified sequences were then also used to produce a series of simple, model peptides for possible SP-B replacement. Two peptide sequences in SP-B were found to significantly reduce surface tension when incubated with DPPC:PC:PG as measured by Langmuir-Wilhemy surface balance tracings. They were also able to increase lung compliance in a fetal rabbit model with surfactant deficiency (*43–45*). The amino acid sequences of these peptides (SP-B_{1-25} and SP-B_{59-80}) are given in Figure 1-9. Furthermore, a study by Gupta and colleagues has determined that the 25 residue peptide based on the N-terminal sequence of SP-B improves surface activity and is also very effective (if not better) in resisting inhibition by fibrinogen, a plasma protein, compared to the full protein and the clinical surfactant, Surfanta™ (*46*). SP-B_{1-25} may also be less susceptible than full length SP-B to degradation by other plasma proteins; understanding how it functions in the lipid environment would allow the development of mimetics which are even less susceptible to degradation. Therefore, SP-B_{1-25} could be a highly effective clinical substitute for the full-length SP-B. These previous studies have also demonstrated the feasibility of utilizing shorter peptides in place of full-length surfactant proteins. They are much easier to make, with high yield and purity. Developing effective therapeutic

peptidomimetics could have a huge impact on the treatment of respiratory illnesses, such as RDS in infants as well as acute respiratory distress syndrome in children and adults.

The sequence of SP-B $_{1-25}$ is FPIPLPYCWLCRALIKRIQAMIPKG, making it highly hydrophobic, and it is thought to form a secondary structure and conformation similar to the parent sequence within the full protein in the presence of lipids. It has been previously established that SP-B$_{1-25}$ maintains the same surface activity as the full protein (*47*), and CD and FTIR data reflect the presence of helical structure in SP-B $_{1-25}$ when it is associated with lipid monolayers (*37*, *48*). It is thought the very hydrophobic N-terminal tail of SP-B is structured for rapid insertion into lipid films and to maintain this association (*8*). SP-B$_{1-25}$ is the peptide focused on in this dissertation and has shown promise as a key factor in LS replacement therapy. Studying the N-terminal portion of the critical protein, SP-B, will lead to an understanding of the importance of the first 25 amino acids of this LS protein and how it associates with LS lipids.

Membrane associated proteins are known to play key roles in many physiological events. To fully understand the structure, dynamics, and function of membrane associated proteins they must be studied in their native lipid environments. The synthetic LS mimics in this study utilized synthetic phospholipids and cholesterol to mirror the primary LS components found in nature or, at the very least, endogenous LS extracts. DPPC was used as the main lipid species along with zwitterionic and negatively charged monounsaturated lipids such as POPC, POPG, and POPE. Binary mixtures of LS lipids were first studied before moving to more complex lipid systems containing several lipid components. Chapters 3 and 4 provide more detail on these LS

mimics. Chapter 2 discusses the theory behind the techniques used in this work. Chapter 5 introduces a mutant peptide of SP-B_{1-25} and its effects on lipid dynamics, while Chapter 6 provides conclusions for this dissertation and ideas for future experiments.

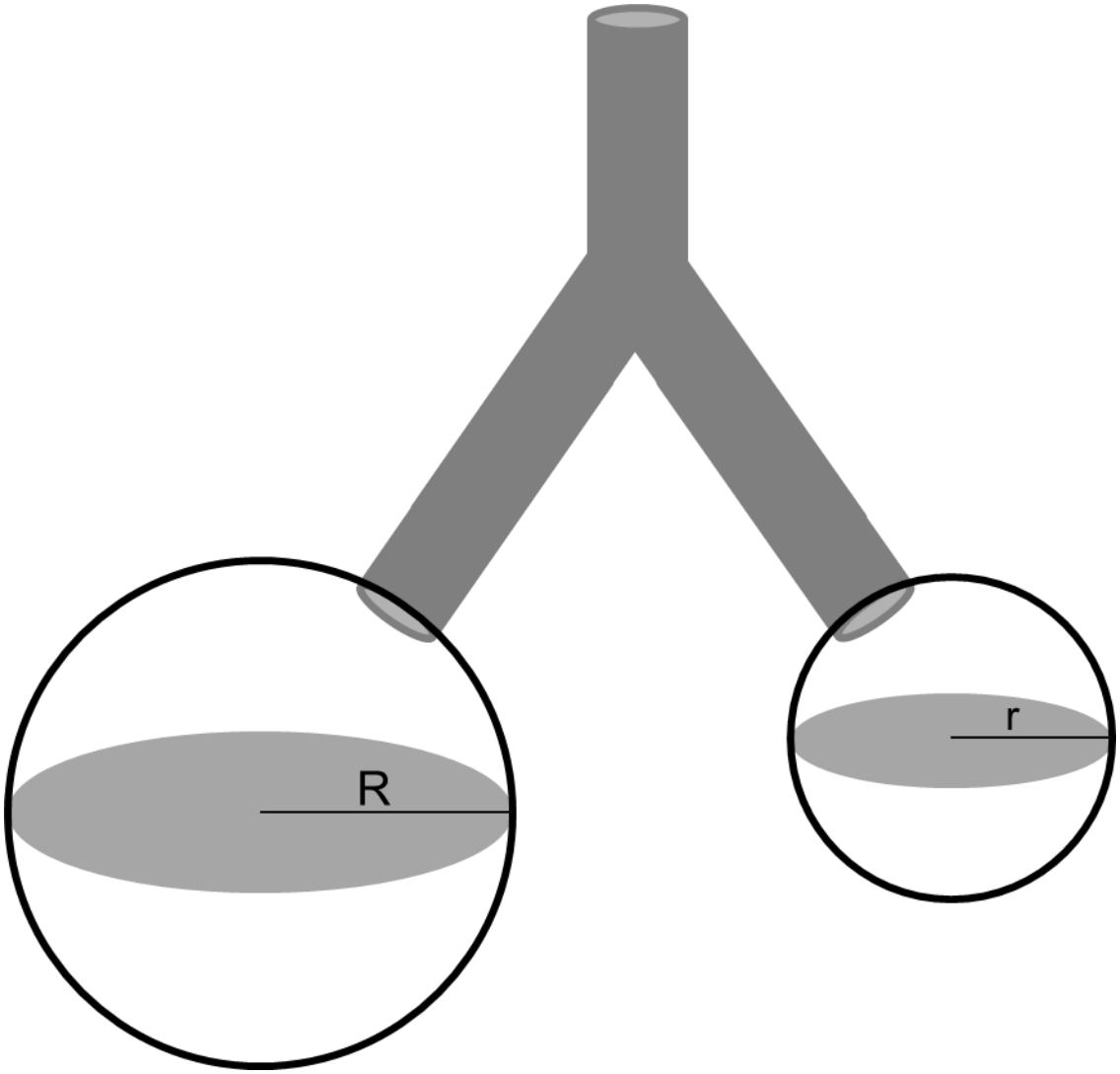

Figure 1-1. The Y-tube model for alveolar inflation showing two bubbles with different radii ($R > r$ and $P_R < P_r$). If only the inner wall has a liquid surface exposed to gas, the pressure (P) is equal to 2 times the surface tension (γ) divided by the radius (r). $P = 2\gamma/r$. Also, bubble r should collapse into bubble R according to this model. Collapse can be prevented if γ also varies with r (*7*). (Adapted from Laplace's Law and the Alveolus: A Misconception of Anatomy and a Misapplication of Physics by Henry D. Prange)

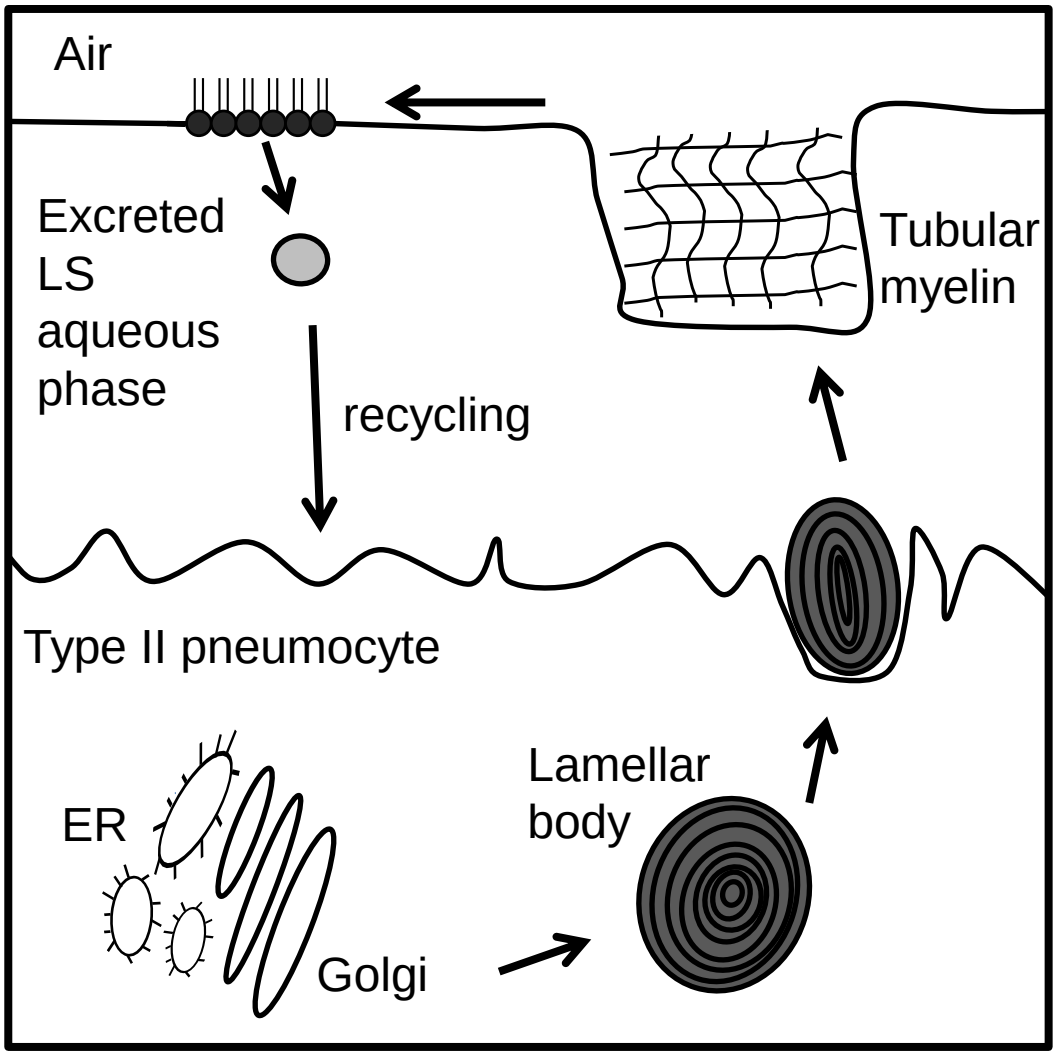

Figure 1-2. The LS cycle in type II alveolar cells. LS is synthesized in the ER, processed through the Golgi, and assembled in lamellar bodies, which are secreted into the alveolar subphase, where they are converted to TM giving rise to the surface film (*49*). (Adapted from Recent Advances in Alveolar Biology: Some New Looks at the Alveolar Interface by Fred Possmayer et al.)

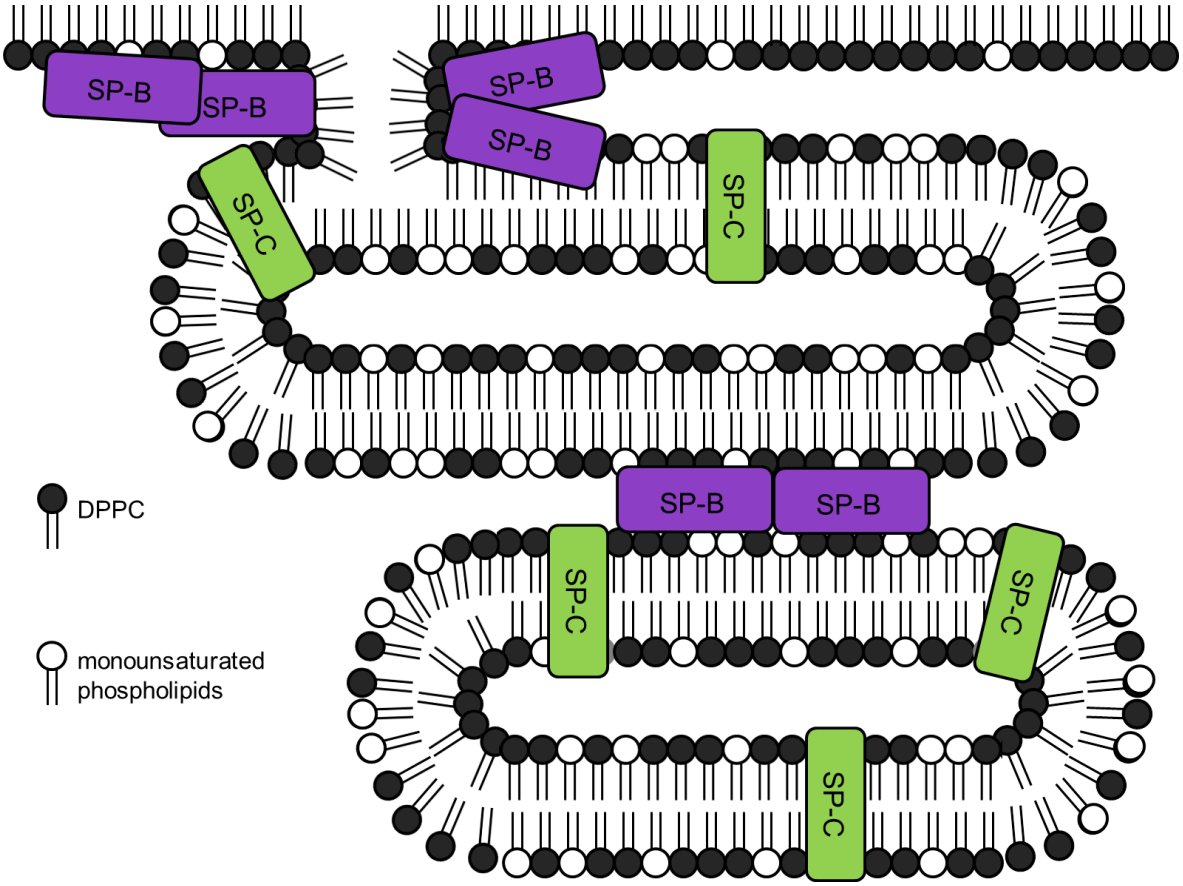

Figure 1-3. Model illustrating lipid trafficking of surface active lipid species to the air/water interface via LS proteins SP-B and SP-C (*50*). The black phospholipid headgroups indicate DPPC lipids and the gray headgroups indicate monounsaturated lipids, mostly POPC. (Adapted from Biochemical and pharmacological differences between preparations of exogenous natural surfactant used to treat Respiratory Distress Syndrome: Role of the different components in an efficient pulmonary surfactant by Odalys Blanco and Jesus Perez-Gil)

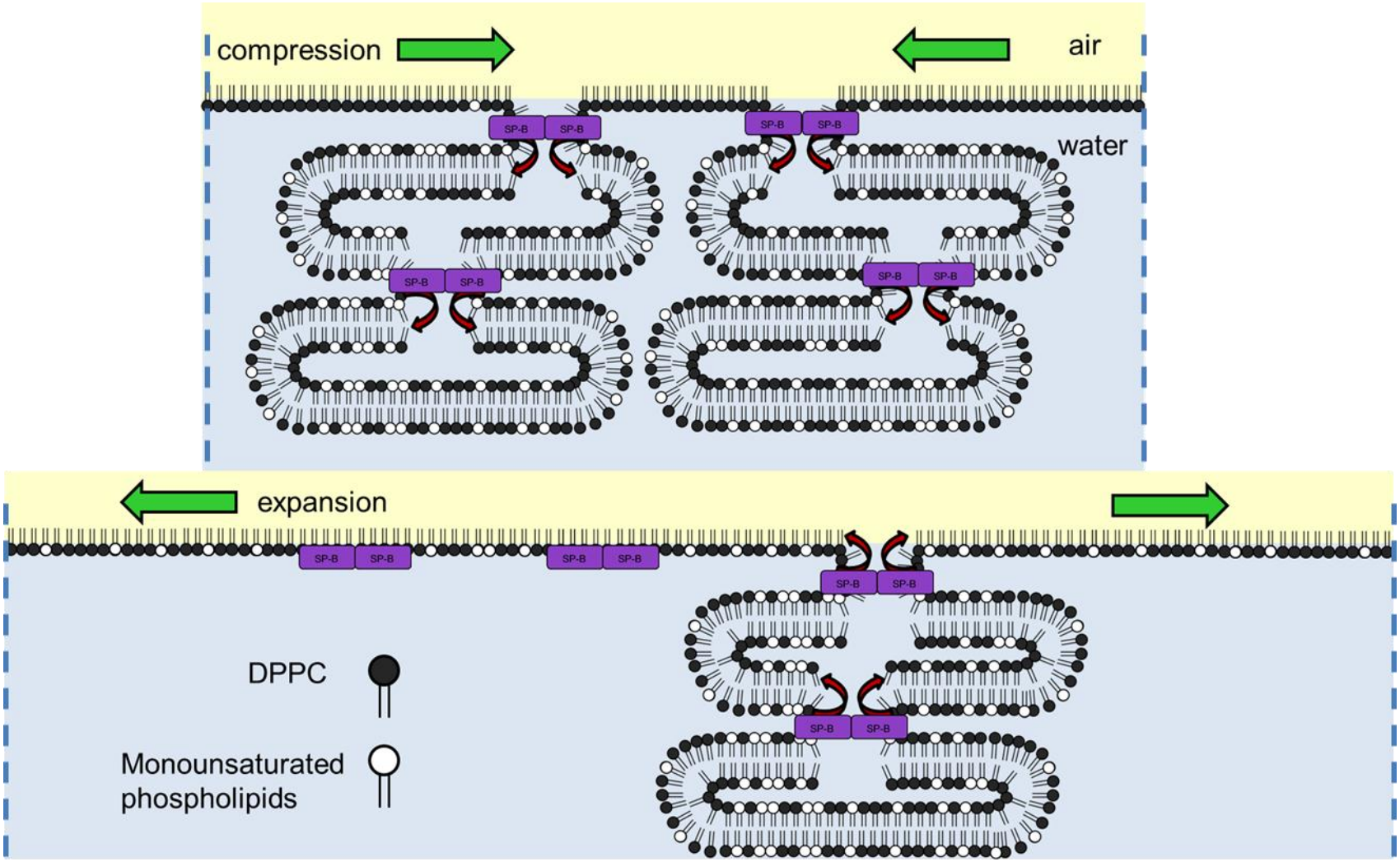

Figure 1-4. Model illustrating the compression and expansion cycle of lung surfactant. The black phospholipid headgroups indicate DPPC lipids and the gray headgroups indicate monounsaturated lipids, mostly POPC. As the lipids are compressed, non-DPPC lipids are thought to be squeezed out into the subphase. During expansion, the air/water interface is comprised of both disaturated and monounsaturated phospholipids.

Table 1-1. Lipid composition of mammalian LS by weight. (Adapted from The role of lipids in pulmonary surfactant by Ruud Veldhuizen et al (*18*))

	Phospholipid composition (% total) [% disaturated]								Cholesterol
	PC	**LPC**	**SM**	**PG**	**PI**	**PS**	**PE**	**LBPA**	**(%chol/PL)**
Mouse	72.3	0	3.3	18.1			1.9		9.7
Rat	82.3 [49.3]	0.3	0.8	7.5 [32.3]	1.8	0.1	5.1	Tr	7.1
Rabbit	80.6 [52.8]	Tr	1.5	7.2 [38.7]	4	1.9	4.4	Tr	
Ovine	81	Tr	1.7	7.9	2.6	Tr	4.8	2	
Bovine	79.2 [49.9]	Tr	Tr	11.3 [33.3]	1.8	Tr	3.5	2.6	3
Human	80.5 [47.7]	Tr	2.7	9.1	2.6	0.9	12.3		7.3

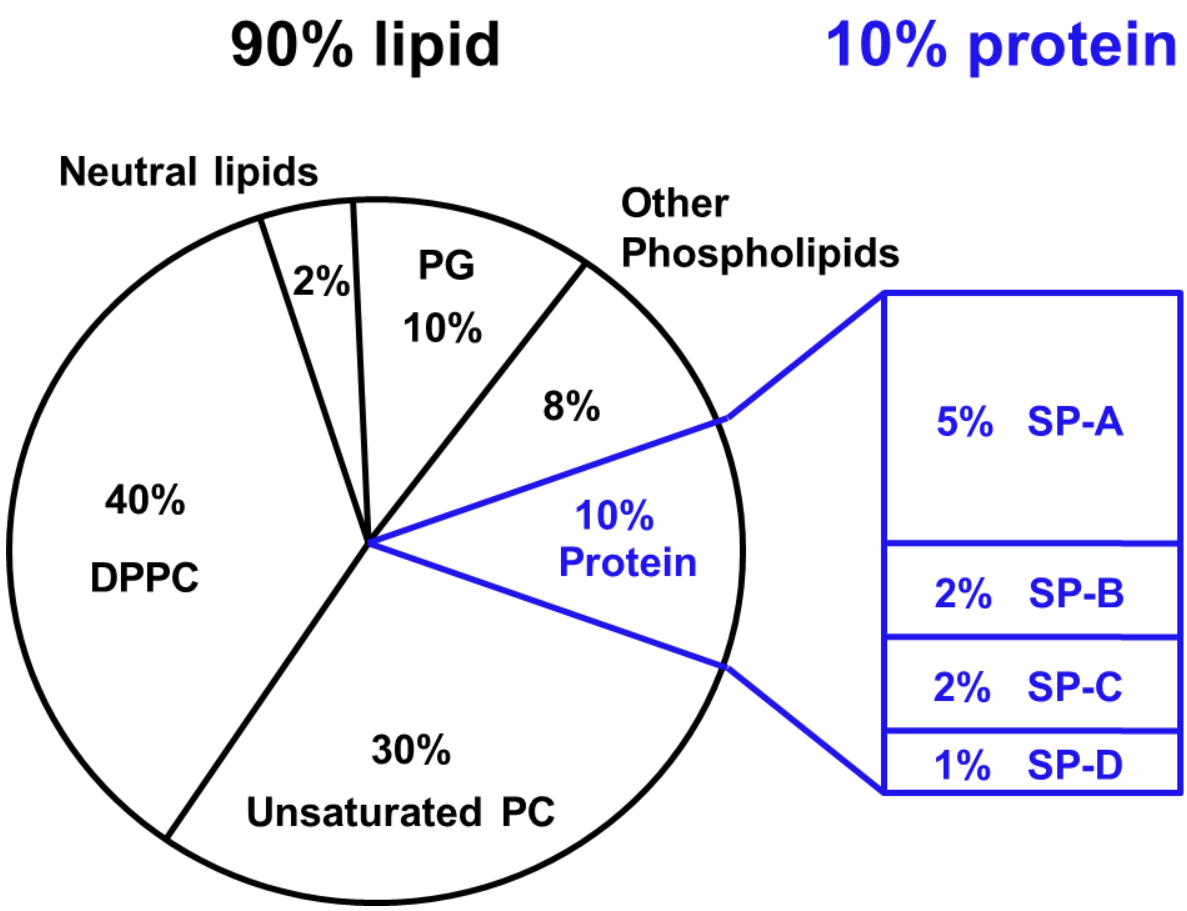

Figure 1-5. Lung surfactant composition. Lung surfactant is comprised of 90% lipid by weight and 10% protein by weight. Most of the lipids are DPPC and unsaturated PCs. The four surfactant proteins, SP-A, SP-B, SP-C, and SP-D, were named in the order they were discovered.

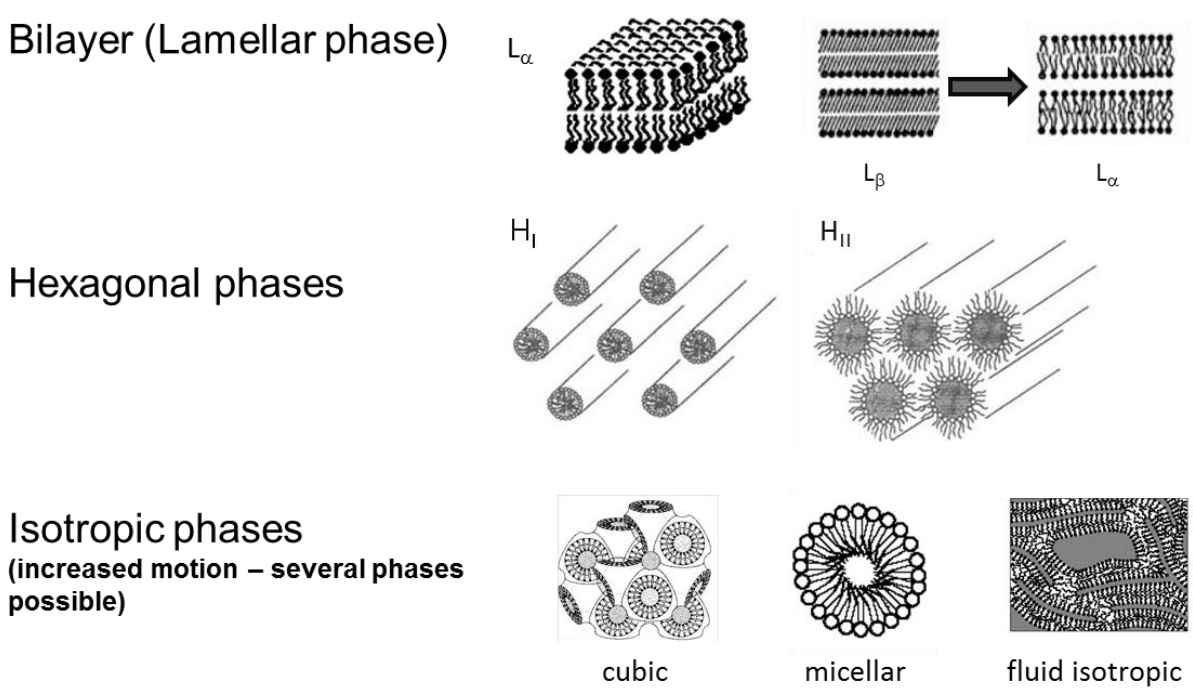

Figure 1-6. Lipid polymorphisms. (*51*) (Adapted from Nonbilayer Phases of Membrane Lipids by Tate et al.)

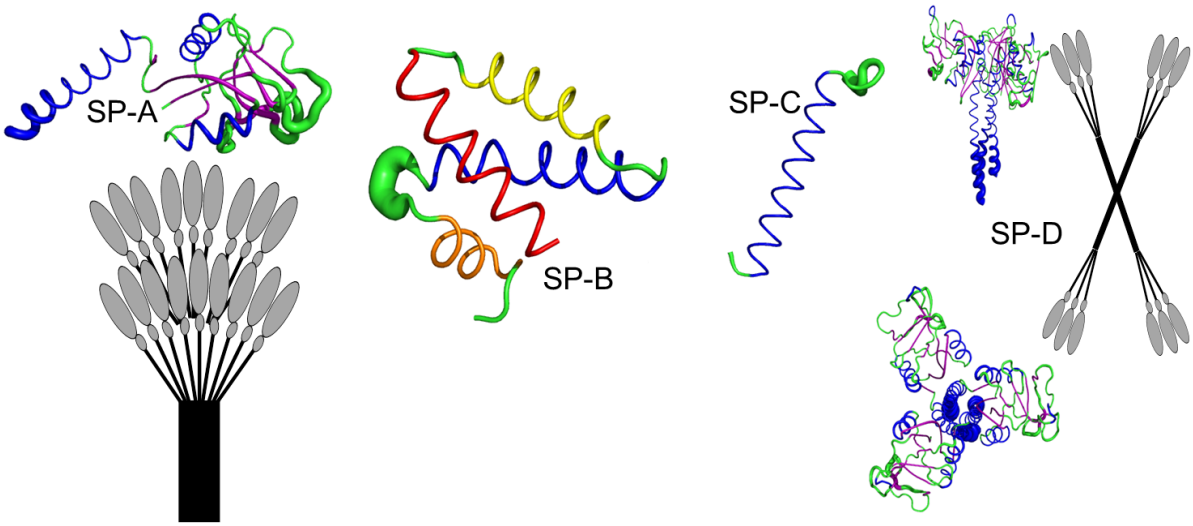

LS Protein	MW (monomer)	AA length (monomer)	Technique	Identifier	Function
SP-A	35 kDa	228	X-ray cryst.	PDB 3PAR	Immune defense/lipid trafficking
SP-B	8.7 kDa	80	Molecular modeling	UniProt P07988	surface tension/lipid trafficking
SP-C	3.7 kDa	35	NMR	PDB 1SPF	surface tension/lipid trafficking
SP-D	43 kDa	355	X-ray cryst.	PDB 3DBZ	Immune defense

Figure 1-7. Lung surfactant proteins. Surfactant protein A (SP-A) and SP-D are both hydrophilic, built of trimers, and play important roles in the immune system. Shown are cartoons of their structures arranged in a bouquet for SP-A. SP-D is a dodecamer complex with crossed helices connecting the trimers. SP-B and SP-C are in the middle and are both small hydrophobic proteins directly involved in lung surfactant function. Only SP-B is essential; humans with genetic SP-B dysfunction die soon after birth, as do genetically engineered SP-B null mice. The SP-B monomer is from molecular modeling based on Saposin A, which is more hydrophilic.

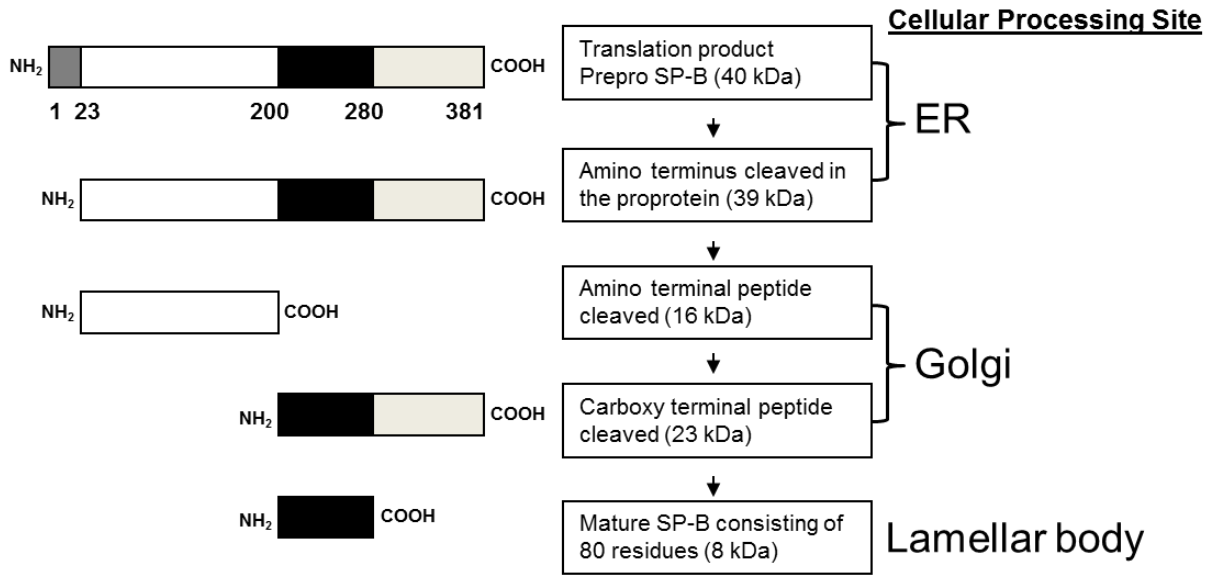

Figure 1-8. Processing steps of SP-B (*52–54*) (Adapted from Surfactant protein B processing in human fetal lung by Susan H. Guttentag et al. and Intracellular Localization of Processing Events in Human Surfactant Protein B Biosynthesis by Annapurna Korimilli et al.)

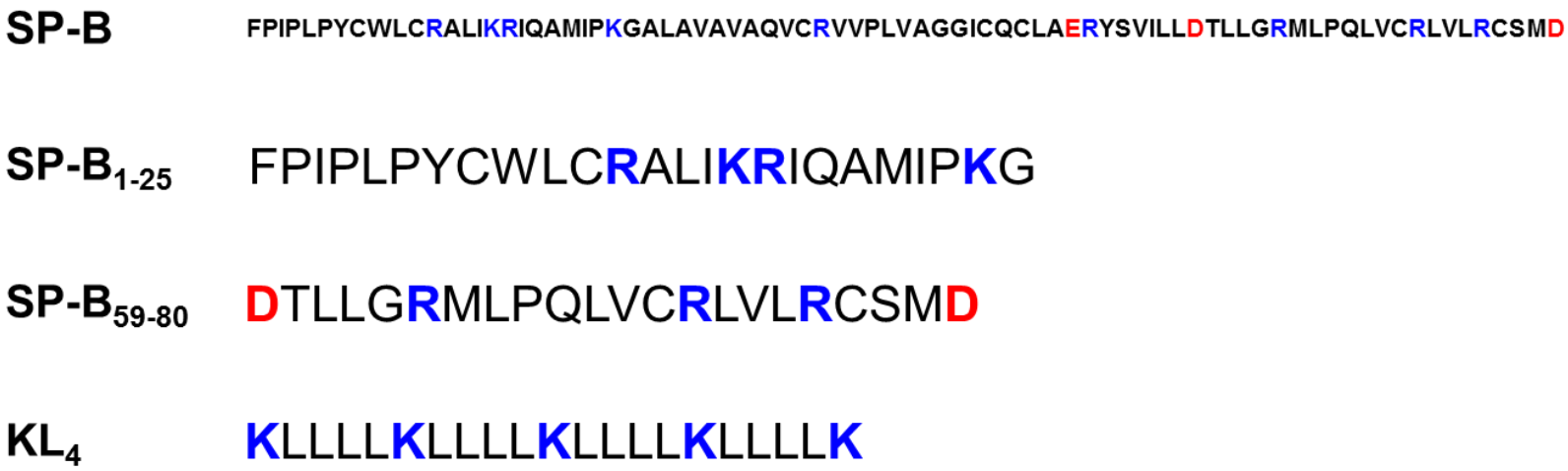

Figure 1-9. Amino acid sequences of SP-B and functionally active peptides

CHAPTER 2
METHODS FOR STUDYING MEMBRANE ACTIVE PEPTIDES AND LIPID POLYMORPHISMS

This chapter provides an overview of the methods used in this dissertation to study lung surfactant (LS) lipids and proteins. The techniques used to study LS can also be used to investigate other membrane protein systems where protein-lipid interactions and lipid dynamics are important.

Differential Scanning Calorimetry

Differential Scanning Calorimetry (DSC) measures the stability of macromolecular interactions by probing their thermotropic phase behavior. Specific physical properties of biomolecules are linked to temperature and the only methods for determining the enthalpy associated with such properties involve calorimetry (*55*). DSC measures the thermal properties of molecules such as the heat consumed or released by samples as a result of changes in their physical state. A common use of DSC is to measure phase transitions of lipids in lipid mixtures and protein-lipid complexes. The stability of proteins can also be studied via DSC by finding the temperature where they denature, although this is more complex for membrane proteins as opposed to soluble proteins. Other biomolecular interactions such as surfactant micellization, nucleic acid melting, and stability of liquid biopharmaceuticals have also been measured via DSC (*56*).

The DSC instrument is a thermal analysis tool that measures the temperature and heat flow associated with phase transitions as a function of time and temperature (*55*). Biomolecular structures are stabilized by weak forces and undergo molecular transitions between conformations or phases when heated or cooled. In a DSC experiment, a sample cell and a reference cell are both heated simultaneously with the temperature in the cells being raised identically over time. The difference in the energy required to

keep the temperature of the sample cell equal to that of the reference cell is the amount of excess heat absorbed during an endothermic process or the heat released during an exothermic process (*55*).

The properties of enthalpy and heat capacity for a given state change can be determined via DSC (*55*, *56*). Changes in heat capacity (C_p) stem from destabilizing the forces that contribute to macromolecular structure such as van der Waals forces, hydrophobicity, electrostatic interactions, and hydrogen bonding. By measuring the molar C_p as a function of temperature, thermodynamic parameters can be monitored. However, DSC actually measures the partial C_p of a sample since the C_p of the solution containing the molecule in question is measured and the C_p of the buffer is subtracted. This is simply the difference in power required to keep both the sample and reference cells at the same temperature at constant pressure which is converted to heat capacity. The partial C_p is graphed vs the sample temperature. The sample can contain any biomolecule such as a protein, tRNA, a protein-DNA complex, a protein-lipid complex, or lipids alone. Other thermodynamic parameters can then be obtained from the DSC thermogram (*55*, *57*).

Heat capacity C_p is obtained from the enthalpy function [$C_p = (\Delta H_{cal}/\Delta T)_p$] and the calorimetric enthalpy ΔH_{cal} can be determined by integrating the thermogram peak

$$\Delta H_{cal} = H(T) - H(T0) \quad (2\text{-}1)$$

$$[H(T) = \int T/T0\ Cp(T)dT + H(T0)] \quad (2\text{-}2)$$

After baseline correction (subtracting the reference), ΔH_{cal} indicates the energy uptake by the sample. Another enthalpy parameter, the van't Hoff enthalpy (ΔH_{VH}), is a measurement of the transition enthalpy as a function of T_m (*57*).

$$\Delta H_{VH} = 4RT_m^2(C_p^{max}/\Delta H_{cal}) \quad (2\text{-}3)$$

R is the universal gas constant and C_p^{max} is the heat capacity measured at the transition peak (Figure 2-1). Furthermore, the above thermodynamic data collected by DSC allows for the transition entropy (ΔS) and the transition-free energy (ΔG) at each temperature to be calculated, but these values are highly variable because of coupling and propagation of errors (*55*).

By comparing the two enthalpy parameters, ΔH_{cal} and ΔH_{VH}, the state of the transition can be evaluated, revealing the cooperative nature of the transition. If ΔH_{cal} and ΔH_{VH} are equal, the transition is a two-state process. If the ratio $\Delta H_{VH}/\Delta H_{cal}$ is less than one, there is intermolecular cooperation; if it is greater than one, there are intermediate transition states. As the temperature is increased, these transitions will be seen depending on the scan rate as they can occur rapidly and may not be detected by the DSC experiment if the relevant temperature range is scanned too quickly.

For my studies, the purpose of the DSC experiment is to reveal lipid phase transition temperatures as the temperature is increased through the melting temperature (T_m) of the lipids. These transitions are thermally induced with a primary transition from an ordered gel state (L_β) to a disordered liquid-crystalline state (L_α) at a specific temperature, which is known as the T_m (Figure 2-2). Above the T_m there is more motion of the lipid acyl chains, or trans-gauche isomerizations, and increased fluidity, or axial diffusion and rotation, as well as deformations of the bilayer. The transition from a gel to a liquid-crystalline state is first-order with a few second-order transition characteristics. A first-order transition is highly cooperative and abrupt with all the lipid molecules experiencing the phase transition at the same time, appearing as a

sharp peak. In second-order transitions the transition is broad and less cooperative with some domain formation in anticipation of thermal change. This is usually seen as a small peak at a lower temperature, a pre-transitional phase, and a broad peak for the main melting transition.

Circular Dichroism

Light is an electromagnetic wave, which is usually unpolarized and propagates in all directions. However, when light waves are polarized their electric vectors lie in the same plane. Furthermore, if the light has two waves in the same plane with equal amplitude differing in phase by 90°, it is circularly polarized light (*58*). The waves of this type of planar polarized light trace the path of a circle over one period of the wave frequency (Figure 2-3). Circular Dichroism (CD) is a technique that uses circularly polarized light and is sensitive to chirality (e.g. molecules lacking a plane of symmetry). A chiral molecule has optical activity when introduced to polarized light because it has the ability to rotate the plane of polarization as the light is passed through the molecule. CD uses the differential absorption of right and left handed circularly polarized light to examine chiral molecules (*59*). A common use of CD is to monitor the secondary structure of proteins in solution, since they are intrinsically chiral due to the chirality of amino acids. The right handed or left handed circularly polarized light differentially excites electronic transitions in the peptide bonds in the Far-UV range (*60*, *61*). The differences in energy absorbed results in both positive and negative absorption in the CD spectrum with different intensities at various wavelengths depending on the secondary structure of the protein.

Secondary structure composition can be determined using Far-UV CD, which covers the wavelength range of 190 to 240 nm. This method can be used to observe how changes in environmental conditions of proteins can affect their secondary structures. The CD signal is mathematically represented as

$$\Delta\varepsilon = \varepsilon_L - \varepsilon_R \quad (2\text{-}4)$$

The CD signal is obtained as ellipticity in units of millidegrees and is normalized according to the protein concentration to yield molar ellipticity m_ε

$$m_\varepsilon = \frac{m\,deg}{\#AA*[M]*l} \quad (2\text{-}5)$$

The number of amino acids in the protein is denoted as #AA, [M] is the molar concentration, m_{deg} is the CD signal in millidegrees, and l is the path length in centimeters of the cuvette (*58*).

Protein secondary structural elements such as α-helix, β-sheet, and turns can be monitored using Far-UV CD data as the various types of secondary structure have characteristic CD lineshapes. The chromaphore for this experiment is the peptide bond and there are energy transitions that occur when it is excited. The lowest energy transition for an α-helix is the n $\rightarrow$ π* transition, which is observed as double minima at ~205 to ~220 nm. Another transition for an α-helix occurs at ~190 nm, which is the p $\rightarrow$ π* transition and is much more intense (*58*, *60*). Other secondary structures will have different transition energetics leading to characteristic lineshapes (Figure 2-4).

Solid State NMR Spectroscopy

Nuclear magnetic resonance (NMR) is a powerful technique used to study the structure and dynamics of molecules. The principle of this method is to measure the absorption and emission of specific radio frequency (rf) waves by the sample when

placed inside a static, homogenous magnetic field (*62*). When the sample is in the magnetic field, its nuclear spins will align with respect to the static magnetic field. When radio frequency waves are introduced, energy is absorbed and the nuclear spins flip from the lower energy state to the higher one, at a matching condition known as resonance. These excited nuclei eventually return to the lower energy level, emitting energy as a result. The energy and time it takes for the spins to return to the lower energy level yields information about the structure and dynamics of the molecules in the sample (*62*).

Those who have experience with NMR most likely are very familiar with solution-state NMR and may not recognize as well the merits of solid-state NMR (ssNMR). In solution-state NMR the molecules in the sample tumble isotropically at rates fast enough to average out anisotropic chemical shifts and dipolar couplings yielding single NMR resonances for chemically equivalent nuclei. During the development of NMR, the fact that these anisotropic interactions were not averaged in solid samples was considered a hindrance. However, anisotropic interactions are now recognized as a valuable source of information. They can be partially averaged by the experimentor using specific ssNMR methods such as Magic Angle Spinning (MAS) ssNMR, but anisotropic interactions can also be retained and observed as they can provide information about the structure, dynamics, and organization of biomolecules in a sample. Particularly, with ssNMR one can obtain orientation dependent information that is lost in solution NMR experiments.

^{31}P Chemical Shift Anisotropy

Phosphorus is a popular probe for studying the structure and dynamics of model and biological lipid membranes as it is almost always present due to the prevalence of

phospholipids. The NMR active isotope of phosphorus, ^{31}P, is 100% naturally abundant, and there is generally only one phosphate group present per lipid (Figure 2-5) (*62*, *63*). Phosphorus-31 has a spin ½ nucleus, which means it is dipolar. Dipolar nuclei are spherical with a uniform charge distribution over their surface, disturbing the external magnetic field independent of direction. This results in a sharp NMR signal in the absence of chemical shielding (*64*). This is in contrast to what is seen for quadrupolar, spin 1 nuclei, described below.

The two anisotropic interactions primarily affecting phosphorus ssNMR spectra are chemical shift anisotropy (CSA) and heteronuclear dipolar couplings to protons. Both contribute to the line broadening seen in 1D ^{31}P ssNMR experiments. The latter is removed with high power proton decoupling and thus the CSA is the dominant interaction typically measured. When a sample is placed in a strong magnetic field, the nuclei of the same NMR-active isotope in different chemical environments resonate at different frequencies as they are experiencing different magnetic fields due to the shielding effect of the surrounding electrons. The characteristic resonance for each nucleus is a result of a reduction of the externally applied magnetic field on the nucleus by the shielding electrons. This is known as the chemical shift and it is measured in units of parts per million (ppm) relative to the external magnetic field. For liquids, the electronic environments of the spins are spatially averaged to yield a single chemical shift for each type of chemical bonding environment. However, for solids the magnitude of the chemical shift depends on the orientation of the molecule with respect to the magnetic field as well as the molecular environment, giving rise to CSA. In other words,

the resonant frequency depends on the orientation of the anisotropic interaction (Figure 2-6).

The anisotropic interaction can be described mathematically by tensors. The static ^{31}P ssNMR lineshape is defined by the shielding tensor and rotation matrices describing the orientation of the molecules with respect to the external magnetic field and the shielding tensor to the molecular frame of reference. There are three principle components of the shielding tensor in its principle axis system, designated σ_{11}, σ_{22}, and σ_{33}. These tensor elements are averaged by molecular motions. Phospholipids in liquid crystalline lipid bilayers undergo fast rotation around the bilayer normal, which is the direction the lipid acyl chains are oriented along. This motion causes the tensor elements to average to an axially symmetric tensor with two unique values oriented in the molecular frame. The resulting tensor has perpendicular ($\sigma_{\perp}$) and parallel (σ_{II}) components which describe the broadened ^{31}P lineshape observed for fluid phospholipid liposomes in a static solid-state NMR experiment. The values of the two tensor elements correspond to the extremes in frequencies of line shape due to the bilayer normal of the lipid membranes being oriented either parallel or perpendicular relative to the external magnetic field. This results in a powder lineshape with a high-field peak and a low-field shoulder and can be described by the difference between the two tensor elements, which is the CSA ($\Delta\sigma$) (*65*). The average tensor is aligned with the bilayer normal and each part of the powder pattern is related to a certain orientation of the bilayer in a spherical liposome to the external magnetic field. The lineshape is affected by both motions (Figure 2-6) and partial orientation of the bilayers in the magnetic field. The more motions that exist the narrower the lineshape compared to

when there are fewer axes of rotation (Figure 2-7). Also, with spherical lipid vesicles there are more perpendicularly oriented lipids than parallel oriented lipids due to the angular distribution of lipids over the sphere relative to the magnetic field axis. The relative probability of orientation, or intensity at a particular frequency, scales with the sine of the angle between the bilayer normal and the external magnetic field (Figure 2-8) (*66*). At high magnetic fields, the plane of the bilayer tends to favor a perpendicular orientation to the magnetic field leading to elongated ellipsoidal liposomes, due to the anisotropy of the magnetic susceptibility of phospholipid molecules being negative (*65*).

^{31}P ssNMR spectroscopy of phospholipids is often used to gather information about lipid polymorphisms as the spectral lineshapes are reflective of the different lipid phases that phospholipids can adopt. The details of the lineshape resonances contain information about lipid orientation with respect to the bilayer normal in lipid bilayers as well as general lipid polymorphisms that can occur if the phospholipid molecules undergo further rearrangement (i.e. out of the plane of the bilayer) under biological and experimental conditions. Different lineshapes are indicative of gel and liquid-crystalline lamellar (bilayer) phases, the inverted hexagonal phase, and isotropic phases such as micellar and cubic phases (Figure 2-9) (*63*). If multiple phases are present, the spectrum will be a superposition of lineshapes. For lamellar phases, the gel phase results in a broad spectrum. When more motion occurs resulting in a liquid-crystalline structure, the lineshape appears narrower than when the sample lipids are in a gel state. ^{31}P spectra of inverted hexagonal phases exhibit a lineshape with reversed asymmetry compared to lamellar phases that is a factor of two narrower. Anisotropic interactions are averaged out in samples with rapid reorientation in three dimensions

(such as micelles and fluid isotropic phases) and their lineshapes are isotropic, single resonances like those seen in solution NMR spectra.

^{2}H Quadrupolar Coupling

^{2}H (deuterium) NMR is another method widely used to study the structure and dynamics of lipid bilayers. In particular, it can be used to study the membrane hydrophobic core of lipid assemblies when the fatty acyl chain protons are replaced with deuterons. Specific lipids can be isotopically enriched allowing one to observe the behavior of a particular lipid in a complex mixture (Figure 2-10). Deuterium has a spin-1 nucleus which leads to a quadrupolar interaction as its shape is not spherical and has an uneven charge distribution. Deuterium is a stable isotope with a natural abundance of 0.02% and it is the second most commonly studied nucleus in lipids by ssNMR (*62*, *67*). There are two quadrupolar spin transitions which results in a doublet of resonances for a specific molecular orientation that are separated by the quadrupolar splitting $\Delta\nu_Q$ (Figure 2-11). The motionally averaged $\Delta\nu_Q$ for each bilayer orientation relative to the magnetic field is represented as follows:

$$\Delta\upsilon_Q = \frac{3}{4}\frac{e^2qQ}{h}(3cos^2\theta - 1)S_{CD} \qquad (2\text{-}6)$$

For saturated C-D bonds, the quadrupolar coupling, $\frac{e^2qQ}{h}$, is 167 kHz in the static limit (*68*, *69*). The static quadrupolar splitting constant (167 kHz) was determined by measuring the splitting values for C-D bonds in several deuterated alkane containing compounds such as ethane and acetonitrile in frozen solids (*69*). Different frequencies arise from the orientational dependence ($3\cos^2\theta$-1) and yield a powder lineshape for liposomes. S_{CD} is the time averaged order parameter for the deuterated labels at each carbon position, which will be described later. The multiple splittings of perdeuterated

lipid acyl chains complicate lipid ^{2}H spectra due to line broadening and overlapping peaks from the different labeled positions having different order parameters. As discussed for the ^{31}P CSA above, at each deuterated position the frequency for the 90° orientation of the bilayer normal is more intense than the 0° shoulder due to their relative probabilities and a broad lineshape is observed due to the many possible orientations for the phospholipid vesicles from perpendicular (90°) to parallel (0°) (*70*).

The spectrum obtained for a chain-perdeuterated lipid molecule is complex since it contains the contribution of every deuteron along the deuterated acyl chain(s). Each pair of deuterons at a particular carbon has a specific quadrupolar splitting and the powder spectrum is a superposition of their powder spectra. As the quadrupolar splitting decreases, the acyl chain order decreases and vice versa. In other words, the more motion at a specific acyl carbon the narrower the lineshape becomes and the two peaks for a particular bilayer orientation separated by the quadrupolar splitting will be closer together (Figure 2-12). Once $\Delta\nu_Q$ is determined for each particular methylene group, the S_{CD} values can be calculated and plotted against the carbon number of the acyl chain from 2 to 16 to show an increase or decrease in order in comparing various lipid samples. The deuterons at the16 carbon position on the deuterated acyl chain will naturally have more motion due to their distal position and fast rotation of the methyl group leading to the lowest order parameter observed for acyl-chain deuterated lipids (Figure 2-13). It will also have 1.5 times the signal of other positions due to the additional deuteron. However, assigning specific frequencies to each peak in the ^{2}H lineshape is quite difficult to do with any degree of accuracy without deconvoluting the spectra. The process used to do this is known as dePaking, described below, and it

transforms complicated, broad lineshapes to individual frequencies. This allows order parameters to be calculated using more accurate splitting values.

As a further complication, a lipid in which both acyl chains are perdeuterated will not always have the same order parameters in both chains for a specific carbon position. DPPC has been shown to possess a different order parameter for the carbon at the second position on the acyl chains. One splitting was measured for the C2 position on the sn-1 chain and two splittings for the same position on the sn-2 chain. This is because the beginning of the sn-1 chain is oriented more perpendicular to the plane of the bilayer, and the beginning of the sn-2 chain is more parallel (*62*). Nevertheless, the order parameters of the C-D bonds, S_{CD}, along the two deuterated acyl chains can be evaluated from the quadrupolar splitting relationship in Equation 2-6. The S_{CD} can be assigned for each C-D bond along the deuterated acyl chain(s) based on prior work with specifically deuterated samples (*71*, *72*). The frequencies for each peak are assigned and converted to order parameters (S_{CD}) using the quadrupolar splitting relationship and then they are used to generate order parameter profiles (Figure 2-14). The internal motions of the phospholipids are reflected in the order parameters obtained for each C-D bond. While order parameters reveal information about the motion in lipid acyl chains, the nature of these motions is not completely definable from ^{2}H NMR spectra alone (*62*). Nevertheless, motion in general is the dynamical property being probed when utilizing static ^{2}H ssNMR to study lipid membranes and the deuterated lipids enable one to “see” what is occurring at the molecular level in a biologically relevant environment when particular variables are

introduced such as proteins. As the lineshapes change with variable temperatures, one can also see when the lipids melt (phase behavior).

Of specific importance to LS, proteins interacting with the lipids in a sample can change the deuterated lipid's dynamics and assembly, causing visible spectral changes allowing one to draw conclusions about the system being studied. Qualitative information can be obtained from ^{2}H static ssNMR data without deconvoluting it any further. However, for a quantitative analysis with more accurate frequency readings, a dePaking analysis is performed when possible. Lipids deuterated either on one or both acyl chains allows for the study of the structure and dynamics of their plateau and tail regions (*63*). The lipid dynamic information can also be useful for inferring relative protein insertion depth. Phase or structure information can be obtained from non-dePaked spectra, but insertion depth requires more precise frequency assignments that are only gathered from deconvoluting the broad powder lineshapes.

DePaking

DePaking transforms a broad NMR lineshape consisting of overlapping Pake powder patterns into one where individual frequencies can be assigned more easily. This procedure generates an "oriented" spectrum from an unoriented sample (*73*). The resonances may still be somewhat broad, but overall the peaks are sharper, better resolved, and more easily assigned (Figure 2-15). This higher resolution data are then used to make more quantitative measurements.

^{31}P and ^{2}H solid state ssNMR interactions are governed by second order tensors (*74*). Second order tensors are normally referred to as "tensors" as 0^{th} and 1^{st} order tensors are actually scalars and vectors, respectively. Tensors have 9 quantities, meaning they are represented by a 3 x 3 matrix. In the nuclear reference frame this

tensor is diagonal and the eigenvalues (the diagonal components) are the quantities known as the tensor principal values. In ssNMR σ_{11}, σ_{22}, and σ_{33} correspond to the principal components of the anisotropic interactions seen in ^{31}P and ^{2}H static ssNMR in the nuclear reference frame.

Lipid molecular motions in the liquid crystalline state render the ssNMR interactions axially symmetric or symmetric with respect to one axis (i.e. $\sigma_{22} = \sigma_{33}$), aligned with the bilayer normal, and the strength of these second rank tensor interactions is dependent on the average orientation of the nucleus of interest relative to the axis of motion (*74*, *75*). Since the molecular motions are anisotropic there is incomplete averaging of the tensor interactions, such as the CSA, dipole-dipole, and quadrupolar interactions, particularly for membrane bilayers where there is little change in the average orientation of the molecules relative to the bilayer normal (*76*). In a sample containing randomly oriented bilayers (i.e. MLVs or LUVs) the mentioned interactions have a spatial dependent component, $3\cos^2\theta$-1, where θ is the angle between the external static magnetic field and the bilayer normal. The spatial component can also be represented in the form of a second order Legendre polynomial:

$$P_2(cos\theta) = \frac{1}{2}(3cos^2\theta - 1) \qquad (2\text{-}7)$$

With this equation, the spatial component varies between 1 and -1/2 (i.e. θ = 0° to 90°). If θ is set to the magic angle, 54.7°, $P_2(\cos\theta) = 0$ and the anisotropic component of NMR interactions (CSA, dipole-dipole, quadrupolar) disappear because the spatial dependence is equal to zero. The spatial dependence of the molecular interactions broadens the resonances in unoriented samples and decreases resolution leading to spectra which are broad superpositions from all the contributions of the possible

orientations of the long axis of the lipid molecules in the sample from 0° to 90° with respect to the external magnetic field, B_0. One solution is to orient lipid bilayers, but for many samples this is not feasible.

To retain orientation information which is important for distinguishing between lipid polymorphisms in the sample and at the same time restore resolution, the orientational distribution for the NMR interactions and the anisotropies that define their strengths need to be separated. The original powder (broad) spectrum can be described by the following two equations (*75*):

$$S(\omega) = \int g(x)\left[\rho(\theta)\frac{\partial\theta}{\partial\omega}\right]dx,\ \theta = \theta(x,\omega)$$

or

$$= \int p(\theta)\left[p(x)\frac{\partial x}{\partial\omega}\right]d\theta,\ x = x(\theta,\omega) \qquad (2\text{-}8)$$

where g(x) is the anisotropy distribution function and p(θ) is the orientation distribution function. The first equation, g(x), is a lineshape function for each anisotropy, such as for a single ^{31}P CSA in a pure phospholipid sample. The second equation, p(θ), is a superposition of spectra from the individual oriented spectra of a powder pattern; there is one orientation distribution function for each orientation, θ.

In a truly random orientation distribution $p(\theta) \propto \sin\theta$. Different ways of dePaking have been used, which are to extract g(x) when p(θ) is known or the opposite where g(x) is known and p(θ) is calculated from the measured data. The latter form of dePaking is possible because of the symmetric relationship between g(x) and p(θ).

For the work in this dissertation dePaking of NMR data was accomplished with previously published algorithms which simultaneously dePake and determine

macroscopic ordering in partially aligned lipid spectra using Tikonov regularization (*75*, *77*). ^{31}P NMR spectra were referenced to phosphate buffer prior to dePaking and dePaked spectra were quantitated by fitting the two peaks with Lorentzian line shapes**.** Assignments of ^{2}H resonances were made based on Petrache, *et al.* (*78*).

If the bilayers adopt random orientations with respect to the magnetic field, the resulting spectra of perdeuterated lipid acyl chains are a superposition of axially symmetric powder patterns, arising from each deuterated position, whose intensities follow the well-established distribution function $p(\theta) \propto \sin(\theta)$ where θ is the angle between the bilayer normal and the magnetic field. The spectra can be deconvoluted using a standard inversion (dePaking) procedure (*77*). For samples in which the lipid bilayers align to some degree in the magnetic field, assuming the magnetic field leads to an ellipsoidal deformation of the MLVs, the probability distribution function becomes (*75*):

$$p_{\varepsilon}(\theta) \propto \sin\theta\,[1-(1-\kappa_{\varepsilon})cos^{2}\theta]^{-2} \qquad (2\text{-}9)$$

where κ_{ε} is the square of the ratio of the long to short axes of the ellipsoids. If κ_{ε} is equal to 1 the lipid vesicle is a sphere. If this value is high the shape is cylindrical with its axis along the external magnetic field. Deconvolution is accomplished using an iterative procedure which simultaneously determines κ_{ε} and dePakes the spectrum. Since our lipid samples showed some degree of alignment in the magnetic field, the latter procedure was utilized. Both ^{31}P and ^{2}H experiments exhibited the same degree of distortion as evidenced by comparable kappa values, further supporting our interpretation that distortion of the lineshapes can be attributed to alignment of the lipids rather than experimental differences (i.e. Bloch decay vs. echo experiments).

Dynamic Light Scattering

Dynamic light scattering (DLS) is a technique used to probe particle size by measuring the diameter of molecular assemblies in solution as they interact with light. DLS is also sometimes referred to as photon correlation spectroscopy (PCS) or quasi-elastic light scattering (QELS) (*79*, *80*). During a DLS experiment, Brownian motion is measured, which is associated with the size of the particles in the sample (Figure 2-16). Brownian motion is random movement of particles in a solution as they collide with the thermally driven solvent molecules surrounding them (*79*). Large particles will have slow Brownian motion, while small particles have more rapid movement due to the force exerted when they hit heavier solvent molecules (*80*). The DLS experiments in this dissertation were used to measure the size of lipid vesicles with various molar concentrations of a peptide at physiologic temperature.

In a DLS experiment, it is important to know the temperature as DLS depends on the viscosity of the solution and viscosity is related to temperature. It is also imperative that the temperature is stable to avoid convection currents in the sample. Convection currents can cause non-random movements, ruining size measurements of the particles as the random motions are linked to particle size in DLS data interpretation (*80*).

The Stokes-Einstein equation (Equation 2-10) is used to determine the hydrodynamic diameter (d(H)) of the particles in a sample from the translational diffusion coefficient (D), which describes the velocity of the Brownian motion.

$$d(H) = \frac{kT}{3\pi\eta D} \tag{2-10}$$

The hydrodynamic diameter is represented as d(H) where, D is the translational diffusion coefficient, k is Boltzmann's constant, T is absolute temperature, and η is

viscosity (*80*). The diameter measured by DLS assumes a spherical shape with the same translational diffusion coefficient as a solid particle, but in reality it depends on other factors in addition to size. Ionic strength, surface structure, and existence of non-spherical particles can all affect the diffusion speed of the particles and thus the measured diameter. In particular, the ionic strength of the medium can affect diffusion speed if the conductivity is too low or too high. Low conductivity promotes extra layers of ions around the particle artificially reducing diffusion speed and high conductivity results in the opposite effect with a smaller apparent diameter. Changes in surface structure such as binding to polymers or conformational changes affect diffusion speed as well, and non-spherical particles can give less accurate results as the Stokes-Einstein equation assumes a spherical shape (*80*). DLS is applicable to a wide range of systems as it can measure the size of particles from ~ 2 nm to ~ 6 μm.

Transmission Electron Microscopy

Transmission electron microscopy (TEM) provides information about the topography (surface features) of a sample and particle morphology (shape and size) by sending a beam of electrons through the sample and monitoring the effects the sample has on the transmitted electrons (*81*). The electron intensity distribution is focused with electromagnetic lenses and the image is viewed on a fluorescent screen or recorded on film or a digital CCD camera (*82*). TEM is another technique that enables observation and characterization of materials on the nm to μm scale (*81*)

During a TEM experiment, current heats up a pin-shaped cathode producing a ray of electrons. These electrons are taken up in a vacuum by the anode's high voltage. Basically, this means a stream of electrons is formed in a vacuum by an electron gun.

Then the stream of electrons is accelerated toward the sample by a positive electrical potential. The electron beam is focused onto the sample by magnetic lenses as a monochromatic beam. The voltage is usually between 100 and 200 kV during acceleration (*83*). When the beam irradiates the sample, interactions occur within the sample which affect the transmitted electron beam, and these effects are detected to form an image (*81*). High voltage results in shorter electron waves and better resolution. However, resolution for TEM is usually only limited by lens quality and sample preparation (*83*, *84*).

There are three types of effects on the electron beam from interacting with the sample, which result in unscattered, elastically scattered, and inelastically scattered electrons. The beam of unscattered electrons is called transmitted because it goes through the sample without interacting with it – this is what is detected in TEM. A thicker area of sample will have fewer transmitted electrons and will have a dark appearance. Other electrons are scattered either elastically by atoms in the sample without a loss of energy or inelastically with a loss of energy. The inelastic collisions can disrupt molecules in the sample by forming free radicals and reactive ions (*83*). All incident electrons hit the sample with the same energy and wavelength and follow Bragg's Law (*81*).

Sample preparation is key for TEM experiments as biomolecules have weak contrast due to their atomic composition, which consists of elements with mostly low atomic numbers (C, H, N, O) that scatter electrons weakly. The samples require a stain to enhance the chemical composition with heavy metals with high atomic numbers (such as lead or uranium) to enhance contrast. The TEM experiments conducted for

this dissertation took advantage of negative staining techniques to prepare lipid vesicles to enhance electron absorption or scattering. The stain aids in absorbing or scattering electrons as the electron beam is projected onto the sample. Also, it is generally unfeasible to study living objects with TEM as the sample is almost completely destroyed by preparation and high temperature from electron absorption. In chapter 3 the use of TEM will be discussed as a tool used to monitor the morphology of lipid vesicles in the presence or absence of a peptide. This experiment was used to shine a light on possible lipid polymorphisms occurring within a particular lung surfactant replacement composition.

Synthesis of Peptides

The experiments in my dissertation utilized peptide sequences of 25 amino acids in length that were prepared synthetically and purified before reconstitution with model lung surfactant lipids and CLSE. SP-B_{1-25} is the synthetic peptide used throughout this dissertation (see Chapter 1 for details about SP-B_{1-25}). The primary accepted method of peptide synthesis is solid phase peptide synthesis (SPPS). This technique allows for the synthesis of natural peptides that are difficult to express in media or even the incorporation of unnatural amino acids, such as isotopically enriched residues.

The main objective in SPPS is to couple the C-terminus of one amino acid to the N-terminus of another amino acid until you have the desired peptide sequence. Peptide chains are built on small, insoluble resin beads with (covalently attached) linkers or supports, keeping the peptide immobilized and intact on the solid phase during filtration and washing away of by-products from the organic reactions. The processes of coupling new amino acids, washing away reactant, deprotecting the end of the growing peptide chain, and washing again are cycled as the peptide chain elongates one

residue at a time, with this growing chain remaining covalently attached to the insoluble resin (*85*, *86*).

Fluorenylmethyloxycarbonyl (Fmoc) protection was used during SPPS of the peptides in this dissertation. Protecting groups are used because of the possibility of adverse reactions occurring during synthesis (*85*). The Fmoc group protects the α-amino group and resin-linkage agents. The side chains are also protected as they commonly contain reactive functional groups. The steps of Fmoc SPPS can be summarized as follows (*85*, *86*):

1. The Fmoc protected amino acid is attached to the resin via a linker.
2. The Fmoc protecting group is removed (usually with piperidine in dimethylformamide (DMF)), deprotecting the residue.
3. The next Fmoc protected amino acid is coupled to the amino acid linker support.
4. The deprotection/coupling cycle is repeated to yield the desired amino acid sequence.
5. The linker/resin support and side-chain protecting groups are cleaved with TFA, yielding a free peptide. Then the peptide is purified with HPLC.

The prominent features of the above SPPS reaction steps are outlined in Figure 2-17.

Gel Permeation Chromatography

Gel permeation chromatography (GPC) was used as a preparative technique to separate the hydrophobic components of a protein-lipid mixture in an organic solvent. GPC is a type of size-exclusion chromatography as it separates sample components based on size; the term GPC is used when organic solvents that cause polymer beads to swell are used as the mobile phase. Nevertheless, the separation process is the same no matter what type of solvent is used (*87*). A column tightly packed with small porous polymer beads of different sizes is used as the stationary phase. Sephadex is a

common gel for GPC stationary phases. The smaller molecules enter the pores while the larger ones do not and thus elute faster. The mobile phase is an organic solvent and should be the same or similar to the sample solvent, such as methanol and/or chloroform (*87*, *88*). Various assays can be done afterwards to determine the contents of the eluent fractions.

For the experiments in this dissertation, proteins and lipids were separated with the large proteins coming off the column first. A rudimentary GPC setup was used for these experiments (Figure 2-18). A gravity column packed with Sephadex beads and hydrated with methanol and chloroform was utilized. The column was packed under pressure from a nitrogen gas cylinder, which was also introduced to the column throughout the separation process to push the mobile phase through.

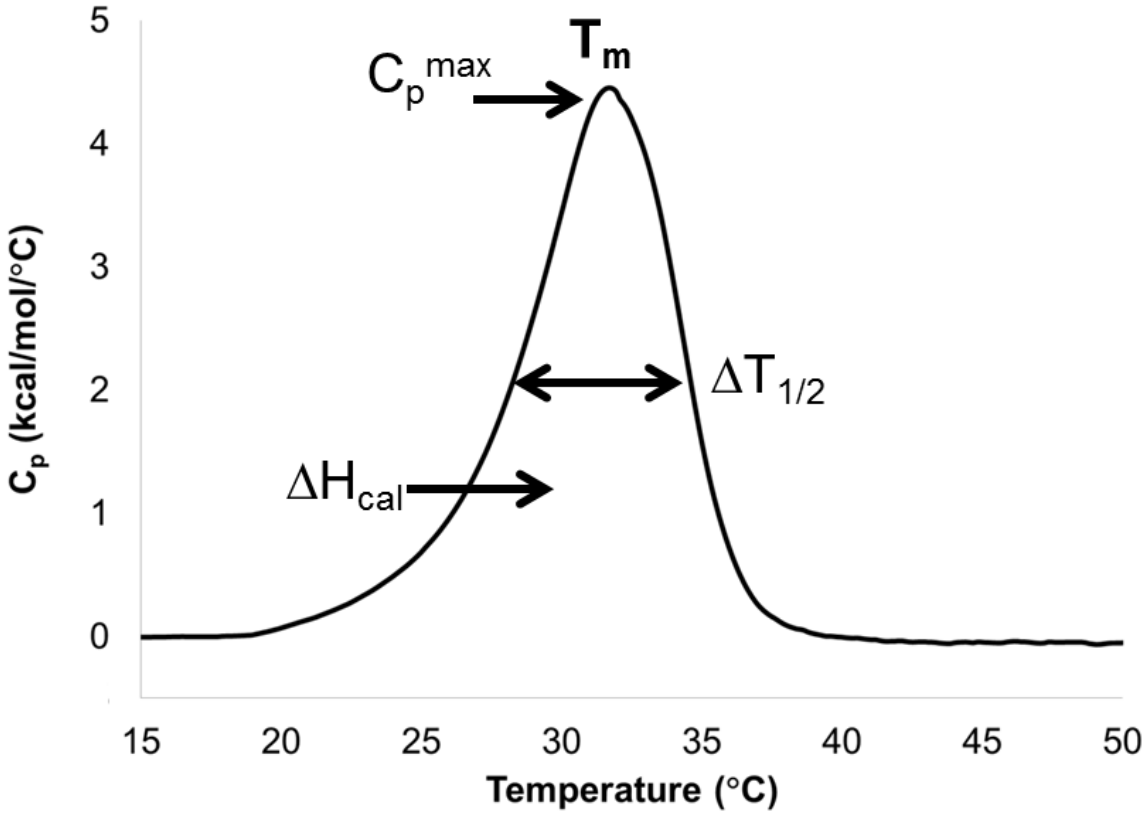

Figure 2-1. DSC thermogram showing the melting of 4:1 DPPC/POPG large unilamellar vesicles (LUVs). The phase transition (T_m) is at ~32°C, the C_p^{max}. $\Delta T_{1/2}$ measures how broad the transition is, and ΔH_{cal} is determined by integrating the peak.

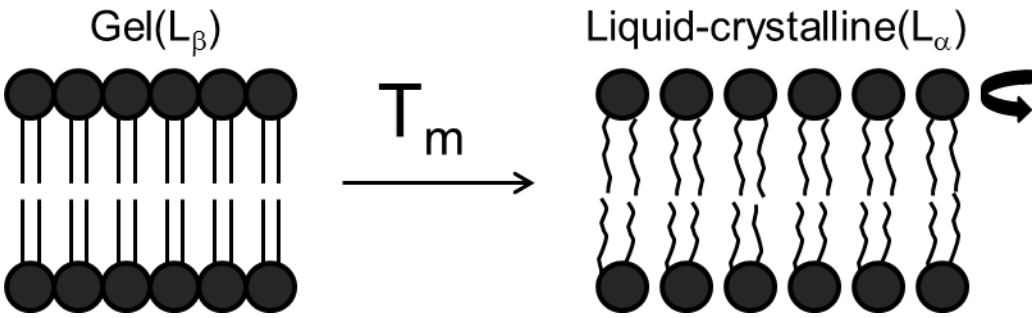

Figure 2-2. Illustration of the gel to liquid-crystalline phase transition. Above the T_m, phospholipids acquire more degrees of freedom as they melt and have more motions associated with their acyl chains, including greater axial rotation.

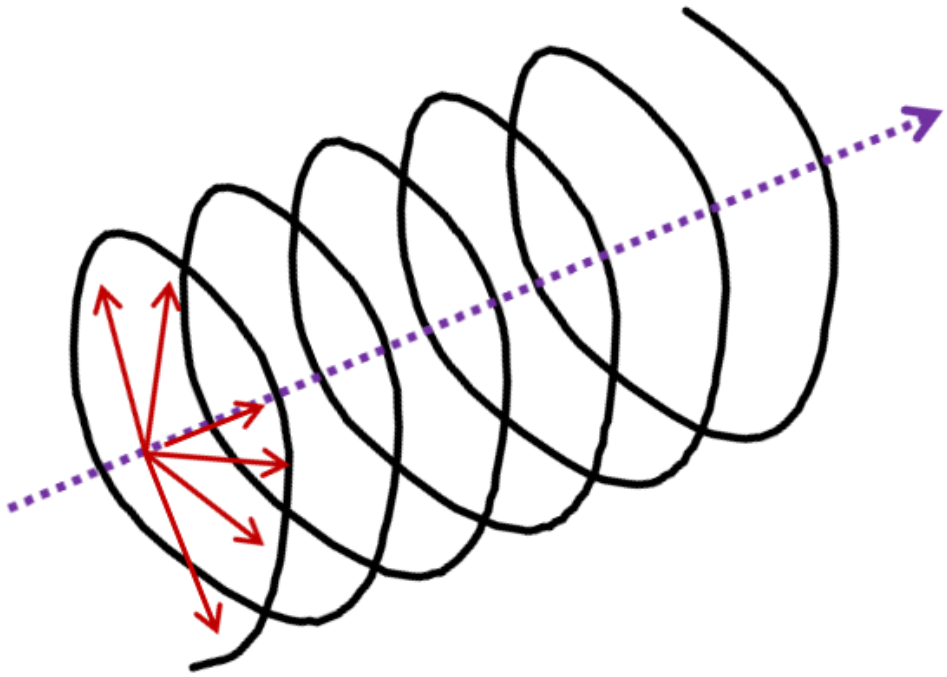

Figure 2-3. Circularly polarized light. Figure made with ACD/ChemSketch program

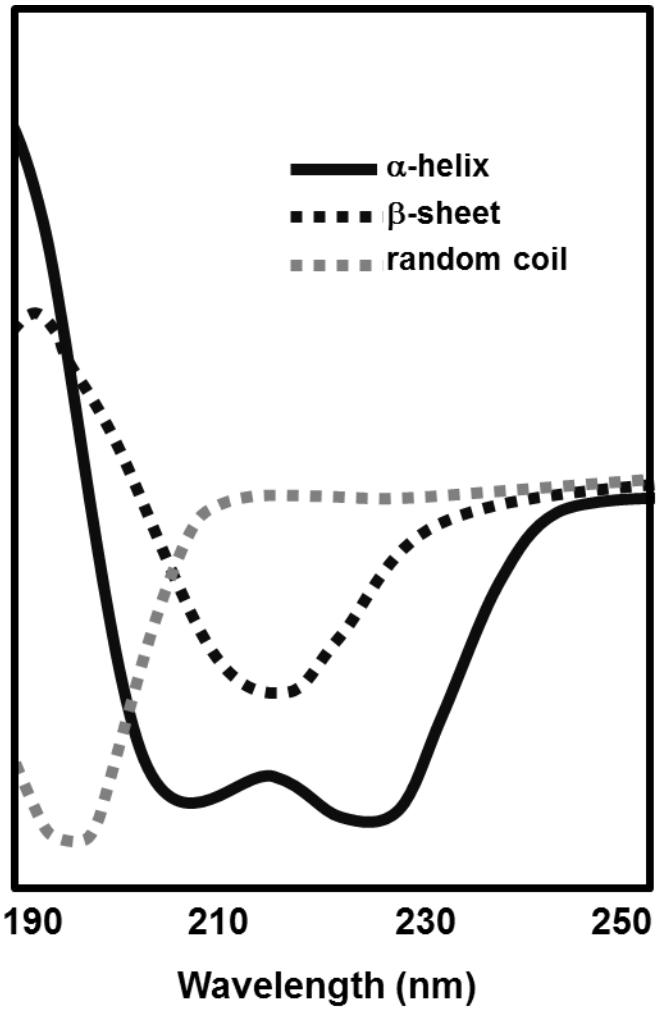

Figure 2-4. CD spectra of different secondary structures. Adapted from figure by Omjoy K. Ganesh.

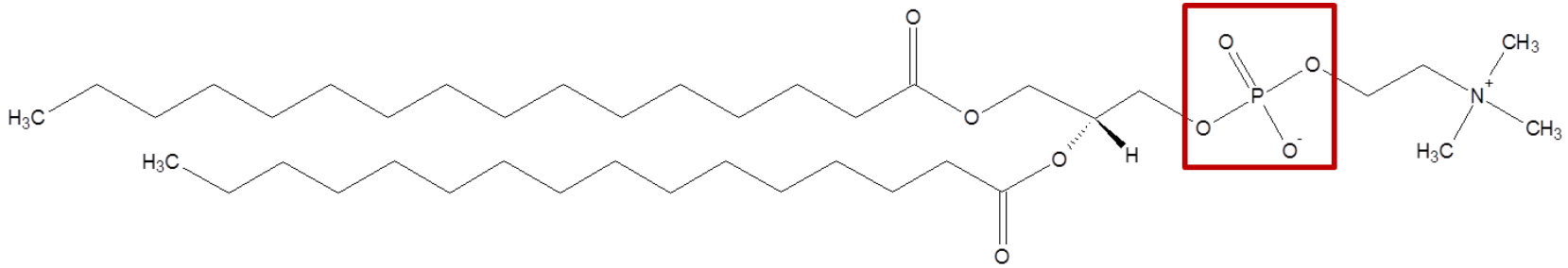

Figure 2-5. Phospholipid with phosphorus atom highlighted. Figure made with ACD/ChemSketch program

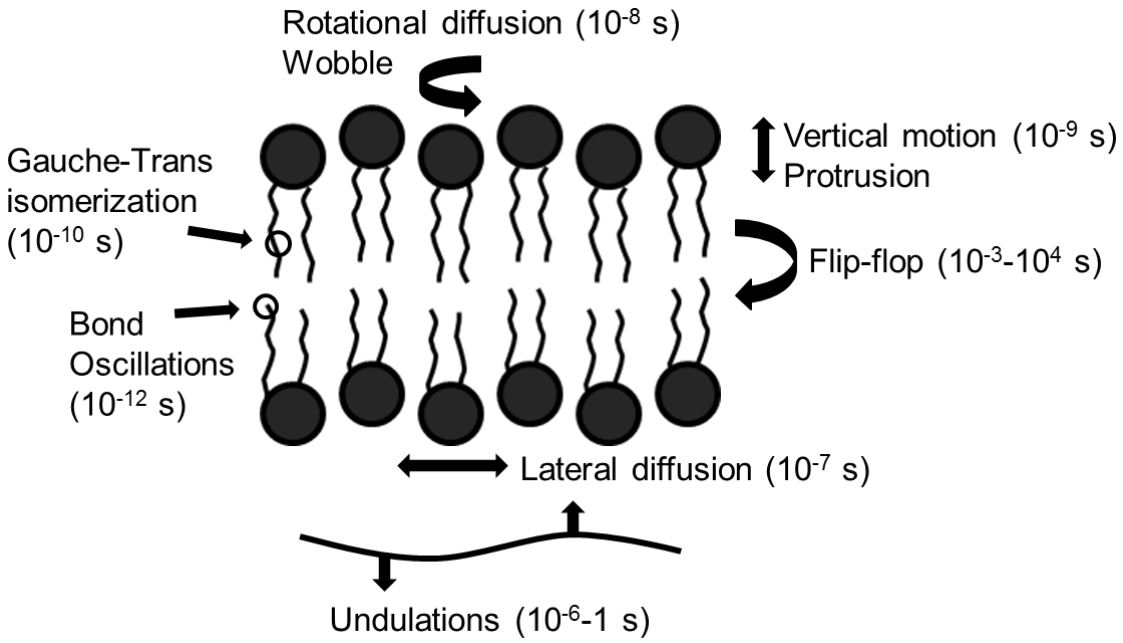

Figure 2-6. Dynamics in a lipid bilayer. Lipids have motions that are NMR sensitive and these are the timescales of the motions. Gauche-trans isomerizations (rotations about chemical bonds), bond oscillations, and lipid flip-flop are some of the motions that are focused on more in lipid dynamics studies of deuterated acyl chains.

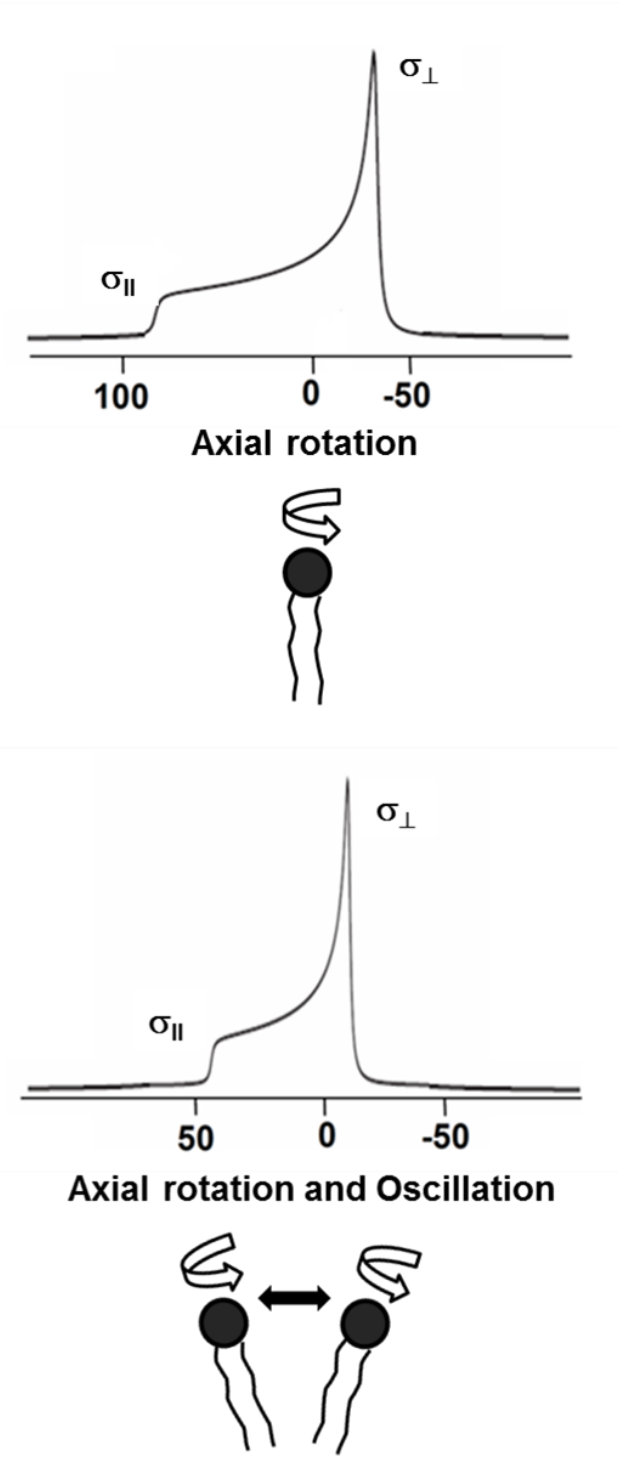

Figure 2-7. Effects of lipid motions on ^{31}P lineshapes. Additional motions cause further averaging and narrowing of the lineshape.

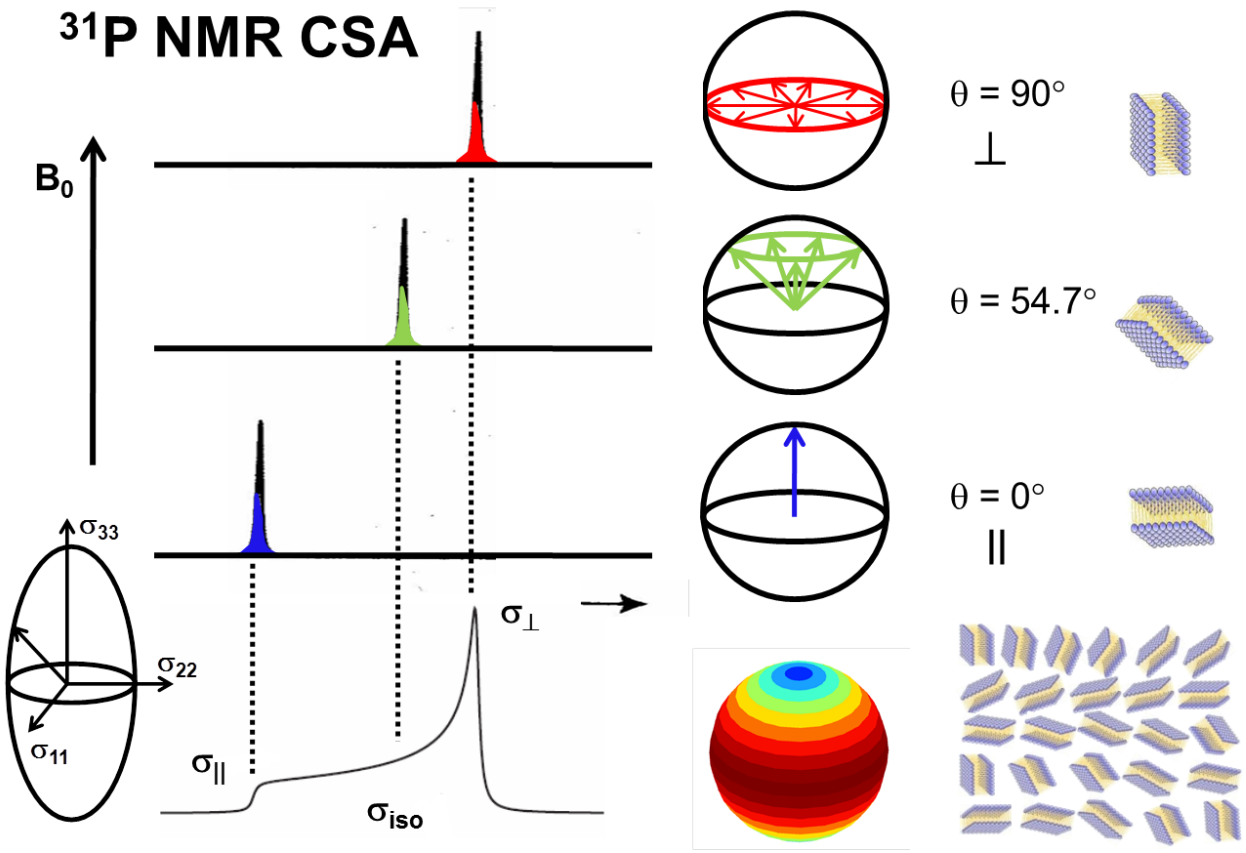

Figure 2-8. Chemical shift anisotropy. The CSA interaction results in a powder pattern due to the distribution of populations of orientations the lipid bilayers adopt. The CSA is defined by a tensor with elements α_{11}, α_{22}, and α_{33} in lipid bilayers that are time averaged to $\alpha_{\perp}$ and $\alpha_{||}$. This is because the average tensor is oriented with respect to the bilayer normal. With ssNMR you can obtain orientation information that is lost in solution NMR. Each part of the powder pattern is related to a certain orientation of the bilayer and each orientation leads to a different frequency. With spherical vesicles you have more perpendicular than parallel orientations. This is illustrated by the colored spheres showing chances are higher for an angle of rotation of the bilayer normal that is 90° relative to the external magnetic field (B_0). As the angle decreases, chances of the lipid orienting at that angle in the magnetic field leads to a lower intensity.

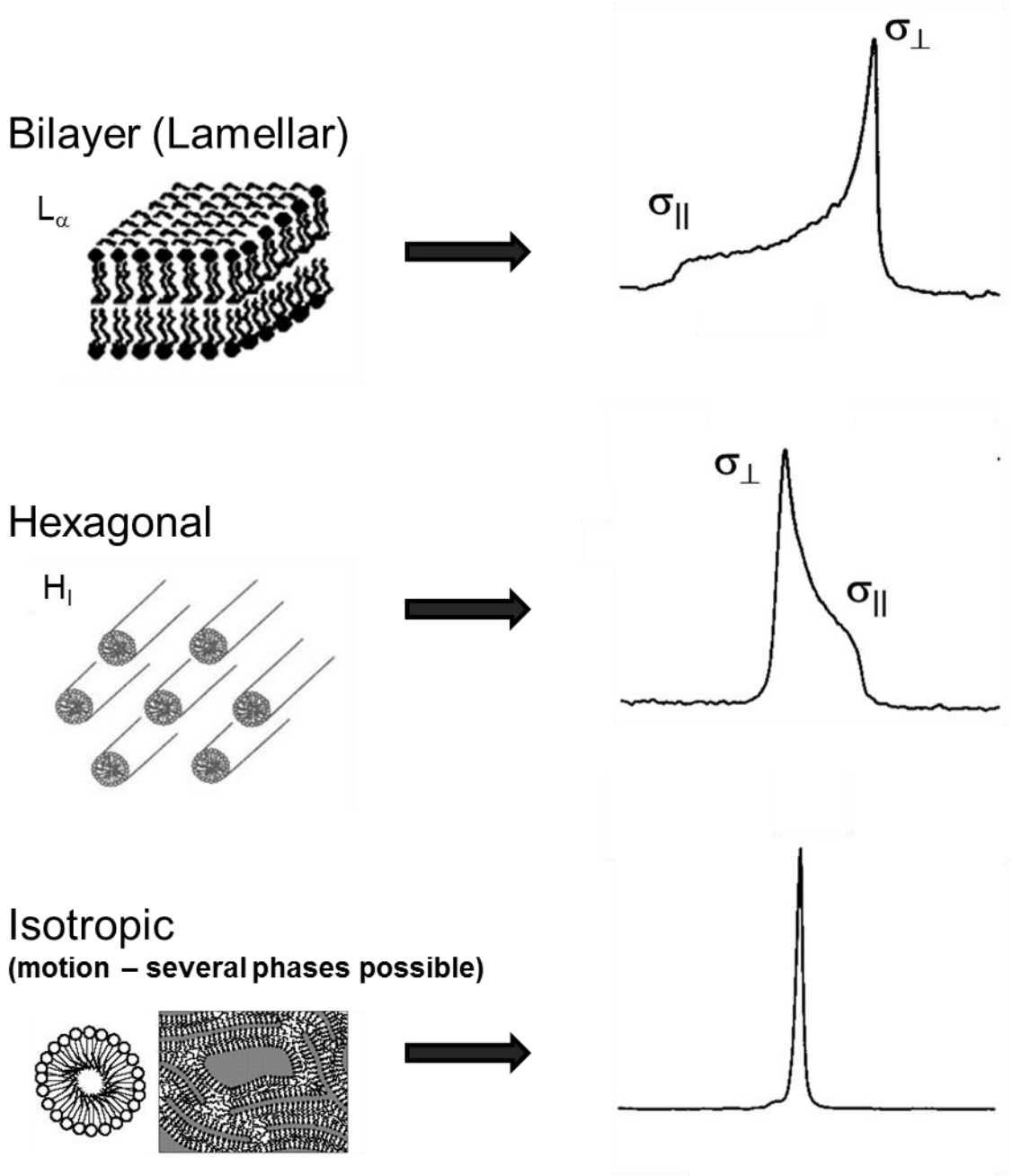

Figure 2-9. Polymorphisms and phosphorus NMR lineshapes (Adapted from Cullis (*89*) and Tate (*51*)). The lineshapes for ^{31}P NMR spectra correspond to different phases or polymorphisms. The phase is shown on the left and its corresponding spectrum on the right. Several phases can result in an isotropic peak.

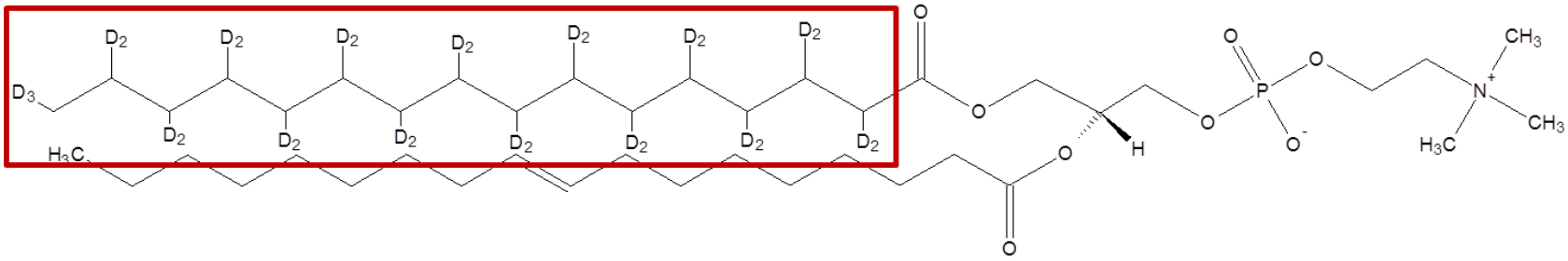

Figure 2-10. Phospholipid with sn-1 acyl chains deuterated. Figure made with ACD/ChemSketch program

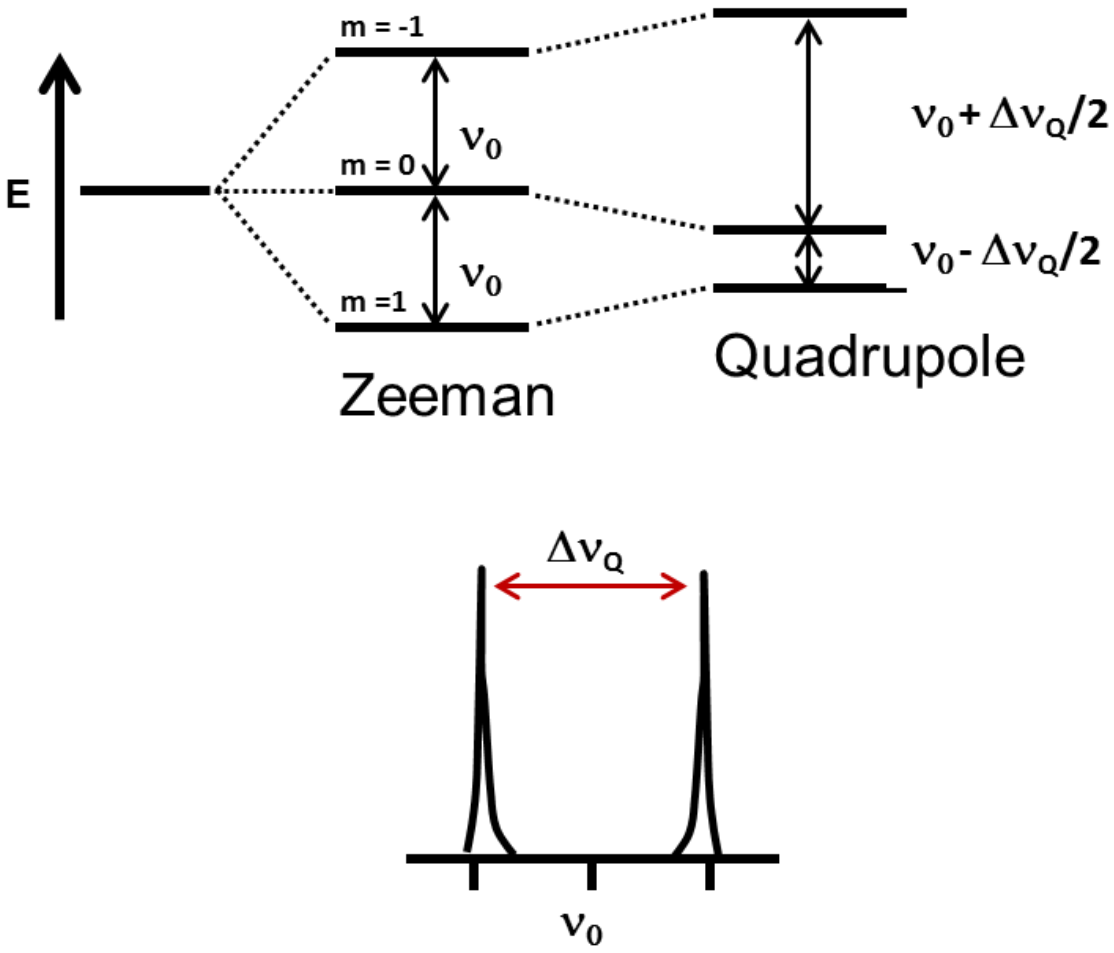

Figure 2-11. The doublet of resonances seen in ^{2}H NMR spectra results from the quadrupolar interaction for spin-1 nuclei. Deuterium is a spin-1 nucleus with a quadrupolar moment that interacts with the electric field gradient at the nucleus, giving rise to the quadrupolar interaction. Two spin transitions exist and a doublet of resonances is observed on a ^{2}H NMR spectrum separated by the quadrupolar splitting $\Delta\nu_{Q.}$

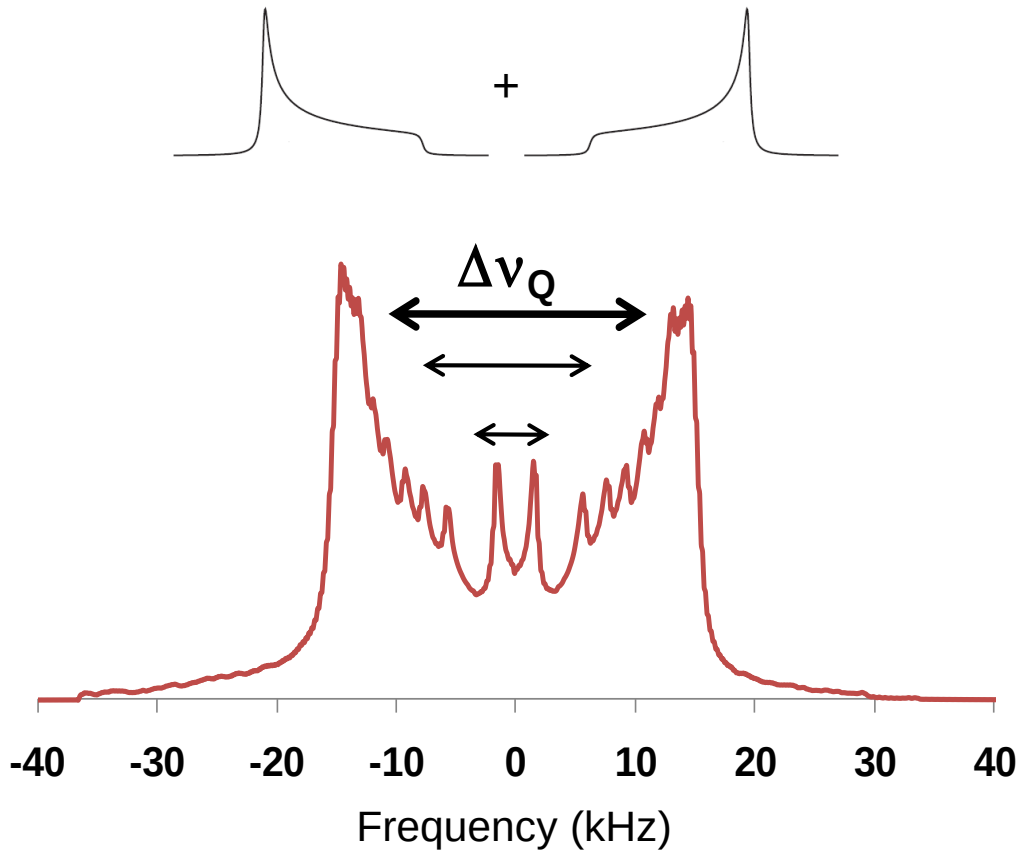

Figure 2-12. Quadrupolar splitting and overlapping of lineshapes. There are two spin transitions in ^{2}H NMR that lead to two powder patterns that overlap. The samples in this dissertation have multiple sites deuterated, which have different motions resulting in a broad spectrum with several overlapping lineshapes.

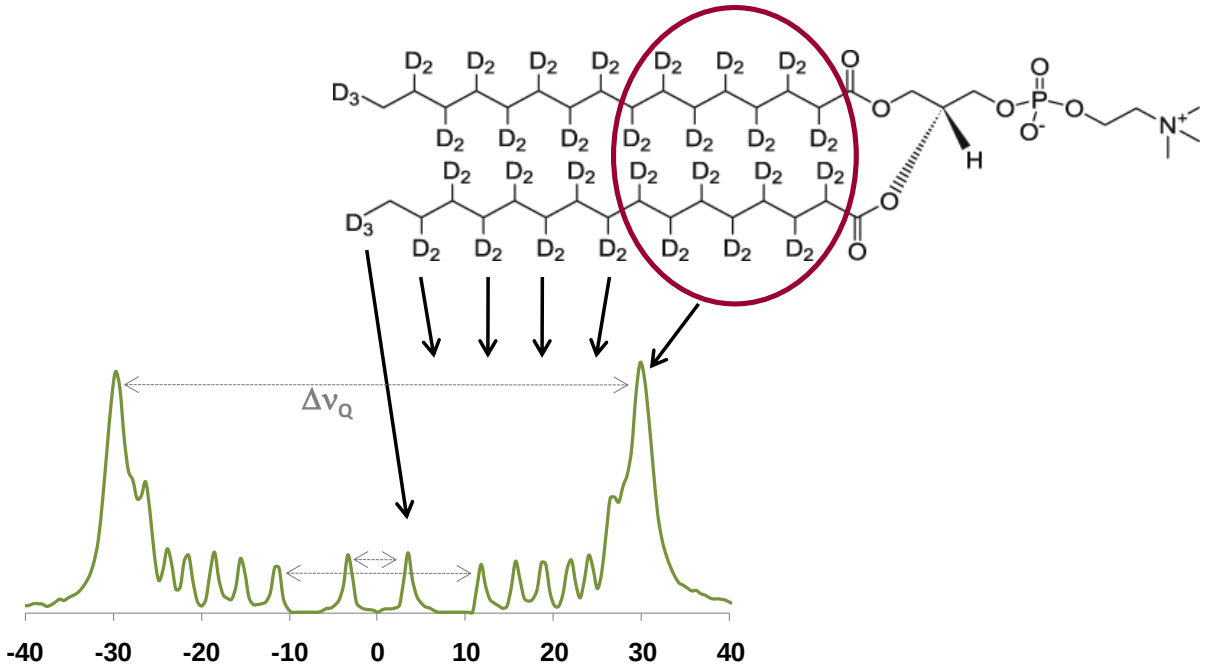

Figure 2-13. Deuterons and their associated resonances in a dePaked deuterium solid-state NMR spectrum. The quadrupolar splitting is affected by lipid mobility. As the quadrupolar splitting decreases, the acyl chain order decreases. The distal end of the lipid molecule exhibits the most motion. The motion decreases closer to the headgroup region.

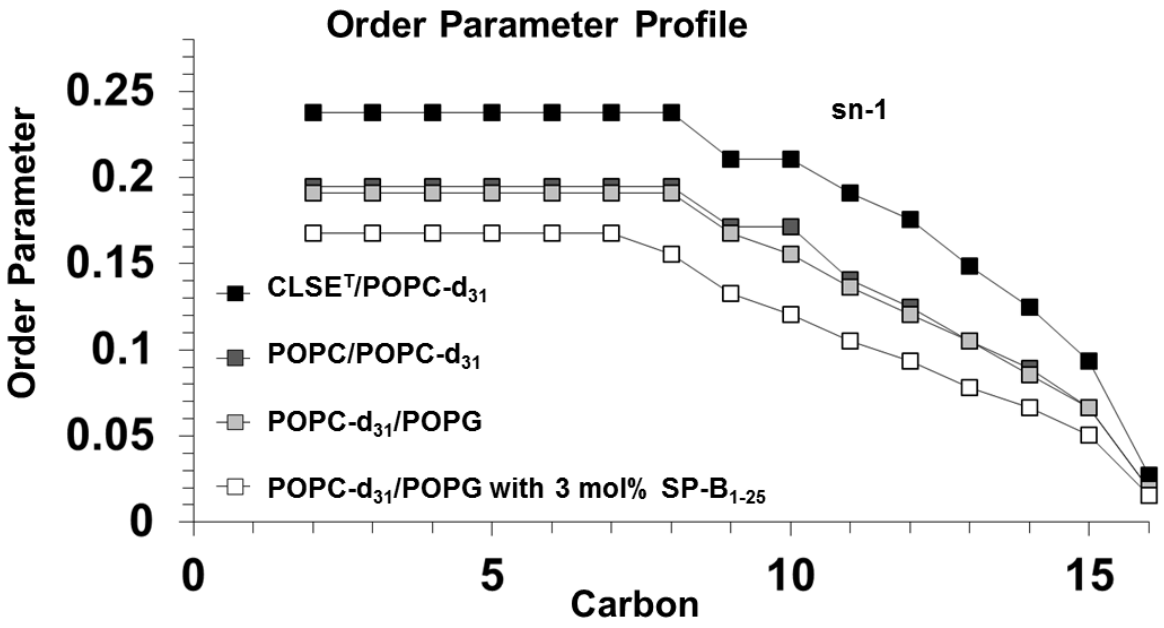

Figure 2-14. Order parameter profile of POPC-d_{31} acyl chains in different lipid environments.

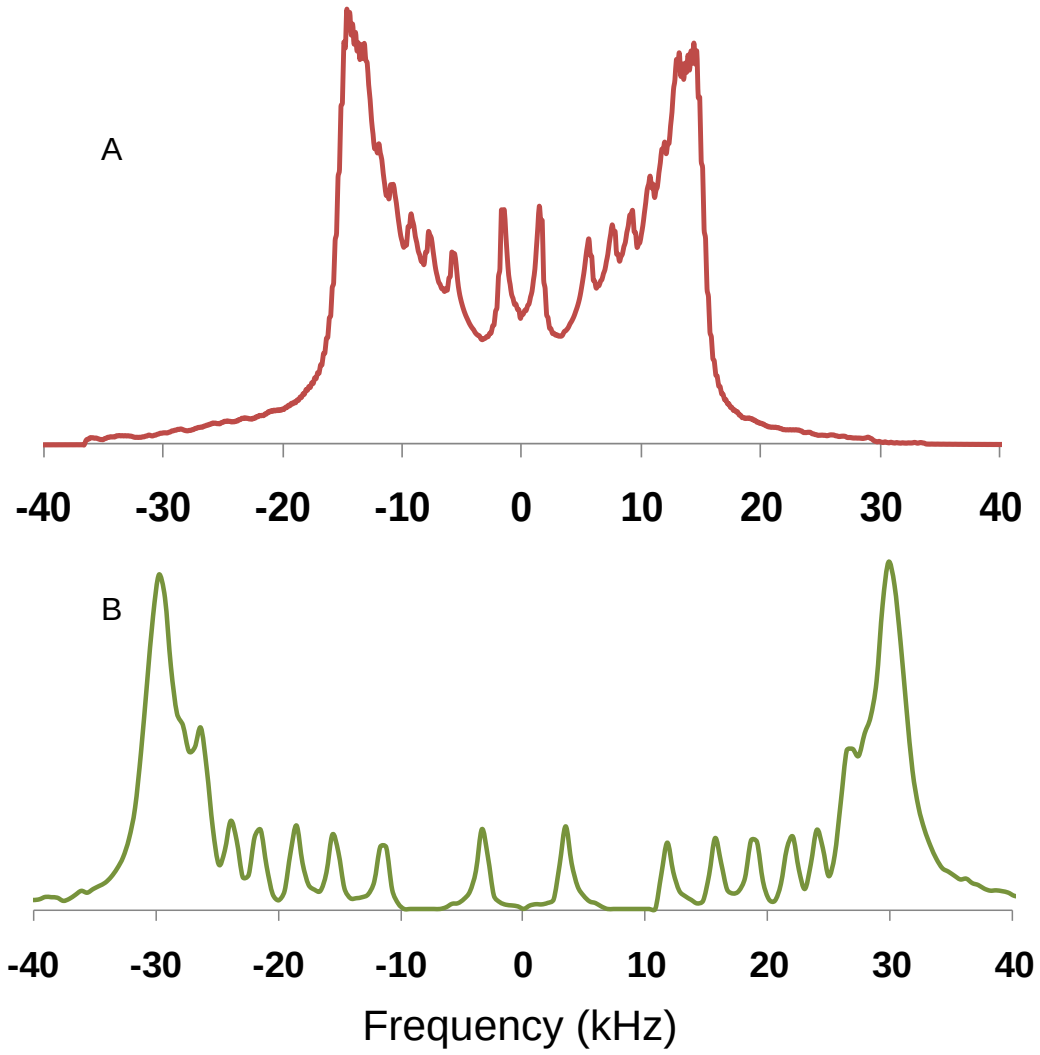

Figure 2-15. A) ^{2}H ssNMR lineshape B) dePaked ^{2}H ssNMR lineshape. Depaking simplifies analysis by transforming powder lineshapes to individual frequencies.

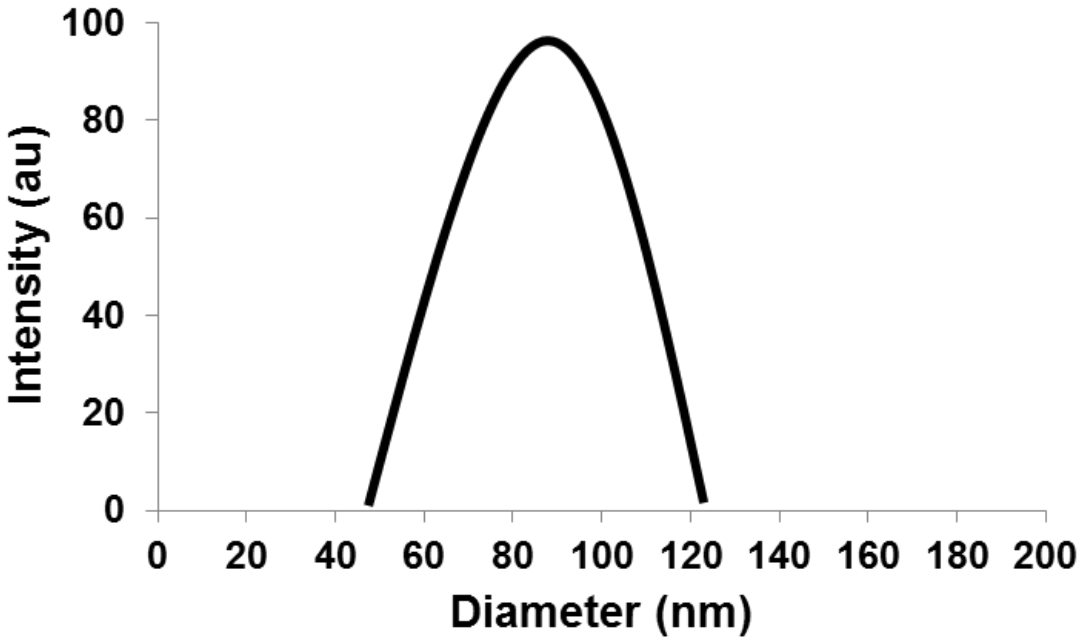

Figure 2-16. Example of a dynamic light scattering spectrum. DLS experiments in this dissertation were used to determine the size of lipid vesicles as a function of peptide concentration.

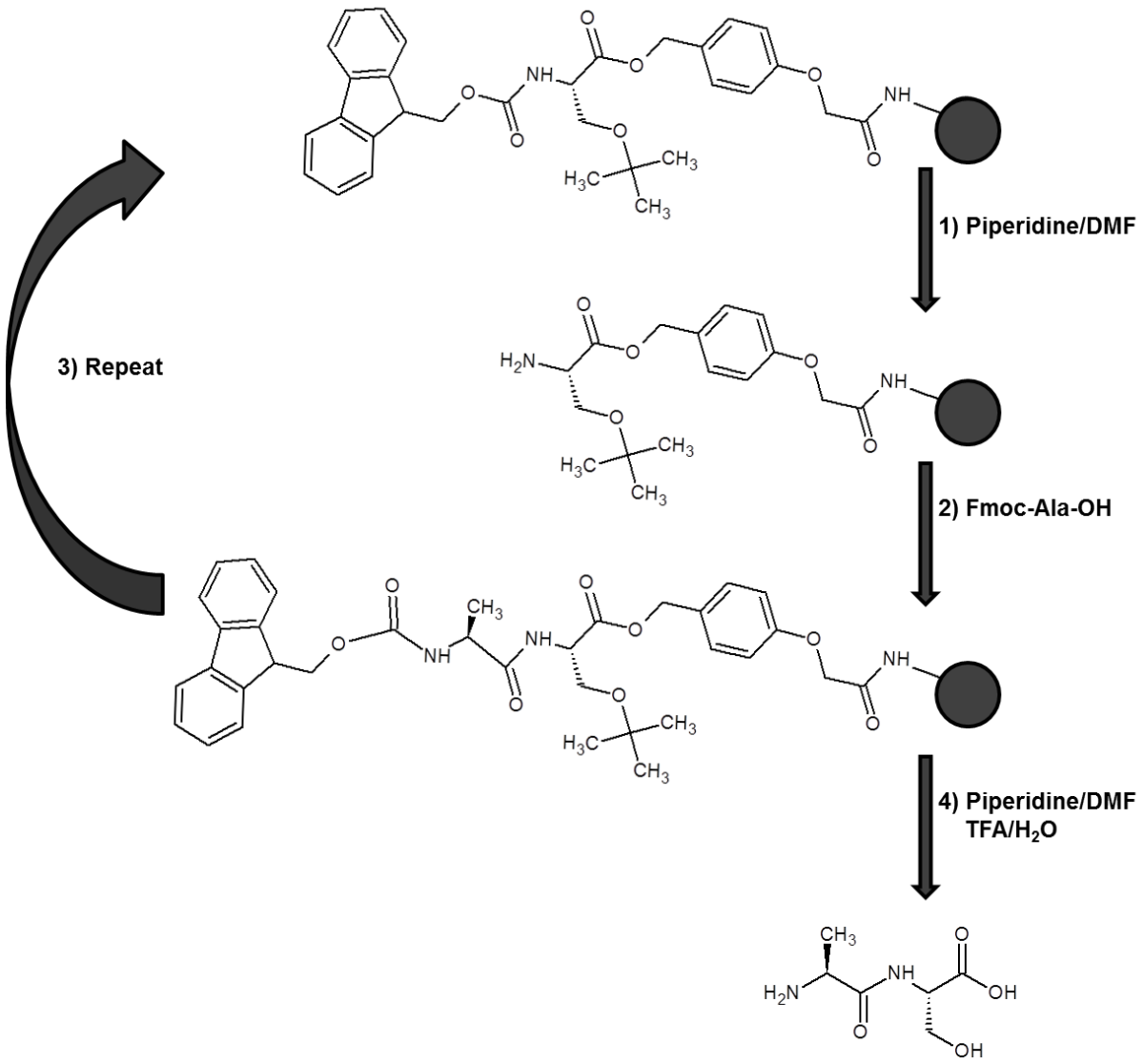

Figure 2-17. A summary of Fmoc SPPS steps. 1) An Fmoc protected amino acid attached to the resin via a linker is deprotected using piperidine. 2) The next amino acid is attached to the growing chain. 3) The deprotection/coupling cycle is repeated. 4) The desired amino acid sequence is cleaved from the resin with TFA to yield a free peptide.

Figure 2-18. Gel permeation chromatography column and fraction tray

CHAPTER 3
LIPID POLYMORPHISM INDUCED BY SURFACTANT PEPTIDE SP-B_{1-25}

This chapter is an article published in *Biophysical Journal* (*15*). The formatting has been altered to fit the requirements of this dissertation.

Introduction

Pulmonary surfactant protein B, SP-B, is an essential protein for lowering surface tension in the alveoli. SP-B_{1-25}, a peptide comprised of the N-terminal 25 amino-acid residues of SP-B, is known to retain much of the biological activity of SP-B. When interacting with negatively charged lipid vesicles, circular dichroism shows that SP-B_{1-25} contains significant helical structure for the lipid compositions and peptide/lipid ratios studied here. The effect of SP-B_{1-25} on lipid organization and polymorphisms was investigated via DSC, dynamic light scattering, transmission electron microscopy, and solid-state NMR spectroscopy. At 1-3 mol% peptide and physiologic temperature, SP-B_{1-25} partitions at the interface of negatively charged PC/PG lipid bilayers. In lipid mixtures containing 1-5 mol% peptide, the structure of SP-B_{1-25} remains constant, but ^{2}H and ^{31}P NMR spectra show the presence of an isotropic lipid phase in exchange with the lamellar phase below the T_m of the lipids. This behavior is observed for both DPPC/POPG and POPC/POPG lipid mixtures as well as for both the PC and PG components of the mixtures. For 1-3 mol% SP-B_{1-25}, a return to a single lamellar phase above the lipid mixture T_m is observed, but for 5 mol% SP-B_{1-25} a significant isotropic component is observed at physiologic temperatures for DPPC and exchange broadening is observed in ^{2}H and ^{31}P NMR spectra of the other lipid components in the two mixtures. DLS and TEM rule out the formation of micellar structures and suggest that SP-B_{1-25} promotes the formation of a fluid isotropic phase. The ability of SP-B_{1-25} to

fuse lipid lamellae via this mechanism, particularly those enriched in DPPC, suggests a specific role for the highly conserved N-terminus of SP-B in the packing of lipid lamellae into surfactant lamellar bodies or in stabilizing multilayer structures at the air-liquid interface. Importantly, this behavior has not been seen for the other SP-B fragments of $SP\text{-}B_{8\text{-}25}$ and $SP\text{-}B_{59\text{-}80}$, indicating a critical role for the proline rich first seven amino acids in this protein.

Pulmonary surfactant (PS) is a lipid-rich substance containing key proteins that minimizes surface tension in the alveoli. PS is required for normal respiration and provides a barrier against disease (*9*, *32*, *90*). PS is synthesized, processed into lamellar bodies, secreted, and recycled by type II epithelial cells, which cover ~5% of the alveolar gas exchange surface. PS lipids undergo a cycle of adsorption and resorption from the fluid subphase to maintain a surface-active layer at the alveolar air-fluid interface, with lung surfactant being completely recycled every 5-10 hours (*91*).

Mammalian PS has a highly conserved lipid composition dominated by zwitterionic phosphatidylcholines (PC) (70-80%) and anionic phosphatidylglycerol (PG) and phosphatidylinisotol (PI) (10-20%) (*18*, *92*). Approximately 50% of the PC lipids and almost all of the anionic lipids in lung surfactant are monounsaturated. However, a significant fraction of PS (>40% of the lipids) is fully saturated DPPC and this component is conserved among mammalian species. DPPC enhances the stability of lipid monolayers at air/water interfaces, which is of particular relevance to lung function. However, the lipid composition of PS alone is not sufficient to maintain the organization and dynamics of the lipid assemblies observed in the lung surfactant fluid of intact lung tissue. It has been postulated that protein-induced lipid polymorphisms and protein-

induced trafficking of lipids to the interface are critical for PS function at ambient pressure (*24*, *31*, *93*, *94*) To support this claim, it has been shown that surfactant proteins B and C (SP-B and SP-C, respectively), which are highly hydrophobic and present at relatively low levels, are essential to imparting the recycling properties of LS. In particular, surfactant protein B (SP-B), which comprises 0.7-1.0% of the dry weight of PS or <0.2 mol% relative to the lipids, is requisite for proper lung function (*95*, *96*). Inadequate PS is a leading cause of respiratory distress syndrome (RDS) in premature infants (*97*).

The native form of SP-B is a highly hydrophobic, 17 kDa sulfhydryl-linked homodimer (*25*). Intramolecular disulfide bridges formed by the remaining six cysteine residues and a sequence similar to sphingolipid-activator proteins place SP-B in the saposin-like protein family. However, SP-B is significantly more lipophilic than other saposin-like proteins and has not been found to activate lipids for enzymatic modification. The hydrophobicity and disulfide bridges within SP-B make it difficult to express and purify heterologously. Animal sources of lung surfactant are the current standard of care therapeutically, posing a risk of infection or immune response (*98*).

Given the tremendous importance of SP-B for surfactant function, surfactant replacement methods employing simple peptide analogs with surface-active properties have been the focus of many investigations. N- and C-terminal peptide fragments of SP-B, 20-25 amino acids in length, possess significant surface activity and can restore lung compliance in mouse models of respiratory distress (*8*, *43*, *99*, *100*). Additionally, a simple peptide analog, known as KL_4, based on the hydrophilic and hydrophobic periodicity in the C-terminus has shown clinical success (*101*), and peptoid analogs are

also surface active (*102*). The N-terminal 25 residue peptide, SP-B_{1-25}, has proven not only to improve the surface activity of lipid mixtures but it is also more resistant to inhibition by the plasma protein fibrinogen compared to the full protein (*46*). More recently, a chimeric construct made up of the C- and N-terminal sequences, termed mini-B, has shown increased activity relative to the individual peptides and it is comparable in activity to native SP-B at similar concentrations (*103*). The success of this synthetic analog suggests that both the N- and C-terminal sequences in SP-B are important to its function and may have complimentary roles.

We recently reported that at therapeutically relevant concentrations both SP-B_{59-80} and KL_4 differentially partition into lipid bilayers of varying saturation while preserving a lamellar phase (*13*, *14*). The helical secondary structures of both SP-B_{59-80} and KL_4 in a lipid bilayer environment vary from canonical α-helices and both undergo changes in helicity with varying lipid composition, suggesting that structural plasticity is important to their mechanism of action. SP-B_{1-25} has also been shown to possess significant helical structure when it is associated with lipid monolayers and bilayers (*37*, *104*, *105*). Based on FTIR and CD measurements, it has been inferred that the proline-rich N-terminal residues of SP-B_{1-25} are not highly structured. Monolayer studies have demonstrated these residues are important to its rapid insertion into lipid films (*8*).

The effect that SP-B_{1-25} has on lipid organization and polymorphisms has not been thoroughly investigated. The ability of SP-B_{1-25} to modulate the macroscopic organization of lipid molecules may play a functional role in maintaining reservoirs of LS lamellar bodies near the air/water interface (*94*). Here, we report that SP-B_{1-25} can induce non-lamellar lipid morphologies when mixed with PS lipids. We utilized static ^2H

and ^{31}P NMR, CD, DLS, TEM and DSC to characterize 4:1 DPPC/POPG and 3:1 POPC/POPG lipid mixtures on addition of varying concentrations of SP-B_{1-25}. The former lipid composition was selected to mirror the lipid composition of several model PS studies and lucinactant, a synthetic formulation under development for treating RDS, whereas the latter composition is similar to formulations used in numerous studies of amphipathic membrane-active peptides (*106*) and allows for the direct comparison of the physical properties of SP-B_{1-25} to SP-B_{59-80} and KL_4. Lipid phases enriched in either POPC/POPG or DPPC/POPG could potentially be found in localized areas of the alveoli during the surfactant cycle.

Materials and Methods

Synthesis of SP-B_{1-25} and Preparation of Peptide/Lipid Samples

SP-B_{1-25}, (FPIPLPYCWLCRALIKRIQAMIPKG) was synthesized via solid-phase peptide synthesis, purified by RP-HPLC, and verified by mass spectrometry (m/z=2928). Peptide was dissolved in methanol and analyzed by amino acid analysis for concentration (Molecular Structure Facility, UC Davis). POPC, DPPC, POPG, POPC-d_{31}, DPPC-d_{62} and POPG-d_{31} chloroform solutions (Avanti Polar Lipids, Alabaster, AL) were quantified by phosphate analysis (Bioassay Systems, Hayward, CA). SP-B_{1-25} in methanol was added to the lipid chloroform solutions resulting in P/L ratios ranging from <1:1000 to 1:20. Samples were dried under nitrogen at >45°C; suspended in warm cyclohexane (>45°C), flash frozen in nitrogen, and lyophilized to remove residual solvent.

CD Experiments

CD spectra were acquired at 45°C on an Aviv Model 215 (Lakewood, NJ). Samples were prepared by hydrating lyophilized peptide-lipid powders in 10 mM

HEPES buffer, pH 7.4, with 140 mM NaCl and 1 mM EDTA, to achieve a final concentration of 36 μM SP-B_{1-25}. Samples were extruded through 100 nm filters (Avanti Polar Lipids, Alabaster, AL) to form LUVs. Spectra of 40 μM SP-B_{1-25} in methanol were also collected.

DSC Analysis

Thermograms were collected on a VP-DSC microcalorimeter (Microcal Inc, LLC Northampton, MA). Samples were prepared by solubilizing peptide-lipid powders as above to achieve a 2.5 mM lipid concentration. Samples were extruded and degassed.

Solid State NMR Analysis

Phosphorus and Deuterium NMR data were collected on a 500 MHz Bruker DRX system (Billerica, MA) with a 5 mm BBO probe. For the ^{31}P NMR experiments, 25 kHz proton decoupling was employed. ^{2}H NMR spectra were collected using a quad echo sequence (90°-τ-90°-τ-acq with τ = 30 μs). For each NMR sample, ~20 mg of peptide-lipid powder was placed in a 5 mm diameter NMR tube and 200 μL of buffer containing 10mM HEPES, pH 7.4, 140mM NaCl, and 1mM EDTA in ^{2}H depleted water (Cambridge Isotopes, Andover MA) was added. The hydrated dispersions were subjected to 5 freeze-thaw cycles to form MLVs. DePaking of NMR data was accomplished with previously published algorithms which simultaneously dePake and determine macroscopic ordering in partially aligned lipid spectra using Tikonov regularization (*75*). Assignments of ^{2}H resonances were made based on Petrache, *et al.* (*78*).

Dynamic Light Scattering

Dynamic light scattering measurements were performed using a Brookhaven 90Plus/BI-MAS ZetaPALS spectrometer with BI-9000AT Digital Autocorrelator and 9KDLSW data acquisition software. The instrument was operated at a wavelength of

659 nm over a temperature range of 25-45ºC. Samples contained a 1 mM suspension of 4:1 DPPC/POPG MLVs.

TEM Analysis

TEM images of 4:1 DPPC/POPG MLVs were captured using a Hitachi H-7000 transmission electron microscope operated at 75 kV with a Soft-Imaging System MegaViewIII and AnalySIS digital camera (Lakewood, Colorado). Samples were prepared as above and contained a 1 mM suspension of 4:1 DPPC/POPG MLVs. Sample grids were prepared by negative staining.

Results

SP-B_{1-25} Adopts a Stable, Primarily Helical Structure in the Presence of Lipid Vesicles

CD spectroscopy was utilized to investigate the conformation of SP-B_{1-25} in the presence of 4:1 DPPC/POPG and 3:1 POPC/POPG unilamellar lipid vesicles (Figure 3-1). The CD spectra at 45ºC are identical for the two lipid environments and have features characteristic of helical secondary structure, with minima at 208 and 222 nm. Standard deconvolution analysis (*107*) gives secondary structure estimates of 60% α-helix, 30-35% random coil, and <10% β-sheet for SP-B_{1-25} interacting with phospholipid LUVs. These findings are consistent with results from previous FTIR studies of isotopically enriched SP-B_{1-25} in POPG, which concluded that the peptide forms a well-structured α-helix from residues 8 to 22 and a β-sheet conformation in the first six residues (*37*). The CD spectra for the peptide in the lipid-containing samples are identical for both lipid mixtures and over a concentration range of 1-5 mol% SP-B_{1-25}. A CD spectrum obtained for SP-B_{1-25} in methanol (dashed line), where the peptide is more helical, is also shown for comparison.

DSC Shows SP-B_{1-25} Decreases Lipid Miscibility

Also shown in Figure 3-1 are DSC thermograms for 4:1 DPPC/POPG LUVs containing varying molar percentages of SP-B_{1-25}. Samples for DSC measurements had the same lipid compositions as those used for NMR investigations described below, i.e. they included deuterated lipids (DPPC-d_{62}), the presence of which is known to lower the lipid phase transition temperature. The main phase transition temperature for the 4:1 DPPC/POPG sample is observed at 32ºC. At 0.5 mol% SP-B_{1-25}, a higher temperature shoulder appears at ~34°C in the thermogram. The intensity of this shoulder grows as the concentration of peptide increases. At 1.5 mol% peptide, two separate melting events are resolved with T_m values of 31 and 34°C, suggestive of lipid demixing or domain separation. This effect on the DSC thermogram is similar to that previously noted for the lung surfactant peptides KL_4 (*108*) and SP-B_{59-80} (*14*). Similar effects on the DSC thermograms for 7:3 DPPC-d_{62}/POPG and 7:3 DPPC/POPG-d_{31} with and without 3.5% SP-B_{8-25} (by weight) have been observed (*109*). From DSC data alone one cannot distinguish whether the two transitions result from the formation of separate POPG-enriched and POPG-depleted DPPC lipid domains or whether the different melting temperatures arise from phase separation of bulk lipids and peptide-associated lipids (*110*) or a combination of the two, such as DPPC-peptide separation from DPPC-POPG domains.

^{2}H NMR Spectra Indicate SP-B_{1-25} Decreases PC/PG Lipid Miscibility and Induces an Isotropic Phase, Particularly for PC Lipids

To obtain a molecular level view of how SP-B_{1-25} modulates lipid organization and mixing, solid state ^{2}H NMR spectra of both saturated and unsaturated lipid mixtures containing varying mol% SP-B_{1-25} were obtained and analyzed. Samples containing

either deuterated PC or PG were prepared, allowing the monitoring of individual lipid components. Figure 3-2 shows stack plots of ^{2}H NMR data obtained for 4:1 DPPC/DOPG samples with varying mol% SP-B_{1-25} over the temperature range of 26°C to 40°C. In the absence of peptide, both the DPPC and POPG components are observed to melt at similar temperatures. The phase transition temperatures for DPPG and POPG were determined from sigmoidal fits to first moment analyses of spectra collected between 22°C and 44°C. The phase transition temperature determined for deuterated DPPC is slightly *lower* (30.8°C) than that for deuterated POPG (32.8°C). This difference is likely due to a larger relative percentage of the fatty acyl chains being deuterated in the DPPC-d_{62} containing sample compared to that of the POPG-d_{31} containing sample (80% vs. 10%) (*111*). For non-peptide containing samples, the spectra at intermediate melting temperatures, from 26 to 32°C, have line shapes that are a superposition of gel phase and liquid crystalline phase spectra, consistent with the broad asymmetric DSC thermogram obtained for this lipid mixture. Addition of 1 mol% SP-B_{1-25} increases the phase transition of the DPPC lipids, with the melting midpoint determined to be 34.3°C, whereas the melting temperature of the POPG component is not altered. These results are consistent with the DSC thermograms, where a shoulder at 34°C is detected for this concentration of SP-B_{1-25}, and they suggest some demixing of DPPC from the mixture on addition of SP-B_{1-25}. More interesting, however, is the phase behavior seen with 3 mol% SP-B_{1-25}. At this peptide concentration, DPPC-d_{62} spectra from 22 to 32°C are dominated by an isotropic peak that changes abruptly to a gel phase spectral lineshape over 34-36°C, followed by the formation of a liquid crystalline lamellar phase at 38-40°C. The lamellar phase spectrum at 38°C has

significant signal intensity at the parallel edges of the lineshape relative to spectra at higher temperatures which is consistent with more rounded vesicles at this temperature. At higher temperatures the vesicles elongate in the magnetic field leading to a loss of signal at the parallel edges, as is commonly seen with lipid mixtures at these high magnetic field strengths. With 5 mol% SP-B_{1-25}, an isotropic phase is observed for DPPC-d_{62} over the entire 26-40°C temperature range with the appearance of an anisotropic phase at 40°C. Spectra acquired up to 44°C contained a significant isotropic component (Figure 3-3). The POPG-d_{31} spectra show less of an alteration in lipid behavior at 5 mol% peptide concentrations, but they are affected nonetheless. At 5 mol% SP-B_{1-25}, the spectra for POPG-d_{31} show trends very similar to those observed for DPPC-d_{62} in the presence of 3 mol% SP-B_{1-25} (Figure 3-2). Given these observations, it is likely that the addition of peptide causes DPPC and POPG to partially demix over the phase transition temperatures with addition of peptide, particularly at physiologic temperatures. This is in agreement with the DSC data presented above. Interestingly, the cationic peptide has a larger effect on the phase behavior of the zwitterionic DPPC rather than the anionic POPG, as the isotropic DPPC spectra suggest the peptide preferentially interacts with the DPPC-enriched domain.

Differences in the peptide's effects on DPPC and POPG lipid morphology in DPPC/POPG lipid mixtures may be attributed to either differing interactions of the peptide with the lipid headgroups, differences in partitioning due to their differing fatty acid saturation, or both. A third major lipid component of lung surfactant is POPC, which has a molecular structure intermediate between DPPC and POPG. We also investigated the effects of SP-B_{1-25} on the thermotropic and phase behavior of 3:1

POPC/POPG mixtures. In order to compare the phase transition behavior of POPC/POPG mixtures on addition of SP-B_{1-25}, ^{2}H NMR data were collected for 3:1 POPC/POPG samples containing either POPC-d_{31} or POPG-d_{31} over the temperature range of the phase transition for the monounsaturated lipids, which is ~40ºC lower than the DPPC/POPG mixture (Figure 3-4). Comparing the trends for the POPC/POPG samples to the DPPC/POPG samples near the respective phase transition temperatures of the lipid mixtures indicates these mixtures behave very similarly with the PC lipids being more affected by the addition of SP_{1-25} and with both systems showing the induction of an isotropic phase by the peptide. The phase transition observed for deuterated POPC is at a slightly lower temperature (midpoint of -4.3°C) than for deuterated POPG (-3.0°C) due to a larger percentage of the lipids being deuterated in the POPC-d_{31} containing sample (75% vs. 25%). Addition of 1 mol% SP-B_{1-25} increases the phase transition temperature of the POPC lipids by almost 6°C, with the melting midpoint at 1.2°C. In contrast, the transition temperature of the POPG lipids increases only 3.1°C, with a midpoint of 0.1°C. With 3 mol% SP-B_{1-25}, the spectra for the POPC-d_{31} lipids exhibit an isotropic peak at temperatures below the T_m of the lipids which coalesces into a gel phase lineshape near the phase transition temperature (-2 to 4°C), followed by the formation of a liquid crystalline lamellar phase at higher temperatures. With 5 mol% SP-B_{1-25}, an isotropic phase is observed for POPC-d_{31} over the entire low temperature range (-6 to 4°C) with the appearance of an anisotropic lineshape beginning at 4°C. The POPG-d_{31} spectra show less of an alteration in lipid behavior at similar peptide concentrations, but they also show the appearance of an isotropic peak at lower temperatures and higher peptide concentrations. The spectra for

POPG-d_{31} in a sample containing 5 mol% SP-B_{1-25} show trends very similar to those observed for POPC-d_{31} in the presence of 3 mol% SP-B_{1-25}.

From the ^{2}H NMR data it is clear that lipid headgroup composition (PC vs. PG) plays a role in determining the phase behavior of the individual lipids in mixtures containing SP-B_{1-25}. The effects of the peptide on lipid morphology are also determined by the degree of saturation in the lipids. This can clearly be seen by comparing the dynamics of each of the lipids in the DPPC/POPG and POPC/POPG mixtures at the average mammalian physiologic temperature of 38°C (Figure 3-5). At this temperature, the DPPC lipids are most affected by addition of peptide and exhibit isotropic phase behavior at 5 mol% SP-B_{1-25}. Even at 3 mol% peptide the DPPC lipids are in exchange between lipid phases as evidenced by the broadened lineshape. In contrast, the POPC and POPG lipids exhibit a lamellar lineshape even at 5 mol% peptide although the lineshape is somewhat broadened suggesting exchange between lipid phases may be occurring.

^{31}P NMR Spectra Are Consistent with Dynamic Exchange Between the Isotropic and Lamellar Phases on a KHz Timescale

At 11.7 T, phospholipid phosphorus chemical shift anisotropy tensors are over an order of magnitude smaller than the deuterium quadrupolar coupling for a methylene group. Thus, static ^{31}P NMR spectra are more sensitive to slower motions, such as exchange between lipid phases. ^{31}P NMR spectra at 38°C for 3:1 POPC/POPG and 4:1 DPPC/POPG MLVs containing varying concentrations of SP-B_{1-25} are also shown in Figure 3-5. Because data were collected on a 500 MHz NMR spectrometer, macroscopic alignment of the vesicles occurred causing a decrease in the downfield features (parallel edges) of the lamellar lineshapes for the phospholipid dispersions.

However, the perpendicular edges of the PG and PC lipid powder lineshapes, at 11 and 15 ppm, respectively, can be clearly distinguished due to slight differences in the average orientation of their respective phosphate headgroups relative to the plane of the lipids (*13*, *14*). In the DPPC/POPG mixtures, addition of 3 mol% SP-B_{1-25} leads to the appearance of an isotropic peak concurrent with a loss of intensity at the perpendicular edge for DPPC. At 5 mol% peptide, the isotropic peak dominates the spectrum and the perpendicular edge of the POPG lineshape is also significantly less intense, consistent with exchange between a lamellar phase and an isotropic phase. In the POPC/POPG mixtures, addition of peptide has less of an effect on the ^{31}P lineshapes at 38ºC; an isotropic peak is not observed. However, there is sufficient lipid exchange to observe altered lineshapes in samples containing 3 and 5 mol% peptide. ^{31}P spectra as a function of temperature for both DPPC/POPG and POPC/POPG are shown in Figure 3-6. Significant isotropic components are observed in the spectra near the phase transition temperatures of the lipid mixtures on addition of SP-B_{1-25}, consistent with the ^{2}H NMR data. The persistence of an isotropic peak in the ^{31}P spectra at temperatures where ^{2}H spectra are anisotropic (e.g. compare ^{2}H and ^{31}P spectra for DPPC/POPG samples containing 3 mol% SP-B_{1-25} in Figure 3-5) is consistent with motions on a kHz timescale contributing to the averaging of the ^{31}P lineshapes.

Addition of SP-B_{1-25} May Lead to a Cubic or Fluid Isotropic Phase Via Vesicle Fusion

The appearance of isotropic lineshapes in the ^{31}P and ^{2}H NMR spectra upon addition of peptide is consistent with formation of either micellar, cubic or fluid isotropic lipid phases (*22*, *112*). To determine the relative sizes of the lipid assemblies and distinguish which lipid polymorphism results from addition of SP-B_{1-25}, we examined the

effects of peptide addition on DPPC/POPG vesicles by dynamic light scattering and electron microscopy. DPPC/POPG vesicles exhibit a broad range of vesicle sizes, with an average size of ~500 nm. Addition of SP-B_{1-25} leads to the formation of larger vesicles in a concentration dependent manner (Figure 3-7); there are no vesicles seen below 150 nm in the peptide-containing samples, ruling out micelle formation, and a rise in vesicles >4000 nm is observed. The DLS instrument setup is unable to determine vesicle sizes above 10,000 nm but a clear trend toward larger sizes is observed for samples containing higher mol% SP-B_{1-25}. Interestingly, the samples containing higher peptide concentrations are visibly less opaque, ruling out the possibility that the DLS data is affected by a decrease in sensitivity due to sample turbidity. Examination of lipid assemblies by electron microscopy also indicates addition of SP-B_{1-25} leads to the appearance of larger interconnected or fused vesicles (Figure 3-7). These observations are consistent with a cubic or fluid isotropic phase via vesicle fusion.

SP-B_{1-25} Partitions at the Lipid Interface in Lipid Lamellae

By analyzing the ^{2}H NMR spectra of the lipid mixtures above their lamellar phase transition temperatures, one can monitor the effect of SP-B_{1-25} on lipid acyl chain dynamics in the fluid phase. From these effects one can infer the partitioning depth of SP-B_{1-25} into the lipid bilayers. Lipid acyl chain order parameters were determined as previously described (*13*). Since our lipid samples show some degree of alignment in the magnetic field, spectra were deconvoluted using a Tikonov regularization procedure to account for vesicle alignment. The resulting order parameter profiles for the *sn*-1 chain in mixtures of DPPC-d_{62}/POPG and DPPC/POPG-d_{31} at 44ºC containing varying levels of SP-B_{1-25} are graphed in Figure 3-8; data for POPC-$_{31}$/POPG and POPC/POPG-d_{31} samples are presented in Figure 3-9. Addition of SP-B_{1-25} results in a

decrease in order parameters with increasing SP-B_{1-25} concentrations for all the lipids in the two types of mixtures. A distinct drop in the order parameters is observed with addition of 5 mol% SP-B_{1-25}. From the order parameter profiles, it can be seen that the methylenes toward the center of the bilayers are more affected than those in the plateau region. This behavior is similar to changes observed in lipid order on addition of antimicrobial peptides (*106*, *113*, *114*) and suggests that the amphipathic helix of SP-B_{1-25} partitions near the lipid headgroups.

Discussion

The ability of SP-B to affect the organization and structures of lipid assemblies on the micron scale is well recognized (*96*). These effects are particularly striking given the low physiologic concentration of SP-B, with 400-800 lipid molecules per protein monomer (*93*). Much of the effort in developing synthetic replacements of PS have focused on identifying which sequences in the highly hydrophobic SP-B are most critical for modifying lipid properties in PS. There is now a general consensus that the N- and C-termini of the protein are the most active portions of the protein (*8*, *43*, *100*). In this study we have focused on the effects of the N-terminal 25 residue peptide, SP-B_{1-25}, on lipid dynamics and morphology. We find that at relatively low concentrations SP-B_{1-25} has a marked effect on lipid morphology.

SP-B_{1-25} is recognized as surface active and a functionally important domain within SP-B, but the molecular mechanisms underlying its activity, specifically its effects on lipid organization and dynamics in bulk PS, had thus far not been fully elucidated. Previous studies have focused on its surface properties via Langmuir monolayer studies of surface tension, lipid adsorption at the air/water interface, surface film stability, and film structure as a function of surface pressure (*48*, *115*, *116*). These studies are

particularly germane given the role of PS in lowering surface tension and the natural air/water interface established within the lung for oxygen exchange. However, electron microscopy studies of alveolar surfaces indicate type II pneumocytes secrete surfactant into a thin aqueous layer which has an average thickness of 0.2 μm, with the bulk of the PS lipids and proteins sequestered in the aqueous subphase (*117*). While SP-B has been demonstrated to promote the rapid transfer of phospholipids between the bulk aqueous phase and the air/water interface, it is not established whether SP-B itself partitions at the interface to accomplish this. For these reasons, we examined the effects of SP-B_{1-25} on lipid dynamics and organization in aqueous suspensions. Our observation by NMR of the coexistence of an isotropic phase in exchange with a lamellar phase on addition of SP-B_{1-25} to aqueous dispersion of DPPC/POPG and POPC/POPG mixtures is in good agreement with the proposed role of SP-B in lipid transfer within the aqueous subphase.

While isotropic NMR spectra for lipids are generally associated with the formation of small lipid micelles, which have correlation times shorter than the NMR timescale, other lipid polymorphisms can lead to isotropic lineshapes if the dynamics of the lipids allow individual lipid molecules to sample a broad array of orientations relative to the magnetic field on a fast enough time scale. In particular, cubic and fluid isotropic lipid phases are also consistent with isotropic NMR spectra. DLS results show that the lipid vesicle assemblies become larger rather than smaller on peptide addition, suggesting vesicle fusion rather than micelle formation. To confirm this, EM data were collected on DPPC/POPG lipid mixtures prepared with SP-B_{1-25}. Clear fusion of the vesicles and an increase in average vesicle size is observed relative to pure lipid mixtures. However, it

appears the vesicle structures are still somewhat lamellar in nature within the resolution of this technique. This suggests the observance of an isotropic phase by NMR is due to fast exchange of the lipids between lamellae facilitated by SP-B_{1-25}. Closer inspection of the ^{2}H and ^{31}P NMR spectra support a model of SP-B_{1-25} supported exchange of lipids between lamellae on a kHz timescale. The ^{2}H quadrupolar interaction is an order of magnitude larger than the ^{31}P chemical shift anisotropy, allowing the concurrent observation of an isotropic lineshape in the ^{31}P spectrum and a lamellar lineshape in the ^{2}H spectrum for a particular sample at temperatures where lipid exchange is intermediate between the timescales of these two interactions. This behavior is consistent with multilayer structures observed in native PS by EM and the induction of cubic phases in POPE suspensions by SP-B and SP-C (*118*). Additionally, electron microscopy (*119*), atomic force microscopy (*120*) and neutron reflection (*121*) studies have demonstrated that the film formed by PS at an air/water interface is thicker than a monolayer with an aqueous, multilayer, surface-associated surfactant reservoir. This reservoir as well as the secreted surfactant-containing lamellar bodies have multi-layer structures which are dependent on SP-B. Our results suggest SP-B_{1-25} may be critical to the juxtaposition of and exchange between lipid lamellae in PS.

SP-B_{1-25} may play a role not only in the organization of PS lipid assemblies but also lipid miscibility. DSC and ^{2}H NMR indicate some lipid phase separation is observed on addition of the peptide to either DPPC/POPG or POPC/POPG mixtures. Our NMR results show SP-B_{1-25} enhances the transfer of DPPC between lipid lamellae relative to POPC and POPG at physiologic temperatures, although there is some transfer of POPC and POPG lipids as well. Alterations in ^{31}P lineshapes can be seen at lower

temperatures for samples containing as little as 1 mol% SP-B_{1-25}. Motional averaging becomes more dramatic at 3 mol% SP-B_{1-25} and the extent of averaging is dependent on both the T_m of the lipid mixtures as well as the identity of the phospholipid headgroups. In particular, ^2H NMR spectra of both POPC and DPPC species exhibit isotropic lineshapes below T_m of the POPC/POPG and DPPC/POPG mixtures, respectively. ^{31}P spectra indicate the POPG species is also isotropic at low temperatures, but returns to a lamellar phase at lower temperatures than the PC lipids. At 5 mol% SP-B_{1-25}, the trend is even more dramatic. The ^2H NMR spectra for POPG-d_{31} and POPC-d_{31} are isotropic below -2ºC and 6ºC, respectively in POPC/POPG mixtures. In DPPC/POPG the resolution back to a lamellar lineshape is seen for POPG-d_{31} at ~34ºC, but DPPC-d_{62} lineshapes remain isotropic below 40ºC. This suggests that SP-B_{1-25} has an effect on lipid miscibility, particularly near the melting temperature of the lipid mixtures. This is especially relevant to PS, which has a melting temperature of ~35ºC, similar to the DPPC/POPG mixture. While physiologic levels of SP-B are much lower, at 0.1-0.2 mol%, our observation that 1 mol% SP-B_{1-25} can lead to significant averaging of the majority of the phospholipids in our mixtures suggests that even lower percentages of peptide could lead to significant transfer of lipids between lamellae. The ability of SP-B_{1-25} to nucleate a cubic or fluidic lipid phase, particularly for lipid mixtures containing DPPC, suggests a role for the N-terminus of SP-B in the packing of lipid lamellae into surfactant lamellar bodies or in stabilizing multilayer structures at the air-liquid interface. Our observation that at physiologic temperature the dynamics of DPPC lipid moiety are much more affected by SP-B_{1-25} is particularly intriguing and suggests that SP-B may enhance the exchange of DPPC between lipid lamellae while POPG and

other lipids remain within a planar lipid structure. It has been postulated DPPC may be specifically enriched at the air/water interface by PS proteins (*31*), and this result gives credence to this model.

While both the N- and C-termini of SP-B have been demonstrated to have some efficacy via both in vivo and in vitro assays, the exact boundaries of the active sequences and their effects on lipid organization at the molecular level have not been fully delineated. Our finding that at relatively low concentrations SP-B_{1-25} has a marked effect on lipid morphology is in contrast to previous studies of SP-B_{8-25} (*109*); the C-terminus, both SP-B_{59-80} (*14*) and SP-B_{63-78} (*122*); and a functional mimic of the C-terminus, KL_4 (*13*). We also note that while an isotropic phase has not been observed for lipid assemblies containing SP-B_{8-25} (*109*), it has been observed for lipid samples containing full length SP-B at a concentration of ~2 mol% (*123*, *124*). This indicates a specific role for the highly conserved, very hydrophobic first seven amino acids (FPIPLPY) as well as the amphiphilic helix from residues 8-22 in lipid association and remodeling. This is consistent with recent findings that the activity of a chimeric construct containing the N- and C-terminal domains of SP-B, mini-B, has superior activity on addition of this sequence (*125*) and that mutations in this sequence lead to poorer reinsertion of lipids into an expanding air/water interface (*8*). Recent studies of surfactant systems at the air/water interface have also demonstrated that the hydrophobic N-terminus is important to stabilizing lipid “nanosilos” in association with POPG-enriched areas of a DPPC/POPG monolayer (*126*).

Molecular dynamics simulations of SP-B_{1-25} in DPPC monolayers suggest that the most likely equilibrium conformation is with the α-helix in SP-B_{1-25} parallel to the

interface (*127*). FTIR studies indicate the first seven hydrophobic residues adopt a β-sheet conformation which penetrates into the interior of the lipid bilayers with residues 8-22 forming an amphiphilic helix at the lipid bilayer interface (*37*). Our CD measurements are consistent with these studies and indicate the overall structure of SP-B_{1-25} is relatively invariant with lipid composition and peptide concentration. The effects of SP-B_{1-25} on lipid acyl chain order parameters in the lamellar phase (Figure 3-8) are also consistent with the peptide partitioning at the lipid interface. However, subtle differences in the effects of SP-B_{1-25} on acyl chain order within PG vs. PC lipids suggest differential partitioning. Specifically, the PG acyl chains become more disordered than PC acyl chains in the lamellar phase on addition of peptide to DPPC/POPG and POPC/POPG mixtures. Increased order in the PC acyl chains can either be due to more peripheral association of the peptide with the bilayers via electrostatic interactions (*128*) or the peptide partitioning more deeply into the bilayer (*13*, *14*, *129*). SP-B_{1-25} has a relatively high percentage of hydrophobic residues relative to other amphipathic peptides, as do all the active PS peptides, and it has a highly hydrophobic N-terminus, which would favor deeper partitioning. This observation, combined with the observed greater effects of SP-B_{1-25} on the overall organization of the PC lipids suggests SP-B_{1-25} might partition more deeply into PC-enriched lipid domains while remaining more surface associated in PG-enriched lipid domains as a consequence of the differences in the charge states at the lipid interfaces (Figure 3-10). This model is consistent with ELISA assays performed using SP-B reconstituted in anionic and zwitterionic bilayers (*130*) where it was found SP-B was more immunoreactive to water soluble antibodies when reconstituted into anionic lipid bilayers. The deeper partitioning of SP-B_{1-25} into

PC-enriched lipids would lead to negative curvature strain which can induce lipid flipping and the formation of a cubic or fluid isotropic phase, or, at the air/water interface, enhanced adsorption of lipids to the surface monolayer from underlying lipid bilayers. The ability of SP-B_{1-25} to fuse lipid lamellae via this mechanism, particularly those enriched in DPPC, suggests a molecular mechanism for how the N-terminus of SP-B can facilitate packing of lipid lamellae into surfactant lamellar bodies or stabilize multilayer structures at the air-liquid interface. Further structural studies will assist in elucidating the mechanism by which the N-terminus modulates lipid organization in both the aqueous subphase and in association with the monolayer at the air/water interface.

Conclusion

In this study we have found that SP-B_{1-25} retains a constant secondary structure when associated with lipids and causes the formation of fluid isotropic lipid phases, particularly for DPPC containing lipid mixtures at physiologic temperatures. These findings can be compared to our previous CD and ssNMR studies on C-terminal SP-B peptides where, in contrast, we found that the helical pitch of the peptide changes as the lipid milieu is altered from saturated PC to unsaturated PC whereas there was no effect on the lipids; they remained in the lamellar mesophase. These contrasting effects suggest the N- and C-termini of SP-B have complementary roles in trafficking of PS lipids. With the findings presented here and elsewhere, a more thorough molecular model is established that provides insights into how these small peptides modulate lipid properties which can drive the development of future SP-B mimetics. The unique interplay observed for the N- and C-termini of SP-B among lipid moieties, peptide penetration, peptide structure, and lipid polymorphisms could explain the unique

properties of SP-B in the dynamic lung environment. Synergism between these peptides is the focus of our current and continuing work.

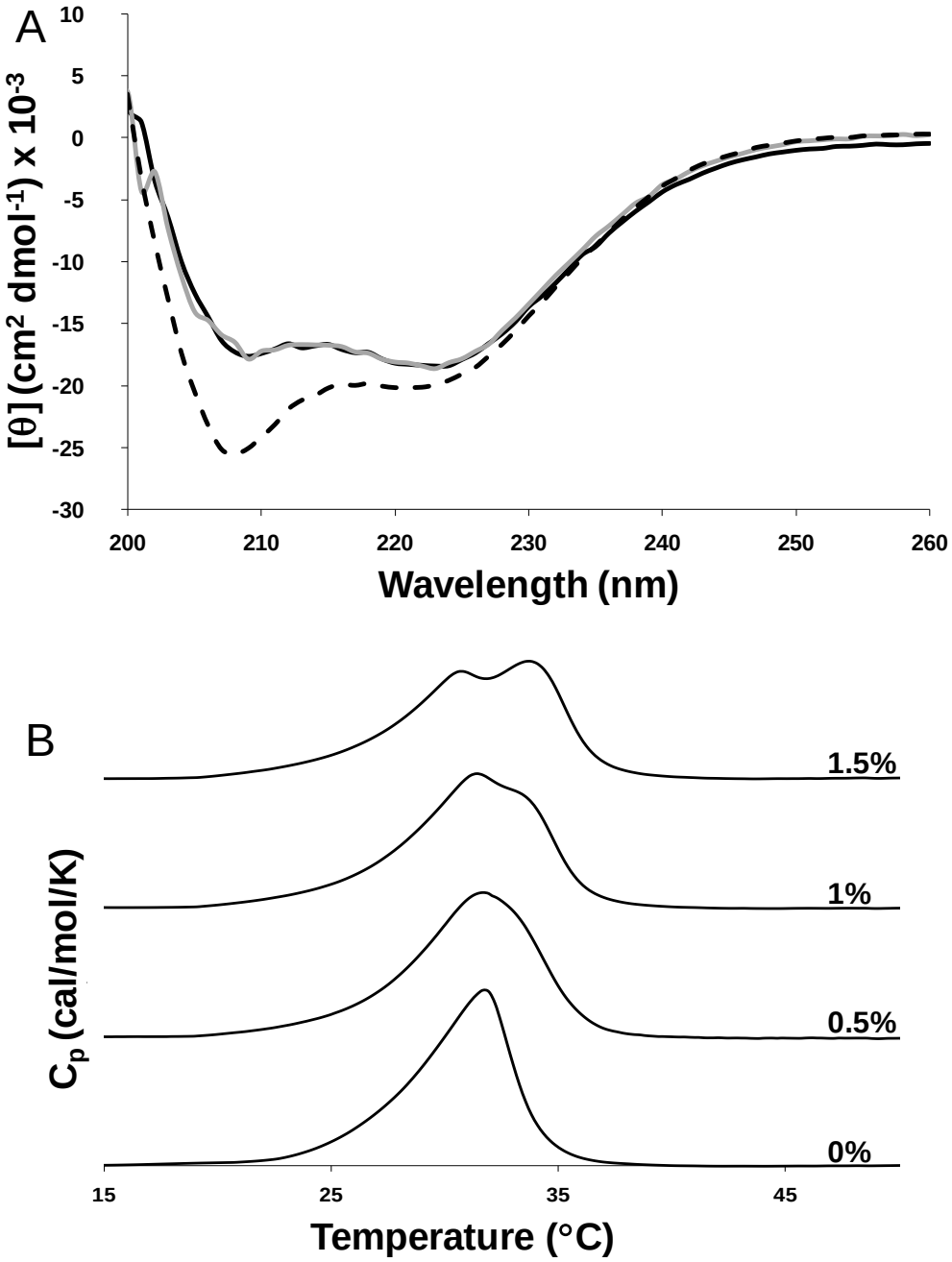

Figure 3-1. CD and DSC of 4:1 DPPC/POPG with SP-B_{1-25}. A) CD spectra at 45°C of SP-B_{1-25} at a P/L molar ratio of 1:100, 1:33, and 1:20 averaged together in 4:1 DPPC/POPG (black solid line) and in 3:1 POPC/POPG (gray solid line). The CD lineshapes for the individual P/L molar ratios are identical. A spectrum of SP-B_{1-25} dissolved in MeOH is shown for comparison (dashed line). The final peptide concentration was ~40 μM in all samples. B) DSC scans for 4:1 DPPC/POPG LUVs with SP-B_{1-25} at the indicated molar peptide percentages. The onset of phase separation is apparent at a P/L ratio of 1:200 and continues with increasing amounts of peptide.

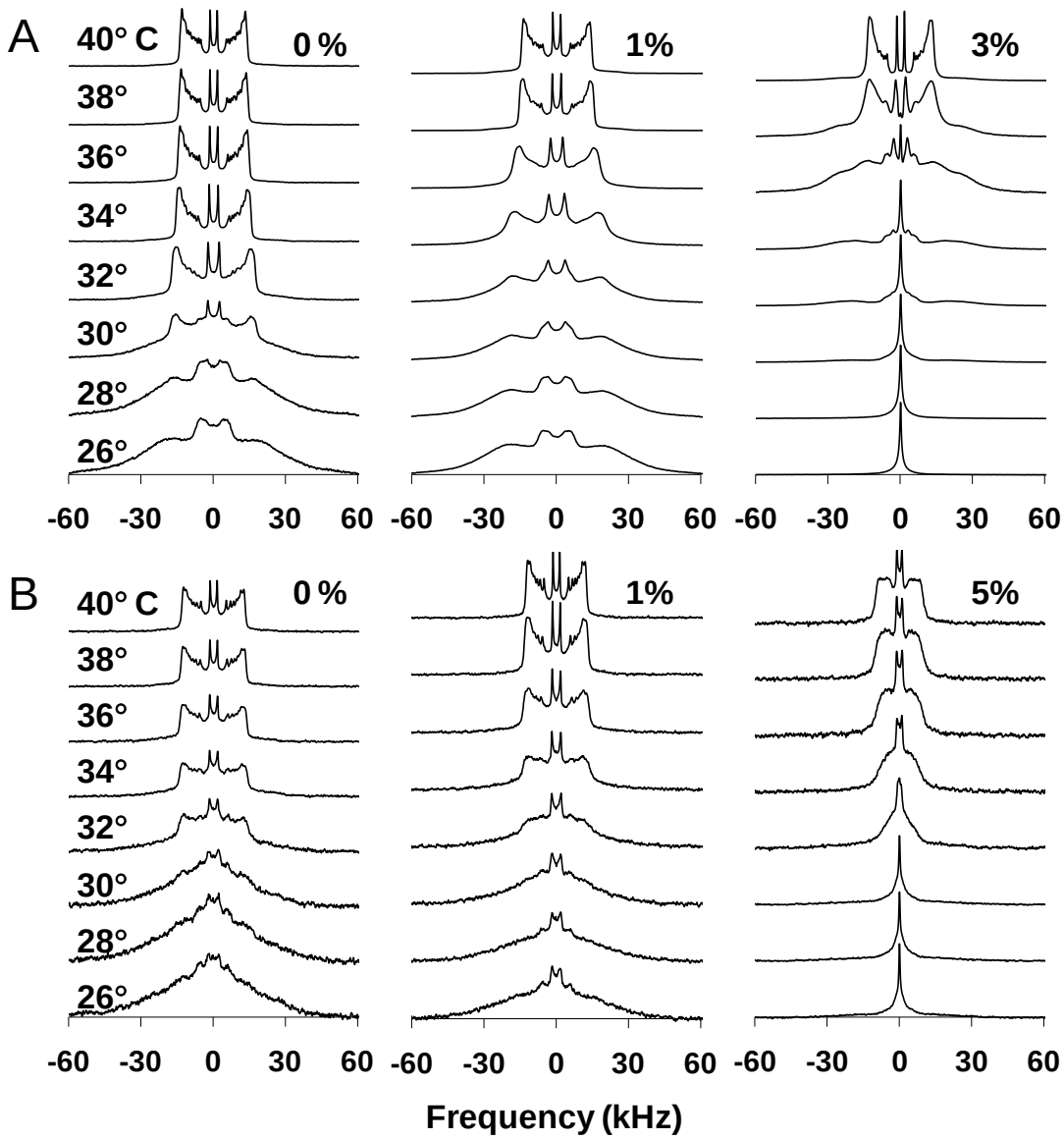

Figure 3-2. Deuterium NMR spectra as a function of temperature for A) 4:1 DPPC-d_{62}/POPG MLVs and B) DPPC/POPG-d_{31} MLVs with SP-B_{1-25} added at the indicated molar percentages.

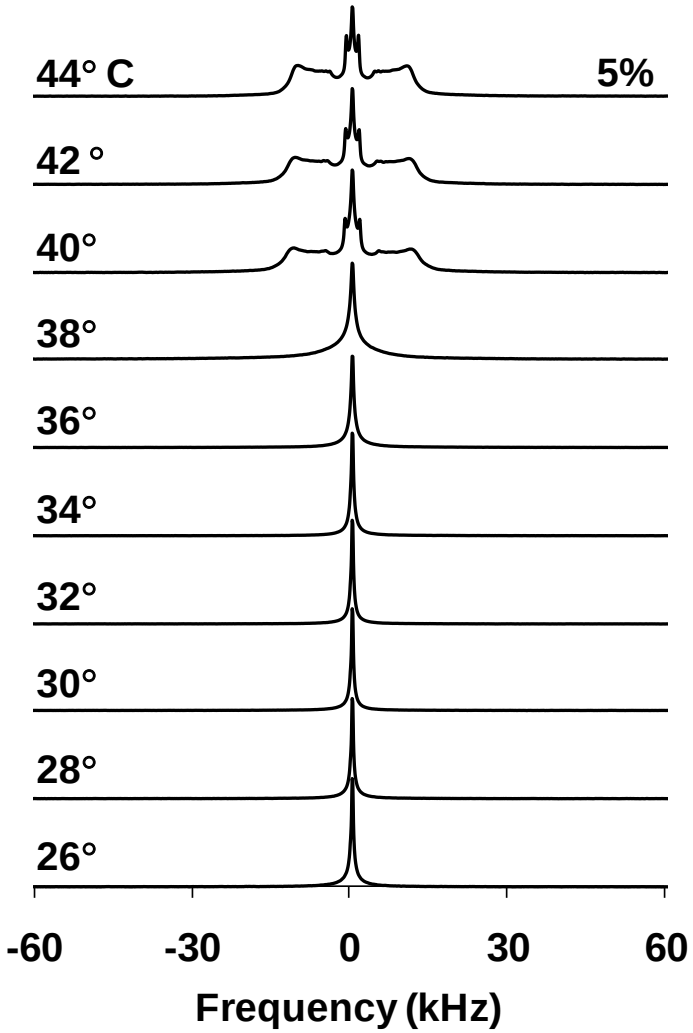

Figure 3-3. Deuterium NMR spectra as a function of temperature for 4:1 DPPC-d_{62}/POPG MLVs with 5% SP-$B_{1\text{-}25}$. An isotropic peak persists until ~ 44°C.

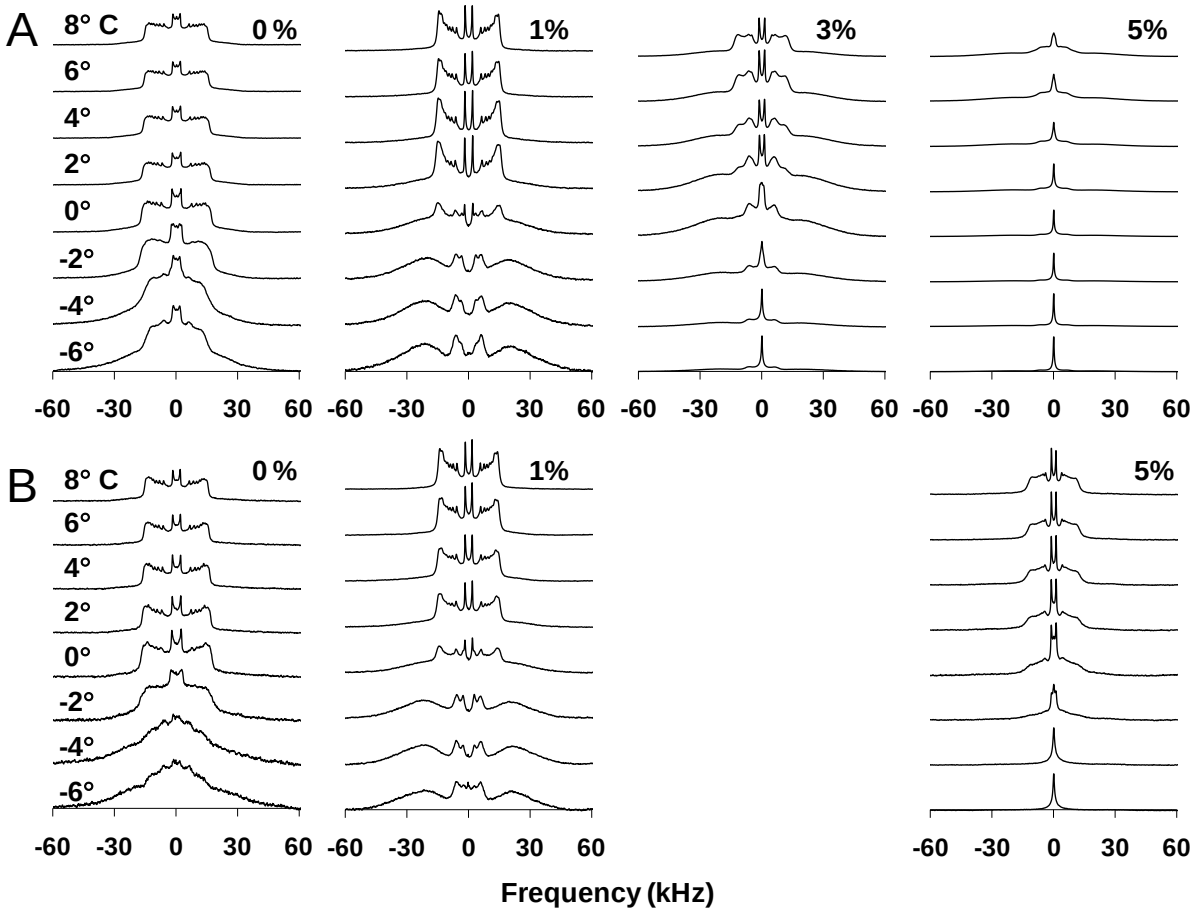

Figure 3-4. Deuterium NMR spectra as a function of temperature for A) 3:1 POPC-d_{31}/POPG MLVs and B) 3:1 POPC/POPG-d_{31} MLVs with SP-$B_{1\text{-}25}$ added at the indicated molar percentages. The temperatures were taken from -6°C to 8°C to allow us to monitor transitions around the melting temperatures of POPC and POPG.

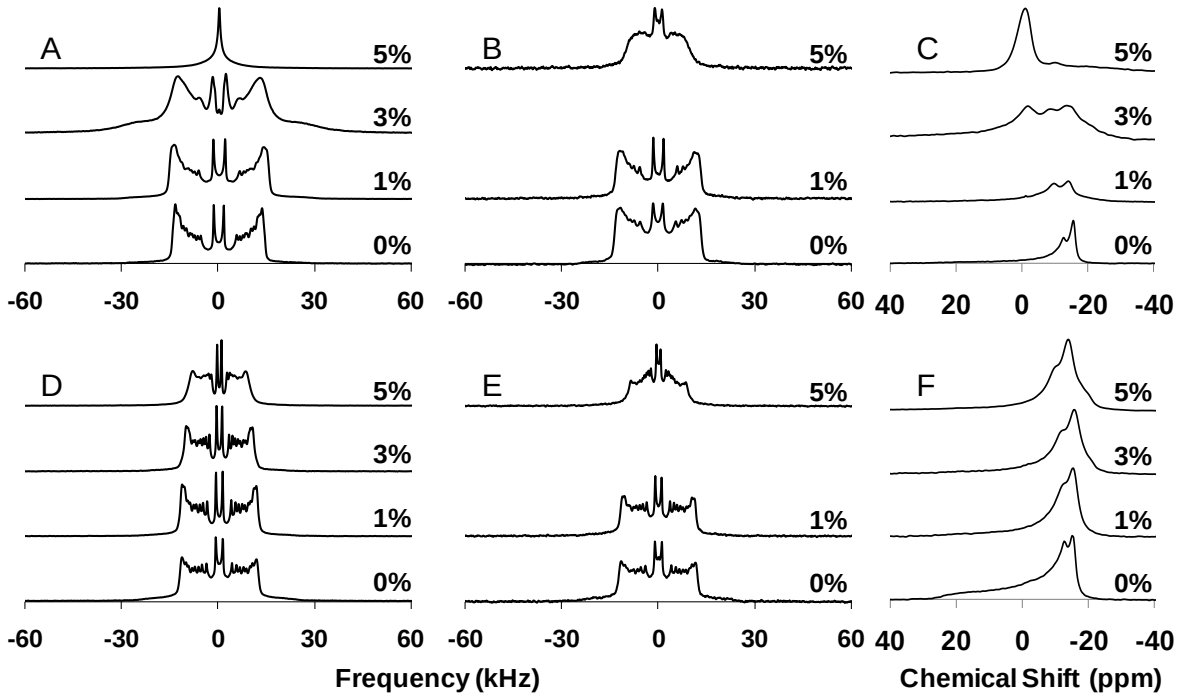

Figure 3-5. Deuterium and phosphorus NMR spectra taken at 38°C. A) ^{2}H spectra of 4:1 DPPC-d_{62}/POPG MLVs, B) ^{2}H spectra of 4:1 DPPC/POPG-d_{31} MLVs, C) ^{31}P spectra of 4:1 DPPC-d_{62}/POPG MLVs, D) ^{2}H spectra of 3:1 POPC-d_{31}/POPG MLVs, E) ^{2}H spectra of 3:1 POPC/POPG-d_{31} MLVs, and F) ^{31}P spectra of 3:1 POPC-d_{31}/POPG MLVs with SP-B_{1-25} at the indicated molar percentages.

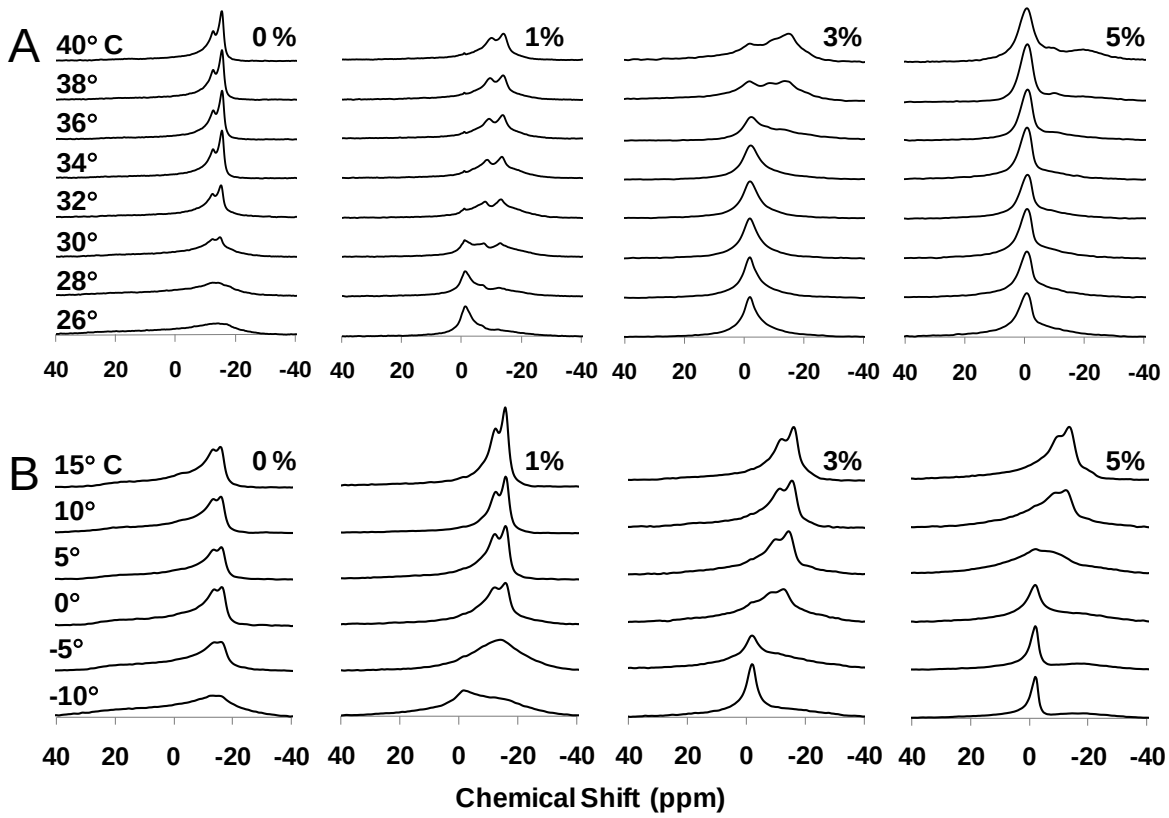

Figure 3-6. Phosphorus NMR spectra as a function of temperature for A) 4:1 DPPC-d_{62}/POPG MLVs and B) 3:1 POPC-d_{31}/POPG MLVs.

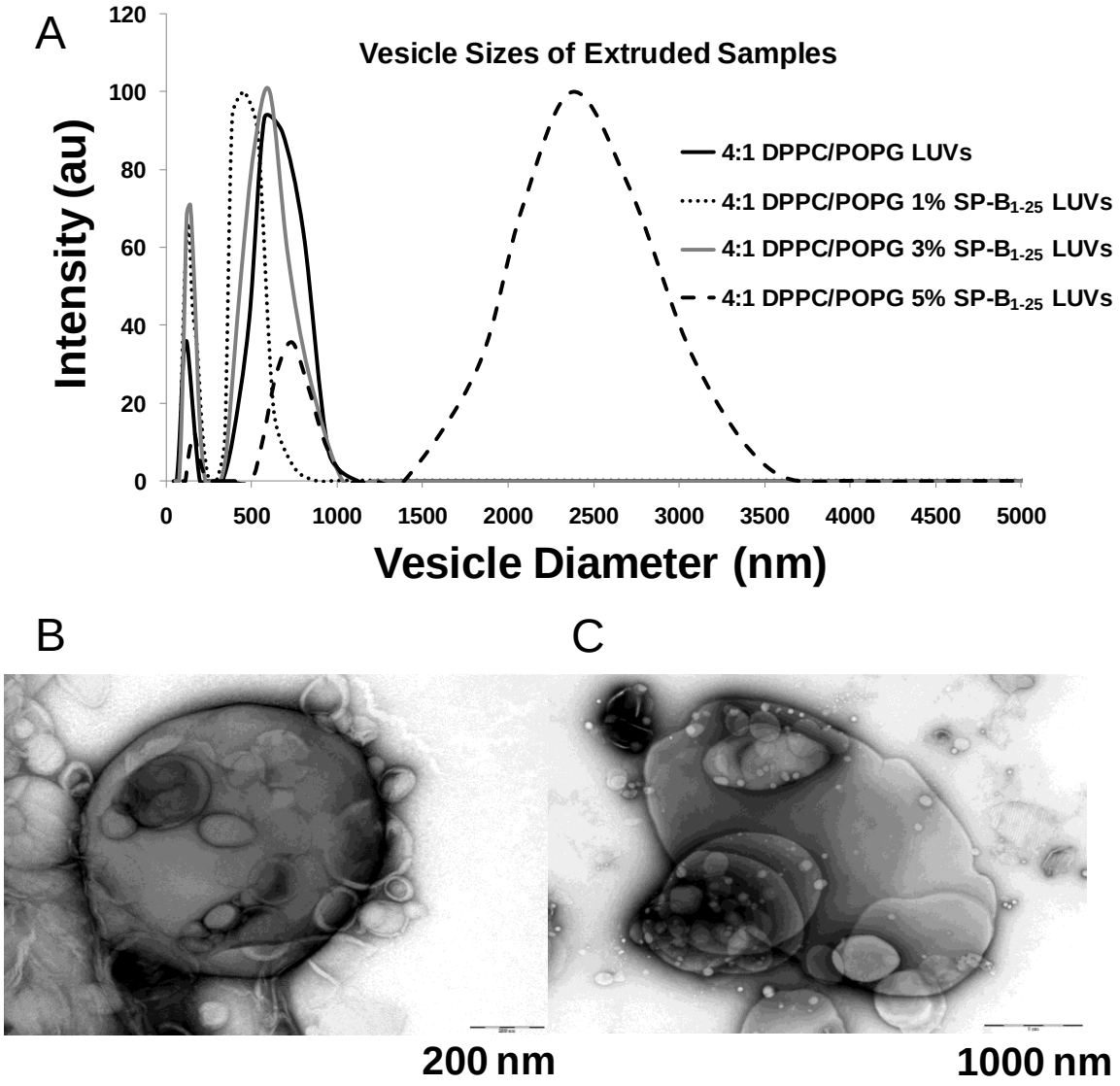

Figure 3-7. A) DLS of 4:1 DPPC/POPG LUVs with 0-5% SP-B_{1-25}. B) EM micrograph of 4:1 DPPC/POPG MLVs C) EM micrograph of 4:1 DPPC/POPG MLVs containing 5 mol% SP-B_{1-25}.

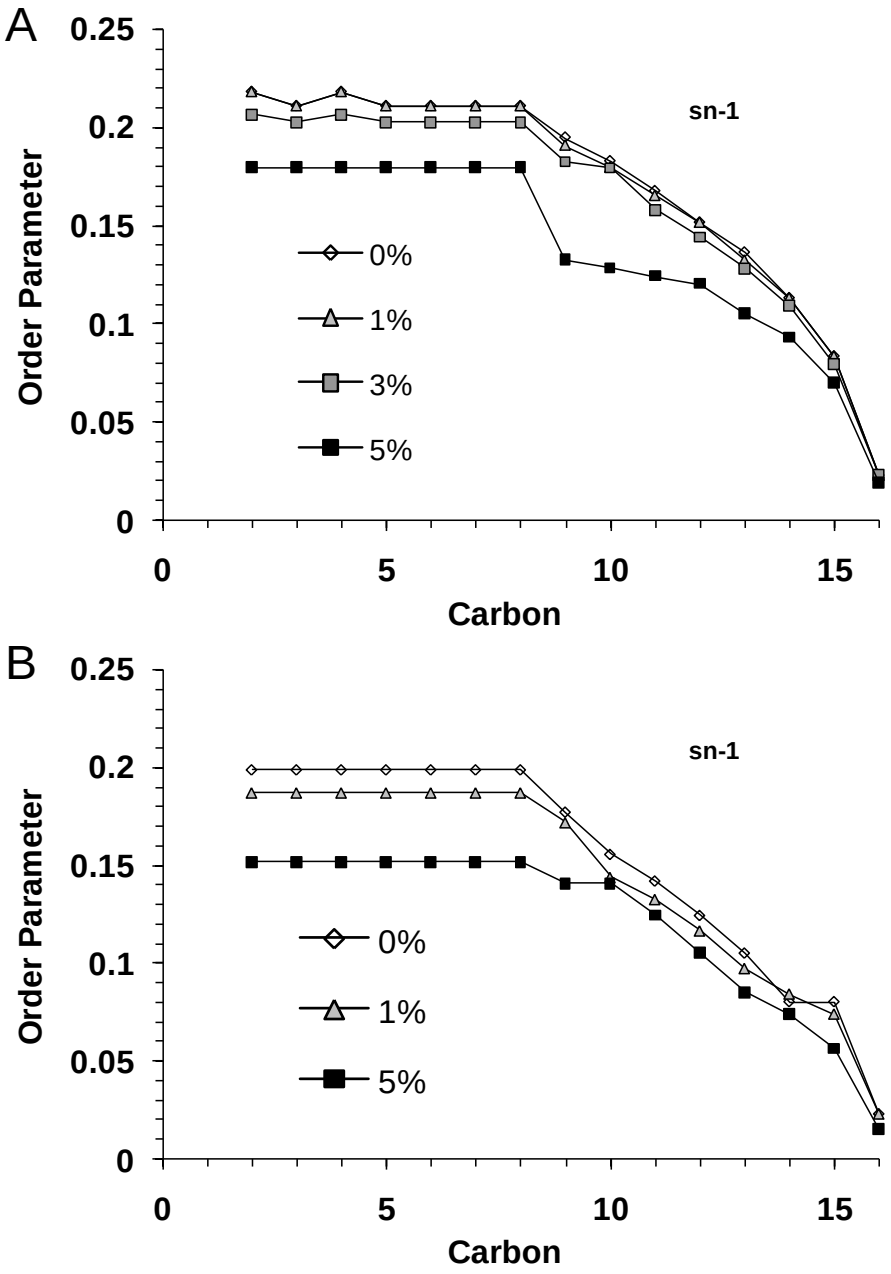

Figure 3-8. Order parameter profiles for the *sn-1* chain of A) DPPC-d_{62} in 4:1 DPPC-d_{62}/POPG and B) POPG-d_{31} in 4:1 DPPC/POPG-d_{31} MLVs at 44°C with SP-B_{1-25} at the indicated molar percentages.

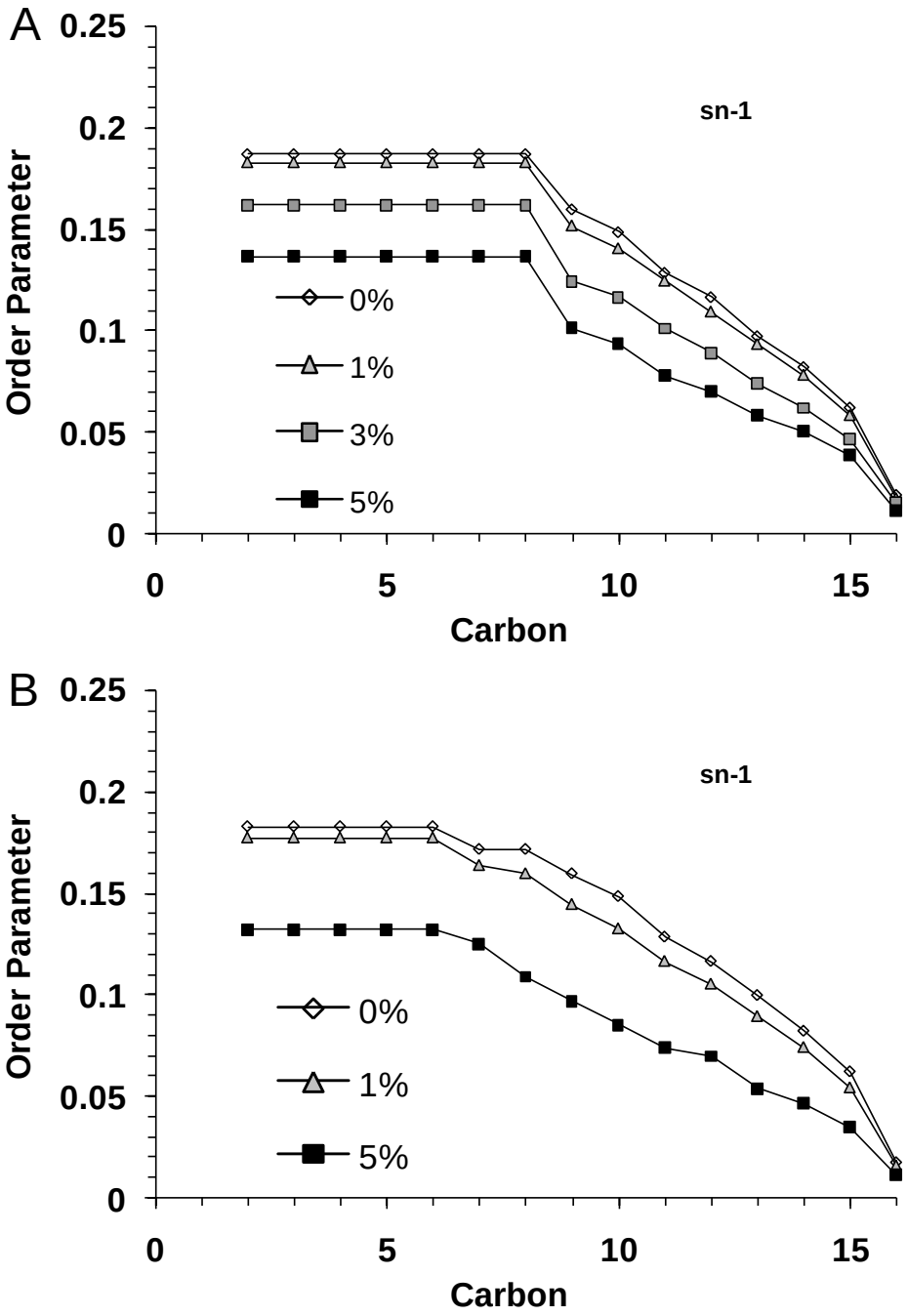

Figure 3-9. Order parameter profiles for the *sn*-1chain of A) POPC-d_{31} in 3:1 POPC-d_{31}/POPG and B) POPG-d_{31} in 3:1 POPC/POPG-d_{31} MLVs at 44ºC with SP-$B_{1\text{-}25}$ at the indicated molar percentages.

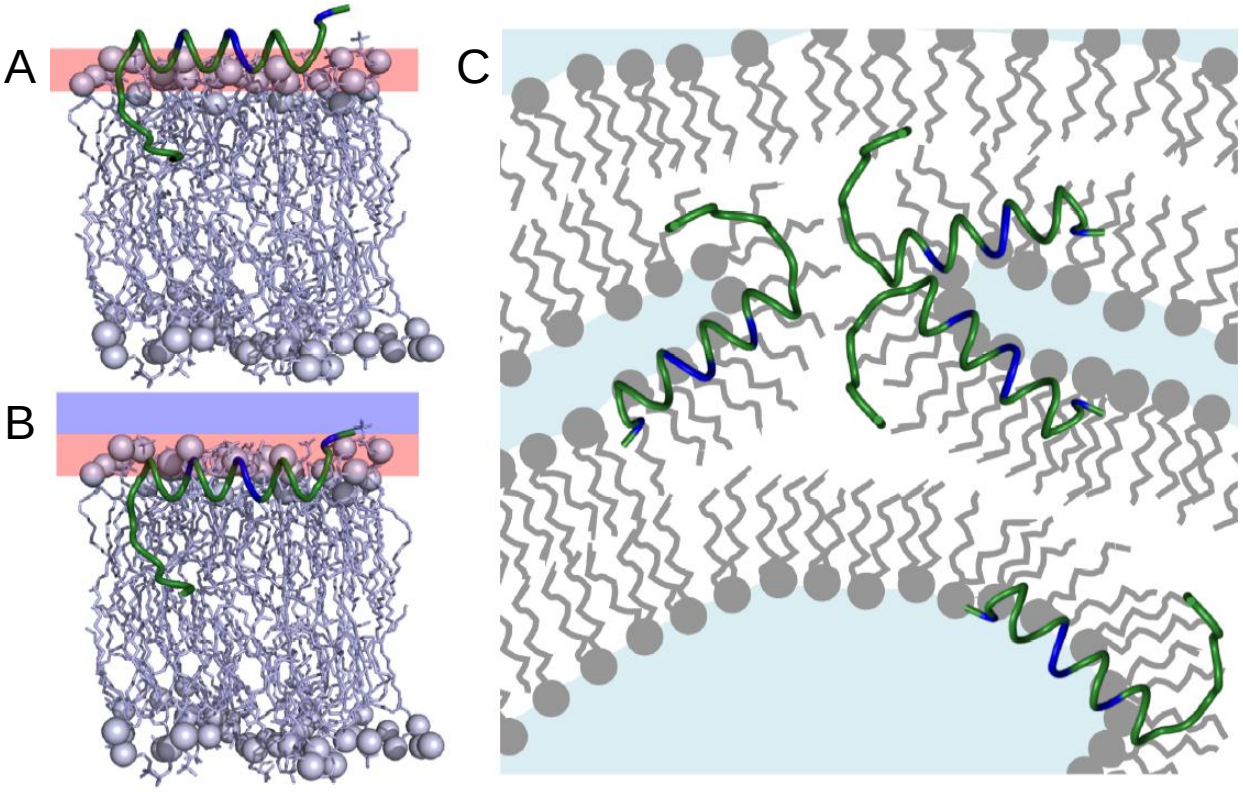

Figure 3-10. Model of SP-B_{1-25} interacting with A) anionic lipids and B) zwitterionic lipids, and C) inducing a fluid isotropic phase in DPPC-rich regions.

CHAPTER 4
COMPARISONS OF CLSE LIPID DYNAMICS TO SYNTHETIC LIPID MIXTURES CONTAINING SP-B_{1-25}

This chapter is a manuscript in preparation for submission to either *Biochemistry* or *Biophysica et Biochimica Acta-Biomembranes*. The final submission may be different from this version due to changes that occur during the peer review process as well as journal formatting differences.

Introduction

Lung surfactant (LS) is a lipid-rich substance containing key proteins that minimizes surface tension in the alveoli. Its lipid composition is highly conserved among mammalian species. However, the lipid composition of LS alone is not sufficient to maintain the organization and dynamics of the lipid assemblies observed in the lung surfactant fluid of intact lung tissue. It has been postulated that protein-induced lipid polymorphisms and trafficking of lipids to the interface are critical for LS function at ambient pressure. In particular, surfactant protein B (SP-B), which is highly hydrophobic and present at low levels, is critical to formation of a stable lipid layer at the air/water interface as demonstrated by in vitro studies. SP-B is absolutely necessary for proper breathing. Several synthetic peptides based on the N- and C- termini of SP-B have shown activity similar to native SP-B and are being pursued as SP-B replacements in synthetic LS formulations for the treatment of respiratory distress syndromes and lung injury, as well as potential drug delivery vehicles.

SP-B_{1-25}, an amphipathic peptide composed of the first 25 amino acids of the N-terminus of SP-B, retains much of the biological activity of SP-B and has shown particular promise as a potential substitute for SP-B in synthetic LS replacement therapy. SP-B_{1-25} is thought to form a secondary structure and conformation similar to

its correlate sequence in the parent protein in the presence of lipids. We have previously characterized SP-B_{1-25} as being ~60% helical in the presence of DPPC/POPG and POPC/POPG unilamellar lipid vesicles and have also observed the induction of uncommon lipid polymorphisms, particularly for DPPC at physiological temperature, by SP-B_{1-25} in these binary lipid systems. This activity may mirror the activity of SP-B in the lung (*15*). In this work, we extend our studies to more complex lipid mixtures which more closely mimic endogenous LS and examine the effects of SP-B_{1-25} on each of the major lipid components of these mixtures. We also characterize the behavior of these same lipids in native LS using calf lung surfactant extract (CLSE) and examine the effect of SP-B_{1-25} in therapeutic CLSE as well as CLSE after the removal of native proteins.

CLSE is a therapeutic surfactant replacement prepared from chloroform extracts of surfactant fluid lavaged from calf lungs. It is commonly administered as a PBS suspension by intratracheal injection into the lungs of premature infants with respiratory distress syndrome under the name *Infasurf*. The lipids in CLSE are unusually surface active and form unique aqueous assemblies due to low levels of surfactant proteins SP-B and SP-C. CLSE contains approximately 93% phospholipid, 5% cholesterol and neutral lipids, and 2% SP-B and SP-C by weight. It is the most successful and widely used surfactant replacement therapy in clinical treatment of ARDS in premature infants.

In this work the properties of individual lipid components in CLSE were investigated and compared to model lipid systems and preparations containing SP-B_{1-25} to guide efforts in developing synthetic lipid/peptide formulations to replace CLSE and other animal derived LS formulations and to better understand the underlying molecular

mechanisms involved in LS function. We utilize ^{2}H and ^{31}P static solid-state NMR to measure lipid phase behavior and dynamics. In particular, ^{2}H NMR is used to distinguish between individual lipid species and investigate lipid acyl chain dynamics and ^{31}P NMR is used to monitor lipid polymorphisms and compare lipid dynamics across sample preparations.

Materials and Methods

Synthesis of SP-B_{1-25}

SP-B_{1-25}, (FPIPLPYCWLCRALIKRIQAMIPKG) was synthesized via automated solid-phase peptide synthesis on a Wang resin (ABI 430, ICBR, UF), cleaved with King's reagent and ether precipitated. Crude product was purified by RP-HPLC using a C18 Vydac column (Grace, Deerfield, IL) with a water/acetonitrile gradient (containing 0.3% TFA). Fractions corresponding to SP-B_{1-25} were collected and purity of the product was verified by mass spectrometry. To ensure only peptide monomers were present, TCEP was added to the peptide in methanol and the monomeric peptide was isolated using a size-exclusion column. The collected monomer fractions were expanded 10 fold in volume with ammonium acetate, pH 8, and compressed air was bubbled through the solution overnight to oxidize the peptide. After this treatment, monomers were observed by non-reducing SDS-PAGE gel analysis and no dimers or other multimers were observed (Figure 4-1). The peptide solution was lyophilized and dried peptide was dissolved in methanol to yield a final concentration of approximately 1 mM and quantitated by UV analysis. A trace amount of TCEP remained and can be seen as a solution NMR resonance in ^{31}P NMR spectra of lipid/peptide preparations. The TCEP likely remains in the aqueous phase of the NMR samples given its polarity and the lack of ^{1}H dipolar couplings observed in ^{31}P spectra.

Calf Lung Surfactant Extract

Research grade calf lung surfactant extract (CLSE) was generously provided as a gift from ONY, Inc. (Amherst, NY). CLSE is a chloroform extract of natural surfactant from calf lungs manufactured by ONY, Inc., as the pharmaceutical drug product *Infasurf*. Upon receipt, the chloroform solution was lyophilized upon arrival for longer storage stability. CLSE contains 93-101 mg/mL of total phospholipid and ~2 mg/mL surfactant proteins B and C (SP-B and SP-C) as indicated on the certificate of analysis from ONY, Inc. For the experiments in this study, CLSE lipids were separated from CLSE proteins after initial characterization of $CLSE^{T}$.

Biochemical Separation of CLSE Lipids and Proteins

The proteins in CLSE were separated from the lipids by gel permeation chromatography using previously established methods (*131*). For each separation, about 200 mg of CLSE in 2 mL of chloroform was loaded onto a 56 x 1.2 cm column containing Sephadex LH-20 (GE Healthcare) and eluted with 95:95:10 chloroform:methanol:0.1 N HCl (v/v/v). Eluent fractions were collected every 2 mL and samples were assayed by phosphate and protein analyses (Figure 4-2). Fractions containing only protein or only phospholipid were pooled and extracted into chloroform to remove acid. Fractions with both lipids and proteins were pooled and concentrated to 2 mL before reloading onto the column. Phosphate and Protein assays determined the successful separation of CLSE lipids and proteins after the second pass through the column. Again, appropriate fractions were pooled and extracted into chloroform. Due to the small, indetectable concentration of cholesterol in the tail end of the eluent with each run, the column was flushed with an additional 150 mL of chloroform:methanol:0.1 N HCl at the end of each separation which was collected and concentrated to recover

the cholesterol. Concentrated cholesterol was identified by TLC and the collected cholesterol was added to the phospholipid fractions. The combined lipid fractions were dried with nitrogen gas and then lyophilized from cyclohexane.

Assays of Phospholipid and Protein Content

Malachite Green reagent was used to quantitate phospholipid content in CLSE fractions. Inorganic phosphate was liberated from the phospholipids by incubation with sulfuric acid at 220°C (*132*) and quantified to determine phospholipid concentration via a colorimetric assay using a reagent known as Malachite Green (Bioassay systems), which forms a green complex between Malachite Green, molybdate, and free orthophosphate. Protein content was assayed via the Amido Black Protein Assay (*133*, *134*). Standard solutions of phosphate and bovine serum albumin were used to calibrate the colorimetric readings. These assays are sensitive to μg quantities and were used as indicators of the presence or absence of phospholipid or protein until CLSE lipids were successfully separated from proteins and the isolates were lyophilized. Actual lipid concentrations for the purpose of making NMR samples were determined after combining all lipid fractions from every pass through the column (~ 2000 mg CLSE) in chloroform at a concentration of ~ 30 mg/mL. The amount of protein isolated was too small for the purposes of this study and was not used further.

Preparation of Synthetic Lipid Mixtures

A purely synthetic surfactant lipid system containing 10:6:3:2:2 DPPC/POPC/POPG/POPE/chol was also studied for comparison to CLSE and earlier studies of the binary mixture 4:1 DPPC/POPG (*13*–*15*). The phospholipids were purchased as chloroform solutions from Avanti, Inc. and mixed after verifying their

concentrations by phosphate analysis (Bioassay Systems, Hayward, CA). Cholesterol was obtained from Avanti, Inc. as a dry powder and dissolved in chloroform. Appropriate volumes of lipid chloroform solutions were mixed to give final lipid molar ratios of 10:6:3:2:2 DPPC/POPC/POPG/POPE/chol for the synthetic LS mimics. Figure 4-42 enumerates the different lipid mixtures discussed in this chapter.

Preparation of NMR Samples

Samples were made with therapeutic CLSE (as received from ONY with both lipids and proteins present), CLSE lipids after removal of proteins, and by combining pure lipids in chloroform based on the lipid composition of CLSE. Acyl chain deuterated lipids, DPPC-d_{62}, POPC-d_{31}, POPG-d_{31}, and POPE-d_{31} were purchased from Avanti (Avanti Polar Lipids, Alabaster, AL) and added to the CLSE and synthetic lipid mixtures as reporters in the ^{2}H NMR experiments. The animal derived LS samples contained 20-50 mg of CLSE (lipids only or with SP-B and SP-C also present) with 2-5 mg added deuterated phospholipid. For peptide containing samples, SP-B_{1-25} in methanol was added to the lipid chloroform solutions resulting in P/L ratios ranging from 1:100 to 1:20. Samples were dried under a stream of nitrogen while in a water bath at 45-50°C; the resulting films were suspended in warm cyclohexane (45-50°C), flash frozen in nitrogen, and lyophilized overnight to remove residual solvent.

For each solid-state NMR sample, ~15-50 mg of peptide-lipid powder was placed in a 5 mm diameter NMR tube and 200 µL of buffer containing 10mM (or 50mM) HEPES, pH 7.4, 140mM NaCl, and 1mM EDTA in ^{2}H depleted water (Cambridge Isotopes, Andover MA) was added. The hydrated dispersions (in NMR tubes) were subjected to 5 freeze-thaw cycles with gentle vortexing to form MLVs

Solid State NMR Analysis

^{31}P and ^{2}H NMR data were collected on a 500 MHz Bruker DRX system (Billerica, MA) using a standard 5 mm BBO probe with the lock channel detuned. For the ^{31}P NMR experiments, data were collected using a Bloch decay (to minimize T_2 relaxation effects due to lipid dynamics); 25 kHz proton decoupling was employed during acquisition to remove dipolar couplings. ^{31}P Spectra were acquired with 256-512 scans and a 5 second recycle delay between scans to minimize RF sample heating. The ^{31}P B_1 field was 52 kHz (4.85 μs 90°pulse). For the ^{2}H NMR experiments, data were collected using a quad echo sequence (90°-τ-90°-τ-acq with τ = 30 μs) with a ^{2}H B_1 field of 42 kHz (5.95 μs 90°pulse). ^{2}H spectra were acquired with 2k-16k scans and a 0.5 second recycle delay between scans.

Results

This study characterizes lipid dynamics in CLSE, compares lipid dynamics in CLSE to a completely synthetic LS mimic system, and examines how lipid dynamics and organization are affected by addition of the LS peptide SP-$B_{1\text{-}25}$ via ^{31}P and ^{2}H static ssNMR experiments. ^{31}P spectroscopy allows monitoring of lipid dynamics and polymorphisms for all lipid species in a given sample while ^{2}H spectroscopy allows monitoring of the dynamics and polymorphisms of individual lipid species that are deuterium enriched and in particular the dynamics of the deuterated lipid acyl chains.

^{2}H NMR Feasibility Measurements

Initial experiments on samples of neat lipids to which a small portion of deuterated lipid of the same type was added were carried out to determine the feasibility of probing the behavior of a small amount of deuterated lipid in a larger environment using NMR, which is an inherently insensitive technique. These experiments were also used to verify

that the phase transition temperatures of the samples were unaffected by addition of a deuterated lipid.

The neat lipids experiments yielded the expected results and demonstrated the small percentages of deuterated lipids used do not alter lipid melting temperatures and are sufficient for collection of adequate NMR spectra in a timely manner. Figure 4-3 shows stack plots of ^{2}H NMR data obtained for DPPC/DPPC-d_{62}, POPC/POPC-d_{31}, POPG/POPG-d_{31}, and POPE/POPE-d_{31} samples as a function of temperature. Each sample contains 5 mg of acyl chain deuterated lipid added to 50 mg of fully protonated lipid, allowing for the monitoring of the deuterated acyl chains within a mostly protonated lipid environment via ^{2}H NMR. The lipid phase transition temperatures were determined from sigmoidal fits to first-moment analyses of spectra collected between -10°C and 55°C for the deuterated lipid in the DPPC/DPPC-d_{62}, POPC/POPC-d_{31}, POPG/POPG-d_{31}, and POPE/POPE-d_{31} samples. The Lα phase transition temperature (T_m) determined for the sample containing deuterated DPPC is 41.4°C, the same melting temperature seen for protonated DPPC as determined by DSC, in contrast to the melting temperature for fully deuterated DPPC which is over five degrees lower (*13*). The T_m determined for deuterated POPE is 28.0°C, while neat POPE is known to melt at ~25°C (*135*, *136*). This discrepancy is likely due to NMR data being collected at 5° intervals. The T_m observed for POPC and POPG are -2.4°C and -2.0°C, respectively, and are reasonable values as these lipids in neat form have been determined to melt at -2°C (*137*). ^{31}P NMR spectra, which monitor both the fully protonated and deuterated lipids, were in agreement with ^{2}H NMR results. POPC and POPG ^{31}P spectra show liquid-crystalline (Lα phase) lineshapes from 0 to 50°C; DPPC and POPE ^{31}P spectra

exhibit gel phase lineshapes below their ^{2}H-NMR-determined transition temperatures and lamellar lineshapes above (Figure 4-4). Above T_m, all lineshapes are lamellar, consistent with lipid bilayers, and do not indicate any other lipid polymorphisms. The phase transition temperature range for all the lipids is very similar to what has been demonstrated with differential scanning calorimetry of protonated lipids (*138*).

Lipid Organization and Behavior in Therapeutic CLSE

Therapeutic CLSE (CLSE as received without separating the hydrophobic proteins and lipids) was combined with low levels of deuterated lipid to probe the behavior of individual lipid species within the CLSE environment, which includes the LS proteins SP-B and SP-C. ^{2}H and ^{31}P NMR spectra of DPPC-d_{62}, POPC-d_{31}, POPG-d_{31}, and POPE-d_{31} containing CLSE^{T} (i.e. four separate samples) were collected at temperatures from -10 to 55°C (Figure 4-5). The phase transition temperatures of the individual lipids were determined by sigmoidal fits to first-moment analyses of the ^{2}H NMR spectra (Figure 4-43). The phase transition of deuterated DPPC is much lower in CLSE^{T} compared to the pure lipid, with deuterated DPPC in the Lα phase above 28.0°C. Deuterated POPE also had a lower T_m at 22.0°C. The T_m of deuterated POPC and POPG are higher compared to the pure lipids at 19.5°C and 21.8°C, respectively. All the lipids clearly transition from gel to liquid-crystalline states between 20 and 30°C at more similar temperatures (compared to neat lipids above) and well below physiologic temperatures. At physiologic temperature, all the lipids exhibit typical lamellar, liquid-crystalline lineshapes.

^{31}P NMR lineshapes for each sample of CLSE^{T} spiked with deuterated lipid are very similar with slight enhancements from the additional lipid showing that adding small

amounts of the individually deuterated lipids to $CLSE^T$ does not change its bulk properties (Figure 4-6). All of the lineshapes indicate the lipids are in the gel phase below 10°C and form liquid-crystalline bilayers well below physiologic temperature. From the ^{31}P data of $CLSE^T$ without any added lipids, it is clear that small amounts of deuterated lipid are not changing the CLSE system (Figure 4-6). Resulting order parameter profiles for the deuterated sn-1 acyl chain in mixtures of $CLSE^T$ with deuterated lipids show higher order parameters for DPPC-d_{62} acyl chains with POPE-d_{31}, POPG-d_{31}, and POPC-d_{31} all having similar, lower acyl chain order parameters, consistent with what is typically observed when comparing saturated to monounsaturated lipids in lipid bilayers of lipid mixtures (Figure 4-7).

Lipid Organization and Behavior of CLSE Lipids After Protein Removal

$CLSE^T$ was subjected to biochemical separation of its hydrophobic constituents via gel permeation chromatography. The lipid constituents of CLSE were combined with individually deuterated lipids and examined by ^2H and ^{31}P NMR spectroscopy. Stack plots of ^2H NMR spectra for $CLSE^T$ and CLSE lipid samples each containing deuterated DPPC-d_{62} are nearly identical as the chromatographic removal of SP-B and SP-C did not significantly change the bulk behavior of DPPC in the two environments (Figure 4-8A). At 25°C in both samples DPPC is in a gel phase. DPPC in the $CLSE^L$ sample melts with a transition midpoint at 28.3°C, which is comparable to the T_m of DPPC in the $CLSE^T$ sample (28.0°C). The deuterated acyl chains also have similar order parameters as seen in Figure 4-8C. Figure 4-9 shows ^{31}P spectra for $CLSE^T$ and $CLSE^L$. The ^{31}P data indicates a slightly larger amount of LPC (lysophosphatidylcholine) lipid species present in the $CLSE^L$ samples compared to the $CLSE^T$ sample, likely due to using two

separate batches of CLSE from ONY to make the samples leading to small differences in the amount of lyso lipids seen as a peak at 0 ppm. The ^{31}P data indicate both lipid environments are in a lamellar phase with a characteristic broad asymmetric lineshape with a low field shoulder and high field sharp peak.

Figure 4-10 shows stack plots of $CLSE^{T}$ and $CLSE^{L}$ with POPC-d_{31}, POPG-d_{31}, or POPE-d_{31} as a function of temperature from 25 to 40°C. From these spectra, we observe that there is little change in the transition temperatures of the lipids between the two CLSE preparations, with the monounsaturated lipids fully melted at 35°C. Small differences are seen between the spectra of the monounsaturated lipids in the two samples, but they primarily arise from differences in bulk alignment of the lipid vesicles, which is very sensitive to bulk hydration rather than differences in lipid dynamics at the molecular level. Depaked spectra, which correct for any changes in bulk alignment, are identical between the two CLSE environments (Figures 4-11, 4-7). All the lipids are in lamellar phases and the monounsaturated lipids have similar order parameters in the presence and absence of low levels of SP-B and SP-C (Figures 4-11, 4-7).

$CLSE^{T}$ preparations contain only ~ 0.2 mol% of SP-B and SP-C. These data indicated that we did not change the lipid phase behavior being studied by removal of the small amounts of SP-B and SP-C. Given the low concentrations of these proteins in CLSE (<0.2 mol%) it is likely their effects on the bulk behavior of the lipids are quite minimal since there are approximately 400-800 lipid molecules for each SP-C or SP-B monomer (*93*). The possibility exists that the proteins are trafficking a small percentage of lipids in the bulk lamellar sample, which is undetectable via the solid-state NMR experiments. The next experiments involved the addition of the LS peptide, $SP\text{-}B_{1\text{-}25}$,

into the CLSE lipid system to measure how this peptide affects lipid dynamics of CLSE lipids. This also allows us to change the peptide/lipid ratio of the samples enough to affect the bulk behavior of the lipids to develop a model of how the lower levels of SP-B may traffick lipids.

Addition of SP-B_{1-25} to CLSE Lipids

The dynamics of DPPC in $CLSE^T$ and the $CLSE^L$ system with 5 mol% SP-B_{1-25} present were studied via ^2H and ^{31}P to measure if a larger concentration of a LS peptide has distinguishable effects on the bulk properties of the lipid in the two CLSE environments. ^2H NMR spectra of DPPC in the two CLSE environments are indistinguishable, but now DPPC remains in a gel phase from 26 to 40°C (Figure 4-12). ^{31}P spectra of $CLSE^T$ and $CLSE^L$ containing 5 mol% SP-B_{1-25} also exhibit very similar lineshapes with a lamellar phase seen at physiologic temperatures, suggesting the monounsaturated lipids are phase separating from DPPC. These data further indicate that we did not change the lipid phase behavior being studied by removal of the small amounts of SP-B and SP-C; when a large amount of SP-B_{1-25} is contained in the sample the two CLSE environments remain indistinguishable.

Temperature and SP-B_{1-25} concentration-dependent behavior of deuterated DPPC is shown in Figure 4-13. Shown in Figure 4-13A are stack plots of $CLSE^L$ with deuterated DPPC with 0-5 mol% SP-B_{1-25} as a function of temperature from 26 to 40°C. The T_m of DPPC-d_{62} increases from 28.3 to 39.1°C with increasing peptide concentration from 0 to 5 mol%. By eye the difference in lipid dynamics are best distinguished at 40°C as the lamellar lineshape for 0 and 1% peptide are very similar and become less resolved with 3 and 5% peptide. The width of the lineshapes is the

same and the intensity of the interior peaks corresponding to the 16 carbon position for the 5% data has decreased. Moreover, the order parameters decrease with increasing peptide concentration as measured by ^{2}H NMR experiments (Figure 4-13C). Also shown are the corresponding ^{31}P spectra that agree with the ^{2}H NMR data by showing lamellar lineshapes with gel phases below the T_m (Figure 4-14).

Shown in Figure 4-15A are stack plots of CLSE^{L} with deuterated POPC with 0-5 mol% SP-B_{1-25} as a function of temperature from 26 to 40°C. The lineshapes for POPC-d_{31} without peptide and with 1 mol% peptide appear the same, however when 3% SP-B_{1-25} is present in the sample the lipid dynamics do change significantly with narrowing of the lineshapes at lower temperatures that gradually widen near physiologic temperature. SP-B_{1-25} has the greatest effect on POPC dynamics at 5 mol% concentration. At this concentration, the peaks are sharper and narrower indicating greater fluidity of POPC in the CLSE^{L} environment when larger amounts of SP-B_{1-25} are present. The phase transitions of these lipids is below 26°C and the spectra indicate solely a liquid-crystalline lamellar phase for POPC up to 40°C. Figure 4-15C shows order parameters for POPC in the CLSE environment with 0-5 mol% SP-B_{1-25}. The order parameters decrease with increasing peptide concentration, which has been true for all samples in this study. Figure 4-16 shows the ^{31}P spectra for CLSE^{L} spiked with POPC-d_{31} with 0-5 mol% SP-B_{1-25} as a function of temperature from 26-40°C. As expected, the lineshapes are identical to those when the CLSE lipid system contains a small amount of DPPC-d_{62} because ^{31}P NMR measures the polymorphisms and dynamics of all the phosphorus atoms and not only the deuterated chains as in ^{2}H NMR.

Figure 4-17A shows stack plots of $CLSE^L$ containing deuterated POPG with 0-5 mol% SP-B_{1-25} as a function of temperature from 26 to 40°C. The lineshapes for POPG-d_{31} with 1 mol% peptide look very similar to that when peptide is not present, however when 3% or 5% SP-B_{1-25} is present in the sample the lipid dynamics do change with narrowing of the lineshapes at lower temperatures that gradually widen near physiologic temperature as they did in the POPC samples. SP-B_{1-25} has the greatest effect on POPG dynamics at 5 mol% concentration. At this concentration, the peaks are sharper and narrower indicating greater fluidity of POPG in the $CLSE^L$ environment when larger amounts of SP-B_{1-25} are present, but other than being slightly narrower they do not appear much different than when 3% peptide is in the sample. The phase transitions of POPG is below 26°C and the spectra indicate solely a liquid-crystalline lamellar phase for POPG up to 40°C. Figure 4-17C shows order parameters for POPG in the CLSE environment with 0-5 mol% SP-B_{1-25}. The order parameters decrease with increasing peptide concentration. Figure 4-18 shows the ^{31}P spectra for $CLSE^L$ spiked with POPG-d_{31} with 0-5 mol% SP-B_{1-25} as a function of temperature from 26-40°C. The lineshapes are identical to those when the CLSE lipid system contains a small amount of DPPC-d_{62} or POPC-d_{31} as ^{31}P NMR measures the polymorphisms and dynamics of all the phosphorus atoms.

Stack plots of $CLSE^L$ with deuterated POPE with 0-5 mol% SP-B_{1-25} as a function of temperature from 26 to 40°C are shown in Figure 4-19A. The lineshapes for POPE-d_{31} with 1 mol% peptide look very similar to the 0% data, however when 3% or 5% SP-B_{1-25} is present again a significant change in lipid dynamics is seen. SP-B_{1-25} has a different effect on POPE dynamics at 3 mol% peptide concentration. At this

concentration, the peaks are less resolved. However, they keep the same width and intensity as the samples with smaller peptide concentrations. It is possible that with 3 mol% SP-B_{1-25} the lipids are fully mixed with the peptide and are flipping between bilayers. With 5% peptide the peaks are sharper and narrower indicating greater fluidity of POPE in the $CLSE^{L}$ environment when larger amounts of SP-B_{1-25} are present. The 5 mol% peptide concentration could be causing phase separation of the lipids instead of lipid flipping as may be the case with 3 mol% peptide. The phase transitions of POPE is below 26°C and the spectra indicate POPE remains in a liquid-crystalline lamellar phase up to 40°C, except for the 3% sample. Figure 4-19C shows order parameters for POPE in the CLSE environment with 0-5 mol% SP-B_{1-25} at 40°C. Again, the order parameters decrease with increasing peptide concentration, much like what was seen for DPPC-d_{62}, POPC-d_{31}, and POPG-d_{31} in the CLSE lipid system. Figure 4-20 shows the ^{31}P spectra for $CLSE^{L}$ spiked with POPE-d_{31} with 0-5 mol% SP-B_{1-25} as a function of temperature from 26-40°C. The lineshapes are mostly identical to those when the CLSE lipid system contains a small amount of DPPC-d_{62}, POPC-d_{31}, or POPG-d_{31} with the exception of one peak close to 20 ppm in the 5% spectra. The 20 ppm peak is an anomaly of a different batch of SP-B_{1-25} WT used to make the sample, which contained a higher level of TCEP.

Of particular interest is the data for the CLSE lipid system containing 5 mol% SP-B_{1-25} with deuterated POPC, POPG, or POPE compared to spectra of DPPC (Figure 4-21), which were shown in the concentration dependent plots and is now being shown side-by-side. In contrast to the monounsaturated lipids, DPPC is affected the most by the LS peptide, remaining in the gel phase above physiologic temperature as seen

previously in Figure 4-12 in the comparison to $CLSE^{T}$. The monounsaturated (POPC, POPG, and POPE) lipid lineshapes are narrower, indicating increased fluidity, and remain in a liquid-crystalline phase from 26 to 40°C unlike DPPC which is not fully melted at physiologic temperature. SP-B_{1-25} may be targeting DPPC the most out of all the CLSE lipids and causing an increased phase transition temperature.

Comparing only the samples of $CLSE^{L}$ with deuterated DPPC, POPC, POPG, and POPE with 0-5 mol% SP-B_{1-25} at physiologic temperature (37-38°C), it becomes clear that peptide introduction affects DPPC dynamics the most with the exception of the sample containing deuterated POPE with 3% SP-B_{1-25} (Figure 4-22). The spectra for $CLSE^{L}$/DPPC-d_{62} with 3% SP-B_{1-25} is very similar to the lineshape at 3% peptide when POPE-d_{31} is in the $CLSE^{L}$ environment.

Fully Synthetic Lipid Systems

The predominantly endogenous CLSE lipid system was also compared to a fully synthetic LS system containing a lipid combination that mimics the major lipids of CLSE (DPPC, POPC, POPG, POPE, and cholesterol), which allows full knowledge of the lipid composition in the sample and better control of relative concentrations. Throughout this chapter synthetic CLSE ($CLSE^{Syn}$) will refer to a 10:6:3:2:2 molar ratio lipid combination of DPPC/POPG/POPG/POPE/cholesterol for simplicity.

Figure 4-23 shows stack plots of $CLSE^{Syn}$ (10:6:3:2:2 DPPC/POPC/POPG/POPE/cholesterol) with DPPC-d_{62}, POPC-d_{31}, POPG-d_{31}, or POPE-d_{31} as a function of temperature from 26 to 40°C (one of the lipids in the mix is deuterated in each sample to ascertain individual lipid dynamics). From these spectra, we observe that there is little change in the lipid dynamics among the individual lipid

species, with all lipids in a lamellar phase and fully melted well below physiologic temperature. The only differences seen are a slightly broader lineshape for DPPC at lower temperatures and a little more noise in the POPE spectra due to low amounts of POPE-d_{31} in the sample. To reiterate the similarity of the multiple lipid samples, ^{31}P spectra are shown for each sample and are identical as ^{31}P NMR measures the polymorphisms and dynamics of all the phosphorus atoms and slight enhancements of a deuterated lipid do not make a large difference in the overall dynamics of the system or appearance of the spectra. This allows us to monitor different polymorphisms for the whole lipid system using ^{31}P NMR and individual lipid dynamics and polymorphisms for deuterated lipids using ^{2}H NMR.

DePaked spectra for DPPC-d_{62} in several lipid environments are shown in Figure 4-25A. The four broader spectra at the top all contain cholesterol; lack of cholesterol leads to considerably narrower spectra. More importantly, the dePaked spectra of DPPC-d_{62} in the CLSE^{Syn} and CLSE^{L} are almost indistinguishable. This results in order parameter profiles which are similarly indistinguishable (Figure 4-25B). A ternary lipid system, DPPC/POPG/cholesterol discussed below, shows slightly more order and the cholesterol-lacking mixtures exhibit less order.

DePaked spectra for POPC-d_{31} in several lipid environments are shown in Figure 4-26A. Again, a clear distinction can be seen between cholesterol-containing and cholesterol-free samples, but POPC-d_{31} in CLSE^{Syn}, CLSE^{T}, and CLSE lipid environments exhibit dynamics which are indistinguishable. Also worth noting is the similarity seen between the dePaked spectra of POPC-d_{31} in the binary POPC-d_{31}/POPG lipid environment and in the CLSE^{L} system when 5 mol% SP-B_{1-25} is present

(Figure 4-15). Adding SP-B to the $CLSE^{L}$ system eventually causes the lipids to return to the monounsaturated binary lipid state that does not contain cholesterol. This is only the case for the monounsaturated lipids. The order parameter profiles for POPC-d_{31} shown in Figure 4-26B quantitate the increased order for the multiple and CLSE lipid samples compared to the binary lipid system, POPC-d_{31}/POPG, and the neat POPC/POPC-d_{31} lipid combination.

DePaked spectra for POPG-d_{31} in several lipid environments are shown in Figure 4-27A. Again, when cholesterol is not present the spectra are narrower. However, the depaked spectra of the $CLSE^{Syn}$ and $CLSE^{L}$ are not completely indistinguishable as was seen for DPPC-d_{62} and POPC-d_{31} and this is reflected in the order parameters shown in Figure 4-27B. The order parameter profiles for POPG-d_{31} show slightly increased order for the multiple and CLSE lipid samples relative to the $CLSE^{T}$ samples. The two monounsaturated binary lipid systems exhibit the least degree of order for POPG-d_{31} with the binary DPPC/POPG-d_{31} showing a higher degree of order as would be expected given DPPC with two saturated acyl chains is the predominant lipid in this mixture.

DePaked spectra for POPE-d_{31} in several lipid environments are shown in Figure 4-28A. The trend for POPE-d_{31} is a little different than what was seen for DPPC-d_{62}, POPC-d_{31}, and POPG-d_{31}. The width of the dePaked spectra is similar for each lipid system but neat POPE is more ordered than all of the other POPE-d_{31}/lipid system combinations. Consequently, the presence of cholesterol does not make a large difference in these samples. This is likely due to the fact that the smaller headgroup in

POPE allows the molecules in the neat POPE sample to pack more tightly, restricting the dynamics of the acyl chains.

Addition of SP-B_{1-25} to Synthetic Lipids and Comparison to CLSE Lipid Systems

In Figure 4-29 are shown ^{2}H NMR spectra of deuterated DPPC in the CLSE and multiple (DPPC-d_{62}/POPC/POPG/POPE/cholesterol) lipids systems with 0-5% SP-B_{1-25} as a function of temperature. The $CLSE^{Syn}$ data reflect a much lower T_m (below 26°C) for DPPC in the $CLSE^{Syn}$ samples relative to DPPC in the CLSE lipid environment, which melts at 28.3°C in the absence of peptide. With the addition of SP-B_{1-25}, the T_m of DPPC in $CLSE^L$ increases from 31.5 to 33.2 to 39.1°C with 1 mol%, 3 mol%, and 5 mol% peptide, respectively. Of particular interest is the addition of SP-B_{1-25}, which raises the melting temperature of DPPC in the multiple lipid samples as well as with the 3 mol% peptide sample exhibiting behavior very similar to the 3 mol% SP-B_{1-25}/$CLSE^L$ sample. In both multiple and CLSE lipid environments exchange broadening is seen with increased peptide concentration at 3-5 mol% peptide. These lineshapes indicate that the DPPC dynamics in the synthetic multiple lipid samples very closely mimic those observed in lipid mixtures isolated from CLSE. Additionally, the multiple lipid samples show the same trend of decreasing order in the DPPC acyl chains with increasing peptide concentration (Figure 4-30) as seen in all order parameter plots showing samples containing SP-B_{1-25}.

Figure 4-31 shows ^{2}H NMR spectra for POPC-d_{31} in CLSE and multiple synthetic lipid environments with 0-5 mol% SP-B_{1-25} as a function of temperature. POPC melts below 26°C in both of these systems and its spectra look very similar between the two lipid preparations as again there are no uncommon polymorphisms. For both the

multiple and CLSE lipid systems, addition of SP-B_{1-25} leads to decreasing order in POPC-d_{31} (Figure 4-32). However, with the $CLSE^{Syn}$ addition of SP-B_{1-25} leads to lipid behaviors similar to what was observed for DPPC-d_{62}; this is not seen for the CLSE lipid samples indicating more lipid phase separation in the $CLSE^{L}$ environment.

Figure 4-33 contains ^{2}H NMR spectra of POPG-d_{31} in the $CLSE^{L}$ and $CLSE^{Syn}$ (10:6:3:2:2 DPPC/POPC/POPG-d_{31}/POPE/cholesterol) environments with 0-5% SP-B_{1-25} as a function of temperature. The lineshapes for POPG-d_{31} look similar to those for POPC-d_{31} with increasing peptide concentration causing the lineshapes to narrow, meaning more motion for POPG in the LS systems. Again, lipid phase separation is not seen as clearly in the multiple lipid system at the lower temperatures and peptide concentrations (Figure 4-33). The order parameter profile for the deuterated POPG acyl chains are shown in Figure 4-34.

Comparing spectra at physiologic temperature, 1 mol% SP-B_{1-25} does not have a significant effect on the dynamics of the deuterated lipids in the $CLSE^{Syn}$ environment, similar to what is observed for $CLSE^{T}$ and $CLSE^{L}$ systems. At 3 mol% peptide the lipid phase behavior changes for DPPC-d_{62}, but not for POPC-d_{31} and POPG-d_{31}. At 5 mol% peptide DPPC-d_{62} is most affected and overall the ^{2}H NMR spectra for DPPC-d_{62} exhibits the most change with increasing concentration of SP-B_{1-25}, but POPC-d31 and POPG-d_{31} also exhibit non-Lα phase lineshapes (Figure 4-35). The behavior of POPC-d_{31} and POPG-d_{31} in the multiple lipid environment compared to $CLSE^{T}$ and $CLSE^{L}$ suggest minor components in endogenous CLSE, such as lysolipids or palmitic acid, may aid DPPC phase separation from the other lipids.

Addition of SP-B_{1-25} to the 8:2:1 DPPC/POPG/cholesterol LS Lipid System

The cholesterol in the CLSE samples affected the T_m and order of the deuterated lipids and we saw the same effects in ternary lipid systems containing cholesterol. Figure 4-36 (top) shows stack plots of ^{2}H NMR spectra for 8:2:1 DPPC-d_{62}/POPG/cholesterol with 0-5 mol% SP-B_{1-25} as a function of temperature from 26 to 40°C. Without peptide, DPPC behaves much like it does in the previous lipid systems melting at 29.9°C (Figure 4-44). However, once SP-B_{1-25} is in the mix phase transition temperatures increase. Interestingly, the 5% sample shows phase separation with an isotropic and gel phase combination at 26°C that persists up to 40°C with gradual narrowing of the outside edges of the lineshape for DPPC-d_{62}. The order of the acyl chains also increases which can be attributed to the cholesterol content. Increased amount of peptide causes the order to decrease for DPPC-d_{62} (Figure 4-37). Previous studies of DPPC/POPG lipid systems with 0-5% SP-B_{1-25} (Chapter 3) also show polymorphisms with increased peptide concentration. However, when cholesterol is present the effect is different. There is a loss of the isotropic peak for the 3% sample and phase separation seen that was not previously measured for the 5% sample although the isotropic peak persists.

Figure 4-36 (bottom) shows stack plots of ^{2}H NMR spectra for 8:2:1 DPPC /POPG-d_{31}/cholesterol with 0-5 mol% SP-B_{1-25} as a function of temperature from 26 to 40°C. This ternary lipid samples with POPG behaves more like the DPPC-d_{62}/POPG lipid system (Chapter 3). POPG melts at ~ 32°C when peptide is not present and the T_m increases with larger concentrations of peptide. At 3 mol% an isotropic peak is observed at 26°C and again at 5 mol% from 26°C to 38°C with the single peak slightly

diminishing at 40°C as POPG transitions into a gel phase. Figure 4-38 shows dePaked spectra and order parameters for POPG-d_{31} in the ternary lipid system, which exhibit the same trends of decreased order with increased peptide content and higher order when cholesterol is present.

The ^{31}P NMR data for both for 8:2:1 DPPC-d_{62}/POPG/cholesterol and 8:2:1 DPPC /POPG-d_{31}/cholesterol with 0-5 mol% SP-B_{1-25} as a function of temperature from 26 to 40°C agree with the ^{2}H data showing both lamellar and isotropic lineshapes at the same temperatures and peptide concentrations (Figure 4-39).

Discussion

The experiments delineated in this study had two major purposes. The first was to guide efforts in developing synthetic lipid/peptide formulations to replace CLSE and other animal derived lung surfactant formulations; the other was to better understand the underlying molecular mechanisms involved in lung surfactant function. With research grade CLSE generously provided by ONY, Inc., we set out to systematically characterize the major lipid constituents of this animal derived lung surfactant replacement and gather information about individual lipids in the CLSE environment.

In prior work we have shown that an analogue of SP-B, SP-B_{1-25}, affects the dynamics of LS lipids in binary lipid systems, particularly the disaturated DPPC as we observed an isotropic phase for its ^{2}H ssNMR spectra as it persisted through physiologic temperature with the addition of 5 mol% SP-B_{1-25} (*15*). With evidence of unusual polymorphisms for lung surfactant mimics, we proceeded to develop a model of lipids fusing together to form a fluid isotropic phase when greater amounts of SP-B_{1-25} are present. With this new perspective on lipid structures in LS, we asked whether such

a model could apply to a clinically used, non-synthetic LS mimic derived from bovine lungs. We wanted to test if our LS system is anything like clinically used endogenous based LS.

Lung surfactant replacements currently used in clinical settings vary in origin, composition, and effect (*41*). There are several LS formulations used today to combat RDS, however they raise concerns regarding purity, immunogenicity, and uniformity. The experiments utilized in this work took advantage of a bovine originating surfactant obtained via bronchiolar lavage. This extract, calf lung surfactant extract or CLSE, is analogous to the clinically used drug, *Infasurf*, which has shown evidence of being the closest formulation to native surfactant available on the market. Its SP-B concentration is the closest to native surfactant (*50*). However, CLSE is an animal-derived formulation, posing risk of immune response and infection (*36*, *98*). One purpose of this study was to aid in developing synthetic LS replacement formulations that show similar activity to animal-derived LS replacements such as CLSE. Current clinically used LS replacements have great efficacy, however a synthetic replacement would be ideal as it would be more stable, having a longer shelf-life, in addition to not posing a risk of immune response and infection. Our beginning efforts with this goal involved systematically characterizing the individual CLSE lipids.

Our initial characterization of CLSE via ^{2}H ssNMR showed that the phase behaviors of deuterated lipids in $CLSE^{T}$ are similar and exhibit a broad phase transition range (Figure 4-5). The broad T_m range from 10-30°C is consistent with what has been observed in DSC traces of LS extracts (*139*). While only lamellar phases were seen in these data, making the data seem rather unremarkable at first glance, the T_m for DPPC

was higher than the monounsaturated lipids. This first spark of interest caused by a difference in DPPC melting temperature (while also somewhat similar to the monounsaturated lipids as all the lipids had broad melting temperature ranges) led us to further investigate the CLSE lipids without protein present to find any differences between protein containing CLSE, $CLSE^{T}$ (therapeutic) and without protein, $CLSE^{L}$ (lipids only).

We removed the surfactant proteins, SP-B and SP-C, from CLSE by gel permeation chromatography, which separates molecules by size as they migrate down a gel filled column. The $CLSE^{L}$ system obtained from the separation technique proved to be indistinguishable from $CLSE^{T}$ as seen by ^{2}H NMR lineshapes and order parameters (Figures 4-8 and 4-10). This led us to investigate a fully synthetic LS formulation based on the main lipids of CLSE, $CLSE^{Syn}$, as a confirmation of the absence of protein in $CLSE^{L}$ and to mimic the CLSE lipid system synthetically.

Also, worth noting is the effect of cholesterol on DPPC behavior, which has been previously studied in cholesterol/DPPC mixtures via ^{2}H NMR and DSC (*140*). There are three phases identified for mixtures of cholesterol and DPPC: the first two are the liquid-crystalline ($L\alpha$) and gel phase and the third is the high cholesterol concentration phase, which is characterized by higher ordered acyl chains and rapid axially symmetric reorientation. In the cholesterol/DPPC study, Davis and Vist identified regions of two-phase coexistence and saw an obvious change in the $L\alpha$ phase as an increase in order of the lipid chains, which has been demonstrated in even earlier work (*141–144*). The increase in chain order indicates an increase in bilayer thickness and a study by Brown and Seelig using ^{2}H NMR head-group labeled DPPC suggests increased motional

freedom from a lack of tight packing in the head-group region (*145*). Cholesterol acts in phospholipid bilayers to increase thickness (hence increased order parameters) or strength of the bilayer while keeping the lipid environment fluid. Davis and Vist saw a gel phase/high cholesterol concentrated phase region below 37°C for 7.5 to 22.5 mol% cholesterol and above 37°C they saw a liquid-crystalline/high cholesterol concentrated phase from 7.5 to 10 mol%. The two phase Lα/cholesterol existence was first discussed in the Davis and Vist publication.

The work by Davis and others has shown that cholesterol effects lipid bilayers and has a larger effect on DPPC. The native CLSE and $CLSE^{Syn}$ samples in this chapter contained ~ 8-10 mol% cholesterol and ~ 40-43 mol% DPPC. The ternary lipid mixture contained 9 mol% cholesterol and 73 mol% DPPC. The data suggest the more DPPC contained in the sample, the larger the effect of cholesterol. Nevertheless, cholesterol was not the only factor contributing to changes in the CLSE-based lipid systems compared to our previous binary lipid systems lacking cholesterol.

$CLSE^{Syn}$ allowed for better control of the lipids system as we knew the exact lipid composition. Most importantly, $CLSE^{Syn}$ had similar behavior compared to $CLSE^{T}$ and $CLSE^{L}$ with the exception of a slightly higher T_m for DPPC-d_{62} with more phase separation from monounsaturated lipids in the $CLSE^{T}$ and $CLSE^{L}$ lipid systems due to a trace amount of palmitic acid (Figure 4-24). Palmitic acid melts at ~63°C, contributing to a higher T_m for associated lipids (*137*). At 40°C the ^{2}H NMR lineshapes were identical for $CLSE^{Syn}$ and native CLSE; the order parameter profiles of both $CLSE^{Syn}$ and $CLSE^{L}$ at 40°C confirmed their similarity (Figures 4-25, 4-26, 4-27, and 4-28). These results indicated we had recapitulated the CLSE environment in a synthetic system as $CLSE^{T}$,

$CLSE^{L}$, and $CLSE^{Syn}$ all had similar lipid dynamics. However, we still did not know how the important LS protein, SP-B, affected the dynamics of the lipids in the CLSE systems. Previously, when we compared $CLSE^{T}$ and $CLSE^{L}$ the differences were indistinguishable even though a small percentage of SP-B and SP-C were present in $CLSE^{T}$. With closer review, we realized that there was only about 0.1 mol% SP-B in $CLSE^{T}$, which is a 1000:1 lipid/SP-B ratio (Figure 4-40). Conceivably there was a very small amount of lipids affected by SP-B in $CLSE^{T}$ and NMR experiments measure bulk properties, which contributed to us not seeing a difference between $CLSE^{T}$ and $CLSE^{L}$. The insensitivity of NMR wouldn't allow us to see a change in the spectral lineshapes in $CLSE^{L}$ when SP-B and SP-C were removed.

The lipid to peptide ratio in clinically used LS replacements is closer to 100:1 or about 1 mol% SP-B and sometimes higher at 2 mol%, such as for KL_4, a synthetic peptide mimic of the C-terminus of SP-B. Considering the importance of SP-B in lung surfactant function (*96*), replacement methods employing simple peptide analogs with surface active properties have been investigated (*43*). These studies have shown that the full protein sequence is not necessary to achieve surface tension reduction. A peptide consisting of the first twenty-five amino acids of SP-B, $SP\text{-}B_{1\text{-}25}$, has been demonstrated to retain the activity of full length SP-B as seen in both animal studies of lung function and air/water interface studies of surface tension (*36*). The proteins in LS, particularly SP-B, are needed for complete surfactant function inside the alveoli and thus we next added the peptide $SP\text{-}B_{1\text{-}25}$ to our native CLSE and synthetic CLSE systems to learn how this peptide affects lipid dynamics and facilitates lipid trafficking in the alveolar subphase. $SP\text{-}B_{1\text{-}25}$ has been demonstrated to affect lipids, facilitating

dynamics exchange between lipid lamellae leading to exchange broadening and non-lamellar lipid polymorphisms. SP-B_{1-25} may be an ideal SP-B replacement in clinical LS formulations.

DPPC, POPC, and POPG are the major lipids found in LS, with DPPC forming stable monolayers at the air/water interface due to its rigid packing abilities. These lipids are all phospholipids with the fatty acid chains attached to the glycerol backbone via ester linkages. The ester bonds of the monounsaturated lipids tend to hydrolyze when the lipids are in aqueous solutions while DPPC is thought to remain packed in bilayer structures. While SP-B_{1-25} affected the dynamics of all the lipids to some extent, DPPC displayed more changes in dynamics compared to the monounsaturated phospholipids. The spectra for deuterated POPC and POPG containing samples show lamellar lineshapes for 0-5 mol% SP-B_{1-25}. Lamellar lineshapes are also seen for deuterated DPPC in the absence of SP-B_{1-25}. However, as more peptide was added, the DPPC lipids showed properties of dynamics exchange between lipid lamellae, seen as exchange broadening in the spectra (Figures 4-21, 4-22, 4-35). This behavior was the same for DPPC in both the animal-derived and fully synthetic lipid samples. In previous work we have shown this exchange broadening for DPPC as a signature of surface active LS peptides. In Figure 4-41 is shown a schematic of how different concentrations of SP-B may affect lipid bilayers in lung surfactant. Increasing concentrations of SP-B cause lipid flipping between bilayers like a connecting doorway, which could explain how the lipids may be fused together with higher amounts of SP-B_{1-25}.

Conclusion

Lipid systems that undergo geometric rearrangement could have a significant impact on lipid transfer to the air/water interface. The underlying aqueous, protein-

containing hypophase is dynamic in that surfactant proteins aid in trafficking and sorting the lipids from secreted surfactant to the surface film lining the alveoli. To date, most studies have focused on the molecular properties of the monolayer phospholipid film at the air/water interface or have investigated low resolution images of intact surfactant, such as electron micrographs of rat intra-alveolar lung surfactant (*30*, *119*, *146*, *147*).

This study presented insights pertaining to the aqueous protein-containing underlying lung surfactant layer below the air/water interface along with the behavior of individual lipid species found in CLSE. Lung surfactant mimics containing an SP-B variant, SP-$B_{1\text{-}25}$, proved to be unique in that DPPC dynamics are preferentially affected and phase separation of the lipids is induced. With this work in addition to similar studies of LS, we are closer to achieving a fully synthetic clinical lung surfactant replacement.

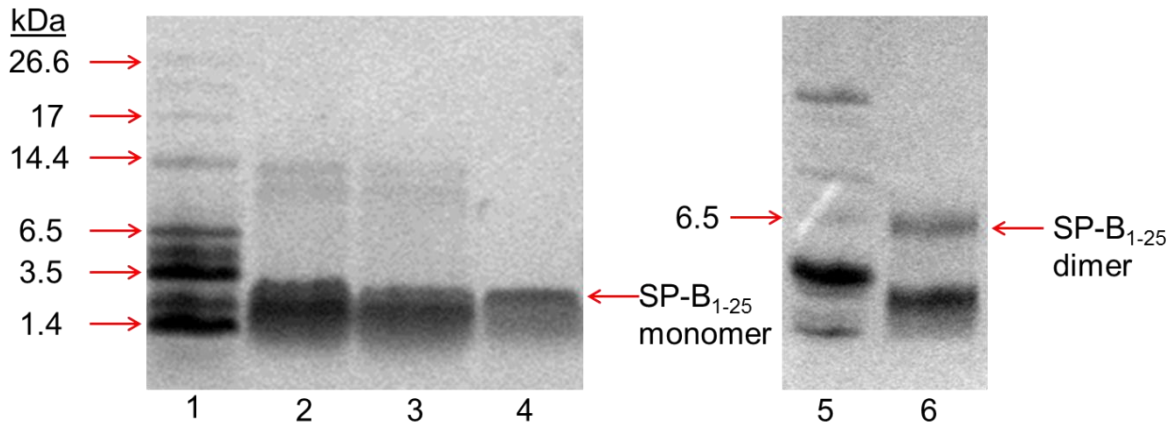

Figure 4-1. Nonreducing SDS PAGE gel of SP-B_{1-25}. Lane 1 is the molecular weight ladder. Lanes 2 - 4 contain monomeric SP-B_{1-25} at different loading amounts. Lane 5 is also the molecular weight ladder and Lane 6 is SP-B_{1-25} before monomerization. There are two bands in lane 6; one is the dimeric form at ~6 kDa and the other is the monomeric form of SP-B_{1-25} at ~3 kDa. The gels were made using a 15% T (Total acrylamide-bisacrylamide monomer concentration) / 2.7% C (Crosslinker concentration) resolving solution and a 5% T / 2.7% C stacking solution in bis-tris (Bis(2-hydroxyethyl)-amino-tris(hydroxymethyl)-methane) gel running buffer.

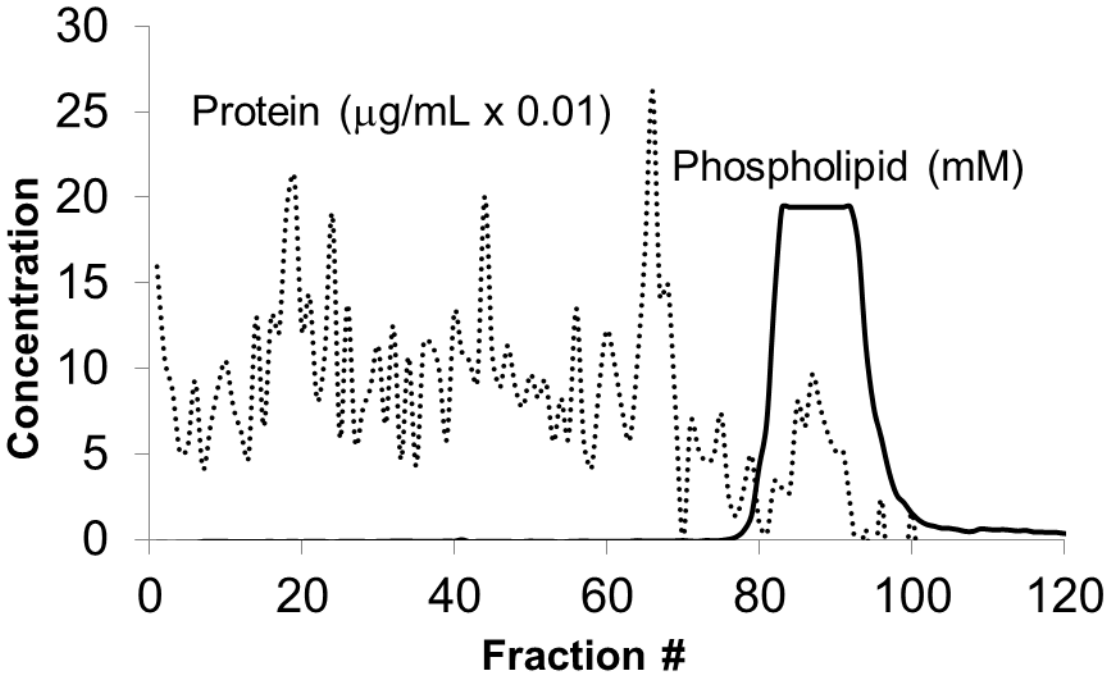

Figure 4-2. Phospholipid and protein concentrations in the first pass of a 2 mL CLSE injection as a function of fraction number. A second pass was conducted to completely separate the protein and lipid fractions. Concentrations were determined via phosphate and protein assays.

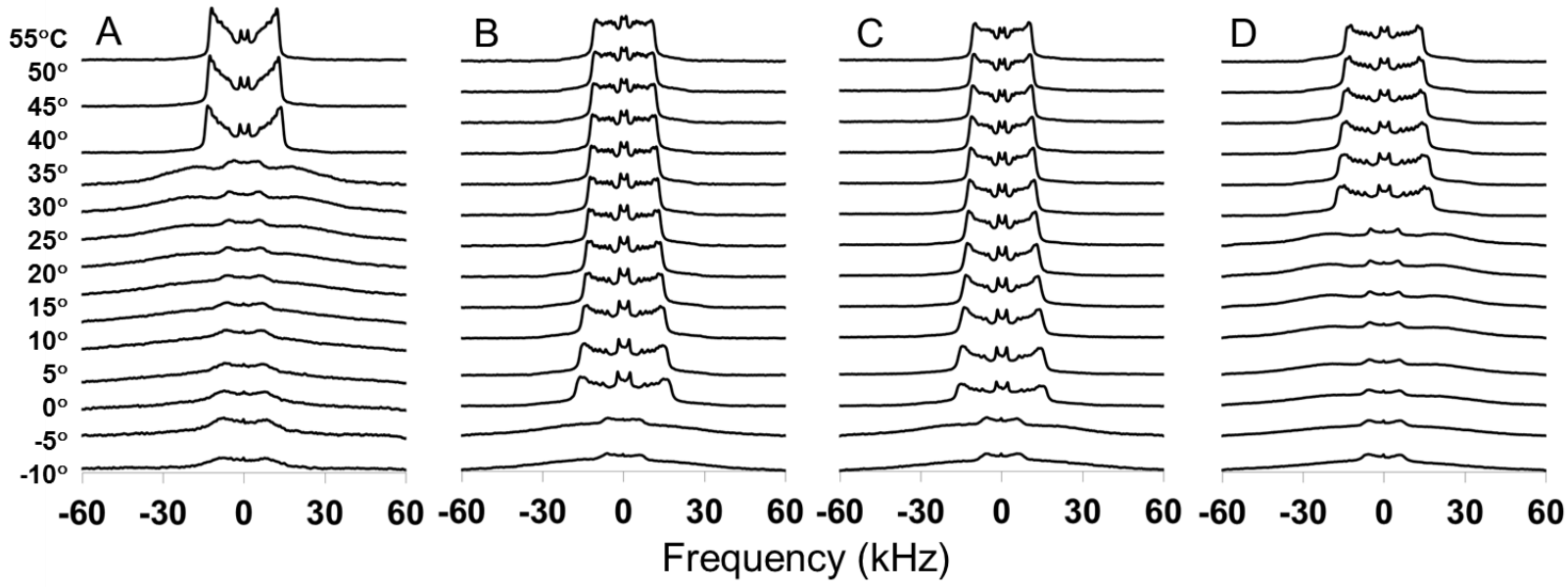

Figure 4-3. Deuterium NMR spectra of neat lipids as a function of temperature. A) DPPC/DPPC-d_{62}, B) POPC/POPC-d_{31}, C) POPG/POPG-d_{31}, D) POPE/POPE-d_{31}

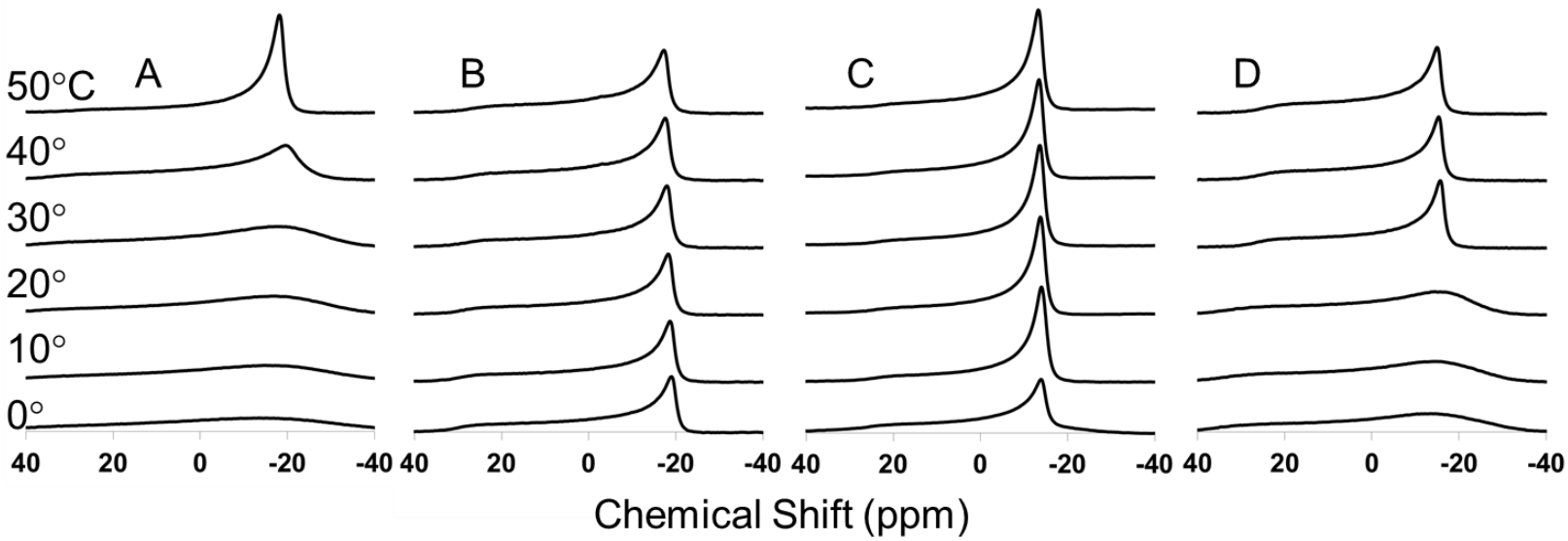

Figure 4-4. Phosphorus NMR spectra as a function of temperature for A) DPPC/DPPC-d_{62}, B) POPC/POPC-d_{31}, C) POPG/POPG-d_{31}, D) POPE/POPE-d_{31}

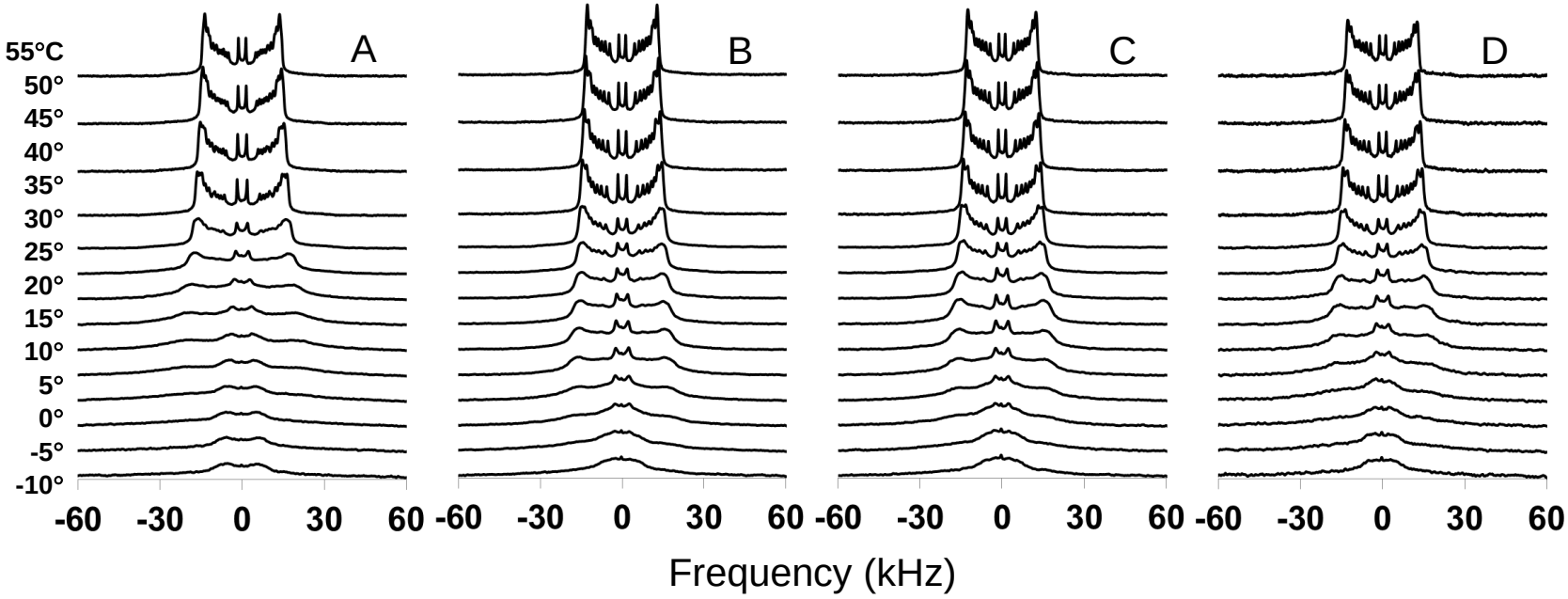

Figure 4-5. Deuterium spectra for A) CLSE^{T}/DPPC-d_{62}, B) CLSE^{T}/POPC-d_{31}, C) CLSE^{T}/POPG-d_{31}, and D) CLSE^{T}/POPE-d_{31} as a function of temperature.

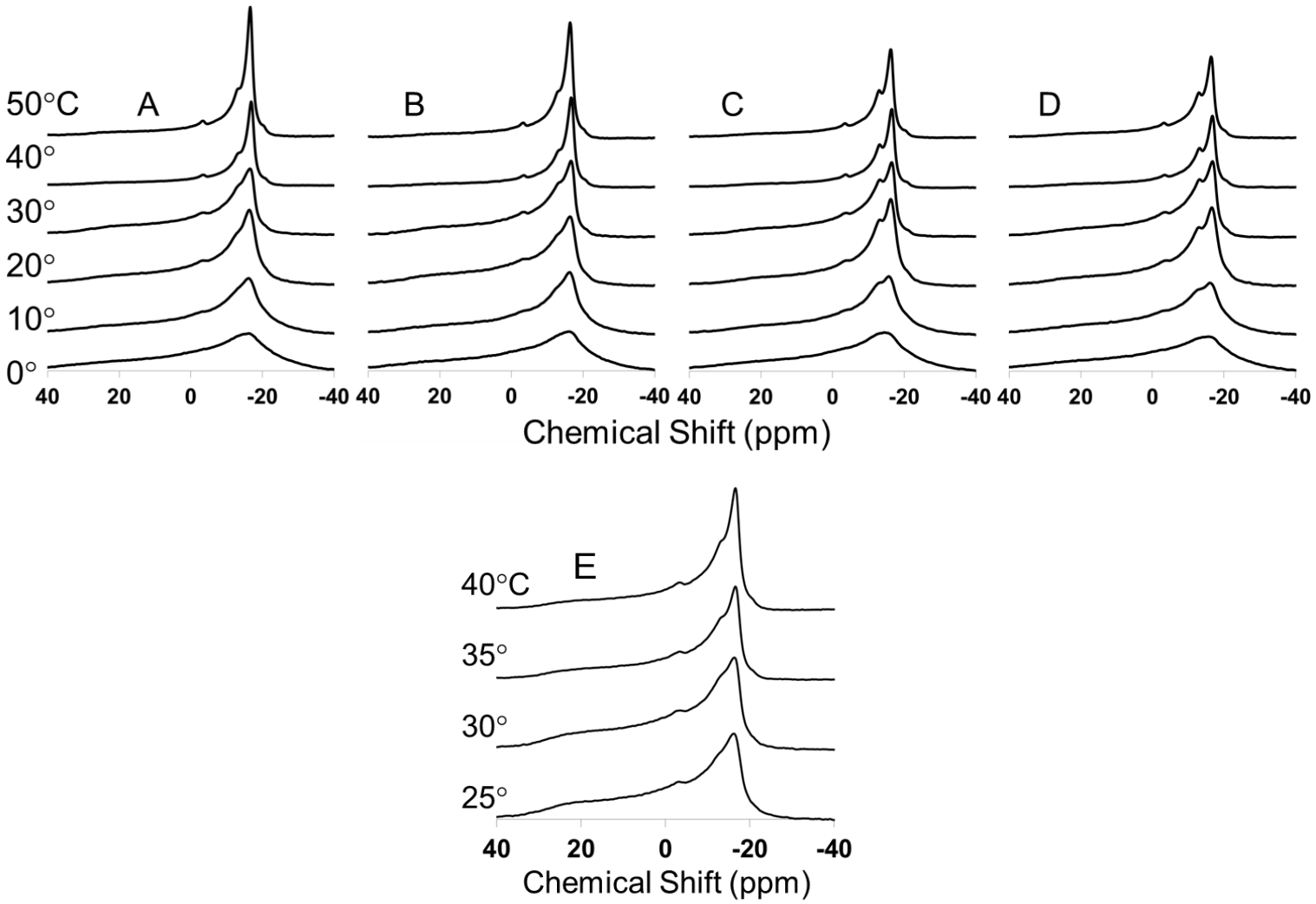

Figure 4-6. Phosphorus spectra for A) CLSE^{T}/DPPC-d_{62}, B) CLSE^{T}/POPC-d_{31}, C) CLSE^{T}/POPG-d_{31}, D) CLSE^{T}/POPE-d_{31}, and E) CLSE^{T} as a function of temperature

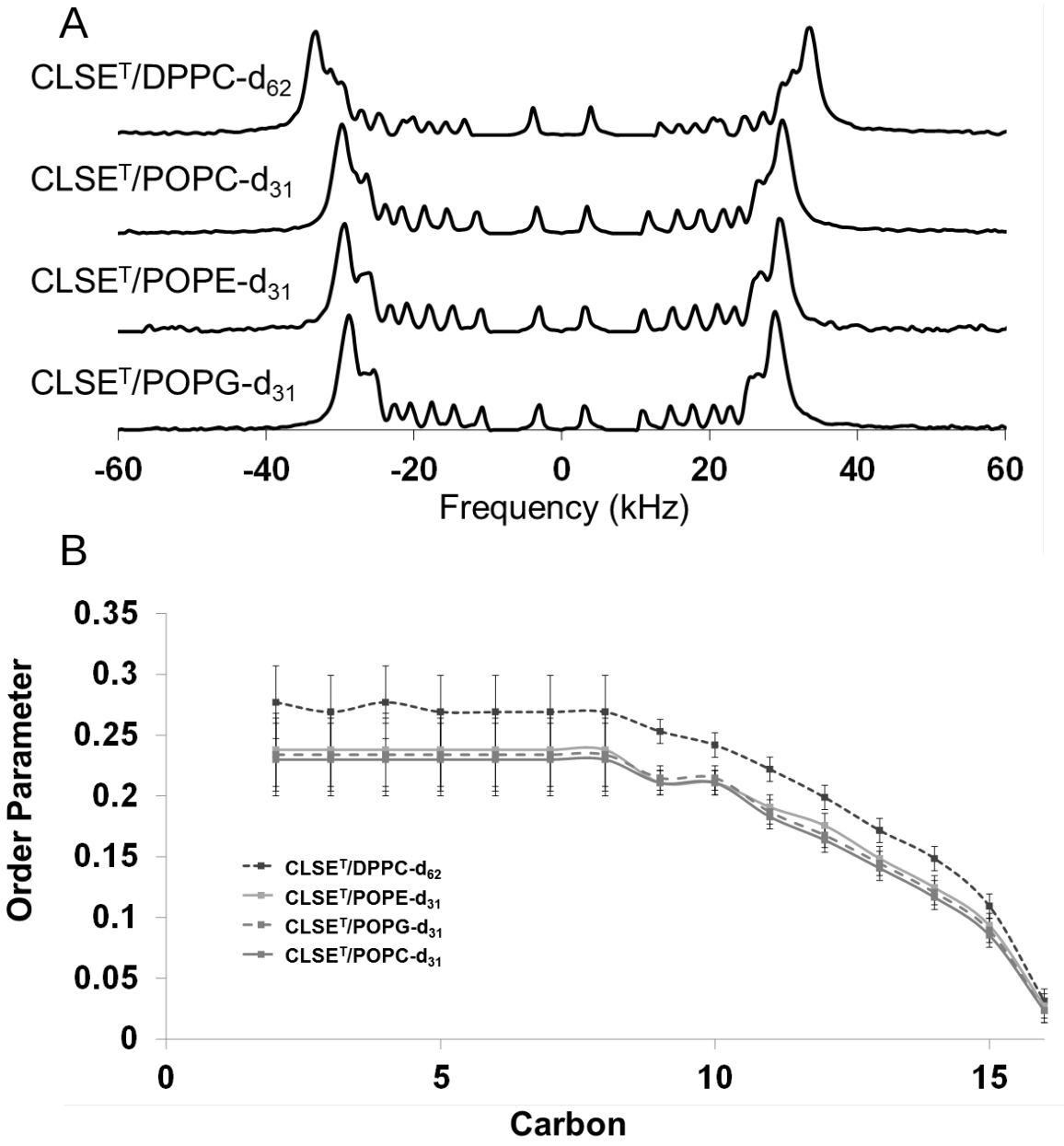

Figure 4-7. A) dePaked ^{2}H NMR spectra of CLSE^T with DPPC-d$_{62}$, POPC-d$_{31}$, POPE-d$_{31}$, and POPG-d$_{31}$ B) Order parameter profile for each deuterated lipid (DPPC-d$_{62}$, POPC-d$_{31}$, POPG-d$_{31}$, or POPE-d$_{31}$) in the CLSE^T environment derived from the dePaked spectra

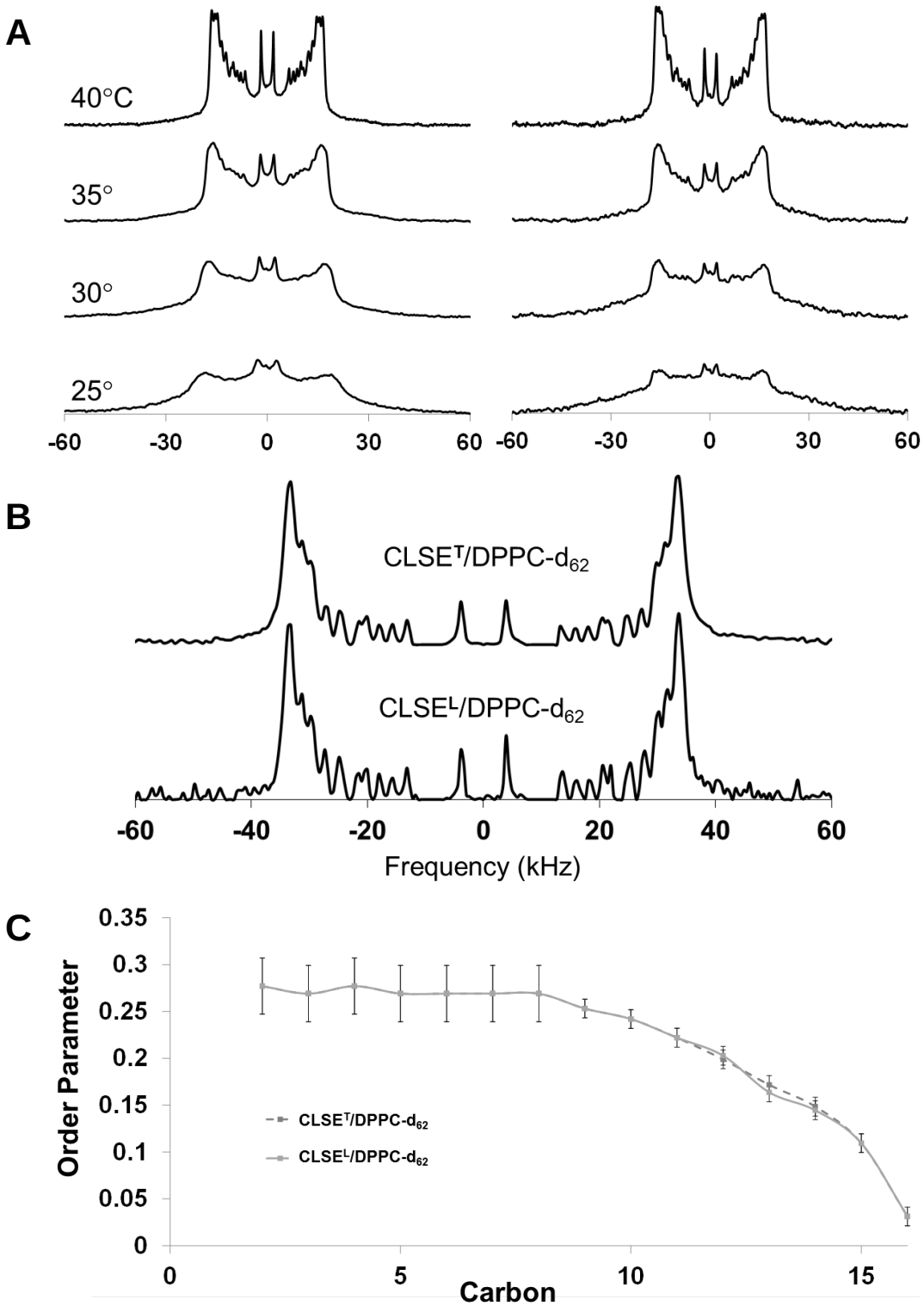

Figure 4-8. A) ^{2}H NMR spectra of CLSE^{T}/DPPC-d$_{62}$ and CLSE^{L}/DPPC-d$_{62}$ B) dePaked spectra of CLSE^{T}/DPPC-d$_{62}$ and CLSE^{L}/DPPC-d$_{62}$ C) Order parameter profile for DPPC-d$_{62}$ in the CLSE^{T} and CLSE^{L} systems

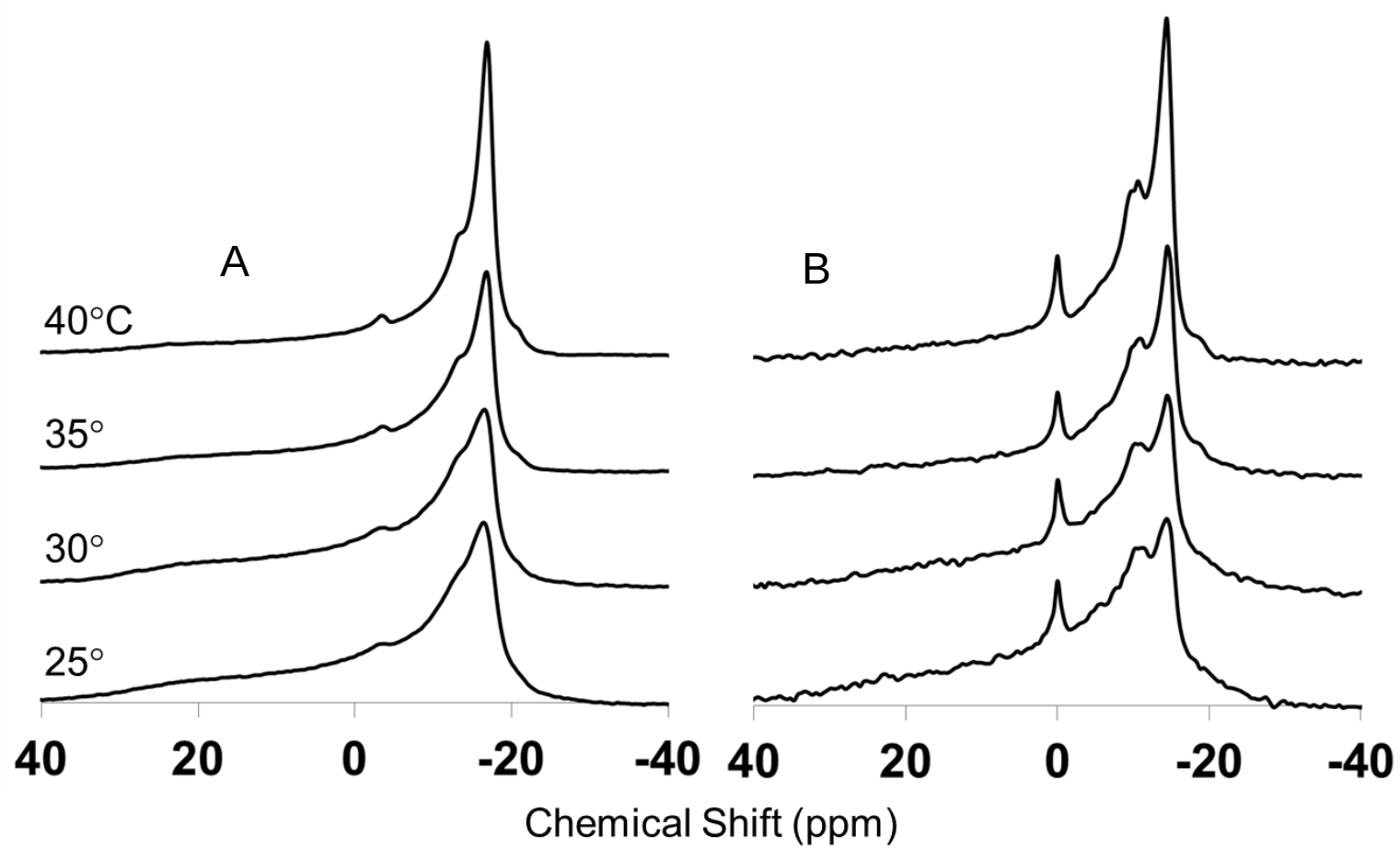

Figure 4-9. ^{31}P NMR spectra of A) CLSE^{T}/DPPC-d$_{62}$ and B) CLSE^{L}/DPPC-d$_{62}$.

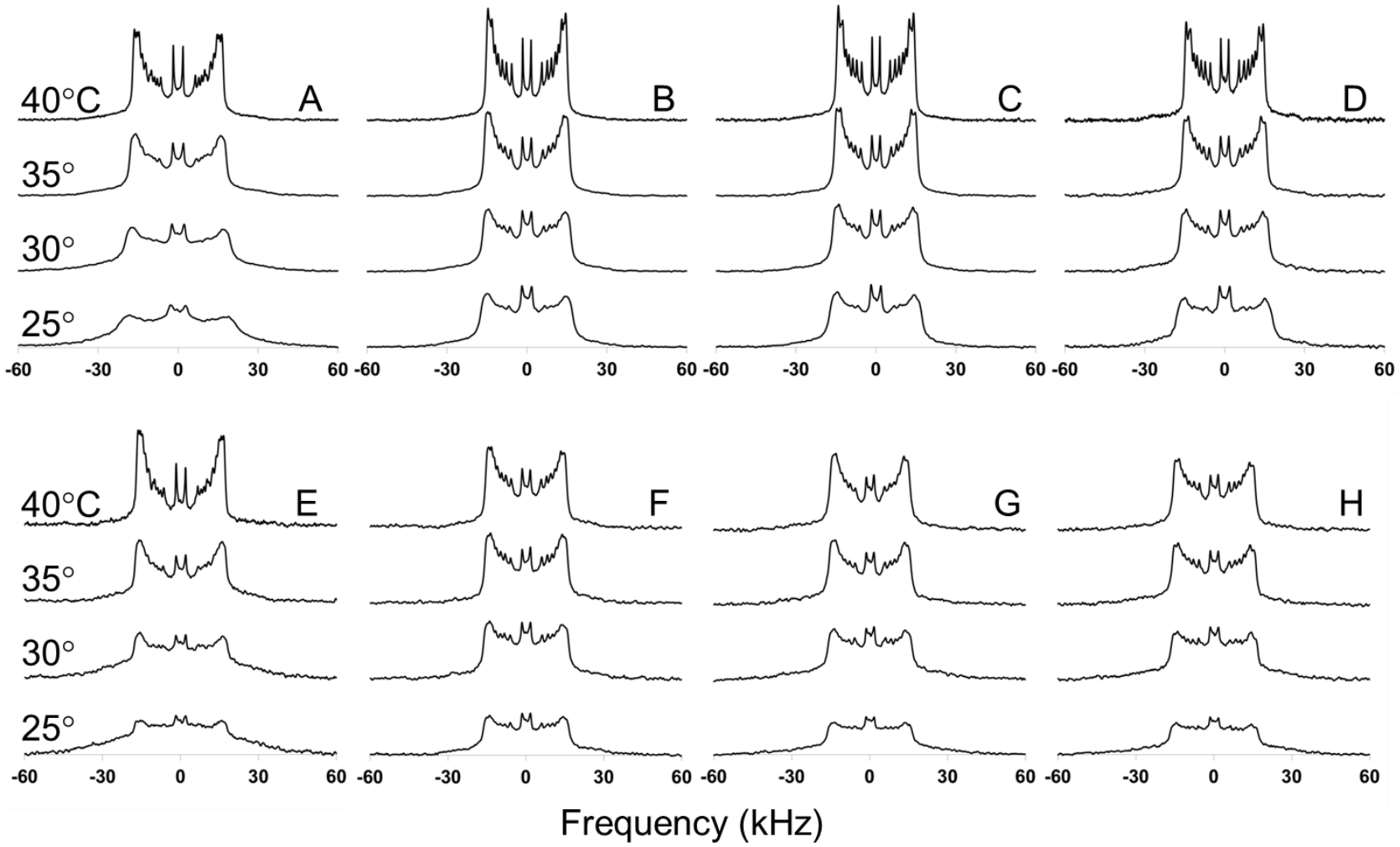

Figure 4-10. Deuterium NMR spectra of A) CLSE^{T}/DPPC-d_{62}, B) CLSE^{T}/POPC-d_{31}, C) CLSE^{T}/POPG-d_{31}, D) CLSE^{T}/POPE-d_{31}, E) CLSE^{L}/DPPC-d_{62}, F) CLSE^{L}/POPC-d_{31}, G) CLSE^{L}/POPG-d_{31}, and H) CLSE^{L}/POPE-d_{31}

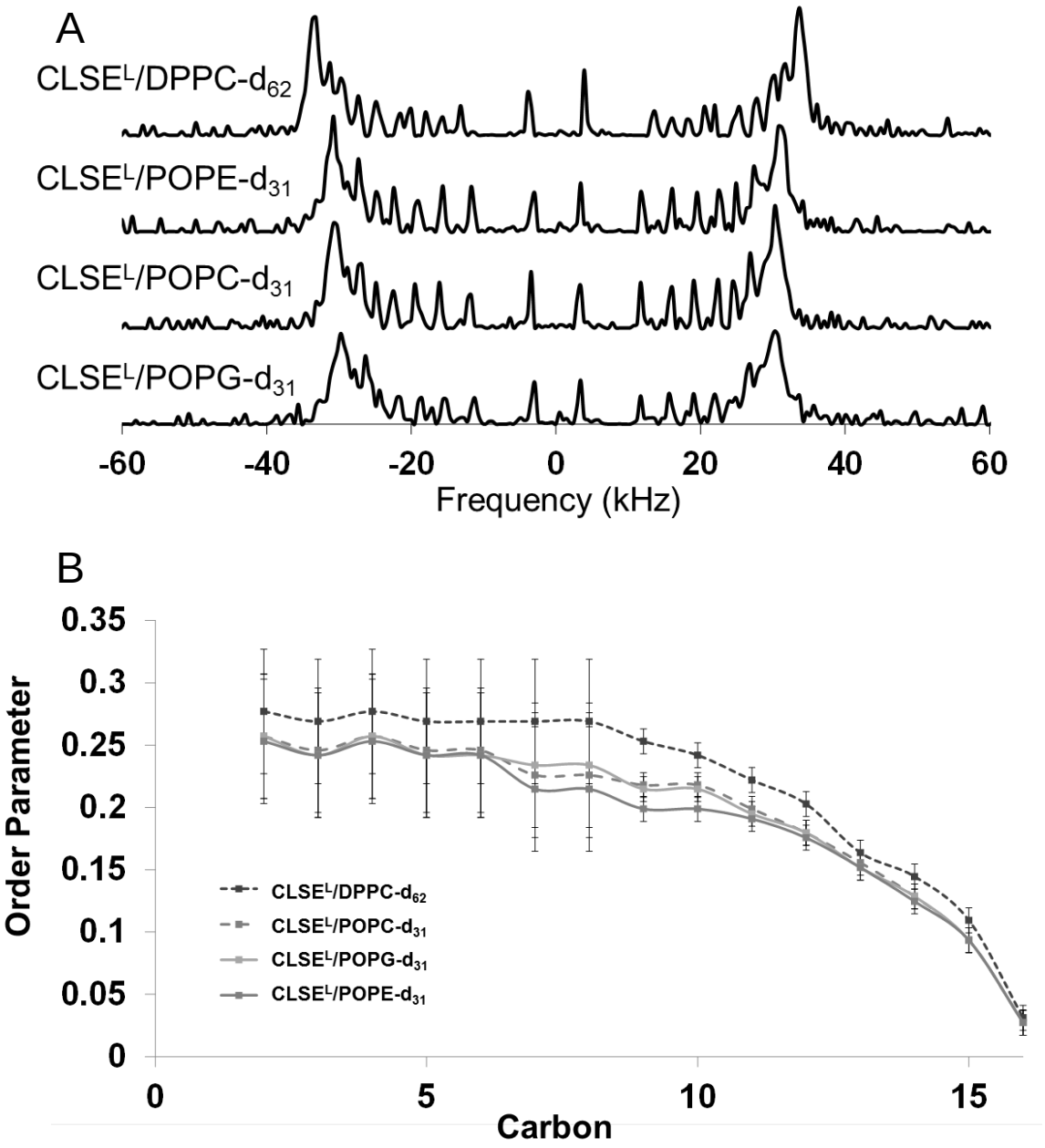

Figure 4-11. A) dePaked ^{2}H NMR spectra of DPPC-d$_{62}$, POPC-d$_{31}$, POPE-d$_{31}$, and POPG-d$_{31}$ in the CLSE^L environment B) Order parameter profile for each deuterated lipid (DPPC-d$_{62}$, POPC-d$_{31}$, POPG-d$_{31}$, or POPE-d$_{31}$) in the CLSE^L environment derived from the dePaked spectra

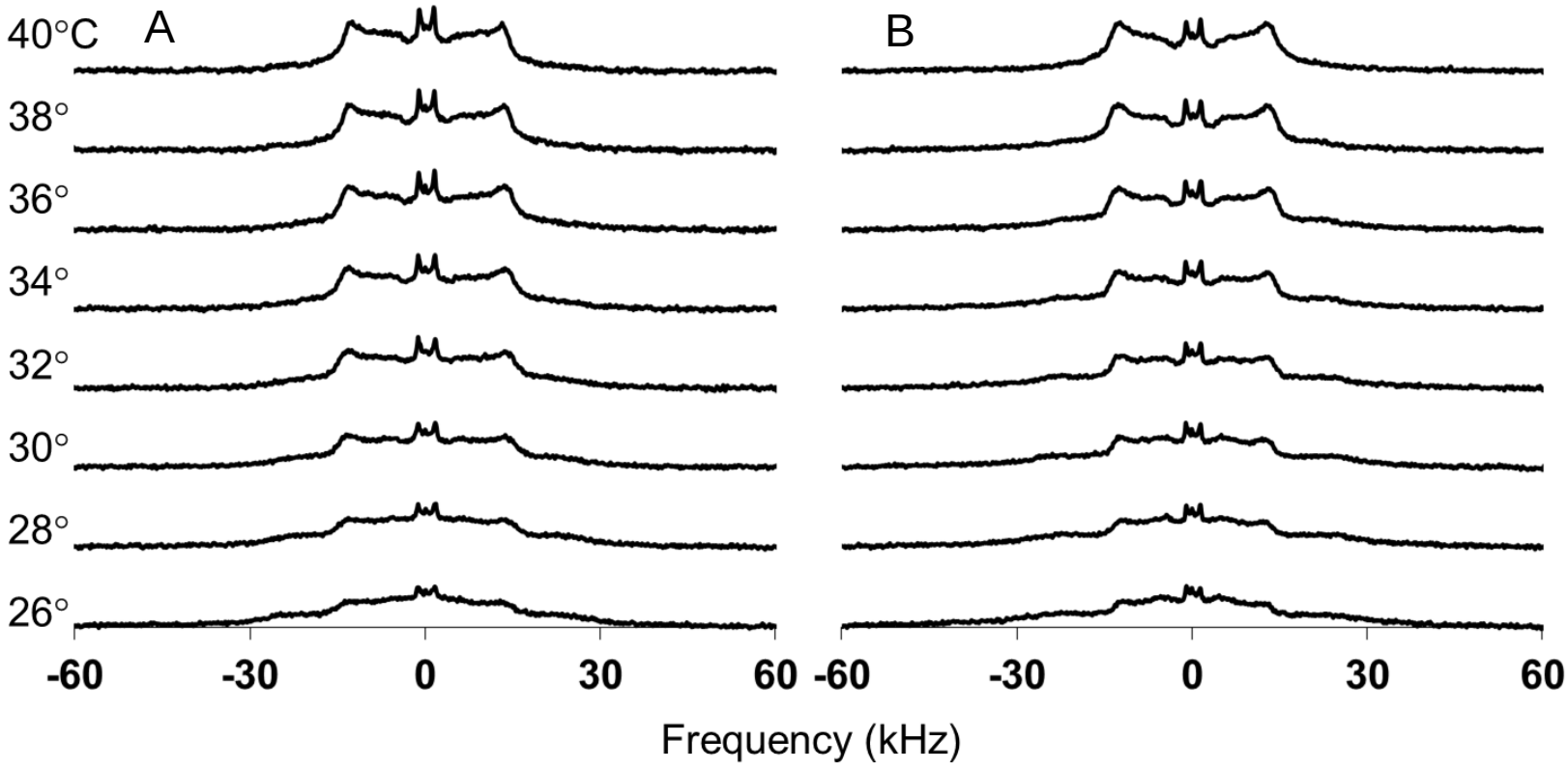

Figure 4-12. ^{2}H NMR spectra of A) $CLSE^{T}$/DPPC-d_{62} containing 5 mol% SP-B_{1-25} and B) $CLSE^{L}$/DPPC-d_{62} containing 5 mol% SP-B_{1-25}

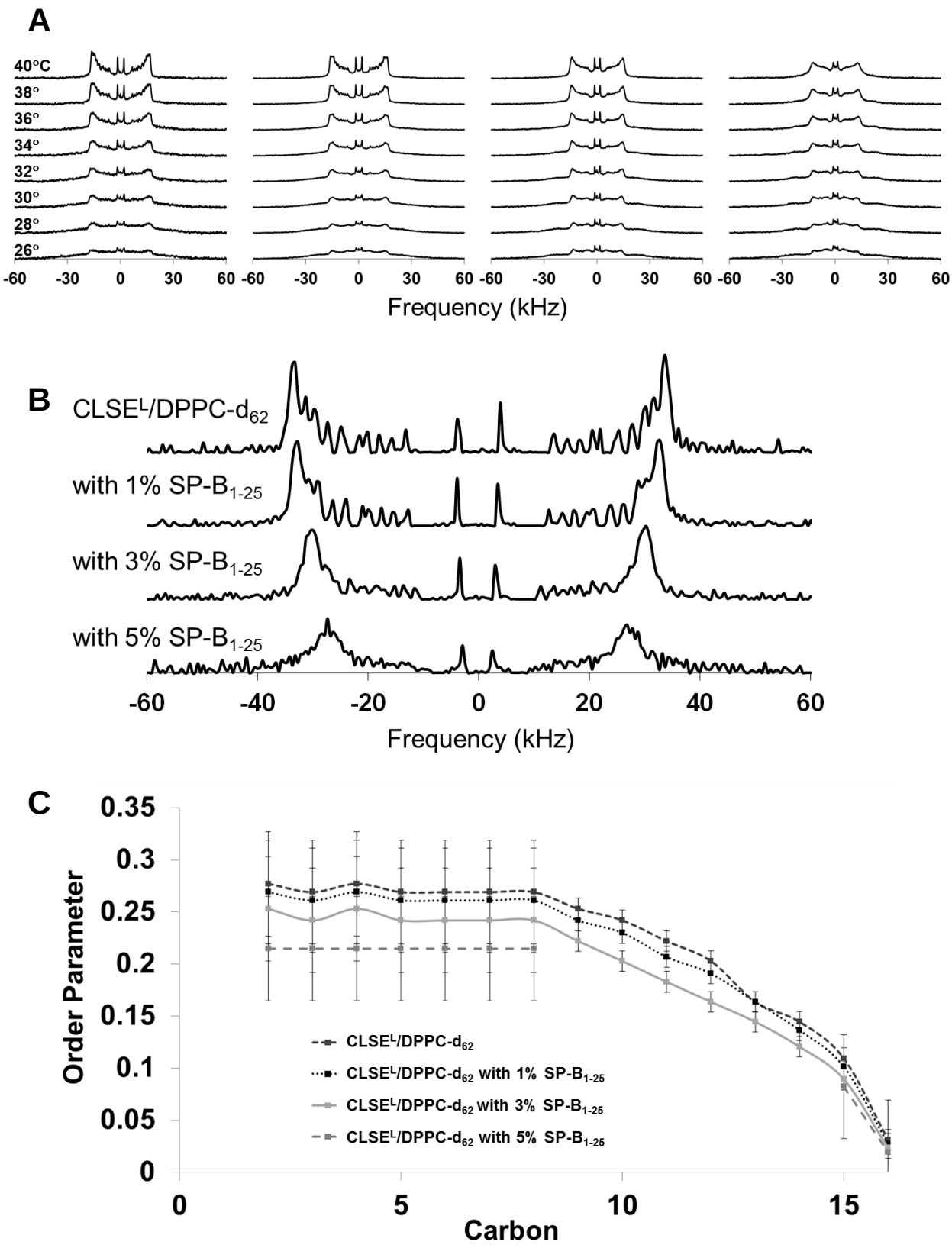

Figure 4-13. A) ^{2}H NMR spectra B) dePaked spectra and C) Order parameter plots of $CLSE^{L}/DPPC\text{-}d_{62}$ containing 0-5 mol% $SP\text{-}B_{1\text{-}25}$

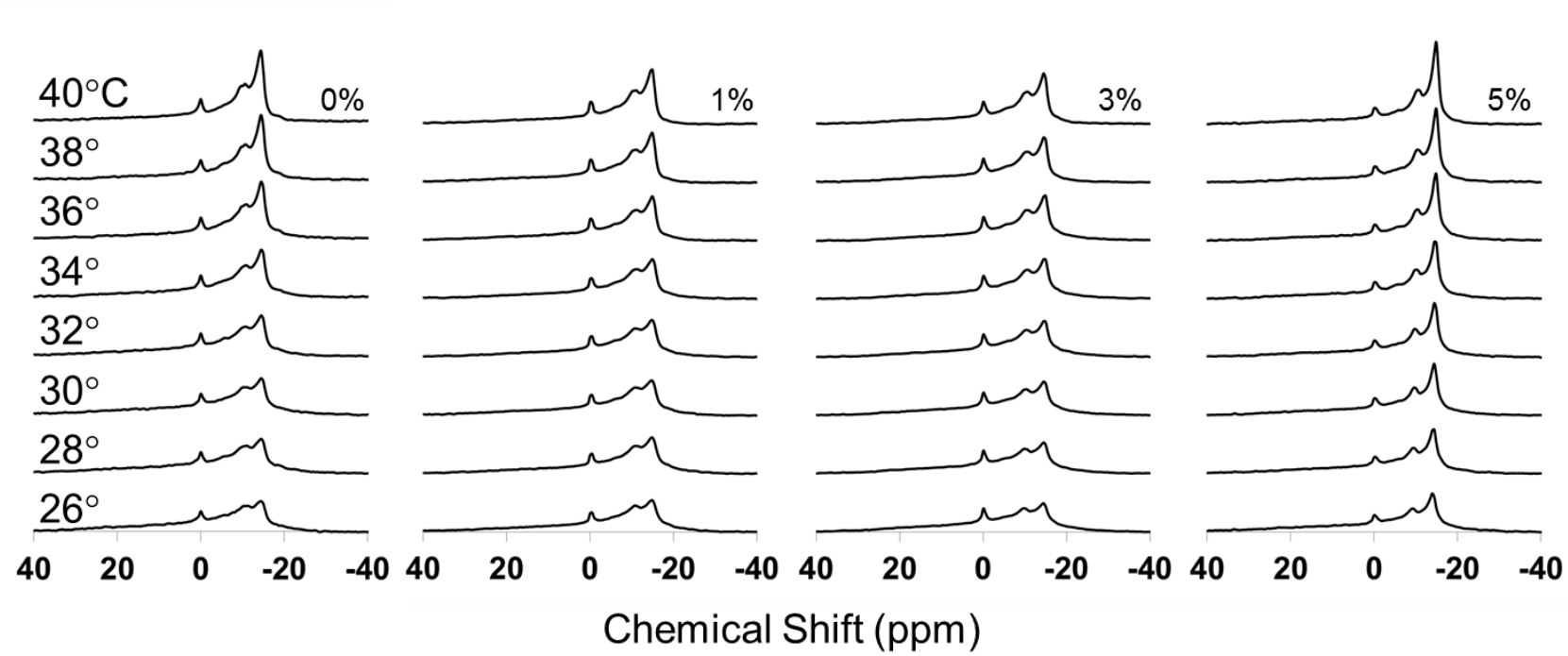

Figure 4-14. ^{31}P NMR spectra as a function of temperature of $CLSE^{L}$/DPPC-d_{62} containing 0-5 mol% SP-B_{1-25}

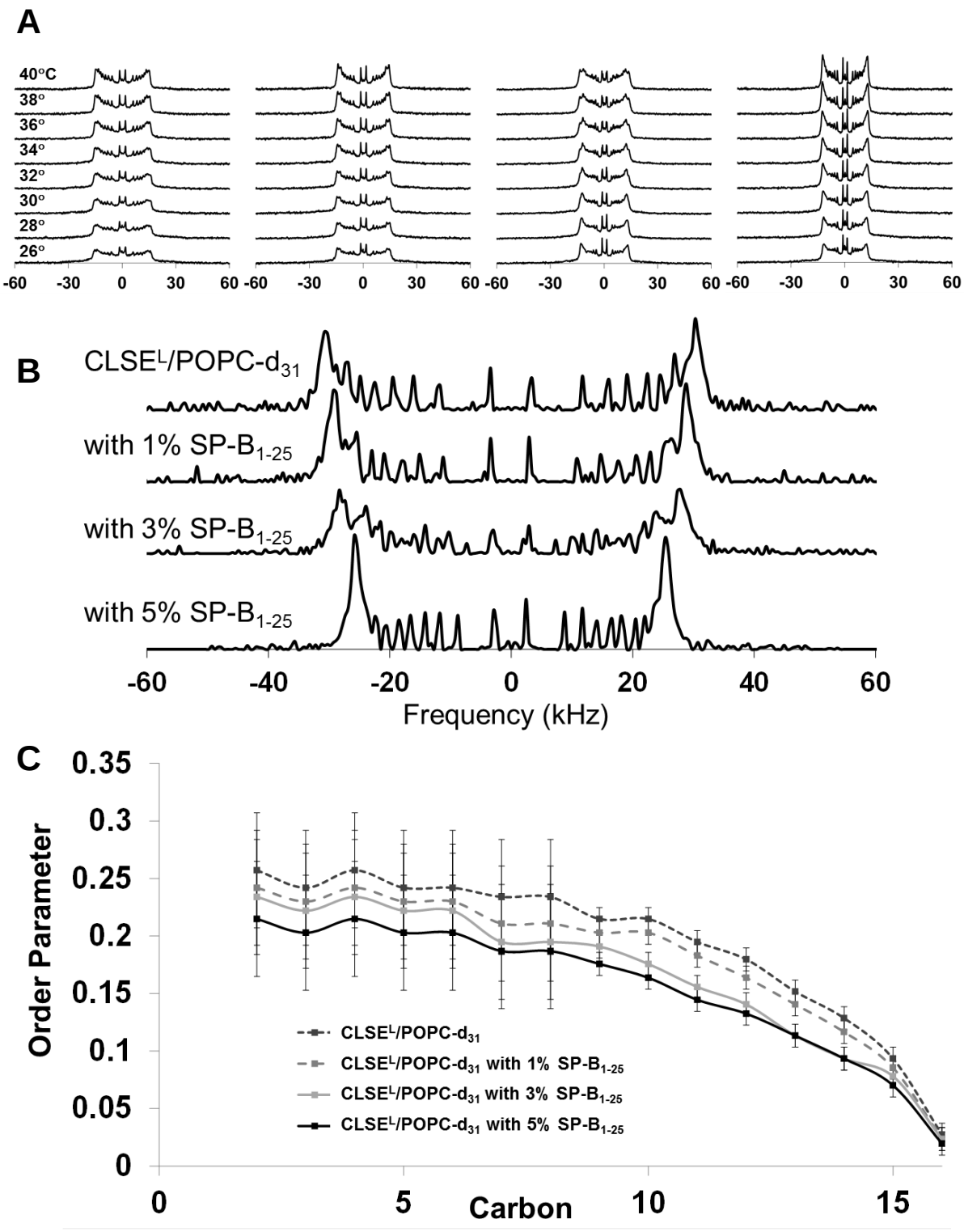

Figure 4-15. A) ^{2}H NMR spectra B) dePaked spectra and C) Order parameter plots of CLSE^{L}/POPC-d$_{31}$ containing 0-5 mol% SP-B$_{1-25}$

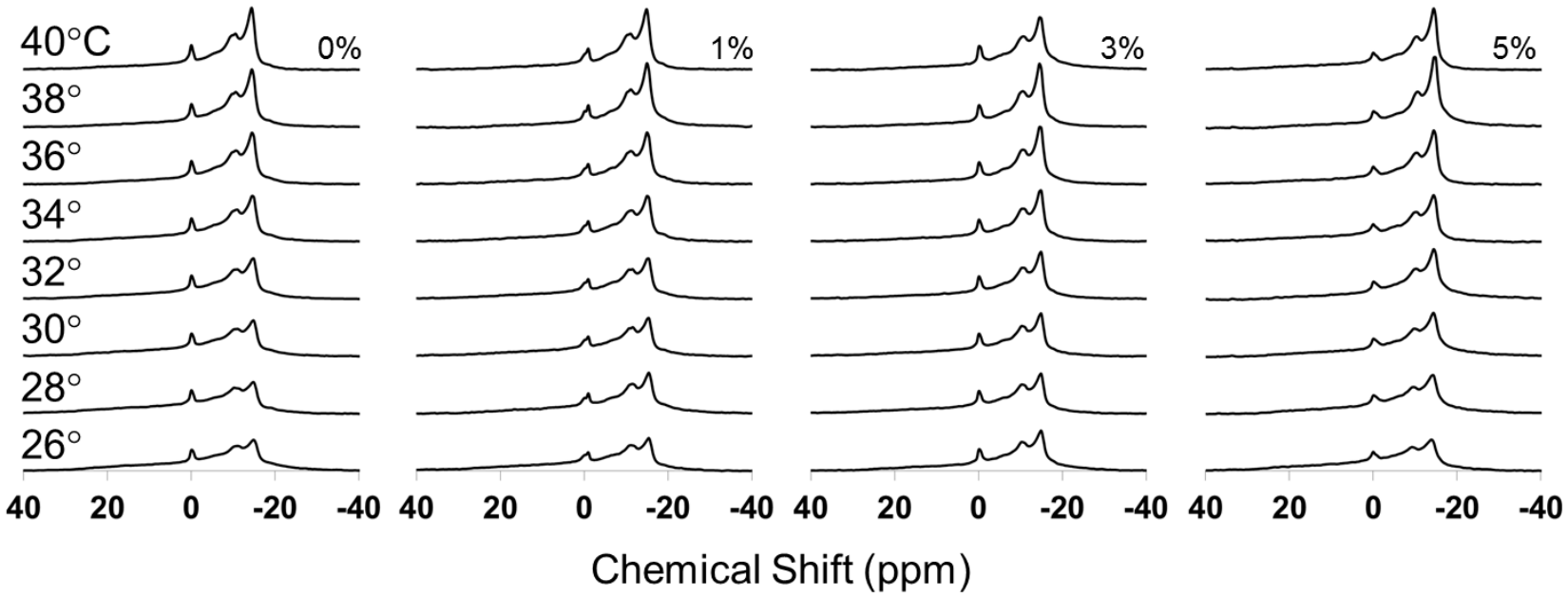

Figure 4-16. ^{31}P NMR spectra as a function of temperature of CLSE^{L}/POPC-d_{31} containing 0-5 mol% SP-B_{1-25}

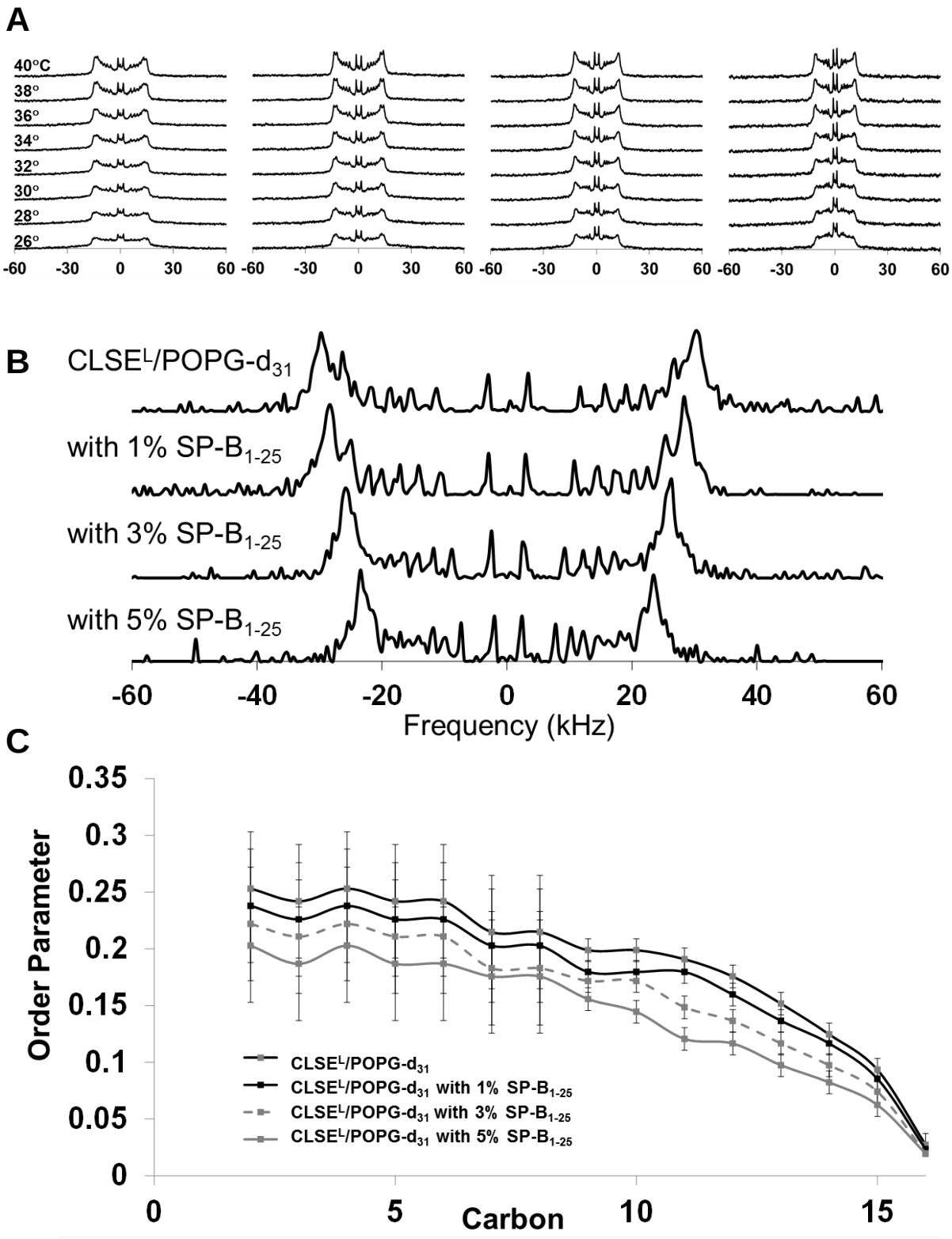

Figure 4-17. A) ^{2}H NMR spectra B) dePaked spectra and C) Order parameter plots of $CLSE^{L}/POPG\text{-}d_{31}$ containing 0-5 mol% $SP\text{-}B_{1\text{-}25}$

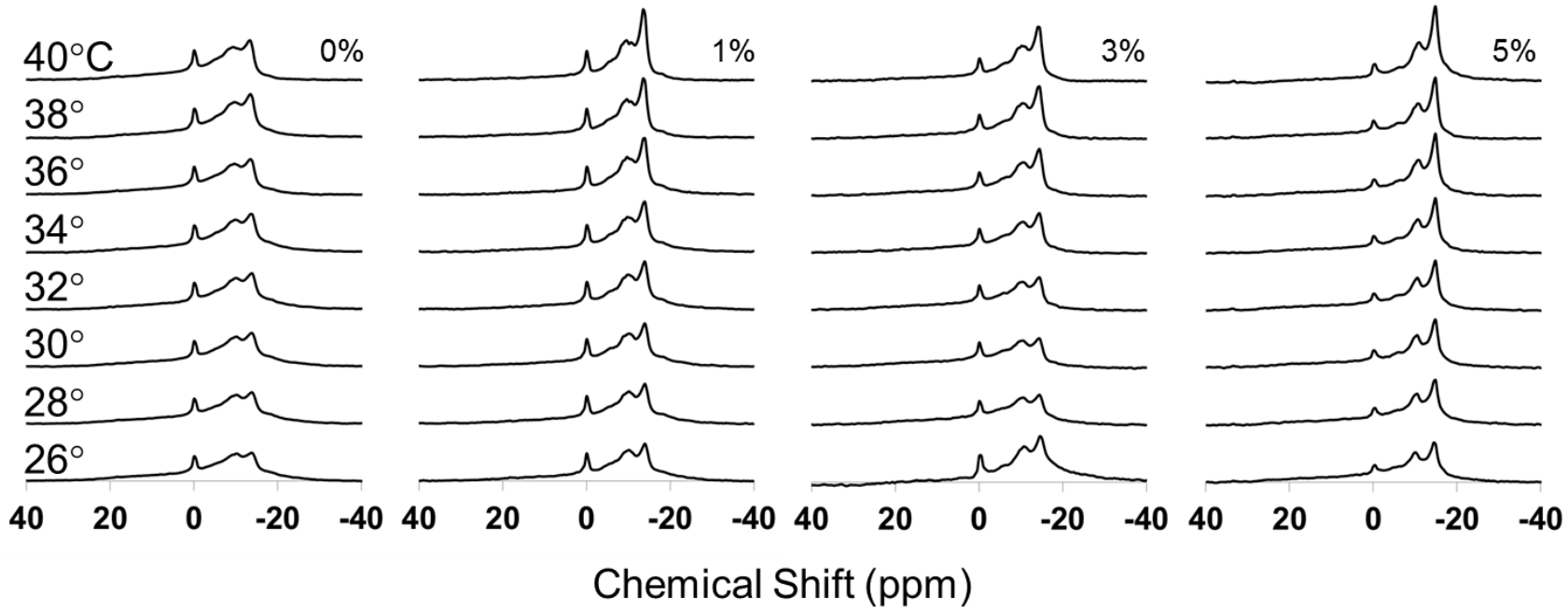

Figure 4-18. ^{31}P NMR spectra as a function of temperature of CLSE^{L}/POPG-d_{31} containing 0-5 mol% SP-B_{1-25}

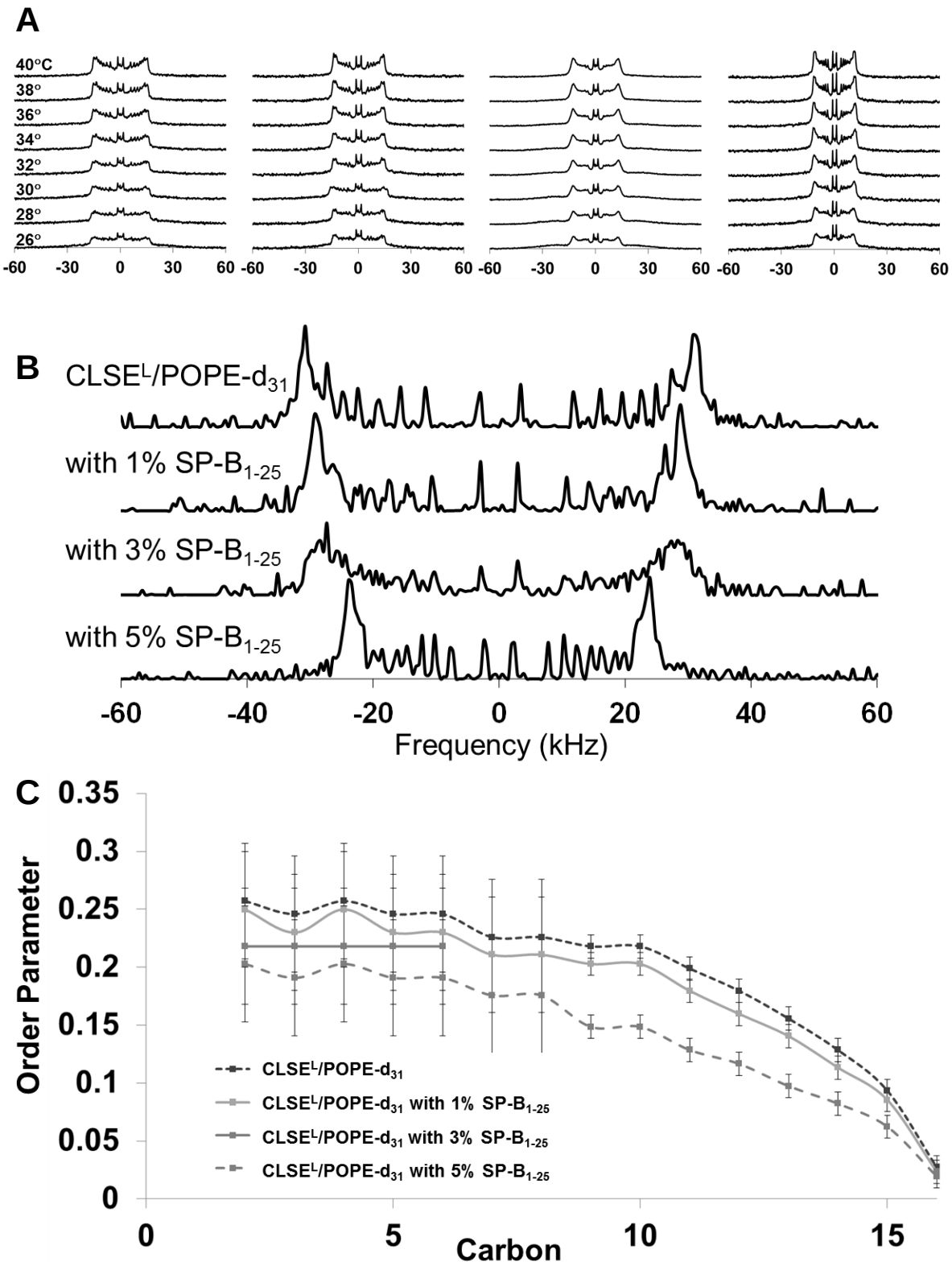

Figure 4-19. A) ^{2}H NMR spectra B) dePaked spectra and C) Order parameter plots of $CLSE^{L}/POPE\text{-}d_{31}$ containing 0-5 mol% $SP\text{-}B_{1\text{-}25}$

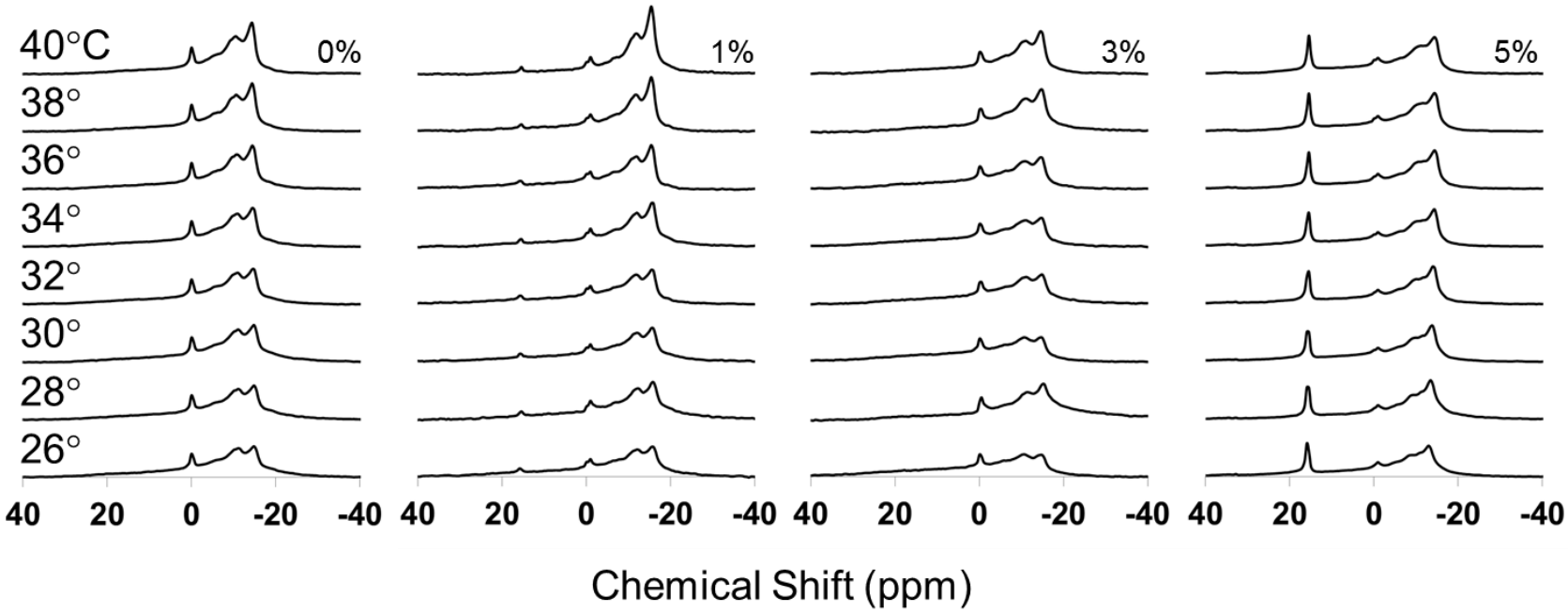

Figure 4-20. ^{31}P NMR spectra as a function of temperature of CLSE^{L}/POPE-d_{31} containing 0-5 mol% SP-B_{1-25}

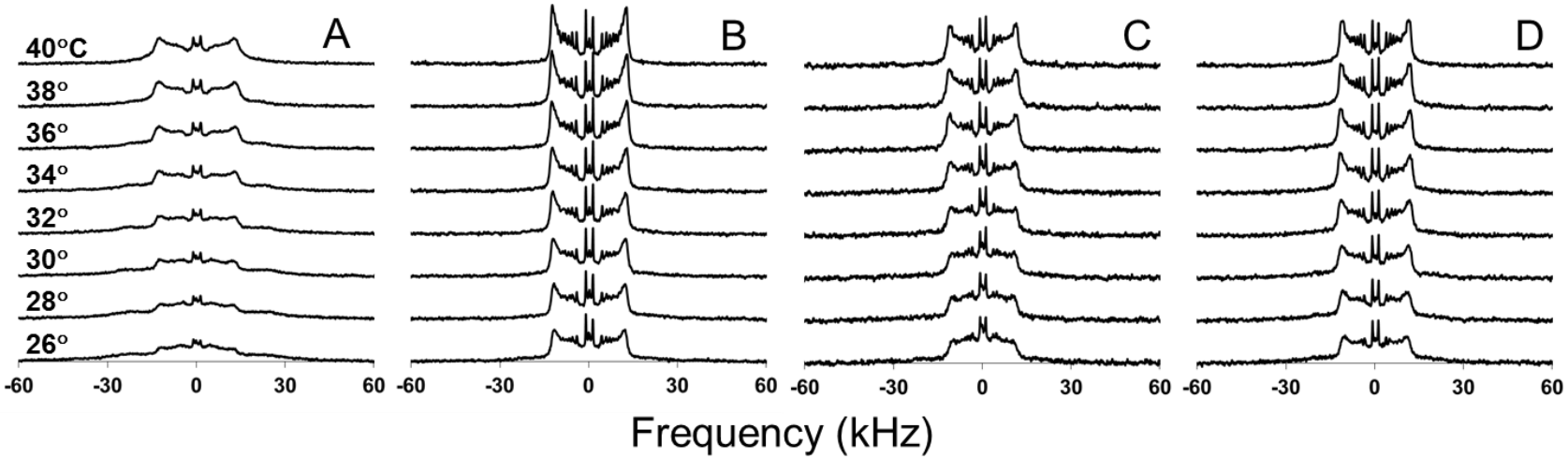

Figure 4-21. Deuterium spectra for A) $CLSE^{L}$/DPPC-d_{62} with 5% SP-B_{1-25}, B) $CLSE^{L}$/POPC-d_{31} with 5% SP-B_{1-25}, C) $CLSE^{L}$/POPG-d_{31} with 5% SP-B_{1-25}, and D) $CLSE^{L}$/POPE-d_{31} with 5% SP-B_{1-25} as a function of temperature.

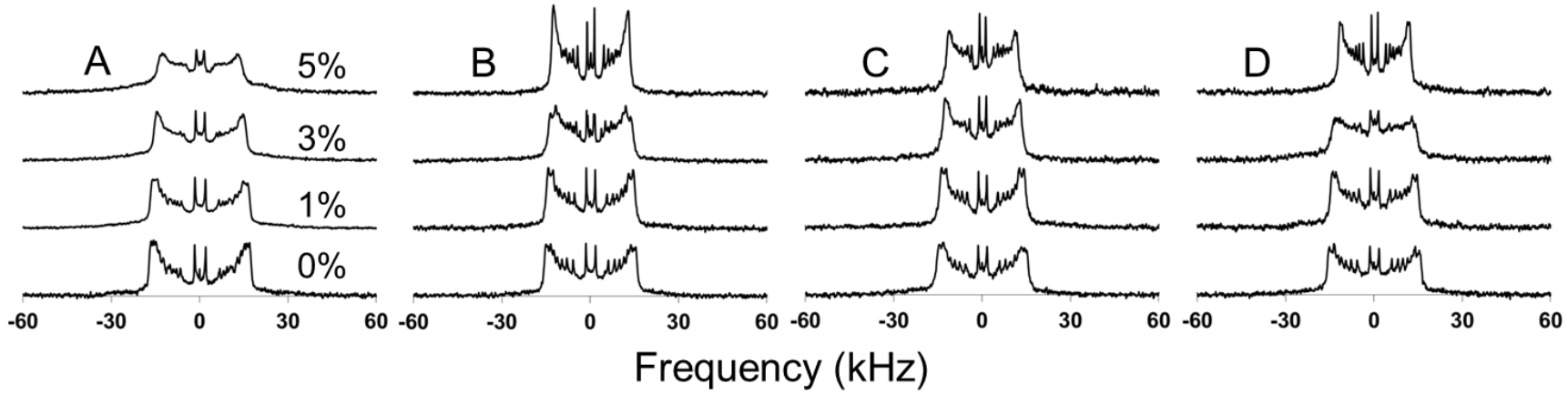

Figure 4-22. Deuterium spectra for A) CLSE^{L}/DPPC-d_{62} with 0-5% SP-$B_{1\text{-}25}$, B) CLSE^{L}/POPC-d_{31} with 0-5% SP-$B_{1\text{-}25}$, C) CLSE^{L}/POPG-d_{31} with 0-5% SP-$B_{1\text{-}25}$, and D) CLSE^{L}/POPE-d_{31} with 0-5% SP-$B_{1\text{-}25}$. All spectra were taken at 38°C.

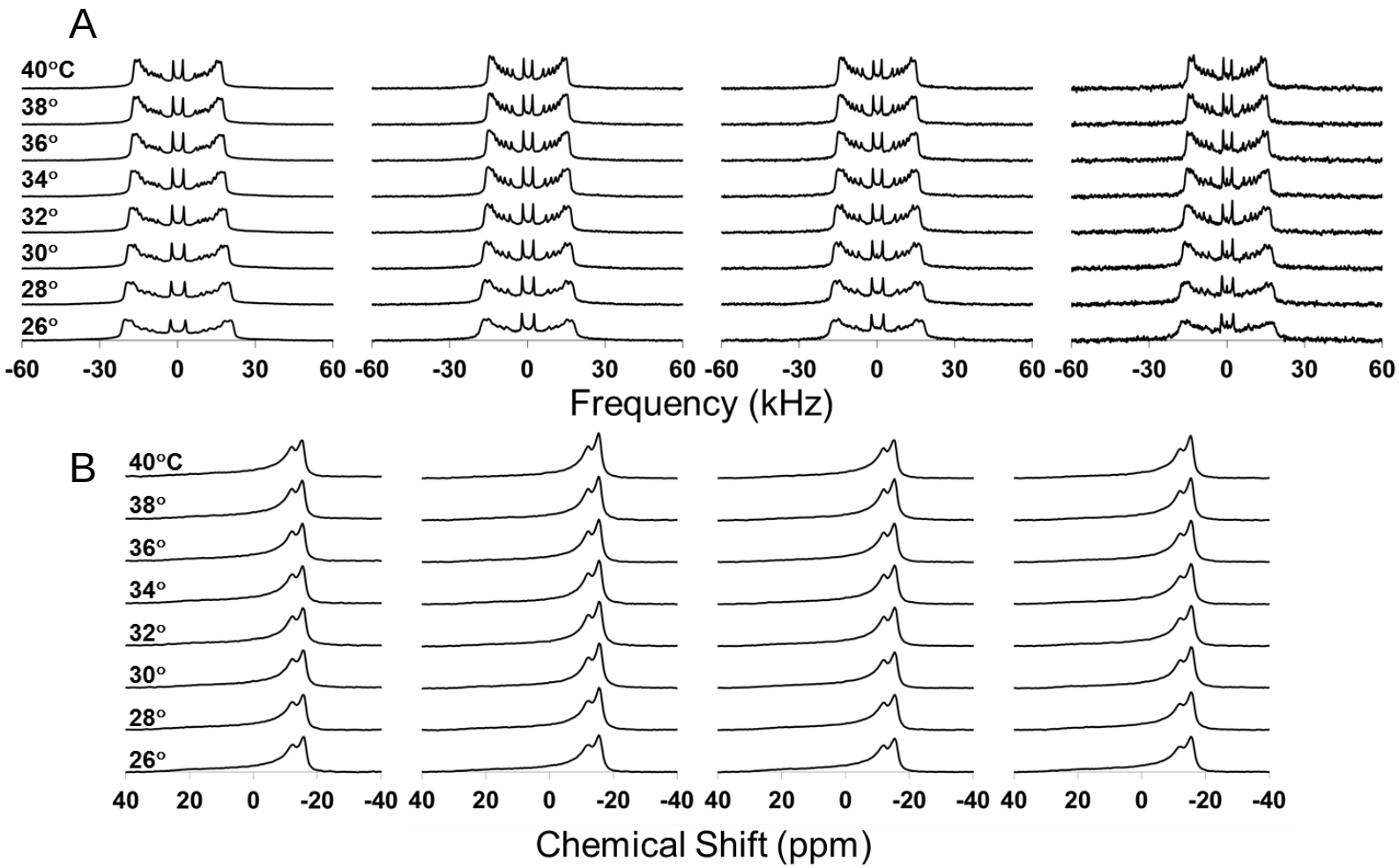

Figure 4-23. A) ^{2}H NMR spectra of (from left to right) DPPC-d_{62}, POPC-d_{31}, POPG-d_{31}, and POPE-d_{31} in the $CLSE^{Syn}$ environment B) Corresponding ^{31}P NMR spectra

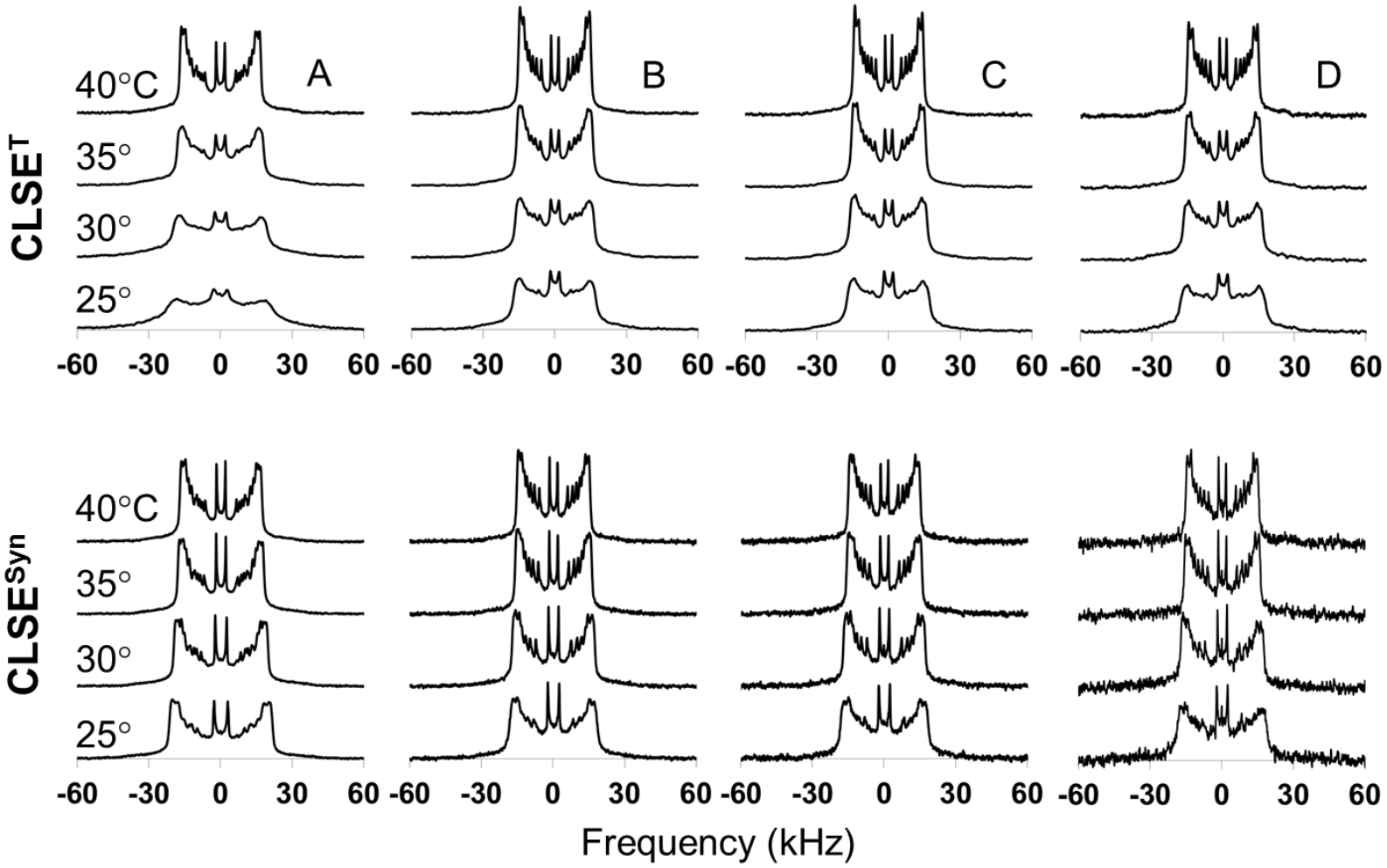

Figure 4-24. ^{2}H NMR spectra of DPPC-d_{62}, POPC-d_{31}, POPG-d_{31}, and POPE-d_{31} in the CLSE^{T} and CLSE^{Syn} systems as a function of temperature from 25 to 40°C. Column A) DPPC-d_{62}, B) POPC-d_{31}, C) POPG-d_{31}, D) POPE-d_{31}

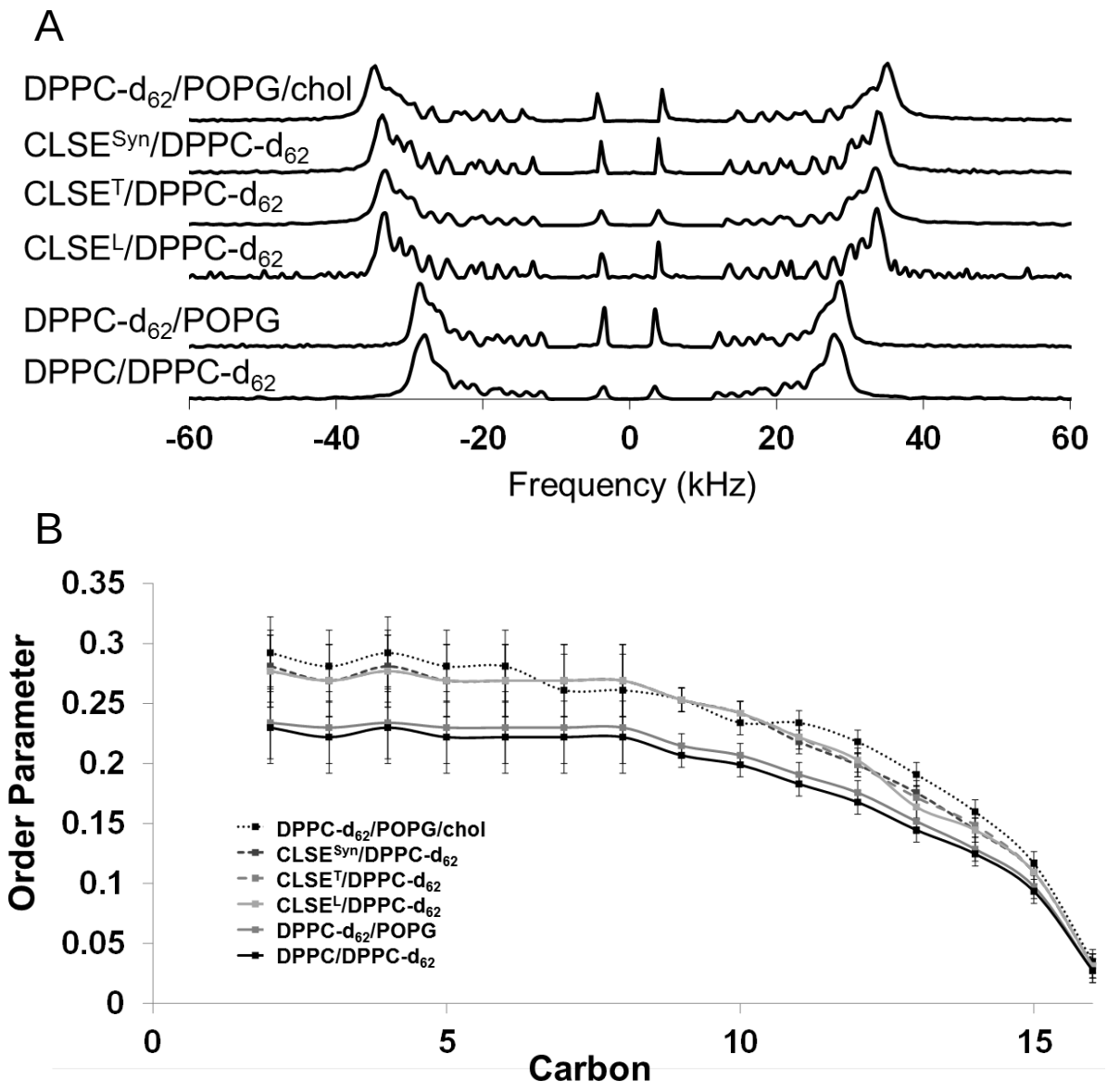

Figure 4-25. A) dePaked ^{2}H NMR spectra of DPPC-d_{62} in several lipid environments B) Order parameter profile for DPPC-d_{62} in different lipid systems

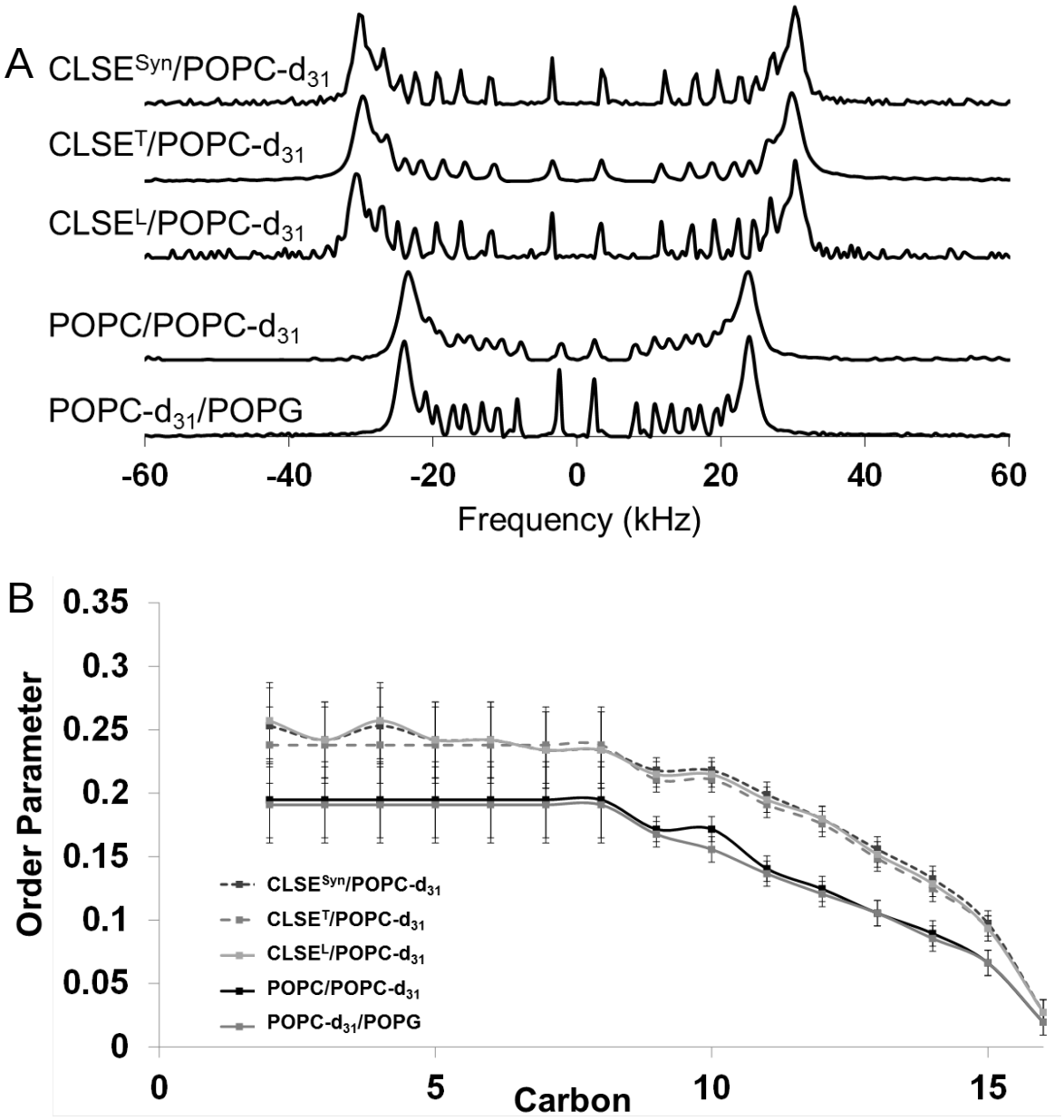

Figure 4-26. A) dePaked ^{2}H NMR spectra of POPC-d$_{31}$ in several lipid environments B) Order parameter profile for POPC-d$_{31}$ in different lipid systems

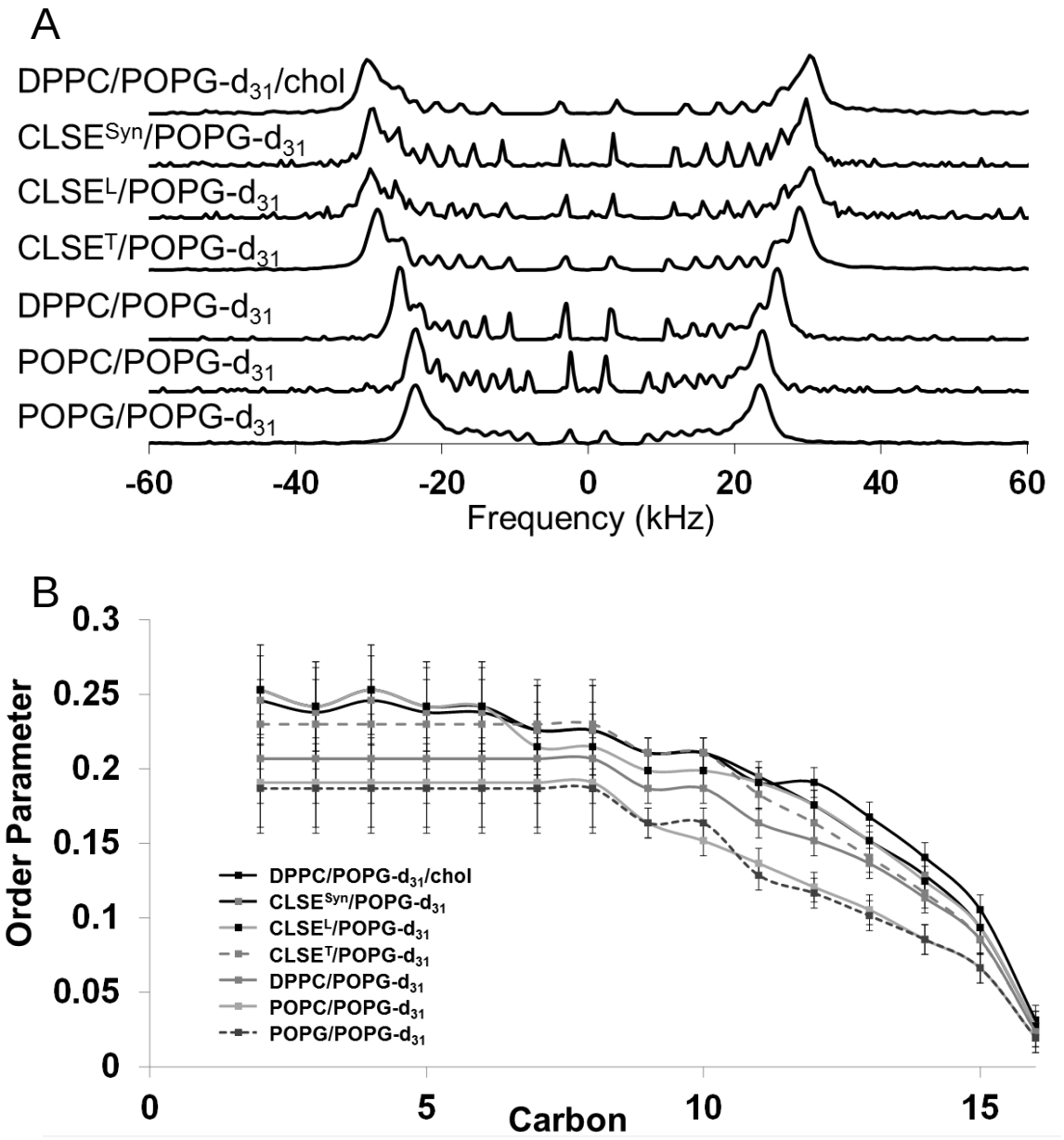

Figure 4-27. A) dePaked ^{2}H NMR spectra of POPG-d_{31} in several lipid environments B) Order parameter profile for POPG-d_{31} in different lipid systems

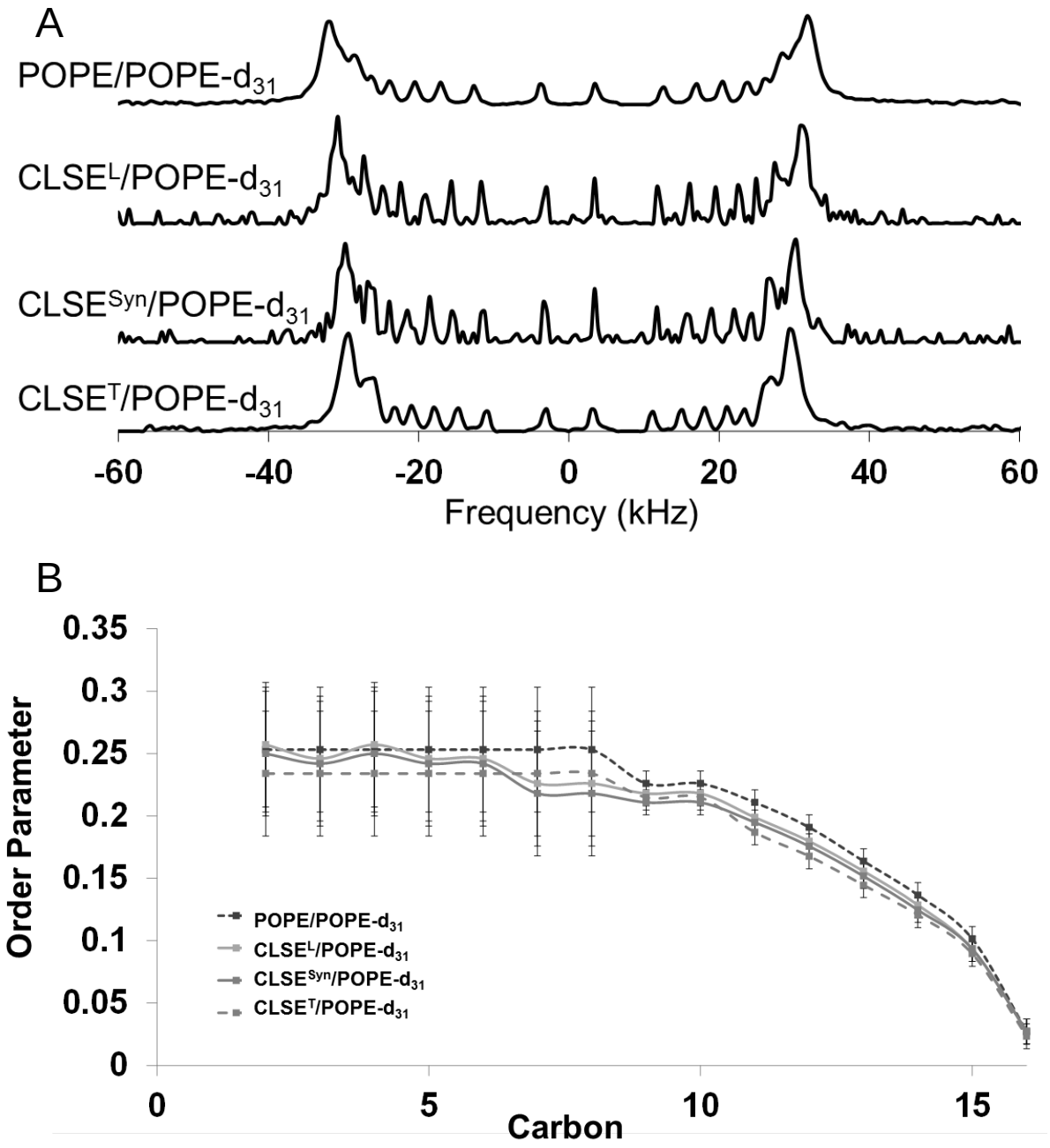

Figure 4-28. A) dePaked ^{2}H NMR spectra of POPE-d_{31} in several lipid environments B) Order parameter profile for POPE-d_{31} in different lipid systems

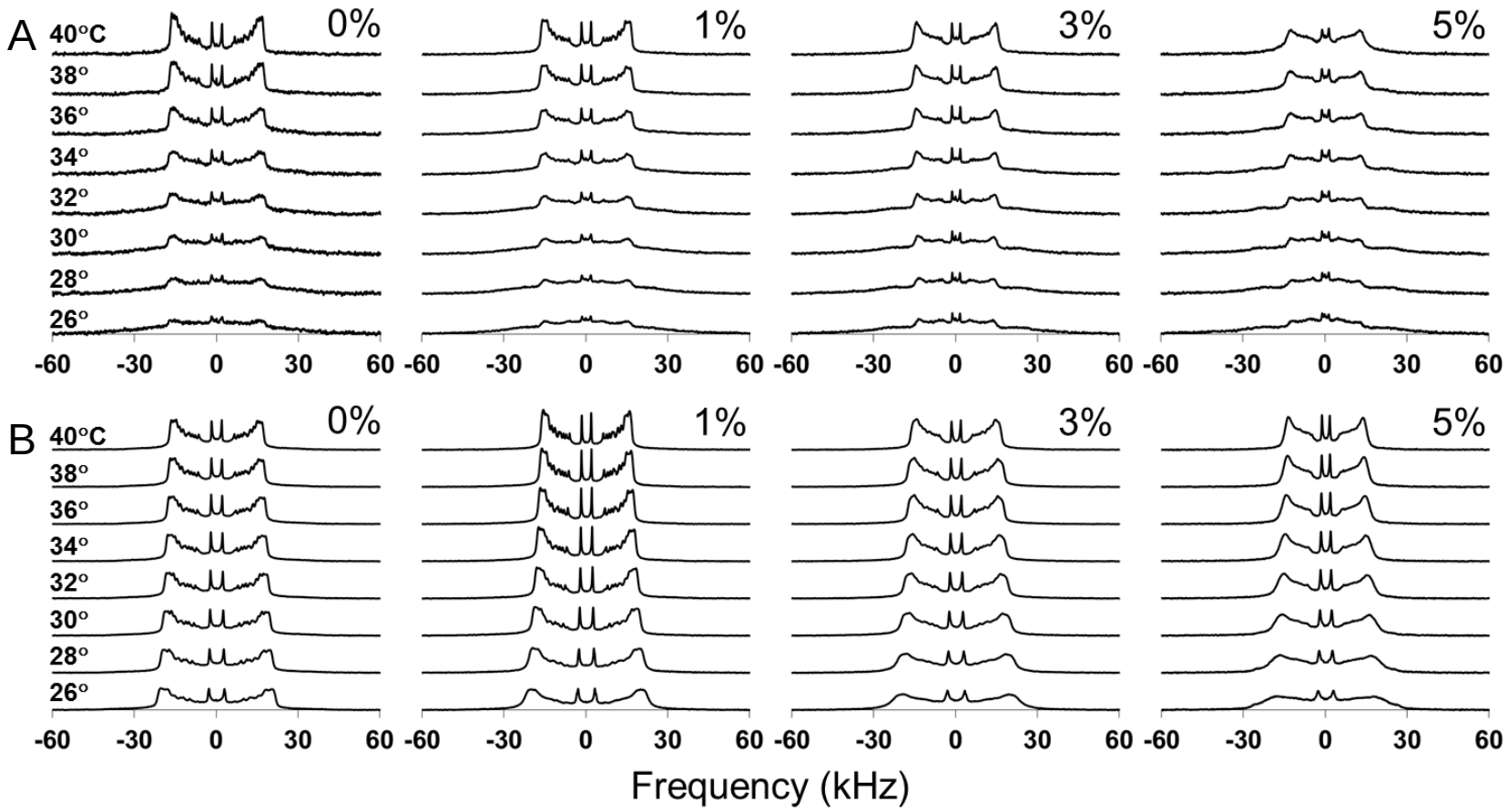

Figure 4-29. Deuterium spectra of A) $CLSE^{L}$/DPPC-d_{62} with 0-5% SP-B_{1-25} and B) $CLSE^{Syn}$ DPPC-d_{62} with 0-5% SP-B_{1-25}

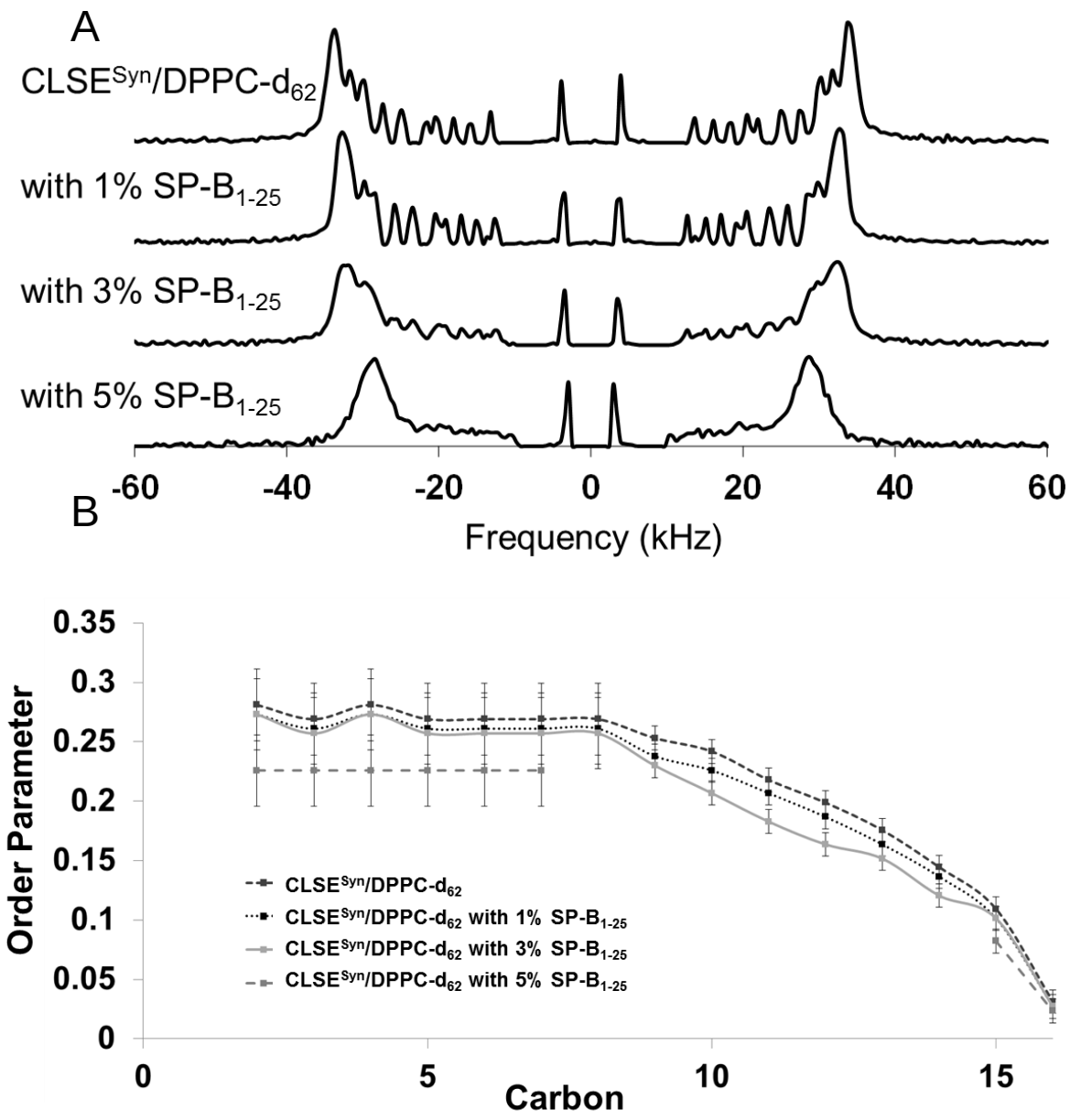

Figure 4-30. A) dePaked ^{2}H NMR spectra and B) Order parameter profile of DPPC-d_{62} in the CLSE^{Syn} environment containing 0-5 mol% SP-B_{1-25}

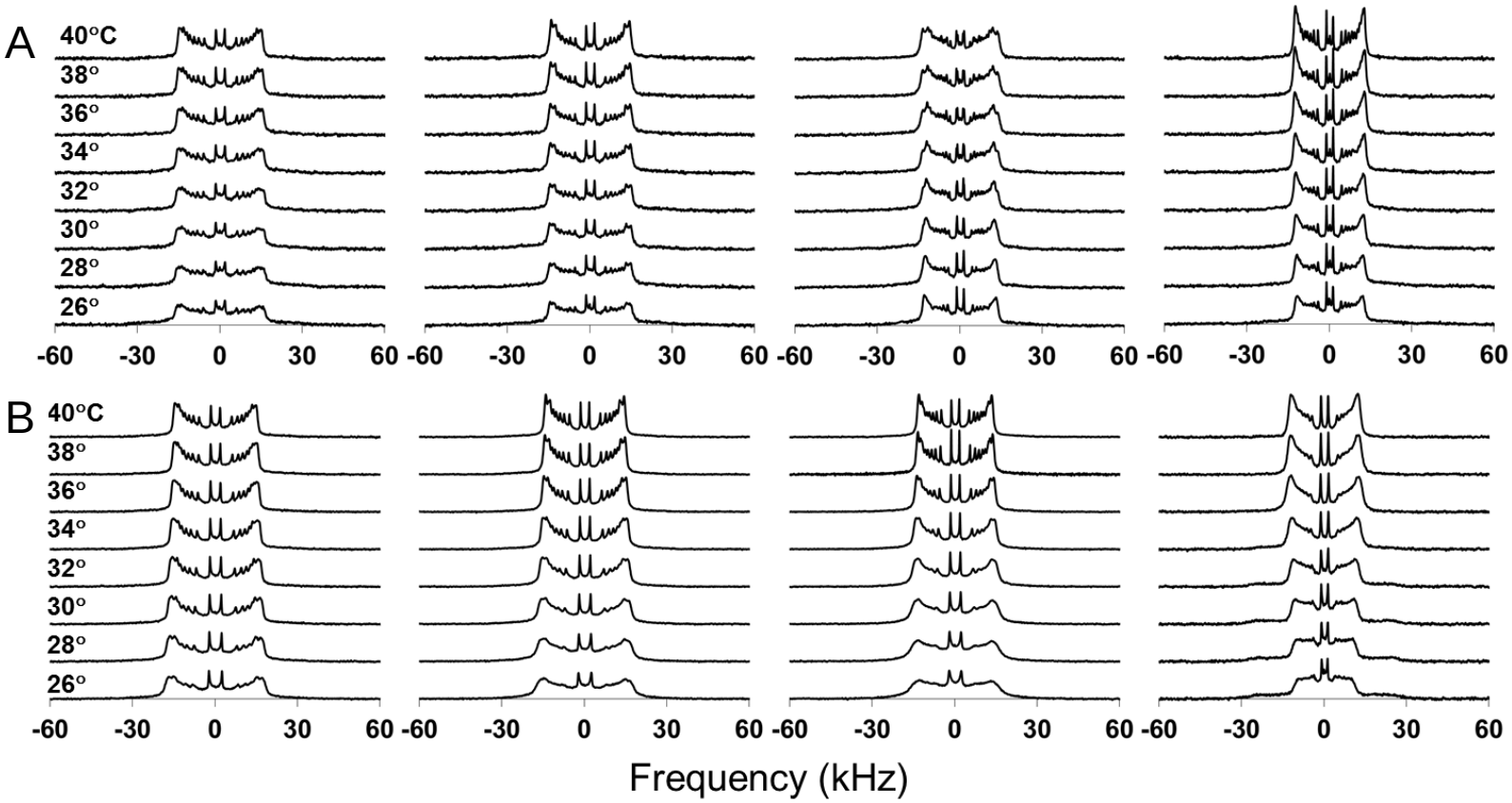

Figure 4-31. ^{2}H NMR spectra as a function of temperature for POPC-d_{31} in A) the $CLSE^{L}$ environment containing 0-5% SP-B_{1-25} and B) the $CLSE^{Syn}$ environment containing 0-5% SP-B_{1-25}

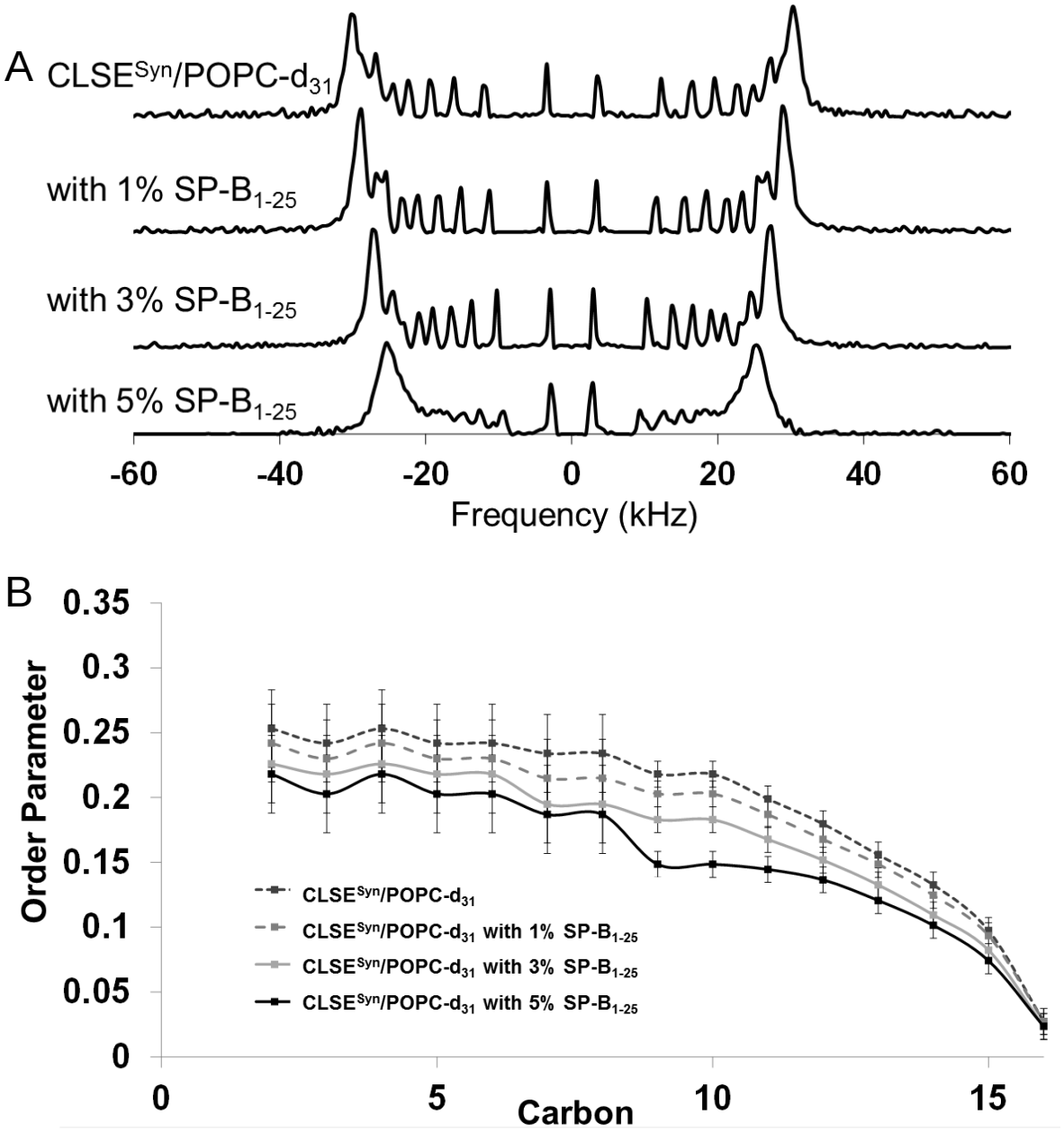

Figure 4-32. A) dePaked ^{2}H NMR spectra and B) Order parameter profile of POPC-d_{31} in the CLSE^{Syn} environment containing 0-5 mol% SP-B_{1-25}

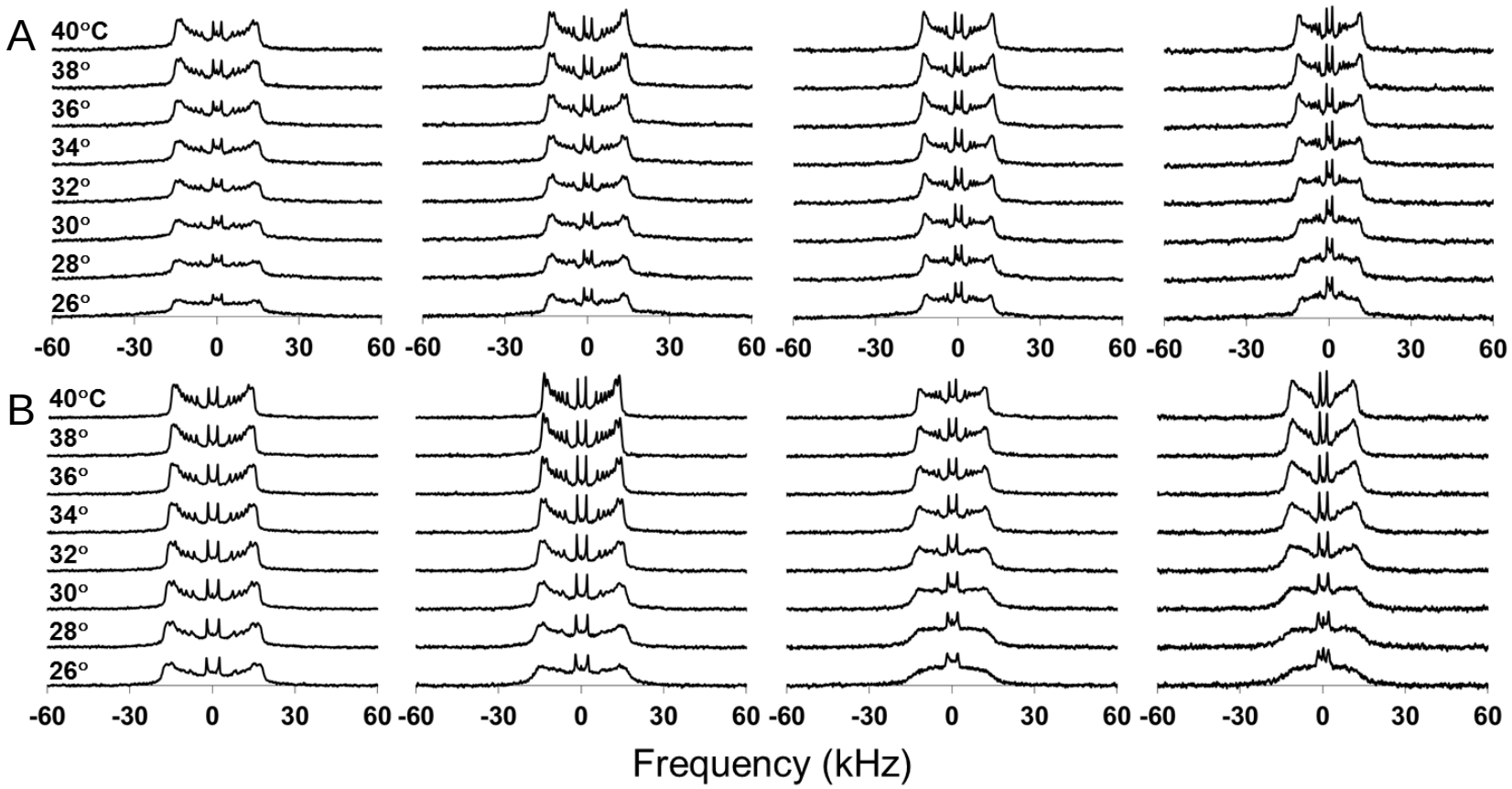

Figure 4-33. ^{2}H NMR spectra as a function of temperature for POPG-d_{31} in A) the $CLSE^{L}$ environment containing 0-5% SP-B_{1-25} and B) the $CLSE^{Syn}$ environment containing 0-5% SP-B_{1-25}

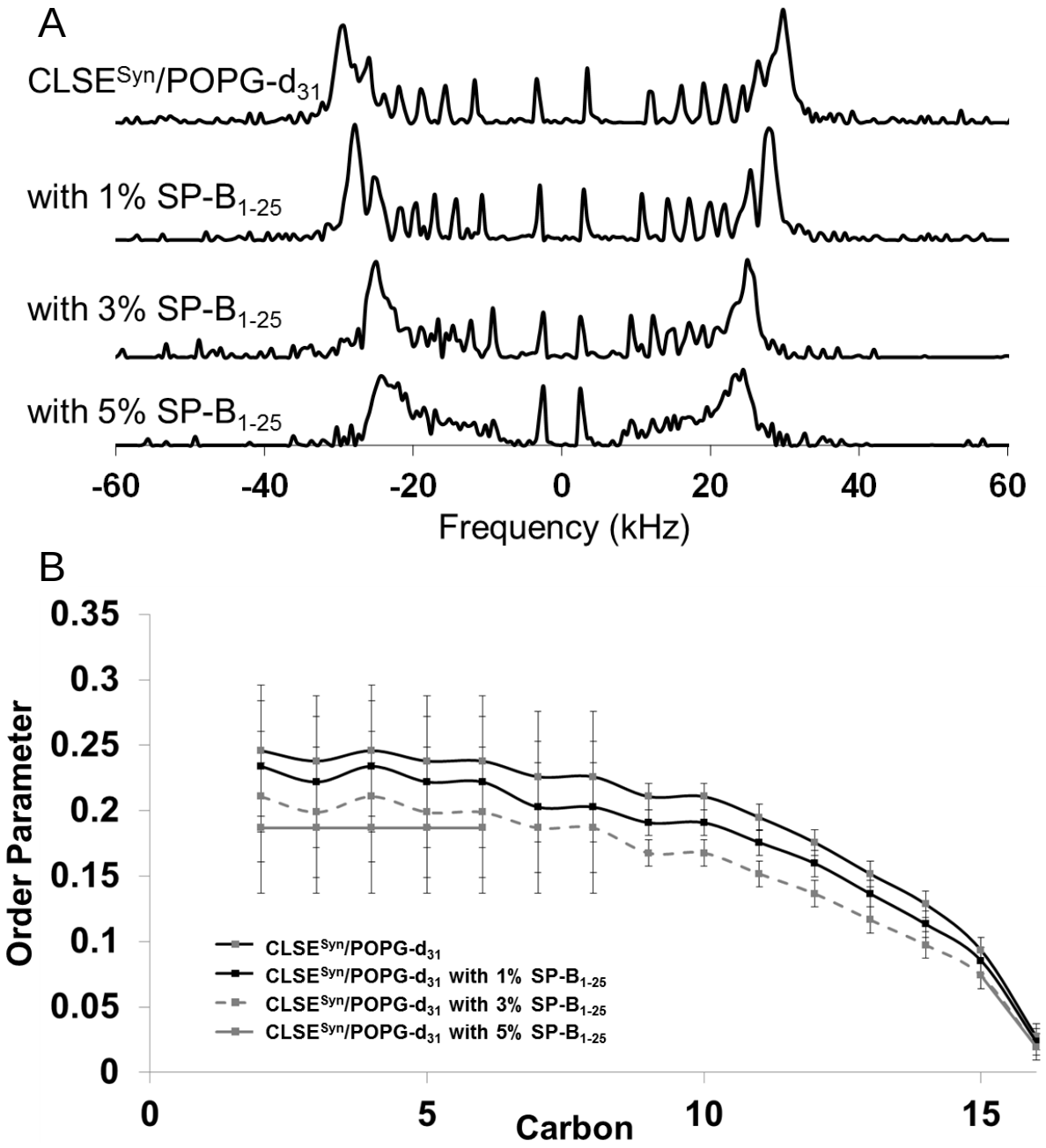

Figure 4-34. A) dePaked ^{2}H NMR spectra and B) Order parameter profile of POPG-d_{31} in the CLSE^{Syn} environment containing 0-5 mol% SP-B_{1-25}

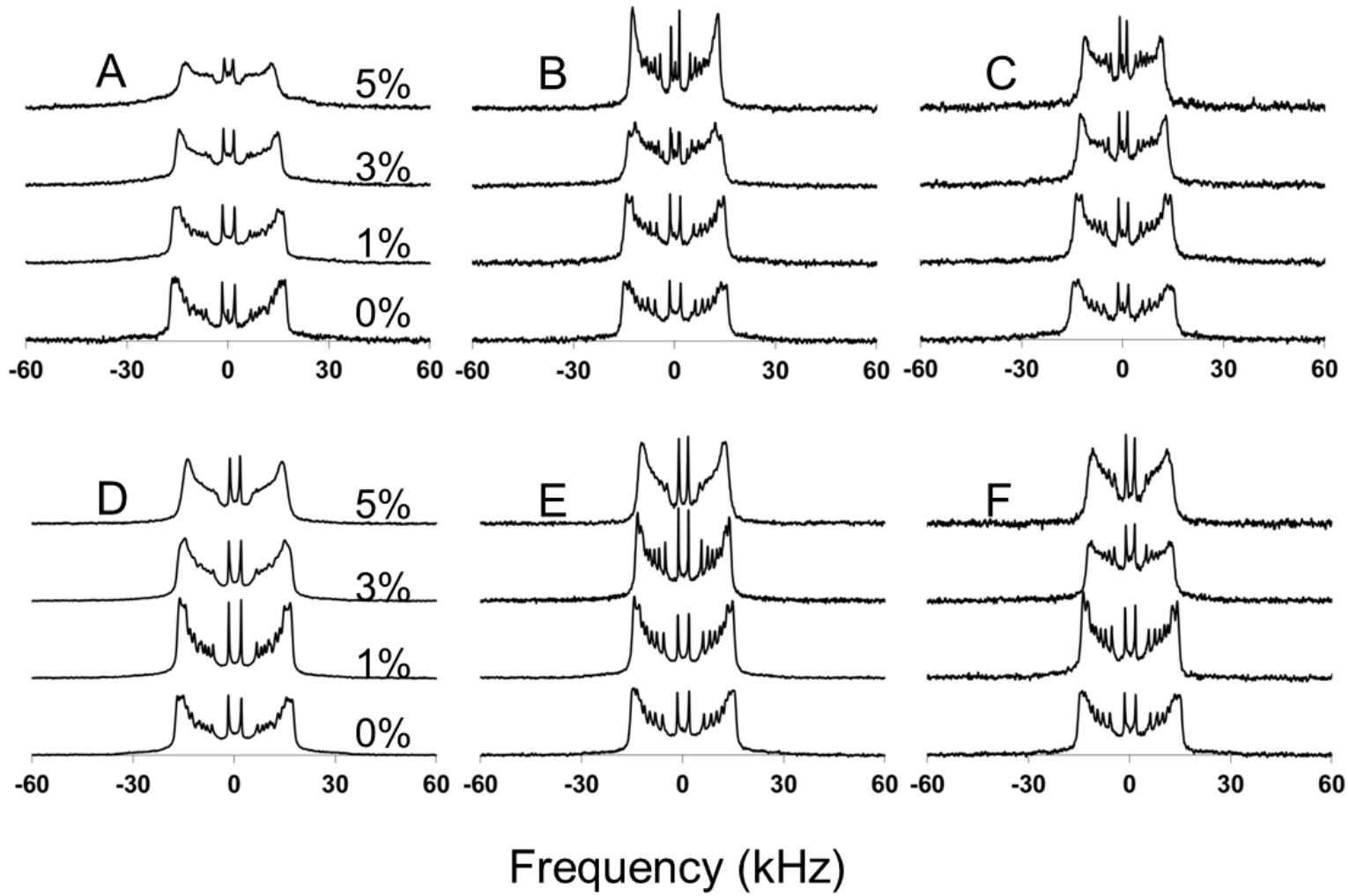

Figure 4-35. ^{2}H NMR spectra of A) $CLSE^{L}/DPPC\text{-}d_{62}$, B) $CLSE^{L}/POPC\text{-}d_{31}$, C) $CLSE^{L}/POPG\text{-}d_{31}$, D) $CLSE^{Syn}/DPPC\text{-}d_{62}$, E) $CLSE^{Syn}/POPC\text{-}d_{31}$, and F) $CLSE^{Syn}/POPG\text{-}d_{31}$ with 0-5 mol% $SP\text{-}B_{1\text{-}25}$ at 38°C

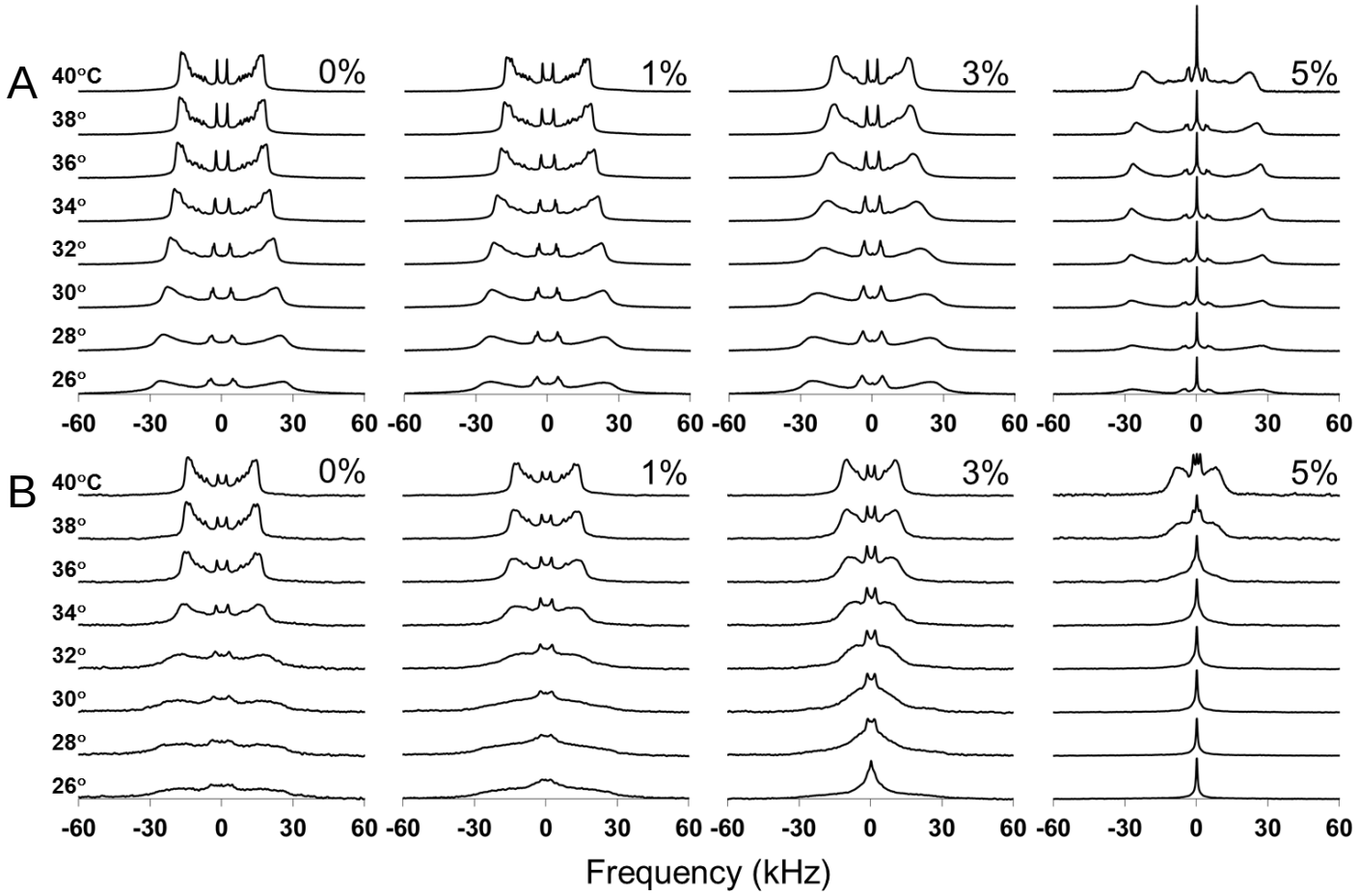

Figure 4-36. Deuterium spectra for A) 8:2:1 DPPC-d_{62}/POPG/cholesterol with 0-5% SP-B_{1-25} and B) 8:2:1 DPPC /POPG-d_{31}/cholesterol with 0-5% SP-B_{1-25} as a function of temperature.

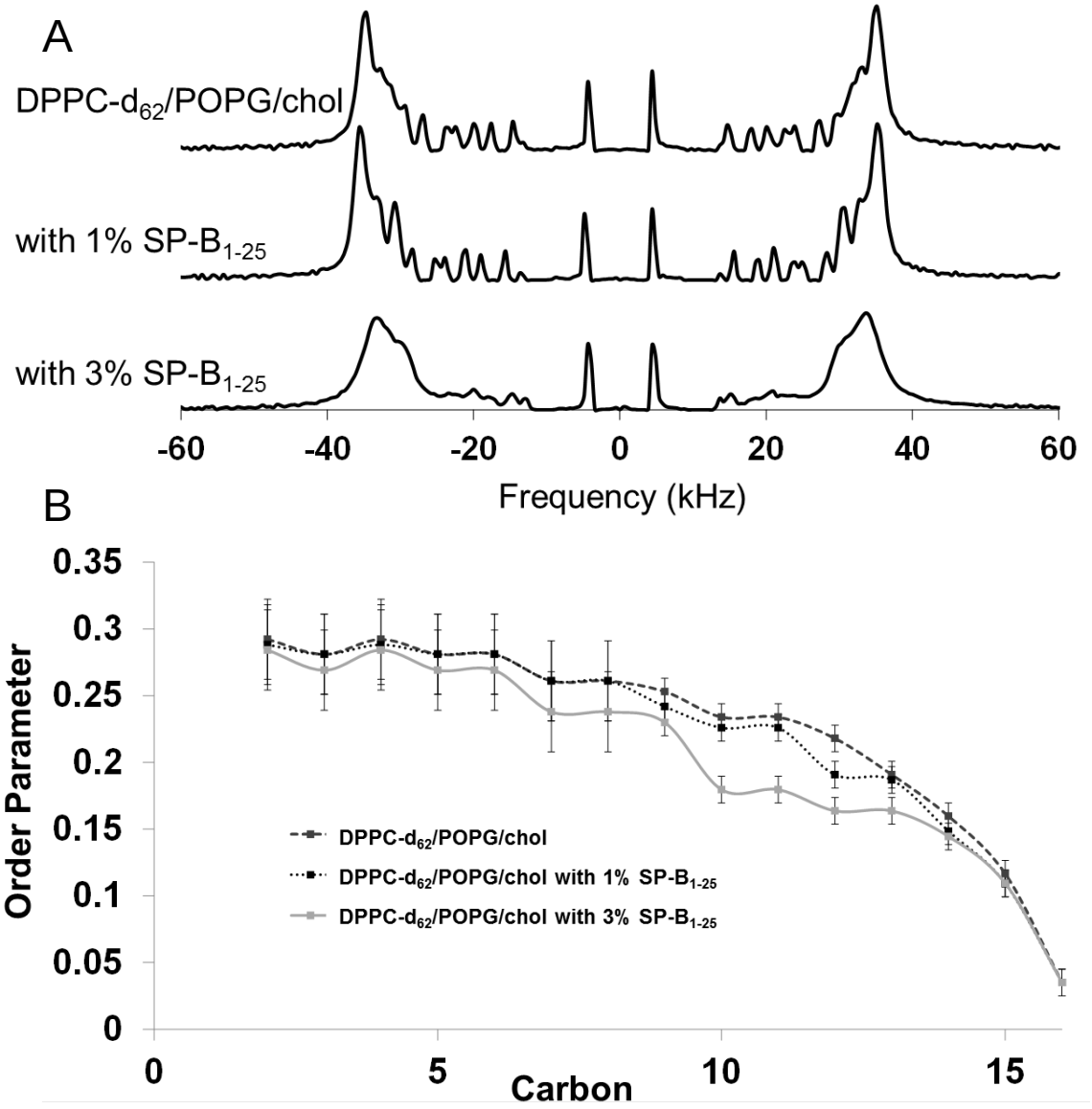

Figure 4-37. A) dePaked ^{2}H NMR spectra and B) Order parameter profile of DPPC-d_{62} in the DPPC/POPG/cholesterol lipid system containing 0-3 mol% SP-B_{1-25}

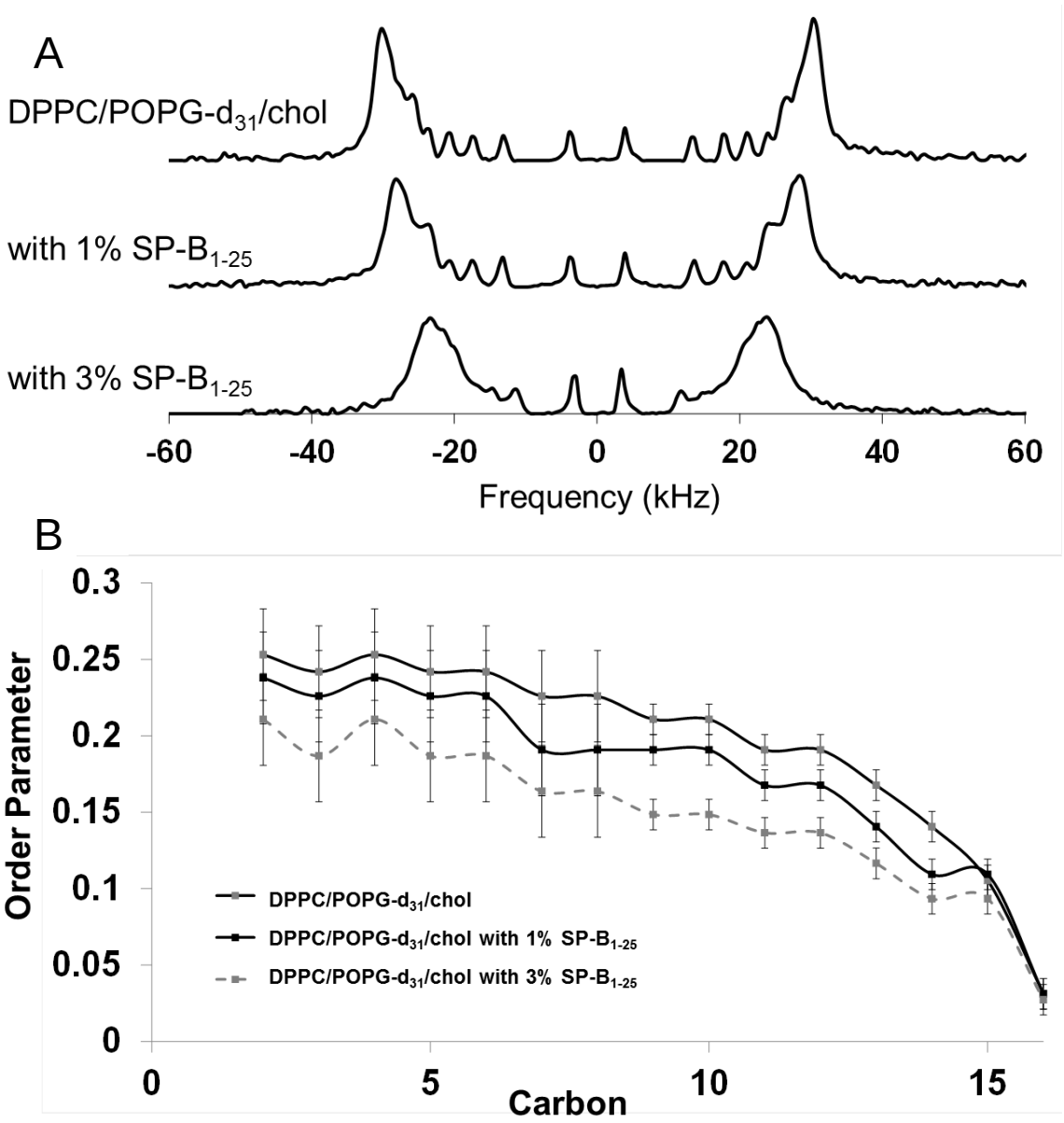

Figure 4-38. A) dePaked ^{2}H NMR spectra and B) Order parameter profile of POPG-d_{31} in the DPPC/POPG/cholesterol lipid system containing 0-3 mol% SP-B_{1-25}

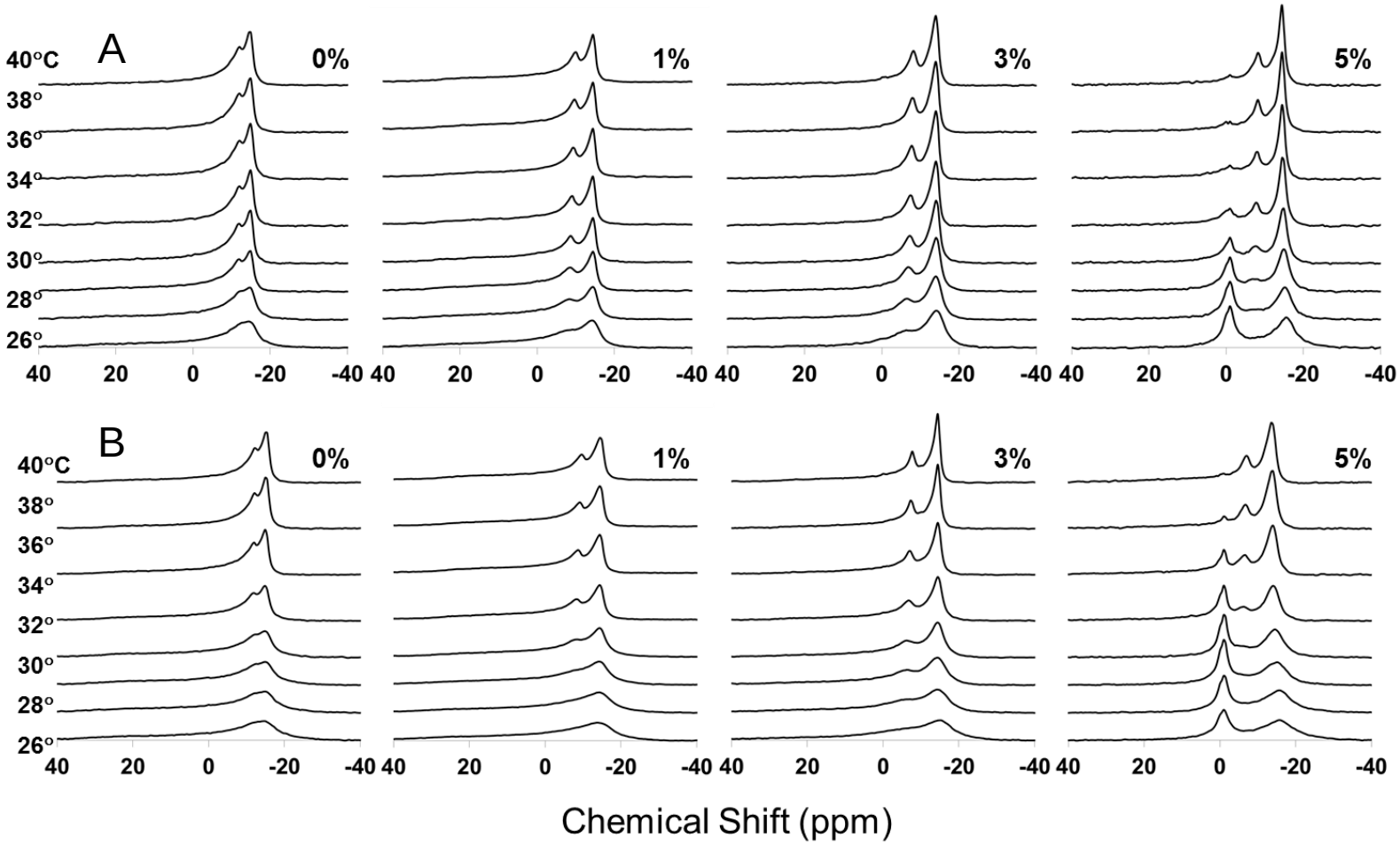

Figure 4-39. ^{31}P NMR spectra as a function of temperature of A) 8:2:1 DPPC-d_{62}/POPG/cholesterol containing 0-5 mol% SP-B_{1-25} and B) 8:2:1 DPPC /POPG-d_{31}/cholesterol containing 0-5 mol% SP-B_{1-25}

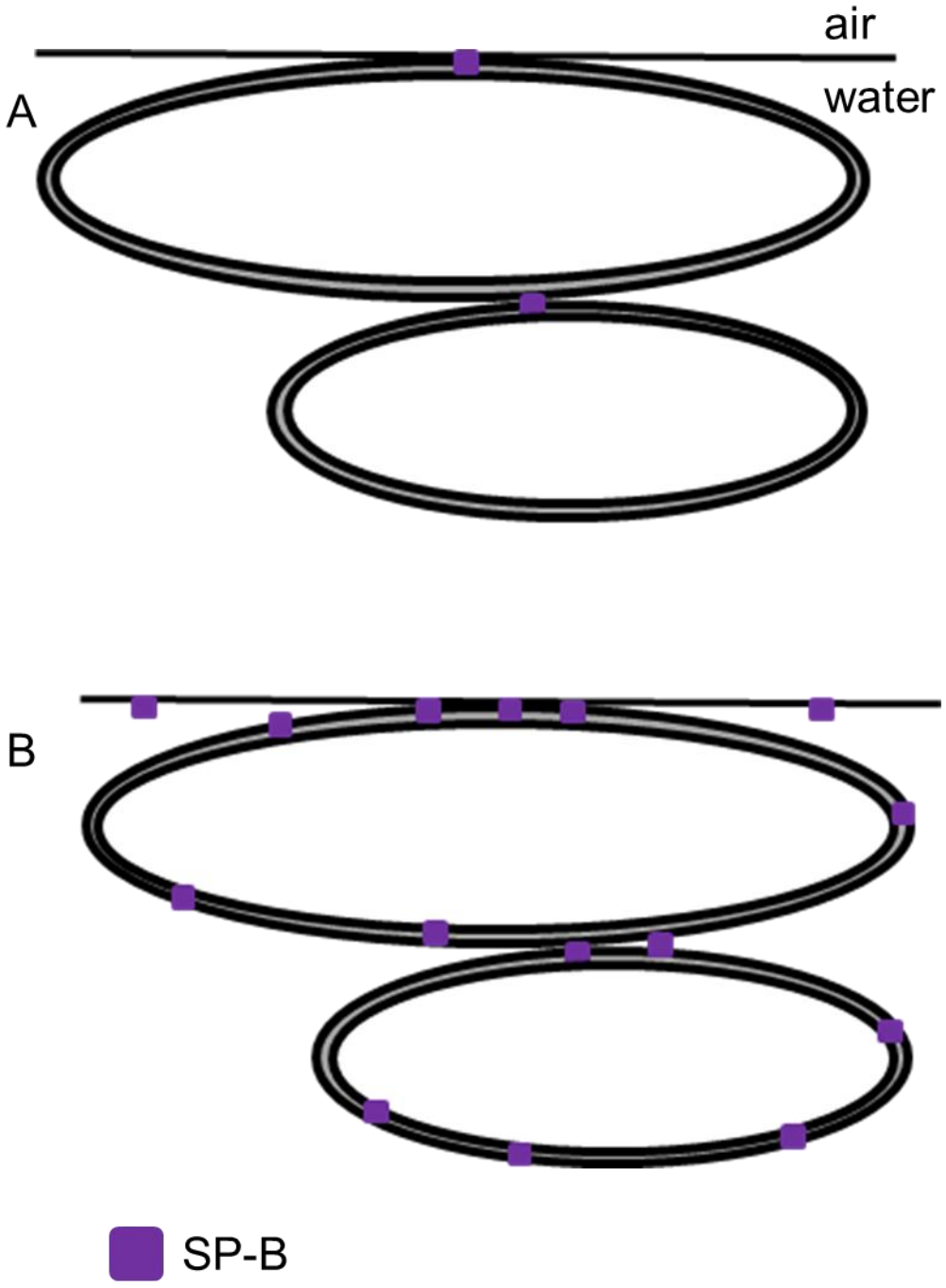

Figure 4-40. Lipid/peptide ratio schematic of 1000:1 vs 100:1. A) 1000:1 lipid/SP-B and B) 100:1 lipid/SP-B. In $CLSE^{T}$ there is about 0.1 mol% SP-B, which is a 1000:1 lipid/SP-B ratio. Clinically used LS replacements generally have a 100:1 ratio of lipid to peptide. There was a very small amount of lipids affected by SP-B in $CLSE^{T}$ and NMR experiments measure bulk properties, which contributed to not seeing a difference between $CLSE^{T}$ and $CLSE^{L}$.

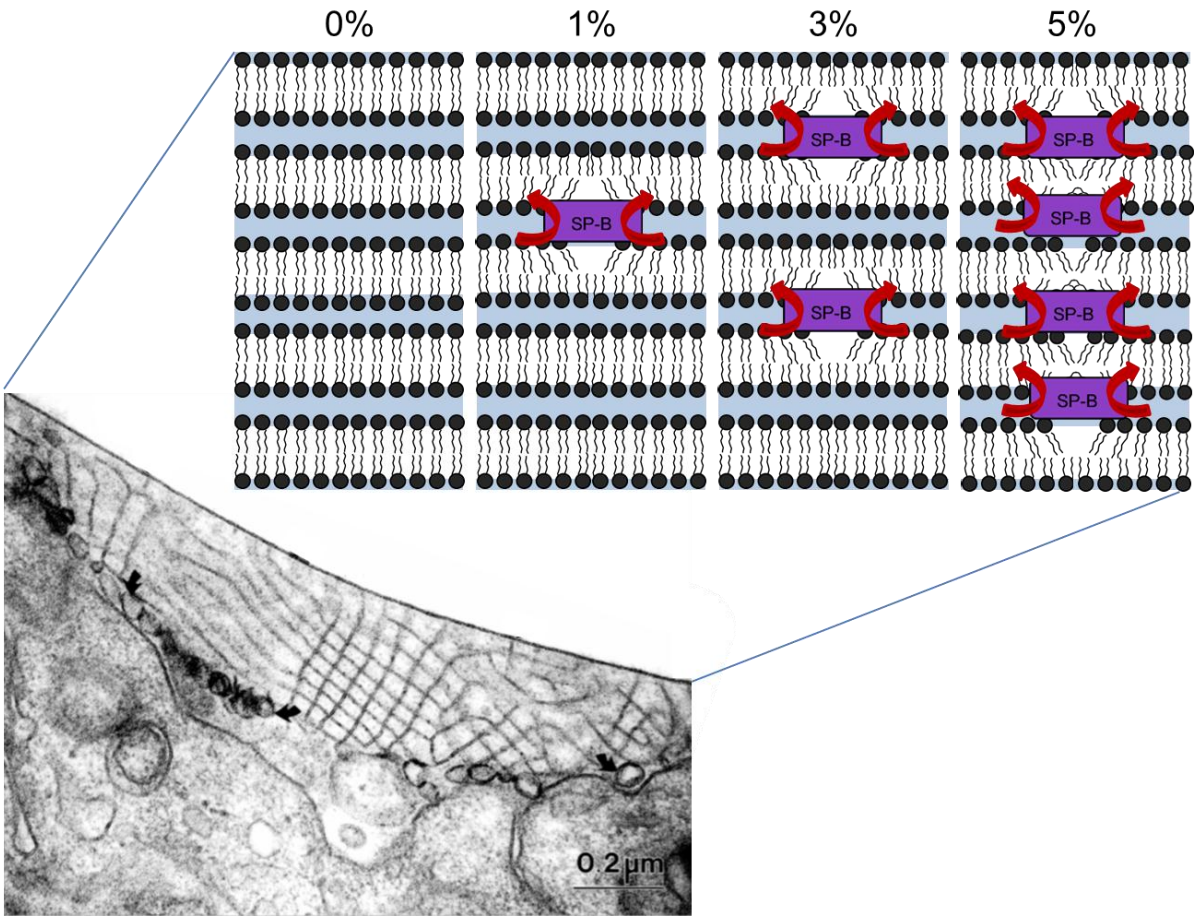

Figure 4-41. Schematic of how different concentrations of SP-B may affect lipid bilayers in lung surfactant. A TEM of rat-intra-alveolar lung surfactant is shown as a reminder of the complicated infrastructure found in alveoli below the air/water interface. Increasing concentrations of SP-B (0-5 mol%) cause lipid flipping between bilayers like a connecting doorway. The TEM image was reproduced with permission from Dr. Heinz Fehrenbach, author of “Alveolar epithelial type II cell: defender of the alveolus revisited" (*146*) (Respir Res 2001, 2:33–46 originally published by Biomed Central).

Neat lipids	Therapeutic CLSE
DPPC/DPPC-d_{62}	$CLSE^{T}$/DPPC-d_{62}
POPC/POPC-d_{31}	$CLSE^{T}$/POPC-d_{31}
POPG/POPG-d_{31}	$CLSE^{T}$/POPG-d_{31}
POPE/POPE-d_{31}	$CLSE^{T}$/POPE-d_{31}
CLSE lipids only	**Synthetic CLSE ($CLSE^{Syn}$)**
$CLSE^{L}$/DPPC-d_{62}	10:6:3:2:2 DPPC-d_{62}/POPC/POPG/POPE/chol
$CLSE^{L}$/POPC-d_{31}	10:6:3:2:2 DPPC/POPC-d_{31}/POPG/POPE/chol
$CLSE^{L}$/POPG-d_{31}	10:6:3:2:2 DPPC/POPC/POPG-d_{31}/POPE/chol
$CLSE^{L}$/POPE-d_{31}	10:6:3:2:2 DPPC/POPC/POPG/POPE-d_{31}/chol
Binary lipids	**Ternary lipids**
4:1 DPPC-d_{62}/POPG	8:2:1 DPPC-d_{62}/POPG/chol
4:1 DPPC/POPG-d_{31}	8:2:1 DPPC/POPG-d_{31}/chol

Figure 4-42. Lipid mixtures

Sample	T_m from 1st Moment
DPPC/DPPC-d_{62}	41.4°C
POPC/POPC-d_{31}	-2.4°C
POPG/POPG-d_{31}	-2.0°C
POPE/POPE-d_{31}	28.0°C
$CLSE^T$/DPPC-d_{62}	28.0°C
$CLSE^T$/POPC-d_{31}	19.5°C
$CLSE^T$/POPG-d_{31}	21.8°C
$CLSE^T$/POPE-d_{31}	22.0°C

Figure 4-43. Phase transition temperatures of deuterated lipids in neat and $CLSE^T$ lipid systems

Sample	T_m from 1st Moment
DPPC/DPPC-d_{62}	41.4°C
DPPC-d_{62}/POPG	30.8°C
DPPC-d_{62}/POPG/chol	29.9°C
$CLSE^{L}$/DPPC-d_{62}	28.3°C
$CLSE^{T}$/DPPC-d_{62}	28.0°C
$CLSE^{Syn}$DPPC-d_{62}	23.8°C

Figure 4-44. Phase transition temperatures of DPPC-d_{62} in various LS lipid systems.

CHAPTER 5
PEPTIDE SEQUENCE AND LIPID ENVIRONMENT AFFECT SP-B_{1-25} BEHAVIOR

This chapter is a brief manuscript in preparation for submission to either Biochemistry or Biophysica et Biochimica Acta-Biomembranes. The final submission may be different from this version due to revisions that occur during the peer review process as well as journal formatting differences.

Introduction

This chapter investigates the differences seen in lipid dynamics as regulated by point mutations in the peptide sequence of SP-B_{1-25}. The function of this peptide in binary lipid systems as well as other lipid environments may be sequence and environment dependent as we have evidence of variations in lipid morphologies as a result of mutating two amino acids in the N-terminus. In Chapter 3 I proposed a model based on evidence of a fluid isotropic phase seen in ^{2}H and ^{31}P NMR data which suggests a molecular mechanism for how the highly hydrophobic N-terminus of SP-B can facilitate packing of lipid lamellae into surfactant lamellar bodies or stabilize multilayer structures at the air/water interface by lipid fusion. Manipulations of the N-terminal sequence and assaying lipid dynamics in different lipid systems has resulted in further characterization of this peptide and its role in modulating lipid organization. In this chapter the three point mutations introduced during peptide synthesis are C8S, C11S, and M21I. The lipid environments include the binary DPPC/POPG lipid system as well as lipids isolated from a CLSE mixture and a synthetic lipid combination based on the CLSE lipid components.

Materials and Methods

Synthesis of SP-B_{1-25} (C8S, C11S, M21I)

SP-B_{1-25} (C8S, C11S, M21I), (FPIPLPYSWLSRALIKRIQAIIPKG), was synthesized via automated solid-phase peptide synthesis on a Wang resin (ABI 430, ICBR, UF), cleaved with King's reagent and ether precipitated as was the WT sequence in Chapter 4. Crude product was purified by RP-HPLC using a C18 Vydac column (Grace, Deerfield, IL) with a water/acetonitrile gradient (containing 0.3% TFA). Fractions corresponding to SP-B_{1-25} were collected and purity of the product was verified by mass spectrometry. The peptide solution was lyophilized and dried peptide was dissolved in methanol to yield a final concentration of approximately 1 mM and quantitated by UV analysis.

Calf Lung Surfactant Extract

Research grade calf lung surfactant extract (CLSE) was generously provided as a gift from ONY, Inc. (Amherst, NY). For the experiments in this study, CLSE lipids were separated from CLSE proteins same as in Chapter 4.

Biochemical Separation of CLSE Lipids and Proteins

The proteins in CLSE were separated from the lipids by gel permeation chromatography using previously established methods (*131*). The separation was performed as in Chapter 4.

Preparation of NMR Samples

Samples were made with CLSE lipids after removal of proteins, by combining pure lipids in chloroform based on the lipid composition of CLSE (10:6:3:2:2 DPPC/POPC/POPG/POPE/cholesterol), and with binary DPPC/POPG mixtures. Acyl chain deuterated lipids, DPPC-d_{62}, POPC-d_{31}, POPG-d_{31}, and POPE-d_{31} were

purchased from Avanti (Avanti Polar Lipids, Alabaster, AL) and added to the CLSE and synthetic lipid mixtures as reporters in the ^{2}H NMR experiments. The animal derived LS samples contained ~20-50 mg of CLSE (lipids only) with 2-5 mg added deuterated phospholipid. For peptide containing samples, SP-B_{1-25} (C8S, C11S, M21I) in methanol was added to the lipid chloroform solutions resulting in P/L ratios ranging from 1:100 to 1:20. Samples were dried under a stream of nitrogen while in a water bath at 45-50°C; the resulting films were suspended in warm cyclohexane (45-50°C), flash frozen in nitrogen, and lyophilized overnight to remove residual solvent.

For each solid-state NMR sample, ~15-50 mg of peptide-lipid powder was placed in a 5 mm diameter NMR tube and 200 µL of buffer containing 10mM (or 50mM) HEPES, pH 7.4, 140mM NaCl, and 1mM EDTA in ^{2}H depleted water (Cambridge Isotopes, Andover MA) was added. The hydrated dispersions (in NMR tubes) were subjected to 5 freeze-thaw cycles with gentle vortexing to form MLVs

Solid State NMR Analysis

^{2}H NMR data were collected on a 500 MHz Bruker DRX system (Billerica, MA) using a standard 5 mm BBO probe with the lock channel detuned. For the ^{2}H NMR experiments, data were collected using a quad echo sequence (90°-τ-90°-τ-acq with τ = 30 μs) with a ^{2}H B_1 field of 42 kHz (5.95 µs 90°pulse). ^{2}H spectra were acquired with 2k-16k scans and a 0.5 second recycle delay between scans.

Results

This chapter details the changes in lipid dynamics seen in LS mimic systems as point mutations are introduced into the peptide sequence and the lipid environment is varied. The two peptides in this study are SP-B_{1-25} (WT) and SP-B_{1-25} (C8S, C11S,

M21I). Binary and quaternary synthetic lipid systems and CLSE lipids are the lipid environments utilized for this study. ^{2}H static ssNMR experiments were used to examine how lipid dynamics and organization are affected by addition of the LS peptides and the differences seen when the lipid system is varied. ^{2}H spectroscopy allows monitoring of the dynamics and polymorphisms of individual lipid species that are deuterium enriched and in particular the dynamics of the deuterated lipid acyl chains.

Temperature dependent behavior of deuterated DPPC in DPPC/POPG, $CLSE^{L}$, and the $CLSE^{Syn}$ environment as measured by ^{2}H NMR is shown in Figure 5-1. The stack plots show that DPPC-d_{62} behaves differently in these LS lipid systems. When mixed with POPG, DPPC remains in a gel phase at lower temperatures and melts at 30.8°C where it continues to exhibit a lamellar phase through physiologic temperature. The T_m for DPPC decreases to 28.3°C in the $CLSE^{L}$ system and shows mostly liquid-crystalline lineshapes throughout the temperature range. In the $CLSE^{Syn}$ environment, the T_m is the lowest at 23.8°C. The spectra are slightly broader at lower temperatures indicating less fluidity and exchange broadening of the lipid phases. Worth noting is the similarity between the $CLSE^{L}$ environment and the $CLSE^{Syn}$ sample. The $CLSE^{Syn}$ system is based on the main lipids of CLSE and is a synthetic CLSE environment. The next experiments involve the LS peptide, SP-B_{1-25}, and its addition to the lipid environments just discussed.

Shown in Figure 5-6 are the sequences of the SP-B analogues used for the experiments in this chapter. The mutant peptide contains two serines instead of cysteines and an isoleucine instead of methionine. Mutating the cysteines to another amino acid with similar hydrophobicity is ideal as disulfide bonds can be very

troublesome in peptide purification and sample preparation when they are not wanted. The reason for choosing serine over isoleucine as a substitute for cysteine is the similarity in size and structure of serine and cysteine. This substitution is common practice, however the hydrophobicity of isoleucine and cysteine are more similar than that of serine (*148*, *149*). While isoleucine has similar hydrophobicity to cysteine, its difference in size could change peptide properties when sitting in a lipid bilayer. The better substitution for cysteine is still under debate as subtle changes in peptide sequence can have a large effect on lipid dynamics as seen in this chapter.

In Figure 5-2 are shown ^{2}H NMR spectra of deuterated DPPC as a function of temperature and peptide concentration in 4:1 DPPC-d_{62}/POPG. The sample peptide for the top panel of spectra is SP-$B_{1\text{-}25}$ (WT) and for the bottom panel, SP-$B_{1\text{-}25}$ (C8S, C11S, M21I). With addition of the peptides, the 1 mol% data look very similar, but when more peptide is added the lipid dynamics change drastically between the different peptide containing samples as seen for the 3 and 5 mol% data. When the wild type SP-$B_{1\text{-}25}$ is present at 3 mol%, an isotropic peak is seen from 26 to 36°C; the isotropic peak is not seen when the mutated form of the peptide is present and the spectra look much like the 1% spectra. Isotropic peaks are seen for both peptide containing samples when 5 mol% SP-$B_{1\text{-}25}$ is present, however up to only 30°C for the mutant peptide, while the isotropic peak persists when the wild type form of SP-$B_{1\text{-}25}$ is present.

In Figure 5-3 are shown ^{2}H NMR spectra of deuterated POPG as a function of temperature and peptide concentration in 4:1 DPPC /POPG-d_{31}. Again, the sample peptide for the top panel of spectra is SP-$B_{1\text{-}25}$ (WT) and for the bottom panel, SP-$B_{1\text{-}25}$ (C8S, C11S, M21I). With addition of the peptides, the 1 mol% data look very similar,

but when more peptide is added the lipid dynamics change between the different peptide containing samples, however POPG behaves differently than DPPC. When the wild type SP-B_{1-25} is present at 5 mol%, an isotropic peak is seen from 26 to 32°C; the isotropic peak persists up to 38°C when the mutated form of the peptide is present and is also seen in the 3% data unlike the DPPC spectra in Figure 5-2 bottom panel. Sp-B_{1-25} (C8S, C11S, M21I) is having the opposite effect on POPG compared to DPPC.

Most striking are the ^{2}H NMR spectra of DPPC-d_{62} shown in Figure 5-4 where each sample contains 5 mol% of either SP-B_{1-25} (WT) or SP-B_{1-25} (C8S, C11S, M21I) and is found in one of three lipid environments: 4:1 DPPC-d_{62}/POPG, $CLSE^{L}$/DPPC-d_{62}, or $CLSE^{Syn}$/DPPC-d_{62}. Figure 5-4 A and D show the lipid dynamics of deuterated DPPC when the wild type peptide is present (top) and the mutant form is present (bottom) in 4:1 DPPC/POPG. These spectra are the most isotropic compared to the spectra of DPPC-d_{62} in other environments and with either peptide. The addition of 5 mol% peptide causes DPPC to go into an isotropic phase. Comparing B and E, one can also see a change in lipid dynamics and polymorphisms for DPPC-d_{62} in the $CLSE^{L}$ environment when wild type or mutant peptide is present as SP-B_{1-25} (C8S, C11S, M21I) causes an isotropic peak to form whereas SP-B_{1-25} (WT) does not in the temperature range from 26 to 40°C. Figure 5-4C and F compare the effect of the peptides in the $CLSE^{Syn}$ environment. DPPC-d_{62} remains in a gel phase at similar temperatures between the two spectra and reach liquid-crystalline Lα phases, however, there are large differences in the widths of the lineshapes indicating increased fluidity when the mutant peptide is in the sample. Comparing spectra from left to right in Figure 5-4, one can see differences in lipid dynamics for DPPC-d_{62} in the three lipid

environments when the same peptide is present. Every spectrum in this figure is different and shows how lipid dynamics can change for a deuterated peptide in an LS mimic system depending on peptide sequence and lipid environment. Figure 5-5 illustrates the lipid phases that occur at different temperatures when 5 mol% peptide is present. At the lower temperatures the spectra are isotropic due to the fluid isotropic behavior of the lipids as they are fused together by SP-B_{1-25}. At higher temperatures the spectra become lamellar as the lipids rearrange into bilayer phases.

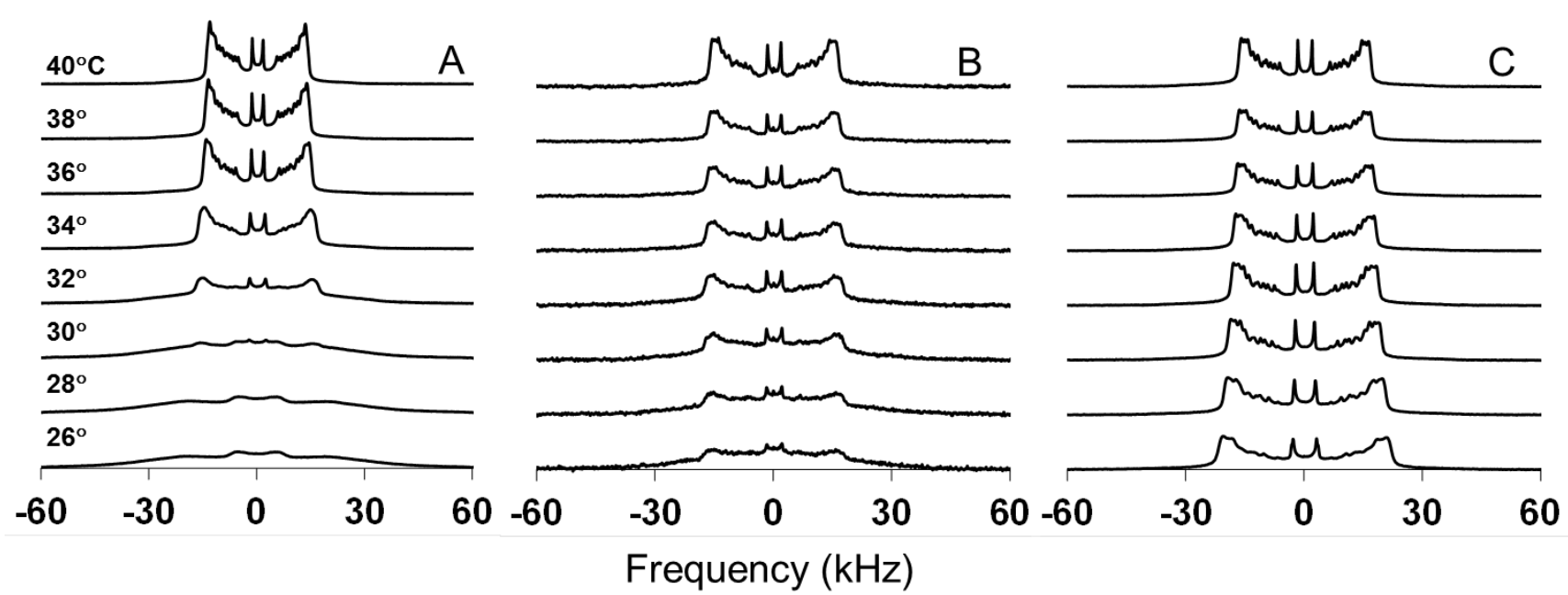

Figure 5-1. ^{2}H NMR spectra as a function of temperature for A) 4:1 DPPC-d_{62}/POPG, B) $CLSE^{L}$/DPPC-d_{62}, and C) $CLSE^{Syn}$/DPPC-d_{62}

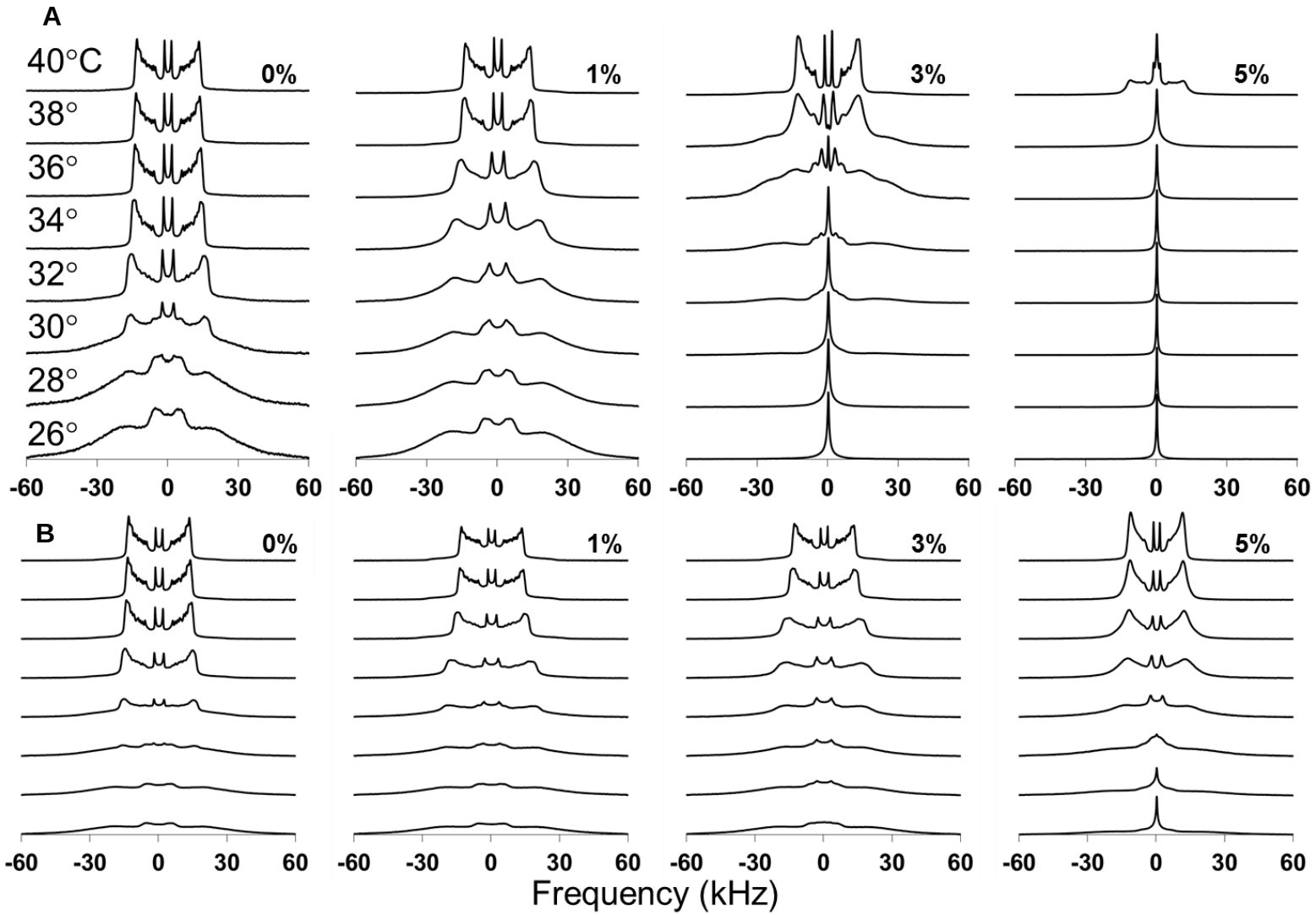

Figure 5-2. Deuterium spectra as a function of temperature for A) 4:1 DPPC-d_{62}/POPG with 0-5 mol% SP-B_{1-25} (WT), and B) 4:1 DPPC-d_{62}/POPG with 0-5 mol% SP-B_{1-25} (C8S, C11S, M21I)

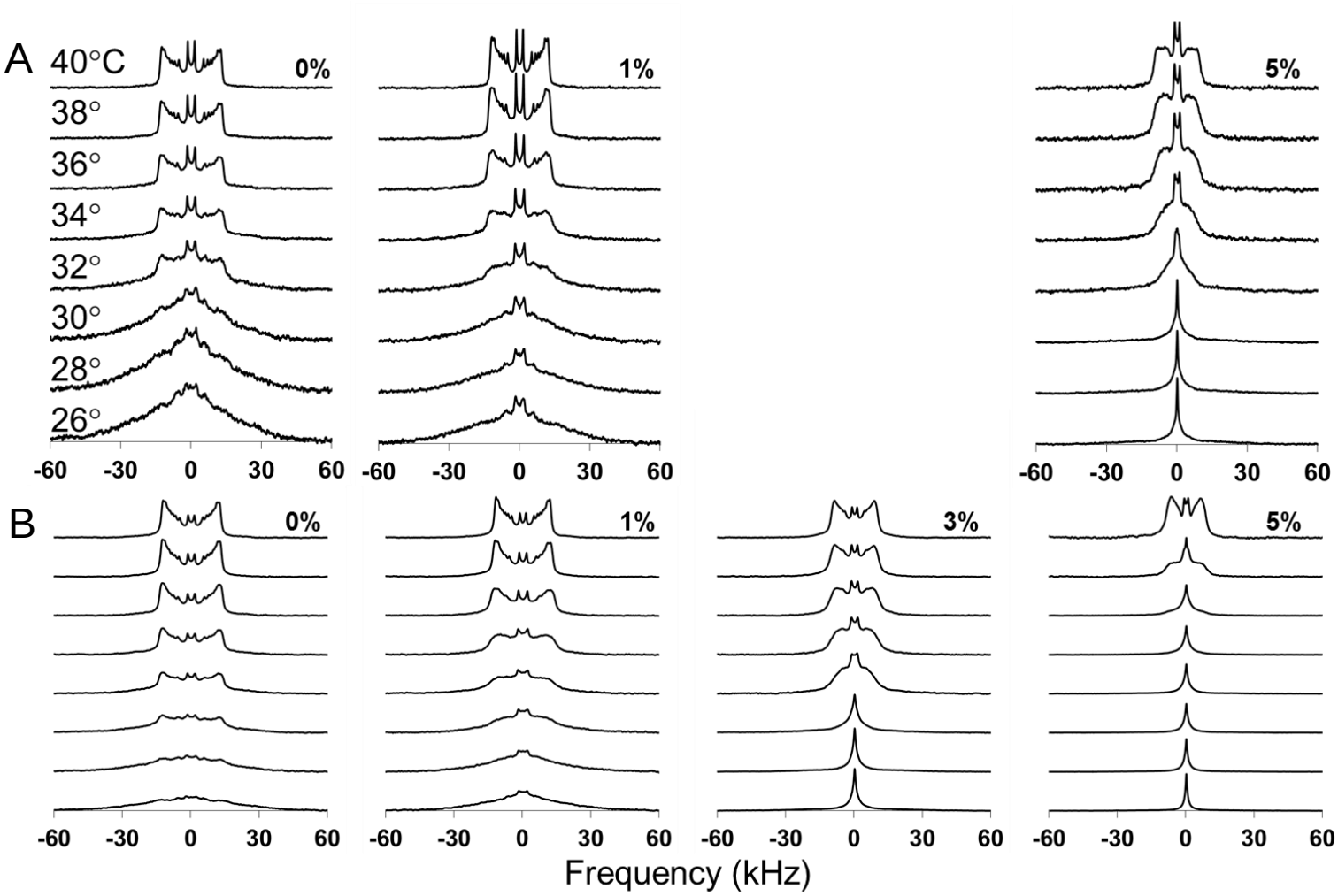

Figure 5-3. Deuterium spectra as a function of temperature for A) 4:1 DPPC /POPG-d_{31} with 0-5 mol% SP-B_{1-25} (WT), and B) 4:1 DPPC /POPG-d_{31} with 0-5 mol% SP-B_{1-25} (C8S, C11S, M21I)

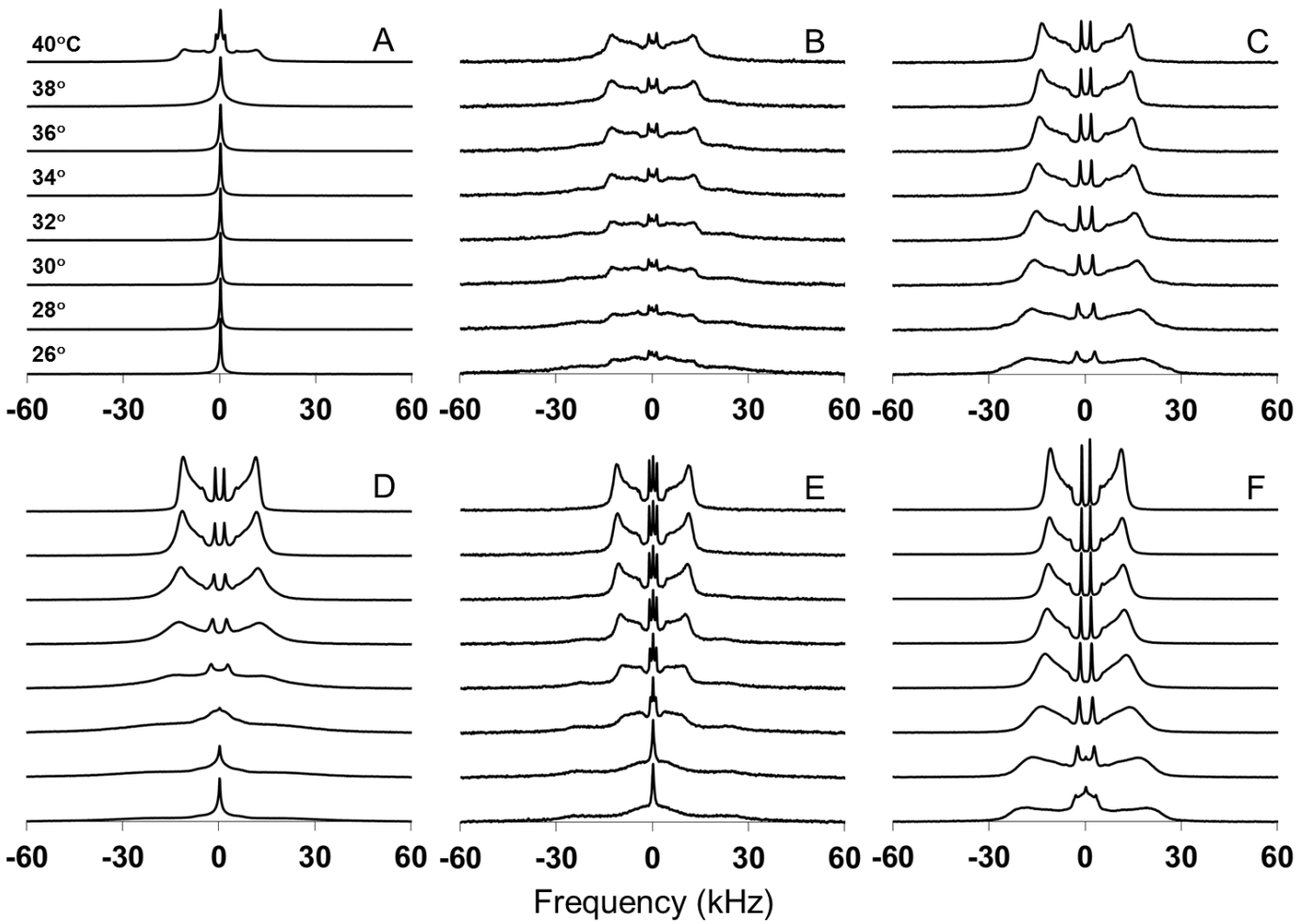

Figure 5-4. Deuterium spectra as a function of temperature for A) 4:1 DPPC-d_{62}/POPG with 5% SP-B_{1-25} (WT), B) $CLSE^{L}$/DPPC-d_{62} with 5% SP-B_{1-25} (WT), C) $CLSE^{Syn}$ /DPPC-d_{62} with 5% SP-B_{1-25} (WT), D) 4:1 DPPC-d_{62}/POPG with 5% SP-B_{1-25} (C8S, C11S, M21I), E) $CLSE^{L}$/DPPC-d_{62} with 5% SP-B_{1-25} (C8S, C11S, M21I), and F) $CLSE^{Syn}$/DPPC-d_{62} with 5% SP-B_{1-25} (C8S, C11S, M21I)

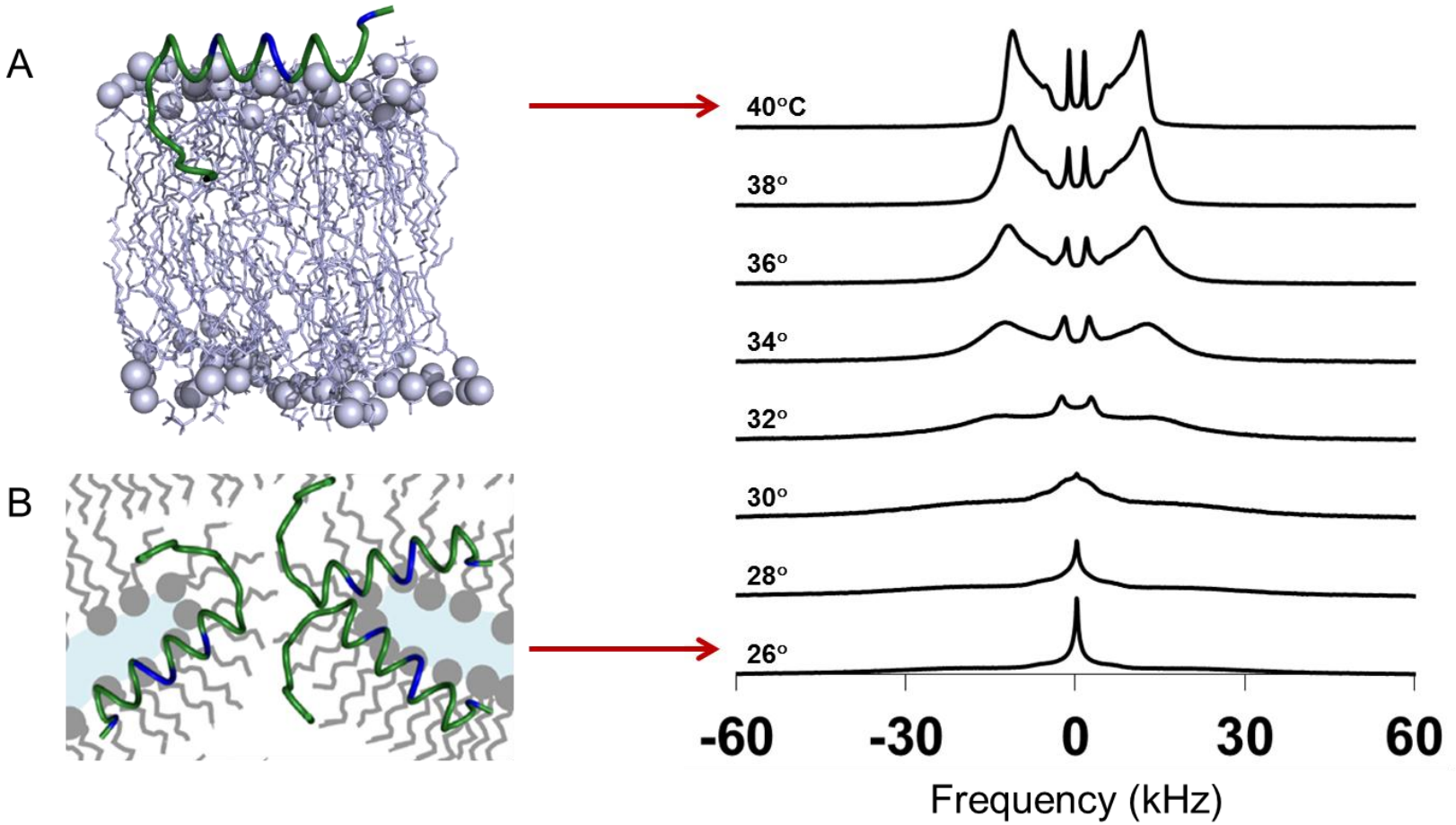

Figure 5-5. Lipid phases at high and low temperatures with 5 mol% SP-B_{1-25}. A) bilayer phase at 40°C B) fluid isotropic phase at 26°C.

Figure 5-6. Full sequence of SP-B and peptide analogues of the N-terminus of SP-B with and without point mutations

CHAPTER 6
CONCLUSIONS AND FUTURE DIRECTIONS

Many lung surfactant deficiency and dysfunction pathologies could potentially be remediated by LS replacement therapies. Current clinical formulations are animal derived which can pose risks to the patient due to their potential of having infectious material and stimulating an immune response. They are used in only a subset of respiratory distress syndromes. The problems and inconsistencies with LS from animal sources have steered current research toward combinations of synthetic LS protein mimics and lipids. Presented here were insights into the molecular level behavior of synthetic LS constituents and comparisons to synthetic and animal derived formulations of varying levels of complexity. This work is a continuation of research aimed at understanding LS on a molecular level to guide development of synthetic formulations and provide effective in vitro assays for testing activity.

In Chapter 3 we showed that SP-B_{1-25} retains a constant secondary structure when associated with DPPC/POPG and POPC/POPG lipid systems and causes the formation of fluid isotropic lipid phases, particularly for DPPC containing lipid mixtures at physiologic temperatures. Previous CD data of the C-terminal SP-B peptide, SP-B_{59-80}, showed contrasting results with peptide secondary structure depending on the lipid environment (*14*). My work on SP-B_{1-25} and the work of my colleagues on SP-B_{59-80} have highlighted their effects on LS lipids, which suggest that the N- and C-termini of SP-B have complementary roles in trafficking of LS lipids. With the findings presented in Chapter 3 and elsewhere, a more thorough molecular model is established that provides insights into how these small peptides modulate lipid properties which can drive the development of future SP-B mimetics. The unique interplay observed for the

N- and C-termini of SP-B among lipid moieties, peptide penetration into the hydrophobic lipid environment, peptide structure, and lipid polymorphisms could explain the unique properties of SP-B in the dynamic lung environment. These peptides could have a synergistic effect whereby both ends of SP-B are important in regulating the dynamic lipid environment of the lung.

Chapter 4 presented a study of lipid dynamics in more complex LS combinations. The goal was to show if our previous synthetic models behaved anything like an animal derived LS formulation known as CLSE and to better understand the dynamics of individual lipid species in this system. We did not see the same polymorphisms in the more complex mixtures containing CLSE or DPPC/POPC/POPG/POPE/cholesterol as we saw in the synthetic binary LS lipid mixtures. However, we did see that adding up to 5% SP-B_{1-25} led to the observation of an isotropic DPPC rich phase in DPPC/POPG/cholesterol. The difference between the binary and ternary synthetic lipid mixtures could be due to the different DPPC concentrations and/or the addition of cholesterol, which is found at a similar concentration in CLSE. More importantly, we saw that the addition of SP-B_{1-25} had an observable effect on DPPC dynamics in complex synthetic lipid mixtures as well as CLSE approaching what we saw in the binary and ternary lipid mixtures in contrast to the other LS lipids. This suggests that SP-B_{1-25} is specifically interacting with the physiologically important disaturated lipid and would explain the existence of an isotropic phase in the binary and ternary mixture as it has a larger concentration of DPPC compared to the LS mimics with more lipid species. The more DPPC present, the more phase separation seen as well as nonlamellar lineshapes. The presence of cholesterol increased the order of the lipids as expected,

and the presence of this sterol along with less DPPC made the deuterium and phosphorus lineshapes appear more like that of $CLSE^{T}$ and $CLSE^{L}$ samples. The ^{2}H and ^{31}P NMR spectra for the samples containing the lipid mix DPPC/POPC/POPG/POPE/cholesterol in a 10:6:3:2:2 molar ratio showed lipid dynamics much like that seen in the spectra for CLSE containing samples. This study has pointed to the probable importance of specifically targeting peptidomimetics that affect DPPC dynamics in LS lipid mixtures and reiterates the ordering effect of cholesterol and suggests low levels of cholesterol may be important to modulating DPPC behavior in LS. Furthermore, a completely synthetic LS replacement formulation might require four to five lipid species rather than two or three to achieve the same lipid behavior seen in CLSE. As the number of lipid species in our LS mimic systems increased, the lipid dynamics we observed more closely mirrored what we observed for lipids in CLSE derived samples. Our five-component lipid system effectively recapitulated the behavior of DPPC while addition of SP-C and other lipids may be necessary for complete phase separation of the monounsaturated lipids.

Chapter 5 focused on differences in the sequence of $SP\text{-}B_{1\text{-}25}$ as well as different lipid environments. We saw differences in lipid dynamics as regulated by point mutations in the peptide sequence of $SP\text{-}B_{1\text{-}25}$ as the function of this peptide in various lipid systems may be sequence dependent. We were interested in whether small changes in the peptide sequence lead to better or worse activity as a result of mutating two amino acids in the N-terminus. As a result, we did see the reemergence of an isotropic peak in $CLSE^{L}$ and $CLSE^{Syn}$. A broad implication of this could be that we have

found a better peptide for LS replacements, which would need to be validated with difference experiments and animal studies.

While we have a good idea of the relative dynamics occurring for the lipid constituents in LS mimics, much work is left if we want to have a better understanding of LS proteins, particularly the N-terminal portion of SP-B, SP-B_{1-25}. The CD studies of SP-B_{1-25} in DPPC/POPG and POPC/POPG lipid environments discussed in this dissertation only tell us that this peptide adopts a consistent secondary structure when associated with different lipid systems. Other structural measurements are needed such as data obtained from solution NMR and MAS solid-state NMR structures to probe the intricacies of this lipophilic peptide. Data from low resolution FTIR has indicated a β-sheet N-terminal tail of about eight amino acids in length (*37*). From the model proposed in this study, the tail is shaped to deeply penetrate into the membrane bilayer. What is most interesting about this tail is its amino acid content, which includes the very hydrophobic residues and three prolines. SP-B_{1-25} may play a functional role of SP-B that anchors the protein deeply into the lipid environment allowing it to distinguish between fully saturated and monounsaturated lipids.

The actual depth of SP-B_{1-25} in the lipid bilayer could be determined at amino acid resolution via power saturation electron paramagnetic resonance (EPR) studies. Experiments of this type would complement our existing deuterium data, confirming conclusions made from our determination of relative order parameters in the acyl chains of the individual lipid species.

APPENDIX A
PROCESSING ^{2}H NMR DATA

Open Matlab®

Current directory → change to wherever you want Matlab® files to be saved on the longlab network (see separate startup protocol)

Type → ndnmr_sam

N-D NMR Workup

1. Click on file type (1st box on top left) and choose user defined 2 (It doesn't change on box-says Raw Binary)

2. Browse, find the fid

3. Read all fids

4. Change limits – to zoom in on the minimum value

5. Cursor value – for ^{2}H will be ~11 (x-axis)

6. Change limits again and double click just outside of spectra box and click ok or read all fids again

7. Baseline correct, shift left, and zerofill
   Shift data points left → 11 and change zerofill points to 4096 (b/c of dePaking)

8. Apodize fid, exponentially multiply – 100 is fine

9. Fourier transform fid

10. Phase spectrum – manual, only change Ph0

11. Click phase spectrum again and apply phase parameters (click yes)

12. Baseline flatten spectrum
    a. Click on baseline twice on both sides of lineshape
    b. Enter order of polynomial – usually 2
    c. Accept baseline flattening

13. Click "process all fids and draw each fid"

14. In main Matlab® window type: save expt#.mat nmr_data (example → save 2.mat nmr_data)

15. For 2000 pts type: real(nmr_data(2048-999:2048+1000))
    imag(nmr_data(2048-999:2048+1000)) copy and paste these into excel file

DePaking

1. Type or copy and paste these lines above the real and imaginary data

2. Open up SSH Secure File Transfer. Quick connect 128.227.76.72 longlab. Password- poPcgels!

3. Left Side- go to Longlab network drive (L:/) to where you will be transferring files. Right side- Fanucci Computer. You should have a folder with 2 sh files. 2Hdepake.sh, 2Hsub.sh, and 2Hdepakelist.sh, make folders and organize

4. Open up new terminal window, cd Suzanne, cd 2HNMR. This is where I modify sh files.

5. But first go to folder to make ftl file. cd expt# inside the folder you want to save the ftl file

6. Type nano expt#.ftl Copy and paste real and imaginary (+ lines before that) into secure shell. Control x to exit, y to save, enter to write file as expt#.ftl

7. Now go back to 2HNMR to modify .sh files. Cd../.. (going back 2 directories) “ls” to see what’s there.

8. Type emacs 2Hdepakelist.sh (**DO NOT** use backspace- only delete button). Example of list- ./2Hsub.sh CLSE_lipids/DPPC expt# can make list of several ftl files to depake. Control x control c to get out or save. Y is yes to save.

9. emacs 2Hsub.sh, modify Kappa values here. 1-20 or one at a time by blocking a line with # symbol. Control x, control c, yes

10. emacs 2Hdepake.sh, page down button 3 times. 2000= number of spectral data points. 1000= number of analyzed data points. 1003= middle point on relative frequency scale. 500= offset for analyzed part of spectrum. 1.0= scaling factor (don’t change). 0.1220703= number point distance of relative scale (SW over TD = 500 kHz over 4096). Control x, control c, control y (yes).

11. Run it (depake) ./2Hdepakelist.sh

12. Find min Kappa value. Cd CLSE_lipids/DPPC enter, more ellipsoid.min, press tab until reach bottom. Find minimum number sig column and its corresponding Kappa value (100 (k-e))

13. Transfer files to Longlab

14. Import data into excel spreadsheet. Files= asc (data read in), rst (fit of data), res (depaked data) and plot all of these.

15. You will have to modify 2Hdepake.sh to get correct midpoint and then depake several ftl files at once. Check peaks to see if they are lined up with 0 frequency exactly in middle of spectrum. Save these files- so you don't forget what you did (all .sh files)

16. Read off frequencies from depaked spectra and calculate order parameters.

APPENDIX B
CLSE SEPARATION PROTOCOL

Gel Permeation Chromatography

Adapted from Hall et al. Journal of Lipid Research Vol 35, 1994 (*131*)

1. **Prepare reagents/solvents** (see AfCS protocols)

2. **Pack the column**: It is a 56 x 1.2 cm glass column.
   - Sephadex LH-20 is the medium either dry or stored in MeOH.
   - Sephadex LH-20 is supplied as a dry powder and must be swollen before use. Swell the medium for at least 3 hours (overnight is better) in an excess of the solvent to be used in the separation.
   - Column volume (CV) = $\pi r^2 L = \pi(1.2)^2 56 = 253\ cm^3 = 253$ mL
   - 4 mL/gram of dry LH-20
   - 253/4 = 63 grams of LH-20 needed for a CV of 253 mL (use more…80 grams)
   - Solvent: Equilibrate with $CHCl_3$/MeOH/0.1 N HCl 950:950:100 (v/v/v) for 2 liters.

     HCl → (12N)(x)=(0.1N)(100mL) x = 0.83 mL + 99.17 mL water (add acid to water) Adjust pH with nanopure water to get a pH of 2 or 3 (not less than 2).
   - Add a piece of glass wool to the bottom of the column before packing to prevent leakage of media. Push it down with a rod. Then pour the slurry into the column without introducing air bubbles. Open the stop cock to check for bead leakage and do over if the glass wool is not sufficiently in place (this is a pain but necessary).
   - If all is well, equilibrate with 250 mL of solvent before using the column. Let solvent flow through as column packs under pressure with nitrogen gas.
   - Label tubes and fill rack

3. **Load CLSE onto the column**.

   Amount to use: 20-30 µmol phospholipid CLSE in 200 µL (up to 2 mL of CLSE can run through column) Add chloroform to CLSE if it is dry.

4. **Elute with chloroform-methanol-0.1 N HCl using pressure.** Collect the fractions in glass culture tubes. Use an automated tray.

5. **Collect fractions** to get about 1-2 mL per tube (adjust the fraction collector)

6. **Take 5-10 µl aliquots** of each fraction for protein and phosphate assays.

7. **Pool appropriate fractions** and extract with chloroform to remove acid (see Bligh Dyer method).

    - Extract protein fractions and lipid fractions using Bligh Dyer Method
    - Save lipid/protein fractions for 2nd pass – do not extract
    - Concentrate (rotovap) the samples that contain both protein and lipid to ~200-500 µl and reload for a second pass through the column.
    - Combine the protein from BD Method and rotovap to remove organic solvent
    - Do the same with the lipids
    - Use Pasteur pipette to transfer remaining solution from round bottom into glass tube
    - Evaporate remaining solvent with N2 gas.
    - Add cyclohexane, vortex, and freeze with liquid nitrogen and lyophilize.
    - Go back to lipid/protein mixed fractions and repeat for a 2nd pass through the column.
    - Follow same protocol yielding the separated proteins and lipids in solid form.

Phospholipid Analysis

See Malachite Green Phosphate Assay protocol →Plot results in excel.

The composition of individual lipids can be determined by TLC (separation based on headgroups)
Find cholesterol with TLC.

Reagents for Lipid Phosphate Assay

- 8.9 N H_2SO_4: dilute 74 mL of 12N H_2SO_4 with 26 mL of deionized water. Add acid to water. Double volumes if you need more than 100 mL.
- Malachite Green Phosphate Assay solution (stored in fridge): 100 volume reagent A + 1 volume reagent B. Example: 25 mL reagent A + 250 uL reagent B. Mix and bring to room temperature before using.

- 1M NaOH solution: Place 20 g of NaOH pellets into a 500 mL volumetric flask. Slowly add ~ 300 mL of water and mix well. Dilute to 500 mL with more water.

- 0.65 mM phosphorus standard solution (stored in fridge in Malachite assay box).

Protein Analysis

1. Prepare samples for a standard curve by pipetting 0, 5, 10, 20, 40, and 80 µl of BSA (0.2 mg/ml →143 uL stock BSA + 857 uL water) into disposable glass culture tubes; this provides known protein amounts of 0, 1, 2, 4, 8, and 16 µg. Adjust the total volume of each tube to 225 µl with deionized water.

2. Or you can use 0, 4, 16, and 32 ug BSA → 0, 20, 80, and 160 uL water adjusted to 225 uL with water.

3. Take 10 µl aliquots of each sample, evaporate off the chloroform/methanol, and dilute to 225 µL with deionized water.

4. Add: 30 µL of Tris-HCl, pH 7.5, 1 M with 2% SDS (Tris-HCl/SDS) to each sample and 50 µL of 90% TCA to each sample

5. Vortex each sample.

6. Following the TCA addition, incubate the samples for at least 3 minutes (10 is fine too) at room temperature to precipitate protein.

7. Number 4 Millipore filters according to the fraction #. Wear gloves when working with the filters and use forceps.

8. Place them in the vacuum funnel and wet each one with water.

9. Then transfer each sample via a Pasteur pipette onto a filter.

10. Filter each sample under vacuum and immediately wash the filter with 100 µL of 6% TCA. Filter again. This will take at least 5 minutes if protein content is high.

11. After all samples have been processed in this manner, remove the filters and place into a beaker containing 200 ml of 0.1% (w/v) Amido Black 10B dissolved in methanol/glacial acetic acid/deionized water, 45/10/45, v/v/v (really just enough to cover the filter).

12. Stain the filters for 20-45 minutes with gentle shaking.

13. Decant the stain (save the stain – can be reused for several weeks) and rinse the filters with 200 ml deionized water once.

14. Wash the filters with 3 successive 200-ml portions of destaining solution (methanol/glacial acetic acid/water, 45/1/4, v/v/v) for 1 minute per wash (with gentle shaking). Then wash with 200 ml of deionized water for 2 minutes (gentle shaking) and place on a paper towel and blot with kimwipes to remove excess water. The filter should sink when organic solvent is removed.

15. Place each filter in a new test tube containing 1 ml of 25 mM NaOH/0.05 mM EDTA/50% (v/v) ethanol. The filters contain stained filtrate (protein).

16. Elute the dye from the filters by incubating for 20 minutes with occasional vortexing. The eluted stain is stable for less than two hours.

17. Measure the absorbance of the eluate at 630 nm. Zero the spectrophotometer against the elution solution (NaOH/EDTA/EtOH) or the 0 ug BSA standard. You want the blank to contain all components except protein.

18. Generate a standard curve by plotting the OD of the protein standards against their content of protein (as µg, ranging from 0 to 32). Plot results in excel→Fit the data by linear regression analysis and calculate the protein concentration (µg/µl) of the unknown samples using the standard curve and the volume of samples used in the assay.

LIST OF REFERENCES

1. Notter, R. H. (2000) Lung surfactants: basic science and clinical applications. CRC Press.

2. Goerke, J. (1974) Lung surfactant, *Biochimica et Biophysica Acta (BBA)-Reviews on Biomembranes 344*, 241–261.

3. Possmayer, F., Nag, K., Rodriguez, K., Qanbar, R., and Schürch, S. (2001) Surface activity in vitro: role of surfactant proteins, *Comp. Biochem. Physiol., Part A Mol. Integr. Physiol 129*, 209-220.

4. Ganong, W. (2005) Review of Medical Physiology 22nd ed. McGraw-Hill Medical.

5. Creuwels, L., Van Golde, L. M. G., and Haagsman, H. P. (1997) The pulmonary surfactant system: biochemical and clinical aspects, *Lung 175*, 1–39.

6. Wrobel, S. (2004) Bubbles, babies and biology: the story of surfactant, *The FASEB Journal 18*, 1624e.

7. Prange, H. D. (2003) Laplace's law and the alveolus: a misconception of anatomy and a misapplication of physics, *AJP: Advances in Physiology Education 27*, 34-40.

8. Serrano, A. G., Ryan, M., Weaver, T. E., and Pérez-Gil, J. (2006) Critical structure-function determinants within the N-terminal region of pulmonary surfactant protein SP-B, *Biophysical journal 90*, 238–249.

9. Goerke, J. (1998) Pulmonary surfactant: functions and molecular composition, *Biochimica et Biophysica Acta (BBA)-Molecular Basis of Disease 1408*, 79–89.

10. Pérez-Gil, J. (2001) Lipid-protein interactions of hydrophobic proteins SP-B and SP-C in lung surfactant assembly and dynamics, *Pediatr Pathol Mol Med 20*, 445-469.

11. Rice, W. R., Sarin, V. K., Fox, J. L., Baatz, J., Wert, S., and Whitsett, J. A. (1989) Surfactant peptides stimulate uptake of phosphatidylcholine by isolated cells, *Biochimica et Biophysica Acta (BBA)-Lipids and Lipid Metabolism 1006*, 237–245.

12. Rooney, S. A., Young, S. L., and Mendelson, C. R. (1994) Molecular and cellular processing of lung surfactant, *The FASEB journal 8*, 957.

13. Antharam, V. C., Elliott, D. W., Mills, F. D., Farver, R. S., Sternin, E., and Long, J. R. (2009) Penetration depth of surfactant peptide KL4 into membranes is determined by fatty acid saturation, *Biophysical journal 96*, 4085–4098.

14. Antharam, V. C., Farver, R. S., Kuznetsova, A., Sippel, K. H., Mills, F. D., Elliott, D. W., Sternin, E., and Long, J. R. (2008) Interactions of the C-terminus of lung surfactant protein B with lipid bilayers are modulated by acyl chain saturation, *Biochimica et Biophysica Acta (BBA)-Biomembranes 1778*, 2544–2554.

15. Farver, R. S., Mills, F. D., Antharam, V. C., Chebukati, J. N., Fanucci, G. E., and Long, J. R. (2010) Lipid Polymorphism Induced by Surfactant Peptide SP-B1-25, *Biophys J 99*, 1773-1782.

16. Raghavendran, K., Willson, D., and Notter, R. (2011) Surfactant Therapy for Acute Lung Injury and Acute Respiratory Distress Syndrome, *Critical Care Clinics 27*, 525–559.

17. Zhang, H., Wang, Y. E., Fan, Q., and Zuo, Y. Y. (2011) On the Low Surface Tension of Lung Surfactant, *Langmuir*.

18. Veldhuizen, R., Nag, K., Orgeig, S., and Possmayer, F. (1998) The role of lipids in pulmonary surfactant, *Biochim. Biophys. Acta 1408*, 90-108.

19. Yeagle, P. L. (2004) The Structure of Biological Membranes, Second Edition 2nd ed. CRC Press.

20. Wang, Z., Gurel, O., Weinbach, S., and Notter, R. H. (1997) Primary importance of zwitterionic over anionic phospholipids in the surface-active function of calf lung surfactant extract, *American journal of respiratory and critical care medicine 156*, 1049.

21. Yu, S. H., and Possmayer, F. (1990) Role of bovine pulmonary surfactant-associated proteins in the surface-active property of phospholipid mixtures, *Biochimica et Biophysica Acta (BBA)-Lipids and Lipid Metabolism 1046*, 233–241.

22. Cullis, P. R., and De Kruijff, B. (1979) Lipid polymorphism and the functional roles of lipids in biological membranes, *Biochimica et Biophysica Acta (BBA)-Reviews on Biomembranes 559*, 399–420.

23. Cullis, P. R., Hope, M. J., and Tilcock, C. P. . (1986) Lipid polymorphism and the roles of lipids in membranes, *Chemistry and physics of lipids 40*, 127–144.

24. Perkins, W. R., Dause, R. B., Parente, R. A., Minchey, S. R., Neuman, K. C., Gruner, S. M., Taraschi, T. F., and Janoff, A. S. (1996) Role of lipid polymorphism in pulmonary surfactant, *Science 273*, 330.

25. Johansson, J., and Curstedt, T. (1997) Molecular structures and interactions of pulmonary surfactant components, *Eur. J. Biochem 244*, 675-693.

26. Kilpatrick, D. C. (2002) Animal lectins: a historical introduction and overview, *Biochimica et Biophysica Acta (BBA)-General Subjects 1572*, 187–197.

27. Van De Wetering, J. K., Van Golde, L. M. G., and Batenburg, J. J. (2004) Collectins, *European Journal of Biochemistry 271*, 1229–1249.

28. McCormack, F. X., and Whitsett, J. A. (2002) The pulmonary collectins, SP-A and SP-D, orchestrate innate immunity in the lung, *Journal of Clinical Investigation 109*, 707–712.

29. Pérez-Gil, J., and Keough, K. M. (1998) Interfacial properties of surfactant proteins, *Biochim. Biophys. Acta 1408*, 203-217.

30. Cruz, A., Worthman, L. A., Serrano, A. G., Casals, C., Keough, K. M., and Pérez-Gil, J. (2000) Microstructure and dynamic surface properties of surfactant protein SP-B/dipalmitoylphosphatidylcholine interfacial films spread from lipid-protein bilayers, *Eur. Biophys. J. 29*, 204-213.

31. Veldhuizen, E. J. A., Batenburg, J. J., van Golde, L. M. G., and Haagsman, H. P. (2000) The role of surfactant proteins in DPPC enrichment of surface films, *Biophysical Journal 79*, 3164–3171.

32. Whitsett, J. A., and Weaver, T. E. (2002) Hydrophobic surfactant proteins in lung function and disease, *New England Journal of Medicine 347*, 2141–2148.

33. Weaver T.E. (1998) Synthesis, processing and secretion of surfactant proteins B and C, *Biochimica et Biophysica Acta (BBA)/Molecular Basis of Disease 1408*, 173-179.

34. Zaltash, S., Palmblad, M., Curstedt, T., Johansson, J., and Persson, B. (2000) Pulmonary surfactant protein B: a structural model and a functional analogue, *Biochim. Biophys. Acta 1466*, 179-186.

35. Liepinsh, E., Andersson, M., Ruysschaert, J.-M., and Otting, G. (1997) Saposin fold revealed by the NMR structure of NK-lysin, *Nat Struct Mol Biol 4*, 793-795.

36. Bringezu, F., Ding, J., Brezesinski, G., Waring, A. J., and Zasadzinski, J. A. (2002) Influence of Pulmonary Surfactant Protein B on Model Lung Surfactant Monolayers, *Langmuir 18*, 2319-2325.

37. Gordon, L. M., Lee, K. Y. C., Lipp, M. M., Zasadzinski, J. A., Walther, F. J., Sherman, M. A., and Waring, A. J. (2000) Conformational mapping of the N-terminal segment of surfactant protein B in lipid using 13C-enhanced Fourier transform infrared spectroscopy, *The Journal of Peptide Research 55*, 330–347.

38. Kurutz, J. W., and Lee, K. Y. C. (2002) NMR Structure of Lung Surfactant Peptide SP-B $_{11-25}$, *Biochemistry 41*, 9627-9636.

39. Sarker, M., Waring, A. J., Walther, F. J., Keough, K. M. W., and Booth, V. (2007) Structure of Mini-B, a Functional Fragment of Surfactant Protein B, in Detergent Micelles †,‡, *Biochemistry 46*, 11047-11056.

40. Engle, W. A., and and the Committee on Fetus and Newborn. (2008) Surfactant-Replacement Therapy for Respiratory Distress in the Preterm and Term Neonate, *Pediatrics 121*, 419-432.

41. Curley, A., and Halliday, H. (2001) The present status of exogenous surfactant for the newborn, *Early human development 61*, 67–83.

42. Halliday, H. L. (2005) History of Surfactant from 1980, *Biology of the Neonate 87*, 317-322.

43. Revak, S. D., Merritt, T. A., Hallman, M., Heldt, G., La Polla, R. J., Hoey, K., Houghten, R. A., and Cochrane, C. G. (1991) The use of synthetic peptides in the formation of biophysically and biologically active pulmonary surfactants, *Pediatr. Res 29*, 460-465.

44. Cochrane, C. G., and Revak, S. D. (1994) Protein-Phospholipid Interactions in Pulmonary Surfactant, *Chest 105*, 57S -62S.

45. Cochrane, C., and Revak, S. (1991) Pulmonary surfactant protein B (SP-B): structure-function relationships, *Science 254*, 566.

46. Gupta, M., Hernandez-Juviel, J., Waring, A., Bruni, R., and Walther, F. (2000) Comparison of functional efficacy of surfactant protein B analogues in lavaged rats, *European Respiratory Journal 16*, 1129.

47. Lipp, M. M., Lee, K. Y. C., Zasadzinski, J. A., and Waring, A. J. (1996) Phase and Morphology Changes in Lipid Monolayers Induced by SP-B Protein and Its Amino-Terminal Peptide, *Science 273*, 1196 -1199.

48. Bruni, R., Taeusch, H. W., and Waring, A. J. (1991) Surfactant protein B: lipid interactions of synthetic peptides representing the amino-terminal amphipathic domain, *Proceedings of the National Academy of Sciences 88*, 7451.

49. Possmayer, F., Hall, S. B., Haller, T., Petersen, N. O., Zuo, Y. Y., Bernardino de la Serna, J., Postle, A. D., Veldhuizen, R. A. W., and Orgeig, S. (2010) Recent advances in alveolar biology: Some new looks at the alveolar interface, *Respiratory Physiology & Neurobiology 173*, S55-S64.

50. Blanco, O., and Pérez-Gil, J. (2007) Biochemical and pharmacological differences between preparations of exogenous natural surfactant used to treat Respiratory Distress Syndrome: Role of the different components in an efficient pulmonary surfactant, *European journal of pharmacology 568*, 1–15.

51. Tate, M. W., Eikenberry, E. F., Turner, D. C., Shyamsunder, E., and Gruner, S. M. (1991) Nonbilayer phases of membrane lipids, *Chemistry and physics of lipids 57*, 147–164.

52. Guttentag, S. H., Beers, M. F., Bieler, B. M., and Ballard, P. L. (1998) Surfactant protein B processing in human fetal lung, *American Journal of Physiology - Lung Cellular and Molecular Physiology 275*, L559 -L566.

53. Guttentag, S. (2008) Posttranslational Regulation of Surfactant Protein B Expression, in *Seminars in perinatology*, pp 367–370.

54. Korimilli, A., Gonzales, L. W., and Guttentag, S. H. (2000) Intracellular localization of processing events in human surfactant protein B biosynthesis, *Journal of Biological Chemistry 275*, 8672.

55. Gill, P., Moghadam, T. T., and Ranjbar, B. (2010) Differential Scanning Calorimetry Techniques: Applications in Biology and Nanoscience, *Journal of biomolecular techniques: JBT 21*, 167.

56. Ladbury, J. E., and Doyle, M. L. (2004) Biocalorimetry 2: Applications of Calorimetry in the Biological Sciences 2nd ed. Wiley.

57. McElhaney, R. N. (1982) The use of differential scanning calorimetry and differential thermal analysis in studies of model and biological membranes, *Chemistry and physics of lipids 30*, 229–259.

58. Bulheller, B. M., Rodger, A., and Hirst, J. D. (2007) Circular and linear dichroism of proteins, *Phys. Chem. Chem. Phys. 9*, 2020.

59. Bertucci, C., Pistolozzi, M., and Simone, A. (2010) Circular dichroism in drug discovery and development: an abridged review, *Anal Bioanal Chem 398*, 155-166.

60. Kelly, S. M., Jess, T. J., and Price, N. C. (2005) How to study proteins by circular dichroism, *Biochimica et Biophysica Acta (BBA)-Proteins & Proteomics 1751*, 119–139.

61. Manta, B., Obal, G., Ricciardi, A., Pritsch, O., and Denicola, A. Tools to evaluate the conformation of protein products, *Biotechnology Journal*.

62. Castro, V. (2005) “Seeing” Lipid Membranes by Solid-State NMR, *From Cells to Proteins: Imaging Nature across Dimensions* 451–458.

63. Auger, M. (2000) Biological membrane structure by solid-state NMR, *Current issues in molecular biology 2*, 119–124.

64. Kühl, O. (Ed.). (2009) Phosphorus-31 NMR Spectroscopy. Springer Berlin Heidelberg, Berlin, Heidelberg.

65. Dubinnyi, M. A., Lesovoy, D. M., Dubovskii, P. V., Chupin, V. V., and Arseniev, A. S. (2006) Modeling of 31P-NMR spectra of magnetically oriented phospholipid liposomes: A new analytical solution, *Solid State Nuclear Magnetic Resonance 29*, 305–311.

66. Levitt, M. H. (2008) Spin Dynamics: Basics of Nuclear Magnetic Resonance 2nd ed. Wiley.

67. Brown, S. P., and Emsley, L. Solid-State NMR 269-326.

68. Burnett, L. J. (1971) Deuteron Quadrupole Coupling Constants in Three Solid Deuterated Paraffin Hydrocarbons: C2D6, C4D10, C6D14, *J. Chem. Phys. 55*, 5829.

69. Seelig, J. (1977) Deuterium magnetic resonance: theory and application to lipid membranes, *Quarterly Reviews of Biophysics 10*, 353–418.

70. Brown, M. F., Lope-Piedrafita, S., Martinez, G. V., and Petrache, H. I. (2006) Solid-state deuterium NMR spectroscopy of membranes, *Modern Magnetic Resonance* 249–260.

71. Seelig, J., and Seelig, A. (1980) Lipid conformation in model membranes and biological membranes, *Q. Rev. Biophys. 13*, 19-61.

72. Seelig, J., and Niederberger, W. (1974) Deuterium-labeled lipids as structural probes in liquid crystalline bilayers. Deuterium magnetic resonance study, *J. Am. Chem. Soc. 96*, 2069-2072.

73. Hemminga, M. A., and Poile, T. W. (1989) Biological applications of solid state NMR., in *In: Dynamic properties of biomolecular assemblies, S.E. Harding & A.J. Rowe (eds.). Royal Soc. Chemistry, Cambridge, UK (1989) 74-89.*

74. Bloom, M., Davis, J. H., and Mackay, A. L. (1981) Direct determination of the oriented sample nmr spectrum from the powder spectrum for systems with local axial symmetry, *Chemical Physics Letters 80*, 198-202.

75. Sternin, E., Schafer, H., Polozov, I. V., and Gawrisch, K. (2001) Simultaneous determination of orientational and order parameter distributions from NMR spectra of partially oriented model membranes, *Journal of Magnetic Resonance 149*, 110–113.

76. Schäfer, H., Mädler, B., and Sternin, E. (1998) Determination of orientational order parameters from 2H NMR spectra of magnetically partially oriented lipid bilayers., *Biophys J 74*, 1007-1014.

77. Sternin, E., Bloom, M., and Mackay, A. L. (1983) De-Pake-ing of NMR spectra, *Journal of Magnetic Resonance (1969) 55*, 274–282.

78. Petrache, H. I., Dodd, S. W., and Brown, M. F. (2000) Area per lipid and acyl length distributions in fluid phosphatidylcholines determined by 2H NMR spectroscopy, *Biophysical journal 79*, 3172–3192.

79. Tscharnuter, W. (2000) Photon correlation spectroscopy in particle sizing, *Encyclopedia of analytical chemistry*.

80. Malvern Instruments. Dynamic Light Scattering: An Introduction in 30 Minutes.

81. Pandey, J., Das, V. M., And Varma, A. (2009) Microscopy: Key to Understand Molecular Biotechnology, *A textbook of molecular biotechnology* 29.

82. Faruqi, A. ., and Henderson, R. (2007) Electronic detectors for electron microscopy, *Current Opinion in Structural Biology 17*, 549-555.

83. Reimer, L., and Kohl, H. (2008) Transmission electron microscopy: physics of image formation. Springer.

84. Williams, D. B., and Carter, C. B. (2009) The Transmission Electron Microscope, *Transmission Electron Microscopy* 3–22.

85. Chan, W. C., and White, P. D. (2000) Fmoc Solid Phase Peptide Synthesis: A Practical Approach 1st ed. Oxford University Press, USA.

86. Grant, G. A. (2002) Synthetic peptides: a user's guide. Oxford University Press US.

87. Stevenson, R., and Johnson, E. L. (1978) Basic Liquid Chromatography. Varian.

88. Yau, W. W., Kirkland, J. J., and Bly, D. D. (1979) Modern Size-Exclusion Liquid Chromatography: Practice of Gel Permeation and Gel Filtration Chromatography 1st ed. Wiley-Interscience.

89. Cullis, P. R., Tilcock, C. P., and Hope, M. J. (1991) Lipid polymorphism, *Membrane fusion* 35–64.

90. Piknova, B., Schram, V., and Hall, S. B. (2002) Pulmonary surfactant: phase behavior and function, *Current opinion in structural biology 12*, 487–494.

91. Wright, J. R., and Clements, J. A. (1987) Metabolism and turnover of lung surfactant, *Am. Rev. Respir. Dis. 136*, 426-444.

92. Postle, A. D., Heeley, E. L., and Wilton, D. C. (2001) A comparison of the molecular species compositions of mammalian lung surfactant phospholipids, *Comp. Biochem. Physiol., Part A Mol. Integr. Physiol. 129*, 65-73.

93. Zuo, Y. Y., Veldhuizen, R. A. W., Neumann, A. W., Petersen, N. O., and Possmayer, F. (2008) Current perspectives in pulmonary surfactant–inhibition, enhancement and evaluation, *Biochimica et Biophysica Acta (BBA)-Biomembranes 1778*, 1947–1977.

94. Pérez-Gil, J. (2008) Structure of pulmonary surfactant membranes and films: the role of proteins and lipid-protein interactions, *Biochimica et Biophysica acta (BBA)-Biomembranes 1778*, 1676–1695.

95. Whitsett, J. A., Nogee, L. M., Weaver, T. E., and Horowitz, A. D. (1995) Human surfactant protein B: structure, function, regulation, and genetic disease, *Physiol. Rev. 75*, 749-757.

96. Clark, J. C., Wert, S. E., Bachurski, C. J., Stahlman, M. T., Stripp, B. R., Weaver, T. E., and Whitsett, J. A. (1995) Targeted disruption of the surfactant protein B gene disrupts surfactant homeostasis, causing respiratory failure in newborn mice, *Proceedings of the National Academy of Sciences 92*, 7794.

97. Ballard, P. L. (2003) Surfactant Protein Profile of Pulmonary Surfactant in Premature Infants, *American Journal of Respiratory and Critical Care Medicine 168*, 1123-1128.

98. Strayer, D., Hallman, M., and Merritt, T. (1991) Immunogenicity of surfactant. II. Porcine and bovine surfactants, *Clinical & Experimental Immunology 83*, 41–46.

99. Walther, F. J., Gordon, L. M., Zasadzinski, J. A., Sherman, M. A., and Waring, A. J. (2000) Surfactant protein B and C analogues, *Molecular Genetics and Metabolism 71*, 342–351.

100. Ryan, M. A., Qi, X., Serrano, A. G., Ikegami, M., Perez-Gil, J., Johansson, J., and Weaver, T. E. (2005) Mapping and Analysis of the Lytic and Fusogenic Domains of Surfactant Protein B, *Biochemistry 44*, 861-872.

101. Sinha, S. K., Lacaze-Masmonteil, T., Valls i Soler, A., Wiswell, T. E., Gadzinowski, J., Hajdu, J., Bernstein, G., Sanchez-Luna, M., Segal, R., Schaber, C. J., and others. (2005) A multicenter, randomized, controlled trial of lucinactant versus poractant alfa among very premature infants at high risk for respiratory distress syndrome, *Pediatrics 115*, 1030.

102. Seurynck, S. L., Patch, J. A., and Barron, A. E. (2005) Simple, Helical Peptoid Analogs of Lung Surfactant Protein B, *Chemistry & Biology 12*, 77-88.

103. Waring, A. J., Walther, F. J., Gordon, L. M., Hernandez-Juviel, J. M., Hong, T., Sherman, M. A., Alonso, C., Alig, T., Braun, A., Bacon, D., and Zasadzinski, J. A. (2008) The role of charged amphipathic helices in the structure and function of surfactant protein B, *The Journal of Peptide Research 66*, 364-374.

104. Gordon, L. M., Horvath, S., Longo, M. L., Zasadzinski, J., Taeusch, H. W., Faull, K., Leung, C., and Waring, A. J. (1996) Conformation and molecular topography of the N-terminal segment of surfactant protein B in structure-promoting environments., *Protein science: a publication of the Protein Society 5*, 1662.

105. Shanmukh, S., Biswas, N., Waring, A. J., Walther, F. J., Wang, Z., Chang, Y., Notter, R. H., and Dluhy, R. A. (2005) Structure and properties of phospholipid-peptide monolayers containing monomeric SP-B1-25:: II. Peptide conformation by infrared spectroscopy, *Biophysical chemistry 113*, 233–244.

106. Ramamoorthy, A., Thennarasu, S., Lee, D. K., Tan, A., and Maloy, L. (2006) Solid-state NMR investigation of the membrane-disrupting mechanism of antimicrobial peptides MSI-78 and MSI-594 derived from magainin 2 and melittin, *Biophysical journal 91*, 206–216.

107. Andrade, M. A., Chacón, P., Merelo, J. J., and Morán, F. (1993) Evaluation of secondary structure of proteins from UV circular dichroism spectra using an unsupervised learning neural network, *Protein Eng. 6*, 383-390.

108. Sáenz, A., Cañadas, O., Bagatolli, L. A., Johnson, M. E., and Casals, C. (2006) Physical properties and surface activity of surfactant-like membranes containing the cationic and hydrophobic peptide KL4, *FEBS J. 273*, 2515-2527.

109. Russell-Schulz, B., Booth, V., and Morrow, M. R. (2009) Perturbation of DPPC/POPG bilayers by the N-terminal helix of lung surfactant protein SP-B: a ^{2}H NMR study, *Eur Biophys J 38*, 613-624.

110. Liu, F., Lewis, R. N. A. H., Hodges, R. S., and McElhaney, R. N. (2002) Effect of Variations in the Structure of a Polyleucine-Based α-Helical Transmembrane Peptide on Its Interaction with Phosphatidylcholine Bilayers, *Biochemistry 41*, 9197-9207.

111. Bunow, M. R., and Levin, I. W. (1977) Raman spectra and vibrational assignments for deuterated membrane lipids. 1,2-Dipalmitoyl phosphatidylcholine-d9 and -d62, *Biochim. Biophys. Acta 489*, 191-206.

112. Epand, R. M. (1998) Lipid polymorphism and protein-lipid interactions, *Biochimica et Biophysica Acta (BBA)-Reviews on Biomembranes 1376*, 353–368.

113. Henzler-Wildman, K. A., Martinez, G. V., Brown, M. F., and Ramamoorthy, A. (2004) Perturbation of the Hydrophobic Core of Lipid Bilayers by the Human Antimicrobial Peptide LL-37, *Biochemistry 43*, 8459-8469.

114. Porcelli, F. (2004) Structure and Orientation of Pardaxin Determined by NMR Experiments in Model Membranes, *Journal of Biological Chemistry 279*, 45815-45823.

115. Longo, M., Bisagno, A., Zasadzinski, J., Bruni, R., and Waring, A. (1993) A function of lung surfactant protein SP-B, *Science 261*, 453 -456.

116. Lee, K. Y. ., Lipp, M. M., Zasadzinski, J. A., and Waring, A. J. (1997) Effects of lung surfactant specific protein SP-B and model SP-B peptide on lipid monolayers at the air-water interface, *Colloids and Surfaces A: Physicochemical and Engineering Aspects 128*, 225–242.

117. Bastacky, J., Lee, C. Y., Goerke, J., Koushafar, H., Yager, D., Kenaga, L., Speed, T. P., Chen, Y., and Clements, J. A. (1995) Alveolar lining layer is thin and continuous: low-temperature scanning electron microscopy of rat lung, *Journal of Applied Physiology 79*, 1615 -1628.

118. Chavarha, M., Khoojinian, H., Schulwitz Jr., L. E., Biswas, S. C., Rananavare, S. B., and Hall, S. B. (2010) Hydrophobic Surfactant Proteins Induce a Phosphatidylethanolamine to Form Cubic Phases, *Biophysical Journal 98*, 1549-1557.

119. Bachofen, H., Gerber, U., Gehr, P., Amrein, M., and Schurch, S. (2005) Structures of pulmonary surfactant films adsorbed to an air-liquid interface in vitro, *Biochimica et Biophysica Acta (BBA)-Biomembranes 1720*, 59–72.

120. Diemel, R. V. (2002) Multilayer Formation upon Compression of Surfactant Monolayers Depends on Protein Concentration as Well as Lipid Composition. An atomic force microscopy study, *Journal of Biological Chemistry 277*, 21179-21188.

121. Follows, D., Tiberg, F., Thomas, R., and Larsson, M. (2007) Multilayers at the surface of solutions of exogenous lung surfactant: direct observation by neutron reflection, *Biochimica et Biophysica Acta (BBA)-Biomembranes 1768*, 228–235.

122. Yang, T. C., McDonald, M., Morrow, M. R., and Booth, V. (2009) The Effect of a C-Terminal Peptide of Surfactant Protein B (SP-B) on Oriented Lipid Bilayers, Characterized by Solid-State 2H-and 31P-NMR, *Biophysical journal 96*, 3762–3771.

123. Morrow, M., Stewart, J., Taneva, S., Dico, A., and Keough, K. W. (2003) Perturbation of DPPC bilayers by high concentrations of pulmonary surfactant protein SP-B, *European Biophysics Journal 33*.

124. Dico, A. S., Hancock, J., Morrow, M. R., Stewart, J., Harris, S., and Keough, K. M. (1997) Pulmonary surfactant protein SP-B interacts similarly with dipalmitoylphosphatidylglycerol and dipalmitoylphosphatidylcholine in phosphatidylcholine/phosphatidylglycerol mixtures, *Biochemistry 36*, 4172-4177.

125. Walther, F. J., Waring, A. J., Hernandez-Juviel, J. M., Gordon, L. M., Wang, Z., Jung, C.-L., Ruchala, P., Clark, A. P., Smith, W. M., Sharma, S., and Notter, R. H. (2010) Critical Structural and Functional Roles for the N-Terminal Insertion Sequence in Surfactant Protein B Analogs, *PLoS ONE* (Morty, R. E., Ed.) *5*, e8672.

126. Frey, S. L., Pocivavsek, L., Waring, A. J., Walther, F. J., Hernandez-Juviel, J. M., Ruchala, P., and Lee, K. Y. C. (2010) Functional importance of the NH2-terminal insertion sequence of lung surfactant protein B, *Am. J. Physiol. Lung Cell Mol. Physiol 298*, L335-347.

127. Kandasamy, S. K., and Larson, R. G. (2005) Molecular dynamics study of the lung surfactant peptide SP-B1-25 with DPPC monolayers: Insights into interactions and peptide position and orientation, *Biophysical journal 88*, 1577–1592.

128. Laroche, G., Dufourc, E. J., Pezolet, M., and Dufourcq, J. (1990) Coupled changes between lipid order and polypeptide conformation at the membrane surface. A deuterium-NMR and Raman study of polylysine-phosphatidic acid systems, *Biochemistry 29*, 6460–6465.

129. Paré, C., Lafleur, M., Liu, F., Lewis, R. N. A. H., and McElhaney, R. N. (2001) Differential scanning calorimetry and 2H nuclear magnetic resonance and Fourier transform infrared spectroscopy studies of the effects of transmembrane [alpha]-helical peptides on the organization of phosphatidylcholine bilayers, *Biochimica et Biophysica Acta (BBA)-Biomembranes 1511*, 60–73.

130. Mari'a Oviedo, J., Casals, C., and Pérez-Gil, J. (2001) Pulmonary surfactant protein SP-B is significantly more immunoreactive in anionic than in zwitterionic bilayers, *FEBS letters 494*, 236–240.

131. Hall, S. B., Wang, Z., and Notter, R. H. (1994) Separation of subfractions of the hydrophobic components of calf lung surfactant., *Journal of lipid research 35*, 1386.

132. Chen Jr, P., Toribara, T. Y., and Warner, H. (1956) Microdetermination of phosphorus, *Analytical chemistry 28*, 1756–1758.

133. Kaplan, R. S., and Pedersen, P. L. (1989) Sensitive protein assay in presence of high levels of lipid, *Meth. Enzymol 172*, 393-399.

134. Schaffner, W., and Weissmann, C. (1973) A rapid, sensitive, and specific method for the determination of protein in dilute solution, *Analytical Biochemistry 56*, 502–514.

135. Epand, R. M., and Bottega, R. (1987) Modulation of the phase transition behavior of phosphatidylethanolamine by cholesterol and oxysterols, *Biochemistry 26*, 1820–1825.

136. Paré, C., and Lafleur, M. (1998) Polymorphism of POPE/cholesterol system: a 2H nuclear magnetic resonance and infrared spectroscopic investigation, *Biophysical journal 74*, 899–909.

137. Gunstone, F. D., Harwood, J. L., and Dijkstra, A. J. (2007) The Lipid Handbook with CD-ROM, Third Edition 3rd ed. CRC Press.

138. Li, X. M., Momsen, M. M., Smaby, J. M., Brockman, H. L., and Brown, R. E. (2001) Cholesterol decreases the interfacial elasticity and detergent solubility of sphingomyelins, *Biochemistry 40*, 5954–5963.

139. Nag, K., Keough, K. M. W., and Morrow, M. R. (2006) Probing perturbation of bovine lung surfactant extracts by albumin using DSC and 2H-NMR, *Biophysical journal 90*, 3632–3642.

140. Vist, M. R., and Davis, J. H. (1990) Phase Equilibria of Cholesterol/Dipalmitoylphosphatidylcholine Mixtures: 2H, *Biochemistry 29*, 1–464.

141. Knoll, W., Schmidt, G., Ibel, K., and Sackmann, E. (1985) Small-angle neutron scattering study of lateral phase separation in dimyristoylphosphatidylcholine-cholesterol mixed membranes, *Biochemistry 24*, 5240-5246.

142. Recktenwald, D. J., and McConnell, H. M. (1981) Phase equilibria in binary mixtures of phosphatidylcholine and cholesterol, *Biochemistry 20*, 4505-4510.

143. Lentz, B. R., Barrow, D. A., and Hoechli, M. (1980) Cholesterol-phosphatidylcholine interactions in multilamellar vesicles, *Biochemistry 19*, 1943-1954.

144. Shimshick, E. J., and McConnell, H. M. (1973) Lateral phase separations in binary mixtures of cholesterol and phospholipids, *Biochemical and Biophysical Research Communications 53*, 446-451.

145. Brown, M. F., and Seelig, J. (1978) Influence of cholesterol on the polar region of phosphatidylcholine and phosphatidylethanolamine bilayers, *Biochemistry 17*, 381-384.

146. Fehrenbach, H. (2001) Alveolar epithelial type II cell: defender of the alveolus revisited, *Respir Res 2*, 33–46.

147. Antonio Cruz, L. V., and others. (2004) Effect of Pulmonary Surfactant Protein SP-B on the Micro-and Nanostructure of Phospholipid Films, *Biophysical Journal 86*, 308.

148. White, S. H., Wimley, W. C., Ladokhin, A., and Hristova, K. (1998) Protein folding in membranes: pondering the nature of the bilayer milieu, *Biol. Skr. Dan. Selsk 49*, 91–98.

149. Wimley, W. C., and White, S. H. (1996) Experimentally determined hydrophobicity scale for proteins at membrane interfaces, *Nat. Struct. Biol. 3*, 842-848.

BIOGRAPHICAL SKETCH

Reba Suzanne Farver got her Bachelor of Science degree in chemistry with a concentration in biochemistry at the University of South Alabama in May of 2006. She graduated with honors and was also a Whiddon Scholar. She joined the PhD program in medical sciences at the University of Florida in the fall of 2006 and joined the lab of Joanna R. Long in 2007. She received her PhD from the University of Florida in the fall of 2011. Her interests include structural biology, playing with Chester (her pet hedgehog), and traveling.